Precision Higgs Physics in the Standard Model Effective Field Theory

CULLEN, JONATHAN,MICHAEL

Precision Higgs Physics in the Standard Model Effective Field Theory

Jonathan M. Cullen

A Thesis presented for the degree of
Doctor of Philosophy

Institute for Particle Physics Phenomenology
Department of Physics
Durham University
United Kingdom

January 2021

Precision Higgs Physics in the Standard Model Effective Field Theory

Jonathan M. Cullen

Submitted for the degree of Doctor of Philosophy

January 2021

Abstract: We consider the application of the dimension-6 standard model effective field theory (SMEFT) as a method to parameterize the effects of heavy new physics in processes involving the Higgs boson. We calculate the full set of next-to-leading order (NLO) corrections to the phenomenologically relevant Higgs decay into fermion pairs, summarized as $h \to f\bar{f}$, for $f \in \{b, c, \tau, \mu\}$. This work forms the basis of precision studies of these decay modes in effective field theory, and is an important constituent to the precision study of the Higgs in the SMEFT.

We address several technical issues relating to the dimension-6 SMEFT at NLO. These issues include subtleties in the Higgs-Z boson mixing, development of a physically consistent electric charge renormalization constant built from two-point functions, our own implementation of gauge fixing, and the treatment of tadpoles in the SMEFT. Additionally, we consider the role of decoupling relations as a method of removing anomalously large tadpole corrections to the decay rate when using a hybrid renormalization scheme, where some parameters are renormalized in the $\overline{\text{MS}}$ scheme, while others are renormalized in the on-shell scheme.

The results are calculated fully analytically. We provide illustrative subsets of analytical results, and full numerical results for the decay rates calculated here. Furthermore, we study the convergence of the results, and estimate the size of uncalculated higher-order corrections by considering scale variations. We also explore the benefits of ratios of decay rates. In these ratios, full or partial cancellation of universal counterterms reduce the Wilson coefficient dependence as compared with decay rates alone. In some scenarios we find an enhanced sensitivity to operators generating the effective hgg and $h\gamma\gamma$ couplings. In particular, we find that these ratios present an interesting test of minimal flavor violation.

Contents

Declaration **9**

Acknowledgements **11**

I Introduction **13**

1 The Standard Model **15**

1.1 Introduction to the Standard Model 15

1.1.1 The Gauge Lagrangian 17

1.1.2 The Higgs Lagrangian 18

1.1.3 The Fermion Lagrangian 23

1.2 Renormalization 27

1.2.1 Loop Integrals 27

1.2.2 UV Divergence Renormalization 31

1.2.3 Tadpole Renormalization 37

1.3 IR Divergences 41

1.4 The Renormalization Group 41

1.4.1 Running Gauge Couplings 42

1.4.2 Running Fermion Masses 44

1.4.3 Observable Invariance 45

1.5 Gauge Fixing and Ghosts 46

1.5.1 Gauge Fixing 46

1.5.2 The Ghost Lagrangian 48

2 Effective Field Theories **51**

2.1 Effective Field Theories 51

2.1.1 Introduction to Effective Field Theories 51

2.1.2 Operator Running and Mixing 55

2.1.3 Minimal Flavor Violation 56

2.2 The Standard Model Effective Field Theory 57

2.2.1 Introduction to the SMEFT 57

2.2.2 Minimal Flavor Violation in the SMEFT 60

2.3 The SMEFT in the Mass Basis 61

2.3.1 The Higgs Doublet, Vacuum Expectation Value, and Mass . 62

2.3.2 Gauge Fields 63

2.3.3 Yukawa sector 66

II Higgs Decay to Fermion Pairs at NLO in the SMEFT 69

3 Preliminaries **71**

3.1 Motivation 71

3.2 Input Scheme 74

3.3 Lagrangian Implementation 77

3.4 Wilson Coefficient Notation 79

3.5 MFV and the Small-Mass Limit 82

3.6 Gauge Fixing in the Dimension-6 SMEFT 85

4 $h \to f\bar{f}$ at NLO in the SMEFT **91**

4.1 Outline of the Calculation 91

4.2 LO Calculation 94

4.3 NLO Calculation 96

4.3.1 Diagonal CKM Approximation 96

4.3.2 The One-Loop Counterterm 99

4.3.3 Electric Charge Renormalization 102

4.3.4 Higgs-Z Mixing 103

4.3.5 Tadpoles . . . 105
4.3.6 The NLO Decay Rate . . . 109
4.4 Select Analytic Results . . . 110
4.4.1 QED-QCD Results and IR Renormalization . . . 110
4.4.2 Large-m_t Results and Input Scheme Revisited . . . 114
4.4.3 Four-Fermion Results . . . 118
4.5 Enhanced NLO Corrections and Decoupling Relations . . . 121
4.5.1 Structure of the NLO Decay Rate . . . 122
4.5.2 Decoupling Relations . . . 126
4.6 Numerical Results . . . 131
4.6.1 Results at $\mu = m_H$ . . . 132
4.6.2 Scale Uncertainties . . . 139
4.7 Ratios of Decay Rates . . . 146

5 Conclusions **153**

A Dimension-6 SMEFT Operators in the Warsaw Basis **157**

B Phase Space Integrals **159**
B.1 2-Body Phase Space . . . 159
B.2 3-Body Phase Space . . . 161
B.2.1 General Phase Space Calculation . . . 161
B.2.2 Phase Space Slicing . . . 164

C Feynman Diagram Subsets **167**
C.1 QED-QCD Diagrams . . . 167
C.2 Large m_t-Limit Diagrams . . . 170

D Numerical Results for $h \to \mu\bar{\mu}$ **173**
D.1 Results at $\mu = m_H$ . . . 173
D.2 Scale Uncertainties . . . 174

E Select Full Mass Dependent Results **175**

E.1 QED-QCD 175

E.2 Four-Fermion Results 177

F Decoupling Constants **181**

Bibliography **187**

Declaration

The work in this thesis is based on research carried out in the Institute for Particle Physics Phenomenology at Durham University. No part of this thesis has been submitted elsewhere for any degree or qualification. This thesis is partly based on joint research as noted below.

- Part II of this work is based on the articles "*NLO corrections to $h \to b\bar{b}$ decay in SMEFT*" [1] and "*Higgs decay to fermion pairs at NLO in SMEFT*" [2], both of which are published in The Journal of High Energy Physics (JHEP).

Acknowledgements

First and foremost, I thank my supervisor Ben Pecjak. Ben's outstanding guidance, patience, and generosity with his time has been invaluable for shaping this work, which would not have been possible without him.

During the past four years I have had the privilege of meeting a great number of wonderful people, both in and out of the IPPP, whom there are too many to name. In particular, to the members of OC118 both past and present, thank you for making these past four years far more fun than I could have ever imagined a PhD in physics could be! I must give a special thanks to those that "volunteered" to proofread parts of this thesis (in order of appearance): Lucy, Elliott, Joey, Andrew, and Darren. Additionally, I thank Darren and Tom, for your discussions and assistance in the early days. Outside the IPPP, I also thank Dom, for making sure life never got boring.

To Rose, thank you for your ceaseless positivity, encouragement, and for the adventures reminding me that there's a world outside of physics.

Finally, I thank my family. Without their endless support (and tolerance for unanswered messages) none of this would have been possible.

Part I

Introduction

Chapter 1

The Standard Model

In this chapter we introduce the *Standard Model* (SM) of particle physics. Although this is a rich theory with a vast number of interesting aspects and nuances, in this chapter we only review the features of the SM which are essential for the understanding of the processes considered in Part II of this work. In particular, in Section 1.1 we introduce the SM and consider the constituents and dynamics of each term in detail. In Section 1.2 we describe *renormalization*, the necessary framework for obtaining UV-finite, analytic results at *next-to-leading order* (NLO) in perturbation theory, while in Section 1.3 we describe the treatment of *infrared* (IR) divergences. In Section 1.4 we consider the *renormalization group* (RG) - a consequence of considering perturbation theory at NLO. Finally we conclude with a discussion of gauge fixing in Section 1.5.

1.1 Introduction to the Standard Model

A quantum field theory (QFT) is a framework in which we are able to unify the laws of quantum mechanics (QM) and special relativity (SR), in which the particles present in QM manifest as excitations of quantum fields. The SM is an example of a QFT which is specifically constructed to describe the properties and interactions of the currently observed fundamental particles and the fundamental forces, except for gravity. Its development has a long history arguably beginning in the 1920s with the initial formulations of *Quantum Electrodynamics* (QED) to describe the interactions of photons and matter, and concluding in the 1970s with the developments of *Quantum Chromodynamics* (QCD) as a description of the strong force [3–14]. Numerous texts are also dedicated to the study of the SM [15–20]. The properties and interactions of the SM are encoded in the *Lagrangian density* of the SM. As is typically the case, we drop the term Lagrangian density and use it interchangeably

u	c	t	γ	h
d	s	b	g	
ν_e	ν_μ	ν_τ	W	
e	μ	τ	Z	

Table 1.1: *The particle content of the SM. The first three columns are the matter content of the SM, specifically comprising of the fermions, with the top two rows containing the quark content of the SM and the bottom two rows containing the leptons of the SM. The fourth column comprises the force mediating gauge bosons of the SM. Finally, the fifth column contains only the Higgs boson. Each electrically charged particle also has a corresponding anti-particle, each (anti-) quark has three (anti-)colors, and there are eight distinct gluons.*

with simply *Lagrangian* throughout the rest of this work. Despite the complexity and numerousness of the properties and interactions of the SM, the SM Lagrangian can be written in a compact form as

$$\begin{aligned}\mathcal{L}_{\text{SM}} = &-\frac{1}{4}F^{\mu\nu}F_{\mu\nu} \\ &+ |D_\mu H|^2 - V(H) \\ &- Y_{ij}\bar{\Psi}_i H \Psi_j + \text{h.c.} \\ &+ i\bar{\Psi}\not{D}\Psi\,. \end{aligned} \tag{1.1.1}$$

We shall explore each line of Eq. 1.1.1 in close detail in Sections 1.1.1 to 1.1.3. The particle content of the SM is summarized in Table 1.1. The SM is a *gauge theory* – specifically it exhibits a local gauge symmetry under the group

$$SU(3)_c \times SU(2)_L \times U(1)_Y\,, \tag{1.1.2}$$

with the subscripts c, L and Y referring to the charges *color*, *left* and *hypercharge* respectively.[1] All fields of the SM thus transform under this symmetry group and leave the SM Lagrangian in Eq. 1.1.1 invariant. The covariant derivative, D_μ, in Eq. 1.1.1 preserves this local gauge invariance[2] and is given by

$$D_\mu = \partial_\mu - ig_1 Y B_\mu - ig_2 \tau^I W_\mu^I - ig_3 T^A G_\mu^A\,, \tag{1.1.3}$$

where g_1, g_2, g_3 are *coupling constants*, Y, τ^a, T^A are the *generators* and B_μ, W_μ^I, G_μ^A are the *gauge fields* of the gauge groups $U(1)$, $SU(2)$ and $SU(3)$ respectively.

[1] Generally throughout the rest of this work, we will drop the subscripts on these gauge groups.

[2] Formally, the gauge group of the SM is a *Lie group* and thus is a manifold such that the non-derivative terms of Eq. 1.1.3 are a connection on that manifold.

Individually, we find that the generators of the groups $SU(2)$ and $SU(3)$ are non-commuting and form a *Lie algebra* defined by

$$[t^a, t^b] = if^{abc}t^c\,, \tag{1.1.4}$$

for some generator t, where the f^{abc} are known as *structure constants*. This feature leads to the non-commutability of gauge-transformation operations for the $SU(2)$ and $SU(3)$ symmetries, and the associated gauge theories are *non-abelian*. The commutability of gauge transformation operations for $U(1)$ lead to an *abelian* gauge theory. Further, we find that invariance under the gauge group $SU(3)$ leads to a description of the *strong force* in QCD, while the $SU(2) \times U(1)$ gauge group unifies the weak and electromagnetic forces as electroweak (EW) theory.

1.1.1 The Gauge Lagrangian

The first line of Eq. 1.1.1 is known as the *gauge part* of the SM Lagrangian owing to it being purely a function of gauge fields. It describes the dynamics and self-interactions of the fields and corresponding gauge bosons of the strong and electroweak forces. The gauge part of the SM Lagrangian is understood as a sum of three such terms, built from *field strength tensors*, with one for each gauge group of the SM

$$\mathcal{L}_{\text{gauge}} = -\frac{1}{4}F^{\mu\nu}F_{\mu\nu} = -\frac{1}{4}B^{\mu\nu}B_{\mu\nu} - \frac{1}{4}W^I_{\mu\nu}W^{I,\mu\nu} - \frac{1}{4}G^A_{\mu\nu}G^{A,\mu\nu}\,. \tag{1.1.5}$$

The field strength tensors for each gauge group are given by

$$\begin{aligned} B_{\mu\nu} &= \partial_\mu B_\nu - \partial_\nu B_\mu\,, \\ W^I_{\mu\nu} &= \partial_\mu W^I_\nu - \partial_\nu W^I_\mu + g_2\epsilon^{IJK}W^J_\mu W^K_\nu\,, \\ G^A_{\mu\nu} &= \partial_\mu G^A_\nu - \partial_\nu G^A_\mu + g_3 f^{ABC}G^B_\mu G^C_\nu\,, \end{aligned} \tag{1.1.6}$$

where, as mentioned in Section 1.1, B_μ, W^I_μ and G^A_μ are the gauge fields of $U(1)$, $SU(2)$ and $SU(3)$ respectively and take the form of spin-1 Lorentz 4-vectors. As the indices, i, for the gauge group $SU(N)$ may take values $i = 1, ..., N^2 - 1$ we see that this corresponds to three bosons associated with the gauge group $SU(2)$ and eight bosons associated with the gauge group $SU(3)$. In the case of $SU(3)$, these gauge bosons are the *gluons* of QCD. For all three symmetry groups of the SM, the Lagrangian generates terms of the form

$$\mathcal{L}_{\text{gauge}} \supset -\frac{1}{2}\partial_\mu F_\nu \partial^\nu F^\mu\,, \tag{1.1.7}$$

for some gauge field F. This term is the *kinetic term* and describes the propagation of the gauge field. We see that it also carries a prefactor of $\frac{1}{2}$, a convention known

as *canonical normalization*. Canonical normalization is only a convention, and while other choices of normalization would describe the same physics, canonical normalization is a convenient choice as it ensures that the residue of the corresponding propagator is i. Under infinitesimal gauge transformations the gauge fields of the standard model transform as

$$\begin{aligned} B_\mu &\to B_\mu - \frac{1}{g_1}\partial_\mu \alpha\,, \\ W_\mu^I &\to W_\mu^I - \frac{1}{g_2}\partial_\mu \alpha^I + f^{IJK}\alpha^J W_\mu^K\,, \\ G_\mu^A &\to G_\mu^A - \frac{1}{g_3}\partial_\mu \alpha^A + f^{ABC}\alpha^B G_\mu^C\,, \end{aligned} \tag{1.1.8}$$

where α is a continuous parameter characterizing the gauge transformation, and where f^{IJK} and f^{ABC} are the structure constants of $SU(2)$ and $SU(3)$ respectively.

For the abelian gauge field B_μ this concludes the gauge part of the Lagrangian, however, for the fields $W_{\mu\nu}^I$ and $G_{\mu\nu}^A$ we find that the gauge bosons also have self-interactions – a unique feature of non-abelian gauge theories. These self-interactions are a result of the non-derivative terms in Eq. 1.1.6, which exist to preserve the gauge symmetry of the non-abelian symmetry groups of the SM.

1.1.2 The Higgs Lagrangian

Line 2 of Eq. 1.1.1 is known as the *Higgs part* of the SM Lagrangian and it summarizes the kinetic terms of the Higgs boson, the interactions of the Higgs with the gauge bosons, and self interactions. It also provides a mechanism for generating gauge boson and chiral fermion masses via a process known as *spontaneous symmetry breaking* (SSB) [8–10].

A symmetry is said to be spontaneously broken when the Lagrangian of the theory possesses some symmetry which is absent in the ground state. The purpose of the introduction of the Higgs sector in the SM is to spontaneously break the $SU(2)\times U(1)$ gauge symmetry of the SM, allowing for the generation of gauge boson and chiral fermion masses, a feature that is not possible in a gauge-invariant theory without SSB. In Eq. 1.1.3 we refrained from specifying the form of the generators for each

Field	$SU(3)$	$SU(2)$	$U(1)$
H	**1**	**2**	$\frac{1}{2}$

Table 1.2: *Representation of the groups under which the Higgs doublet H transforms. Here, **1** represents the trivial representation.*

of the gauge groups; this was because each field of the SM transforms in different representations of each gauge group. We summarize the group representation which the Higgs field transforms under in Table 1.2, where $\mathbf{N} \neq \mathbf{1}$ represents the fundamental representation of an $SU(N)$ group. We find that the Higgs sector consists of an $SU(2)$ doublet of complex, spin-0 scalars

$$H = \begin{pmatrix} -i\phi^+ \\ \chi \end{pmatrix} . \tag{1.1.9}$$

To see how the generation of masses by SSB is achieved we consider the *Higgs potential*, $V(H)$, in Eq. 1.1.1

$$V(H) = \lambda(H^\dagger H)^2 - \mu^2 H^\dagger H + \frac{\mu^4}{4\lambda} , \tag{1.1.10}$$

where both λ and μ are chosen to be positive such that the minima of this potential occurs for a non-vanishing value of the Higgs doublet. Note that the constant term in Eq. 1.1.10 does not in any way change the dynamics of the Higgs doublet, and is simply included as a convenience such that the minima of the potential is at $V = 0$ after SSB. The minima of this potential is found at a non-zero value of the Higgs field, H_0, where H_0 satisfies

$$H_0^\dagger H_0 = \frac{v_0^2}{2} , \tag{1.1.11}$$

where

$$v_0 = \sqrt{\frac{\mu^2}{\lambda}} . \tag{1.1.12}$$

The quantity v_0 in Eqs. 1.1.11 and 1.1.12 is known as the *vacuum expectation value* (vev). For reasons we will explore in Section 1.2.3, we refer to this vev as the *classical Higgs vev*, or *leading order* (LO) vev. The condition in Eq. 1.1.11 represents a continuum of possible minima defining an S^3 surface. As a result of invariance under $SU(2)$ rotations we are free to choose that the minima occurs at

$$H_0 = \frac{1}{\sqrt{2}} \begin{pmatrix} 0 \\ v_0 \end{pmatrix} . \tag{1.1.13}$$

Considering small perturbations about this minima we may write the Higgs doublet as

$$H = \frac{1}{\sqrt{2}} \begin{pmatrix} -\sqrt{2}i\phi^+ \\ v_0 + h + i\phi^0 \end{pmatrix} , \tag{1.1.14}$$

where h and ϕ^0 are scalar fields representing the real and imaginary components

of χ in Eq. 1.1.9 respectively. It is the h field that we interpret to be the physical *Higgs boson*,[1] while ϕ^0 and $\phi^\pm$ are the *Goldstone bosons*. Using the form of the potential in Eq. 1.1.10 we find that the Higgs is the only massive particle in this doublet, with the Goldstone bosons being massless, as is guaranteed by Goldstone's theorem [21, 22]. Using the expression in Eq. 1.1.12 we also find that we may write the mass of the Higgs as

$$m_H^2 = 2\lambda v_0^2 \,. \tag{1.1.15}$$

We can interpret this result in terms of the form of the Higgs potential in Eq. 1.1.10 as the Higgs mass being generated by the small radial perturbations about an approximately quadratic potential, and the Goldstone bosons being perturbations in the flat direction of the potential, orthogonal to the radial perturbations.

Another result of the Higgs Lagrangian's gauge invariance is that we are able to "rotate" the Higgs doublet in Eq. 1.1.14 until it takes the form

$$H = \frac{1}{\sqrt{2}} \begin{pmatrix} 0 \\ v_0 + h \end{pmatrix} \,. \tag{1.1.16}$$

Doing so constitutes a gauge choice, in this case the *unitary gauge*, which we will explore in more detail in Section 1.5. In this gauge we have removed the Goldstone bosons, emphasizing their non-physical nature.

The vev of the Higgs doublet in Eqs. 1.1.14 and 1.1.16 breaks the $SU(2)_L \times U(1)_Y$ symmetry present in the SM Lagrangian to $U(1)_{\text{EM}}$, where the subscript EM refers to the residual symmetry of the electromagnetic interaction. As this pattern of symmetry breaking (known as *electroweak symmetry breaking* (EWSB)) transitions from four generators to one generator, we have three generators of broken symmetry groups (which we call *broken generators*) and one generator of an unbroken symmetry group (which we call *unbroken generators*). As we shall soon see, this pattern of breaking of the generators results in the expectation of the theory containing three massive and one massless gauge boson after SSB.

To see how mass is generated for the gauge bosons we consider the $|D_\mu H|^2$ term in Eq. 1.1.1. A powerful notation which we will occasionally adopt throughout this thesis is to write the $SU(2) \times U(1)$ covariant derivative as

$$D_\mu = \partial_\mu - i(g\tau)^a A_\mu^a \,, \tag{1.1.17}$$

[1] For the remainder of this thesis we will refer to the physical Higgs boson simply as the Higgs boson or the Higgs, and the doublet in Eq. 1.1.14 as the Higgs doublet.

where

$$(g\tau)^a = \begin{pmatrix} g_2\tau^1 \\ g_2\tau^2 \\ g_2\tau^3 \\ g_1 Y \end{pmatrix}, \quad A^a_\mu = \begin{pmatrix} W^1_\mu \\ W^2_\mu \\ W^3_\mu \\ B_\mu \end{pmatrix}, \tag{1.1.18}$$

such that the terms quadratic in the gauge boson fields from $|D_\mu H|^2$ are now given by

$$|D_\mu H|^2 \supset \frac{1}{2}(g\tau)^a \phi_0 (g\tau)^b \phi_0 A^a_\mu A^{b,\mu}\,, \tag{1.1.19}$$

where $\phi_0 = (0, v_0/\sqrt{2})$ is the vacuum state of the Higgs doublet. We also see that Eq. 1.1.19 gives us the form of a mass matrix for the gauge bosons

$$(m^2_A)^{ab} = (g\tau)^a \phi_0 (g\tau)^b \phi_0\,. \tag{1.1.20}$$

The form of Eq. 1.1.20 also makes it clear why broken generators produce massive gauge bosons, while unbroken generators produce massless gauge bosons: unbroken generators acting on the vacuum are vanishing, producing a vanishing element of the mass matrix, while broken generators acting on the vacuum are not, producing non-vanishing elements of the mass matrix in Eq. 1.1.20.

We may consider the explicit form of the terms quadratic in the gauge boson fields from Eq. 1.1.19 by making a choice of $SU(2) \times U(1)$ generators. From Table 1.2 we see that an appropriate choice is to use $Y = \frac{1}{2}$ and $\tau^a = \frac{1}{2}\sigma^a$ where σ^a are the Pauli matrices. Keeping terms which are quadratic in the gauge boson fields we find

$$|D_\mu H|^2 \supset g_2^2 \frac{v_0^2}{8}\left[(W^1_\mu)^2 + (W^2_\mu)^2 + \left(\frac{g_1}{g_2}B_\mu - W^3_\mu\right)^2\right]. \tag{1.1.21}$$

Here we see that the W^1_μ and W^2_μ fields are already mass-diagonal, however, the B_μ and W^3_μ fields are not. From Eq. 1.1.21 we also see the requirement of a non-vanishing vev for the generation of gauge boson masses. To diagonalize these terms we rotate these fields according to

$$\begin{pmatrix} W^3_\mu \\ B_\mu \end{pmatrix} = \begin{pmatrix} \cos(\theta_w) & \sin(\theta_w) \\ -\sin(\theta_w) & \cos(\theta_w) \end{pmatrix} \begin{pmatrix} Z_\mu \\ A_\mu \end{pmatrix}, \tag{1.1.22}$$

where θ_w is the *weak mixing angle*,[1] and Z_μ and A_μ are the physical Z-boson and

[1] In the remainder of this thesis we will use the abbreviations $\cos(\theta_w) = c_w$ and $\sin(\theta_w) = s_w$.

photon respectively. Specifically, the weak mixing angle is found to be

$$\tan(\theta_w) = \frac{g_1}{g_2}\,. \tag{1.1.23}$$

Further, to match the experimentally observed electric charges of the remaining two bosons (± 1) we recognize that the physically observed W bosons are a linear combination of the W^1_μ and W^2_μ fields

$$\begin{pmatrix} W^1_\mu \\ W^2_\mu \end{pmatrix} = \frac{1}{\sqrt{2}} \begin{pmatrix} 1 & 1 \\ i & -i \end{pmatrix} \begin{pmatrix} W^+_\mu \\ W^-_\mu \end{pmatrix}\,. \tag{1.1.24}$$

In total, we find that the mass spectrum for the gauge bosons is

$$M_W = \frac{g_2 v_0}{2}\,, \quad M_Z = \frac{g_2 v_0}{2c_w}\,, \quad M_A = 0\,. \tag{1.1.25}$$

These rotations and scalings from the weak basis gauge boson fields to the mass basis can be summarized as

$$\hat{A}^a_\mu = \hat{R}^{ab} A^b_\mu\,, \tag{1.1.26}$$

where A_μ is given in Eq. 1.1.18 and

$$\hat{R}^{ab} = \begin{pmatrix} \frac{1}{\sqrt{2}} & \frac{1}{\sqrt{2}} & 0 & 0 \\ \frac{i}{\sqrt{2}} & \frac{-i}{\sqrt{2}} & 0 & 0 \\ 0 & 0 & c_w & s_w \\ 0 & 0 & -s_w & c_w \end{pmatrix}\,, \quad \hat{A}^a_\mu = \begin{pmatrix} W^+_\mu \\ W^-_\mu \\ Z_\mu \\ A_\mu \end{pmatrix}\,, \tag{1.1.27}$$

such that $\hat{A}^a_\mu$ contains the gauge fields in the mass basis. We also find that the mass matrix, (m^2_A), in Eq. 1.1.20 is now diagonalized by

$$(m^2_{D,A})_{ab} = (\hat{R}^{-1})_{ac} (m^2_A)_{cd} (\hat{R}^{-1})_{db}\,, \tag{1.1.28}$$

where $(m^2_{D,A})_{ab} = \mathrm{diag}(M_W, M_W, M_Z, 0)$ is the diagonalized gauge boson mass matrix.

Returning to our explicit notation, we find that the electroweak covariant derivative may be written

$$\begin{aligned} D_\mu = \partial_\mu - ieQ_f A_\mu - i\frac{e}{c_w s_w}(\tau^3 - s^2_w Q_f) Z_\mu \\ - i\frac{e}{s_w}(\tau^+ W^+_\mu + \tau^- W^-_\mu)\,, \end{aligned} \tag{1.1.29}$$

where $Q_f = \tau^3 + Y$, $\tau^\pm = (\tau^1 \pm i\tau^2)/\sqrt{2}$ and e is the electric charge.

With some manipulations we can also recover some useful relations between the

electric charge, the vev, the weak mixing angle, and the gauge boson masses

$$\begin{aligned} c_w &= \frac{M_W}{M_Z}\,, & g_1 &= \frac{e}{c_w}\,, \\ v_0 &= \frac{2M_W s_w}{e}\,, & g_2 &= \frac{e}{s_w}\,, \\ e &= \frac{g_1 g_2}{\sqrt{g_1^2 + g_2^2}}\,. \end{aligned} \tag{1.1.30}$$

1.1.3 The Fermion Lagrangian

We now consider the final two lines of Eq. 1.1.1, which describe the dynamics of fermions and their interactions with the bosons of the SM. Fermions can be classified into two distinct categories, quarks and leptons depending on their charges under the SM symmetry group. The most important of these distinctions is that leptons transform in the trivial representation of $SU(3)$, while quarks transform in the fundamental representation of $SU(3)$, the result of which is that leptons have no coupling to gluons. A summary of the charges of the fermions under each gauge group is given in Table 1.3. Each fermion can be described by a four-component spin-$\frac{1}{2}$ *spinor*, which gives rise to fermionic statistics, although for the purposes of this thesis we can consider these spinors as a whole rather than concern ourselves with each component of a particular spinor.

Under $SU(3)$ the quarks of the SM are arranged in triplets, such that for some generic quark, q

$$q = \begin{pmatrix} q^r \\ q^b \\ q^g \end{pmatrix}\,, \tag{1.1.31}$$

where r, b, g represent the three "colors" of QCD: red, blue and green respectively.

Field	$SU(3)_c$	$SU(2)_L$	$U(1)_Y$
l_L	**1**	**2**	$-\frac{1}{2}$
e_R	**1**	**1**	-1
q_L	**3**	**2**	$\frac{1}{6}$
u_R	**3**	**1**	$\frac{2}{3}$
d_R	**3**	**1**	$-\frac{1}{3}$

Table 1.3: *Representation of the groups under which the fermionic field content of the SM transforms. Again, here* $\mathbf{N} \neq \mathbf{1}$ *denotes the fundamental representation of the group* $SU(N)$.

The chiral nature of the SM is apparent due to the different representations under which the *left-* and *right-handed* components of the fermion fields transform. We can project the handedness of a field, ψ, using the projection operators, $P_{L,R}$ as

$$\psi_{L,R} = P_{L,R}\psi\,, \quad P_L = \frac{1}{2}\left(1-\gamma_5\right)\,, \quad P_R = \frac{1}{2}\left(1+\gamma_5\right)\,. \tag{1.1.32}$$

In the SM the left-handed fermionic fields are arranged in an $SU(2)$ doublet, with one doublet for each of the three fermion generations of the SM. These doublets are denoted l_L and q_L[1] for the left-handed lepton and quark fields respectively, and explicitly are

$$l_L^i = \begin{pmatrix} e_L^i \\ \nu_{eL}^i \end{pmatrix}\,, \quad q_L^i = \begin{pmatrix} u_L^i \\ d_L^i \end{pmatrix}\,, \tag{1.1.33}$$

where the index $i = 1,\, 2,\, 3$ denotes the generation, and each of the components is a left-handed projection of the corresponding field.

The problem of writing an explicit mass term in the SM Lagrangian is now apparent: the chiral nature of fermions leads to two distinct particles of different handedness, meaning an explicit mass term must be written as $\sim -m\bar{\psi}\psi = -m\bar{\psi}_L\psi_R - m\bar{\psi}_R\psi_L$, which breaks gauge symmetry. Clearly, we must use the SSB properties of the Higgs field to ensure this symmetry is preserved before SSB, but have a mechanism to generate masses after SSB.

The generation of fermion masses comes from the third line of Eq. 1.1.1, known as the *Yukawa* interactions. This part of the Lagrangian can be written in full as

$$\mathcal{L}_{\text{yuk.}} = -[Y_e]_{ij}\bar{l}^i H e^j - [Y_u]_{ij}\bar{q}^i \tilde{H} u^j - [Y_d]_{ij}\bar{q}^i H d^j + \text{h.c.}\,, \tag{1.1.34}$$

where h.c. represents the hermitian conjugate of the terms already present, $\tilde{H}^i = \epsilon_{ij}(H^j)^*$ where ϵ_{ij} is the two-dimensional antisymmetric Levi-Civita tensor (defined such that $\epsilon_{12} = +1$), and Y_f is the *Yukawa matrix* for fermions of flavor f. As we can see, the Yukawa matrix defines the coupling between the various components of the Higgs and fermionic fields. Importantly, Eq. 1.1.34 is invariant under the unbroken symmetry group of the SM.

We now consider Eq. 1.1.34 in the broken phase of the theory, i.e. when the Higgs doublet takes the form of that seen in Eq. 1.1.14. Substituting the form of the Higgs doublet in Eq. 1.1.14 into Eq. 1.1.34 and looking only at terms linear in the Higgs

[1] These are often simply abbreviated to l and q with the handedness implicitly assumed. We will also often suppress the R subscript on right-handed fermions. Throughout this work, fermion singlets should be assumed to be right-handed, unless an L or R subscript denotes otherwise.

and vev we find

$$\begin{aligned}\mathcal{L}_{\text{yuk.}} \supset & -\frac{1}{\sqrt{2}}(v_0+h)[Y_e]_{ij}\bar{e}_L^i e_R^j - \frac{1}{\sqrt{2}}(v_0+h)[Y_u]_{ij}\bar{u}_L^i u_R^j \\ & -\frac{1}{\sqrt{2}}(v_0+h)[Y_d]_{ij}\bar{d}_L^i d_R^j + \text{h.c.}\,. \end{aligned} \tag{1.1.35}$$

This equation describes the coupling between the Higgs and the fermionic fields of the SM, as well as the mass terms of the SM fermions. We note here that the lack of a leptonic term involving $\tilde{H}$ in Eq. 1.1.34 prevents the generation of neutrino masses. Massless neutrinos are a feature of the SM, although this is in contention with the experimentally measured non-zero neutrino masses. We have no way of knowing a priori what form the Yukawa matrices may take, or any general properties which they might have, however, assuming only that the Yukawa matrices are diagonalizable[1] we know from the fundamentals of linear algebra that they may be diagonalized by two unitary matrices, S and K. We therefore diagonalize the Yukawa matrices according to

$$\begin{aligned} M_e &\equiv S_e^\dagger Y_e K_e = \text{diag}(y_e,\, y_\mu,\, y_\tau)\,, \\ M_u &\equiv S_u^\dagger Y_u K_u = \text{diag}(y_u,\, y_c,\, y_t)\,, \\ M_d &\equiv S_d^\dagger Y_d K_d = \text{diag}(y_d,\, y_s,\, y_b)\,, \end{aligned} \tag{1.1.36}$$

where the form of the y_f are yet to be determined. To bring the fermions into the mass basis, we must correspondingly transform the fermion fields according to

$$\begin{aligned} &e_L \to S_e e_L\,, \qquad u_L \to S_u u_L\,, \qquad d_L \to S_d d_L\,, \\ &e_R \to K_e e_R\,, \qquad u_R \to K_u u_R\,, \qquad d_R \to K_d d_R\,. \end{aligned} \tag{1.1.37}$$

From the above notation we see that the matrices S_i act on left-handed fermion fields and K_i act on right-handed fermion fields. We now find that in the mass basis Eq. 1.1.35 takes the form

$$\begin{aligned}\mathcal{L}_{\text{yuk.}} \supset & -[m_e]_{ij}\bar{e}_L^i e_R^j - [m_u]_{ij}\bar{u}_L^i u_R^j - [m_d]_{ij}\bar{d}_L^i d_R^j \\ & -[m_e]_{ij}\frac{h}{v_0}\bar{e}_L^i e_R^j - [m_u]_{ij}\frac{h}{v_0}\bar{u}_L^i u_R^j - [m_d]_{ij}\frac{h}{v_0}\bar{d}_L^i d_R^j + \text{h.c.}\,, \end{aligned} \tag{1.1.38}$$

where

$$\begin{aligned} [m_e]_{ij} &= \frac{v_0}{\sqrt{2}}[M_e]_{ij} = \text{diag}(m_e,\, m_\mu,\, m_\tau)\,, \\ [m_u]_{ij} &= \frac{v_0}{\sqrt{2}}[M_u]_{ij} = \text{diag}(m_u,\, m_c,\, m_t)\,, \\ [m_d]_{ij} &= \frac{v_0}{\sqrt{2}}[M_d]_{ij} = \text{diag}(m_d,\, m_s,\, m_b)\,, \end{aligned} \tag{1.1.39}$$

[1] The diagonalizability of the Yukawa matrices is a reasonable assumption due to the experimentally measured non-zero masses of the SM fermions [23].

such that we now see that the y_f of Eq. 1.1.36 take the form $y_f = \sqrt{2}m_f/v_0$. Again, we see the importance of the non-vanishing vev for the generation of fermion masses. We also note from the bottom line of Eq. 1.1.38 that the coupling of the Higgs to SM fermions is proportional to the fermion mass.

Lastly, we consider the final line of Eq. 1.1.1. This term describes the dynamics and interactions between the SM fermions and the gauge bosons. Here we will specifically consider the interactions of the W bosons and the left-handed quarks[1] which is given by

$$\mathcal{L}_{\text{fer.}} \supset \frac{e}{\sqrt{2}s_w}\left(\bar{u}_L^i \gamma^\mu W_\mu^+ d_L^i + \bar{d}_L^i \gamma^\mu W_\mu^- u_L^i\right) . \tag{1.1.40}$$

We note that the quark fields in Eq. 1.1.40 are in the weak basis, and so we must transform this equation to the mass basis using the transformations listed in Eq. 1.1.37 in order to understand the physical behavior of this component of the Lagrangian. Performing this transformation brings the terms in Eq. 1.1.40 into the form

$$\mathcal{L}_{\text{fer.}} \supset \frac{e}{\sqrt{2}s_w}\left([S_u^\dagger]_{ik}[S_d]_{kj}\bar{u}_L^i \gamma^\mu W_\mu^+ d_L^j + [S_d^\dagger]_{ik}[S_u]_{kj}\bar{d}_L^i \gamma^\mu W_\mu^- u_L^j\right) , \tag{1.1.41}$$

where the fermions are now in the mass basis. We also find the emergence of a combination of the unitary matrices S_u and S_d, which we denote as

$$V \equiv S_u^\dagger S_d = \begin{pmatrix} V_{ud} & V_{us} & V_{ub} \\ V_{cd} & V_{cs} & V_{cb} \\ V_{td} & V_{ts} & V_{tb} \end{pmatrix} , \tag{1.1.42}$$

and is known as the *Cabibbo-Kobayashi-Maskawa* (CKM) matrix [25, 26]. While all other interactions between fermions in the SM occur between fermions of the same type and generation, the CKM matrix is the only source of interactions between fermions of different generations and different flavors, so called *flavor violating* interactions in the SM. While the components of the CKM matrix must be measured experimentally we can use the fact that both S_u and S_d are unitary to infer that V too must be unitary and use residual symmetries of the SM to reduce the free parameters of the CKM matrix to three angles and one phase. The experimental measurements of these free parameters allows us to drop the numerically less significant components of the CKM matrix and approximately write it in terms of a single parameter, λ,

[1] In the SM (and verified by experiments) the W bosons only couple to left-handed fermions [24].

known as the *Wolfenstein parameterization* [27]

$$|V| \approx \begin{pmatrix} 1-\frac{\lambda^2}{2} & \lambda & \lambda^3 \\ -\lambda & 1-\frac{\lambda^2}{2} & \lambda^2 \\ \lambda^3 & \lambda^2 & 1 \end{pmatrix}, \tag{1.1.43}$$

where experimentally we find $\lambda \simeq 0.22$ [23].

1.2 Renormalization

While calculating beyond LO in QFT is desirable for the purposes of increasing the precision of predictions within a theory, an additional complication that often arises when performing calculations beyond LO is the emergence of loop diagrams. These loops are often formally divergent, with the divergences classified as either *ultraviolet* (UV) or *infrared* (IR) divergent. Naïvely, these divergences often lead to infinities when calculating observables in perturbation theory. There are various methods available to treat these divergences. The methods of removing the UV divergences from a theory are discussed throughout this section, with these techniques known as *renormalization*. The removal of IR divergences are instead discussed in Section 1.3.

Throughout this section we explore how these UV divergences are dealt with at NLO. In Section 1.2.1 we explore how these divergences emerge in loop integrals, and how they may be regularized. In Section 1.2.2 we discuss how we may remove UV divergences by refining our interpretation of parameters appearing the the Lagrangian of a theory. Finally, in Section 1.2.3 we present a consistent manner for renormalizing the tadpoles that may emerge in a theory.

1.2.1 Loop Integrals

A common object to emerge from perturbation theory in QFTs is the *loop integral*. A loop integral occurs in Feynman diagrams that feature a closed loop, and thus have some unspecified momenta running through the loop, which we must integrate over all possible values. Multiple loops may appear in a single diagram, where a diagram containing N loop(s) is described as an N-loop diagram. In some commonly studied processes, such as flavor changing neutral currents, loops first emerge at LO in perturbation theory, however, in most cases and in the processes studied in this work loops first emerge at NLO and so we often use the terms one-loop and NLO interchangeably

One-loop diagrams can be entirely classified by the number of propagators in the loop. We describe integrals with one propagator to be A-integrals, integrals with

two propagators to be B-integrals, etc. Generally, we may write a loop integral with N internal propagators as

$$\int \frac{d^4k}{(2\pi)^4} \frac{k_{\mu_1}..k_{\mu_P}}{D_0 D_1 ... D_{N-1}}\,, \tag{1.2.1}$$

where

$$D_0 = k^2 - m_0^2 + i\varepsilon\,, \qquad D_i = (k+p_i)^2 - m_i^2 + i\varepsilon\,, \qquad i = 1, ..., N-1\,, \tag{1.2.2}$$

and p_i are the external momenta. We first consider the emergence of UV divergences. For an integral with P powers of momenta in the numerator evaluated in d-dimensions, a diagram is UV divergent if $P + d - 2N \geq 0$, that is, the integral diverges as the loop momenta variable, k, tends to infinity. We can however regularize this divergence by deforming the number of spacetime dimensions of the theory. Specifically, we may perform the integral in a non-integer number of dimensions, a technique known as *dimensional regularization*. A common choice, and the choice made for UV-divergent integrals throughout this work is $d = 4 - 2\varepsilon$ dimensions, where $\varepsilon > 0$. Dimensional regularization is by no means the only method of regularizing divergent loop integrals; another method is *Pauli-Villars* regularization, where a cut-off is placed on the range of the integration to avoid the divergent region, however, this method of regularization is not employed in this work.[1]

Choosing that our theory is now defined in d dimensions, we additionally find that this has an implication for the mass dimensions of the coupling constants and field content of our theory. Considering, for example, some parameters of the SM we find

$$[\phi] = \frac{d-2}{2}\,, \qquad [\psi] = \frac{d-1}{2}\,, \qquad [A] = \frac{d-2}{2}\,, \qquad [g] = \frac{4-d}{2}\,, \tag{1.2.3}$$

where ϕ, ψ, A, and g represent some scalar field, fermionic field, gauge field, and gauge coupling constant respectively. We also find that masses and partial derivatives retain their mass dimensions of 1. To avoid non-integer dimensional couplings we factor out a parameter μ from the couplings, where $[\mu] = 1$ as

$$g \to \mu^{\frac{4-d}{2}} g\,. \tag{1.2.4}$$

[1] In fact, Pauli-Villars regularization presents several disadvantages as compared to dimensional regularization, the most prominent of which being that it breaks several important symmetries, such as gauge symmetries. Additionally, Pauli-Villars regularization breaks the EFT power-counting, with it being preserved only in renormalized quantities [28]. We can see how the power counting (discussed further in Section 2.1.1) is affected by considering, for example, a quadratically divergent loop diagram with either two dimension-5, or one dimension-6 operator insertions, which would scale as $\sim \Lambda^2/M^2$ for cut-off scale Λ and heavy-EFT scale M. The emergent ratio of $\Lambda/M \sim 1$ thus spoils the EFT power counting at the level of unrenormalized quantities.

Considering the integral in Eq. 1.2.1, we can write this generically in d dimensions as [29]

$$T^N_{\mu_1...\mu_P}(p_1,...,p_{N-1},m_0,...,m_{N-1}) = \frac{(2\pi\mu)^{4-d}}{i\pi^2}\int d^dk \frac{k_{\mu_1}..k_{\mu_P}}{D_0D_1...D_{N-1}}\,, \tag{1.2.5}$$

where we have introduced some constant factors for convenience. The factor of $(2\pi)^{-d}$ comes from the integral measure seen in Eq. 1.2.1, while the remaining factor of $(2\pi)^4/(i\pi^2) = -i16\pi^2$ is introduced by hand to explicitly factor out this term which always arises from such integrals. Finally, the factor of μ^{4-d} is a result of the shifts of the coupling constants seen in Eq. 1.2.4. When calculating a one-loop amplitude in d dimensions, there is always an accompanying factor of μ to the power of any potential function of d that may arise as a result of the shifts in the couplings seen in Eq. 1.2.4. When accompanied by divergent loop integrals, these powers of μ will produce terms proportional to $\ln(\mu)$ when expanded around $\varepsilon = 0$. Although the shifts in Eq. 1.2.4 sometimes result in an amplitude being a function of powers of μ which differ from that seen in Eq. 1.2.5, we always include the factor of μ^{4-d} into the definition of the loop integrals. The reason for this it that this always leads to logarithms of the dimensionless ratio of μ and some function of the scales of the loop integral, as is discussed later in this section. While there may be remaining powers of μ in the one-loop amplitude, these result in logarithms of dimensionful scales which cancel at the level of observables, and are thus typically ignored in intermediate steps [16]. In this way, for one-loop calculations the factors of μ arising due to the shifts in Eq. 1.2.4 are entirely accounted for at the level of the observable by only including them in the form seen in Eq. 1.2.5.

From Eq. 1.2.5 we also now see that $T^1 = A$, $T^2 = B$ etc. using the notation discussed earlier. From the 4-momenta in the numerator of Eq. 1.2.5 we see that, in general, the result of such integrals are tensors. The work of Passarino and Veltman (amongst others) [30–33] shows that by taking advantage of Lorentz covariance we may write the result of any of these tensors as a finite set of scalar integrals multiplying some tensoral quantities built from some combination of the external momenta and the metric. Following the prior naming conventions, these scalar integrals are denoted A_0, B_0, C_0 etc. and any one-loop integral may be written as some combination of these integrals multiplying the aforementioned tensoral structures. While we do not report the generic results for these scalar integrals, they can be found throughout the literature [29, 34], and we later report specific examples of these integrals when necessary.

When employing dimensional regularization to calculate integrals that are UV divergent, we always find that the result of these calculations are a function of the scales

present in the integral, with one term multiplying a function we denote Δ, where

$$\Delta(d) = \frac{2}{4-d} - \gamma_E + \ln(4\pi) + \ln\left(\frac{\mu^2}{f(\{m\})}\right), \tag{1.2.6}$$

such that with the choice of $d = 4 - 2\varepsilon$

$$\Delta(4-2\varepsilon) = \frac{1}{\varepsilon} - \gamma_E + \ln(4\pi) + \ln\left(\frac{\mu^2}{f(\{m\})}\right), \tag{1.2.7}$$

where γ_E is Euler's constant, and $f(\{m\})$ is some function of the scales of the integral. These $f(\{m\})$ may be different for each integral and have the property $[f(\{m\})] = 2$ such that the argument of the log is unitless. The $1/\varepsilon$ part of Eq. 1.2.7 is known as a *UV pole*, and by examining these poles the divergent nature of these integrals in $d = 4$ dimensions (the limit $\varepsilon \to 0$), becomes clear. In this way we see that we have completely separated the UV-divergent part of the integral. Further, from Eq. 1.2.7 we see that the factor of $1/\varepsilon$ always comes accompanied by the constant factors γ_E and $\ln(4\pi)$[1] and so it is common to combine these as a single quantity

$$\frac{1}{\hat{\varepsilon}} \equiv \frac{1}{\varepsilon} - \gamma_E + \ln(4\pi)\,. \tag{1.2.8}$$

Throughout the remainder of this work, when referencing UV-divergences we will use only $\hat{\varepsilon}$, but drop the hat notation.

UV divergences are not the only type of divergences that can occur in loop integrals. In loop integrals arising from Feynman diagrams with the exchange of a massless particle, divergences can sometimes also occur when the loop momenta $k \to 0$. Divergences occurring in this way are IR divergences. Like UV divergences, there are several ways in which to regularize such IR divergences. One common method is to introduce a fictitious mass for the massless particles, however, in this work we choose to again adopt dimensional regularization to explicitly separate out the IR divergent components of such integrals. Unlike for UV divergences however, for IR divergences we find we must instead set the number of spacetime dimensions to $d = 4 + 2\varepsilon$. As with UV divergences, when regularizing IR divergences in this way we again find that the IR divergences manifest as $1/\varepsilon$ poles. These IR poles also come accompanied by the set of constant terms found in Eq. 1.2.8, except in this instance the constant terms have relative minus signs compared to that seen in Eq. 1.2.8, such that IR poles emerging from IR-divergent loop integrals always appear in the combination $1/\varepsilon + \gamma_E - \ln(4\pi)$ [18].

[1]The factor of $1/\varepsilon$ also always comes accompanied by a factor of $\ln(\mu^2/f(\{m\}))$, however, as we will see, it is useful to keep this quantity separate from the rest of the constant terms in Δ.

1.2.2 UV Divergence Renormalization

As we have seen in Section 1.2.1, UV divergences emerge in loop integrals which tend to infinity as the unconstrained loop momenta tends to infinity. The divergent nature of these integrals is apparent in the UV poles of the form $1/\varepsilon$ which emerge in dimensional regularization. In order to remove these divergences as $\varepsilon \to 0$ it is therefore necessary to remove these UV poles, which also removes the theory's dependence on the regulator allowing us to safely take the limit $\varepsilon \to 0$ without any part of our matrix element diverging.

At LO we can make predictions by identifying parameters in the Lagrangian (known as bare parameters) with physical quantities (for example, the experimentally measured masses or charges). However, as we have seen at NLO, UV divergences spoil this relation such that parameters appearing in the Lagrangian differ from the physical counterparts by a divergent amount. To resolve this issue, the approach we take is to separate these bare parameters into a finite physical parameter (also known as a renormalized parameter) and a UV-divergent part (known as a counterterm). These shifts are not just limited to masses and charges but to all independent physical parameters of the Lagrangian, even extending to the normalization of the physical fields themselves; with these normalizations not being observable quantities we are free to shift any normalization factors by any amount. As an example we provide a set of these shifts which are relevant to the processes explored in Part II of this work. The shifts in the fields are

$$\begin{aligned}
h^{(0)} &= \sqrt{Z_h} h = \left(1 + \frac{1}{2}\delta Z_h\right) h\,, \\
f_L^{(0)} &= \sqrt{Z_f^L} f_L = \left(1 + \frac{1}{2}\delta Z_f^L\right) f_L\,, \\
f_R^{(0)} &= \sqrt{Z_f^R} f_R = \left(1 + \frac{1}{2}\delta Z_f^R\right) f_R\,, \\
\begin{pmatrix} Z^{(0)} \\ A^{(0)} \end{pmatrix} &= \begin{pmatrix} \sqrt{Z_{ZZ}} & \sqrt{Z_{ZA}} \\ \sqrt{Z_{AZ}} & \sqrt{Z_{AA}} \end{pmatrix} = \begin{pmatrix} 1 + \frac{1}{2}\delta Z_{ZZ} & \frac{1}{2}\delta Z_{ZA} \\ \frac{1}{2}\delta Z_{AZ} & 1 + \frac{1}{2}\delta Z_{AA} \end{pmatrix} \begin{pmatrix} Z \\ A \end{pmatrix}\,,
\end{aligned} \tag{1.2.9}$$

where fields with superscript (0) represent bare fields, fields without a superscript represent renormalized fields, Z_X are the *renormalization constants*, and δX represents the UV-divergent counterterm related to the field X. The apparent mixing of the fields Z and A through counterterms is a consequence of these fields mixing into each other at the one-loop level (when these fields are off-shell). Similarly, for the masses and charges the subset relevant to our later calculations are

$$\begin{aligned}
M^{(0)} &= Z_M M = M + \delta M\,, \\
e^{(0)} &= Z_e e = e + \delta e\,,
\end{aligned} \tag{1.2.10}$$

where M is a generic mass and e is the electric charge. In Eq. 1.2.10 we are able to write the mass renormalization constant as a *multiplicative renormalization constant* in the on-shell scheme due the fact that $\delta M \sim M$. This ensures that particles which are massless at the level of the Lagrangian do not acquire a mass as a result of renormalization. This is useful in ensuring that global symmetries (such as chiral symmetries) which preserve particles being massless are not broken by this renormalization scheme.

After substituting the bare parameters written in terms of renormalized parameters and counterterms as in Eqs. 1.2.9 and 1.2.10 into the Lagrangian of our theory, we may similarly split our Lagrangian into a part containing only bare fields and parameters, and a part containing only counterterms as

$$\mathcal{L}^{(0)} = \mathcal{L} + \delta\mathcal{L}\,, \tag{1.2.11}$$

where $\mathcal{L}$ is simply equal to $\mathcal{L}^{(0)}$ with bare parameters replaced by renormalized ones, and $\delta\mathcal{L}$ contains all counterterms. As UV divergences first emerge at the one-loop level, so too the counterterms are NLO corrections, and so it is possible to expand $\delta\mathcal{L}$ to NLO in the coupling; doing so produces the *counterterm Lagrangian* at NLO.

There are several *schemes* available to us when deriving the form of the counterterms. The simplest of these is the minimal subtraction (MS) scheme where the counterterms are purely UV-divergent quantities such that the only function of the counterterms is to exactly cancel the UV divergences appearing in the bare NLO matrix element. A related, more common scheme is the modified minimal subtraction ($\overline{\text{MS}}$) scheme. This scheme functions in much the same way as the MS scheme except that along with the UV pole we also remove the universal constants, γ_E and $\ln(4\pi)$ which appear in Eq. 1.2.7. The advantages of this scheme are that it is typically very simple to calculate renormalized matrix elements (allowing us to calculate at NLO using bare quantities, and renormalize results by simply ignoring the poles and corresponding constant factors) and allows us to sidestep needing to define terms in the Lagrangian in terms of observables, which for some parameters (such as quark masses) are not well defined. It also allows us to resum potentially large logarithms that may appear in physical renormalization schemes such as the one we shall discuss shortly. A downside is that any parameter renormalized in this scheme does not have the additional $\ln(\mu^2)$ term removed from the bare NLO corrections, resulting in this parameter being a function of μ, obscuring the connection of the theory to the physical picture.

Another common scheme is the *on-shell* scheme. In the on-shell scheme we relate quantities in the Lagrangian to observables. The result is that as well as containing identical UV pole structures to those found in the MS and $\overline{\text{MS}}$ scheme, the

counterterms also contain finite parts to ensure a correspondence between the renormalized quantity and the observable. Once a counterterm is obtained in the on-shell scheme it is easy to convert to the $\overline{\text{MS}}$ scheme by simply removing all finite parts besides the constant $-\gamma_E + \ln(4\pi)$ factor. A consequence of relating the parameters in the Lagrangian to observables is that parameters have a physical definition. As a result, any dependence on the scale μ cancels between the NLO bare and counterterm corrections. This cancellation of μ is a result of poles from the bare corrections and the counterterm corrections both being generated by loop integrals so that in both instances the poles are accompanied by $\ln(\mu)$ terms according to Eq. 1.2.7. Therefore, a cancellation between the poles necessarily also results in a cancellation of the μ-dependent terms.

We continue our study of the on-shell scheme by writing the set of two-point functions for the physical particles in our theory [29,35]. What follows is presented in Feynman gauge, which we define in Section 1.5.1. Using the Lagrangian in Eq. 1.2.11, we may write the renormalized two-point functions which are relevant to the processes considered in this work at NLO in terms of scalar functions, Σ_b^a, and counterterms as (where hatted quantities are renormalized, and where we have omitted fermion mixing)

$$
\begin{aligned}
\hat{\Gamma}^W_{\mu\nu}(k^2) = \;& W_\mu \;\underset{\overrightarrow{k}}{\sim\!\!\bigcirc\!\!\sim}\; W_\nu \\
&= -ig_{\mu\nu}(k^2 - M_W^2) - i\left(g_{\mu\nu} - \frac{k_\mu k_\nu}{k^2}\right)\left(\Sigma_T^W(k^2) - \delta M_W^2 - \delta Z_{WW}(M_Z^2 - k^2)\right) \\
&\quad - i\frac{k_\mu k_\nu}{k^2}\left(\Sigma_L^W(k^2) - \delta M_W^2 - \delta Z_{WW}(M_W^2 - k^2)\right) \\
&= -ig_{\mu\nu}(k^2 - M_W^2) - i\left(g_{\mu\nu} - \frac{k_\mu k_\nu}{k^2}\right)\hat{\Sigma}_T^W(k^2) - i\frac{k_\mu k_\nu}{k^2}\hat{\Sigma}_L^W(k^2)\,,
\end{aligned}
$$

$$
\begin{aligned}
\hat{\Gamma}^{ZZ}_{\mu\nu}(k^2) = \;& Z_\mu \;\underset{\overrightarrow{k}}{\sim\!\!\bigcirc\!\!\sim}\; Z_\nu \\
&= -ig_{\mu\nu}(k^2 - M_Z^2) - i\left(g_{\mu\nu} - \frac{k_\mu k_\nu}{k^2}\right)\left(\Sigma_T^{ZZ}(k^2) - \delta M_Z^2 - \delta Z_{ZZ}(M_Z^2 - k^2)\right) \\
&\quad - i\frac{k_\mu k_\nu}{k^2}\left(\Sigma_L^{ZZ}(k^2) - \delta M_Z^2 - \delta Z_{ZZ}(M_Z^2 - k^2)\right) \\
&= -ig_{\mu\nu}(k^2 - M_W^2) - i\left(g_{\mu\nu} - \frac{k_\mu k_\nu}{k^2}\right)\hat{\Sigma}_T^{ZZ}(k^2) - i\frac{k_\mu k_\nu}{k^2}\hat{\Sigma}_L^{ZZ}(k^2)\,,
\end{aligned}
$$

$$\hat{\Gamma}^{AA}_{\mu\nu}(k^2) = \; A_\mu \;\vec{k}\; A_\nu$$

$$= -ig_{\mu\nu}k^2 - i\left(g_{\mu\nu} - \frac{k_\mu k_\nu}{k^2}\right)\left(\Sigma^{AA}_T(k^2) + k^2\delta Z_{AA}\right)$$
$$- i\frac{k_\mu k_\nu}{k^2}\left(\Sigma^{AA}_L(k^2) + k^2\delta Z_{AA}\right)$$
$$= -ig_{\mu\nu}(k^2 - M_W^2) - i\left(g_{\mu\nu} - \frac{k_{\mu\nu}}{k^2}\right)\hat{\Sigma}^{AA}_T(k^2) - i\frac{k_\mu k_\nu}{k^2}\hat{\Sigma}^{AA}_L(k^2)\,,$$

$$\hat{\Gamma}^{AZ}_{\mu\nu}(k^2) = \; A_\mu \;\vec{k}\; Z_\nu$$

$$= -ig_{\mu\nu}k^2 - i\left(g_{\mu\nu} - \frac{k_\mu k_\nu}{k^2}\right)\left(\Sigma^{AZ}_T(k^2) - \frac{1}{2}k^2\delta Z_{AZ} - \frac{1}{2}\delta Z_{ZA}(M_Z^2 - k^2)\right)$$
$$- i\frac{k_\mu k_\nu}{k^2}\left(\Sigma^{AZ}_L(k^2) - \frac{1}{2}k^2\delta Z_{AZ} - \frac{1}{2}\delta Z_{ZA}(M_Z^2 - k^2)\right)$$
$$= -ig_{\mu\nu}(k^2 - M_W^2) - i\left(g_{\mu\nu} - \frac{k_\mu k_\nu}{k^2}\right)\hat{\Sigma}^{AZ}_T(k^2) - i\frac{k_\mu k_\nu}{k^2}\hat{\Sigma}^{AZ}_L(k^2)\,,$$

$$\hat{\Gamma}^{H}(k^2) = \; h \;\vec{k}\; h$$

$$= i(k^2 - m_H^2) + i\left(\Sigma^H(k^2) - \delta m_H^2 - \delta Z_h(m_H^2 - k^2)\right)$$
$$= i(k^2 - m_H^2) + i\hat{\Sigma}^H(k^2)\,,$$

$$\hat{\Gamma}^{f}(k^2) = \; f \;\vec{k}\; f$$

$$= i(\not{k} - m_f) + i\Big\{\not{k}P_L\left(\Sigma^L_f(k^2) + \delta Z^L_f\right) + \not{k}P_R\left(\Sigma^R_f(k^2) + \delta Z^R_f\right)$$
$$+ m_f\Bigg[P_L\left(\Sigma^S_f(k^2) - \frac{1}{2}\delta Z_L - \frac{1}{2}\delta Z_R - \frac{\delta m_f}{m_f}\right)$$
$$+ P_R\left(\Sigma^{S*}_f(k^2) - \frac{1}{2}\delta Z_L - \frac{1}{2}\delta Z_R - \frac{\delta m_f}{m_f}\right)\Bigg]\Big\}$$
$$= i(\not{k} - m_f) + i\Big\{\not{k}P_L\hat{\Sigma}^L_f(k^2) + \not{k}\hat{\Sigma}^R_f(k^2) + m_f\left[P_L\hat{\Sigma}^S_f(k^2) + P_R\hat{\Sigma}^{S*}_f(k^2)\right]\Big\}\,. \tag{1.2.12}$$

As stated, in the on-shell scheme we may define the form of the renormalization constants appearing in Eq. 1.2.12 by imposing a set of conditions that relate the renormalized parameters to measurable quantities. Firstly we can impose that the renormalized mass is equal to the observed mass; this condition is equivalent to imposing that the real part of poles of the corresponding propagators (found from

taking the inverse of the two-point functions in Eq. 1.2.12) appear at the propagator momenta $k^2 = M^2$ for a particle of mass M. We can also fix the field normalization counterterms by imposing that the residues of the renormalized propagators are equal to one. These two conditions give us the set of renormalization conditions for the renormalized scalar functions, $\hat{\Sigma}$. The renormalization conditions given by imposing the position of the pole for the SM bosons result in the expressions

$$\begin{aligned} \widetilde{\mathrm{Re}}\hat{\Sigma}_T^W(M_W^2) &= 0\,, & \mathrm{Re}\hat{\Sigma}_T^{AZ}(M_Z^2) &= 0\,, \\ \widetilde{\mathrm{Re}}\hat{\Sigma}_T^{ZZ}(M_Z^2) &= 0\,, & \hat{\Sigma}_T^{AA}(0) &= 0\,, \\ \hat{\Sigma}_T^{AZ}(0) &= 0\,, & \mathrm{Re}\hat{\Sigma}^H(m_H^2) &= 0\,, \end{aligned} \tag{1.2.13}$$

while imposing the form of the residue of the propagators for the SM bosons gives

$$\begin{aligned} \widetilde{\mathrm{Re}}\frac{\partial\hat{\Sigma}_T^W(k^2)}{\partial k^2}\Big|_{k^2=M_W^2} &= 0\,, & \mathrm{Re}\frac{\partial\hat{\Sigma}_T^{AA}(k^2)}{\partial k^2}\Big|_{k^2=0} &= 0\,, \\ \mathrm{Re}\frac{\partial\hat{\Sigma}_T^{ZZ}(k^2)}{\partial k^2}\Big|_{k^2=M_Z^2} &= 0\,, & \mathrm{Re}\frac{\partial\hat{\Sigma}_T^{H}(k^2)}{\partial k^2}\Big|_{k^2=m_H^2} &= 0\,, \end{aligned} \tag{1.2.14}$$

where $\widetilde{\mathrm{Re}}$ is defined as taking only the real part of the loop integrals. The renormalization conditions for the SM fermions allow us to write

$$\begin{aligned} &\widetilde{\mathrm{Re}}\hat{\Sigma}_f^L(m_f^2) + \widetilde{\mathrm{Re}}\hat{\Sigma}_f^S(m_f^2) = 0\,, \\ &\widetilde{\mathrm{Re}}\hat{\Sigma}_f^R(m_f^2) + \widetilde{\mathrm{Re}}\hat{\Sigma}_f^{S*}(m_f^2) = 0\,, \\ &\widetilde{\mathrm{Re}}\hat{\Sigma}_f^L(m_f^2) + \widetilde{\mathrm{Re}}\hat{\Sigma}_f^R(m_f^2) \\ &+ 2m_f^2\frac{\partial}{\partial k^2}\left(\widetilde{\mathrm{Re}}\hat{\Sigma}_f^L(k^2) + \widetilde{\mathrm{Re}}\hat{\Sigma}_f^R(k^2) + \widetilde{\mathrm{Re}}\hat{\Sigma}_f^S(k^2) + \widetilde{\mathrm{Re}}\hat{\Sigma}_f^{S*}(k^2)\right)\Big|_{k^2=m_f^2} = 0\,. \end{aligned} \tag{1.2.15}$$

The renormalization conditions in Eqs. 1.2.13 to 1.2.15 thus allow us to find that the bosonic field normalization counterterms are

$$\begin{aligned} \delta Z_W &= -\mathrm{Re}\frac{\partial\Sigma_T^W(k^2)}{\partial k^2}\Big|_{k^2=M_W^2}\,, & \delta Z_{AZ} &= -2\mathrm{Re}\frac{\Sigma_T^{AZ}(M_Z^2)}{M_Z^2}\,, \\ \delta Z_{ZZ} &= -\mathrm{Re}\frac{\partial\Sigma_T^{ZZ}(k^2)}{\partial k^2}\Big|_{k^2=M_Z^2}\,, & \delta Z_{ZA} &= -2\frac{\Sigma_T^{AZ}(0)}{M_Z^2}\,, \\ \delta Z_{AA} &= -\mathrm{Re}\frac{\partial\Sigma_T^{AA}(k^2)}{\partial k^2}\Big|_{k^2=M_Z^2}\,, & \delta Z_h &= -\mathrm{Re}\frac{\partial\Sigma^H(k^2)}{\partial k^2}\Big|_{k^2=m_H^2}\,, \end{aligned} \tag{1.2.16}$$

and the counterterms for the boson masses are

$$\begin{aligned} \delta M_W^2 &= \widetilde{\mathrm{Re}}\Sigma_T^W(M_W^2)\,, \\ \delta M_Z^2 &= \widetilde{\mathrm{Re}}\Sigma_T^{ZZ}(M_Z^2)\,, \\ \delta m_H^2 &= \mathrm{Re}\Sigma^H(m_H^2)\,, \end{aligned} \tag{1.2.17}$$

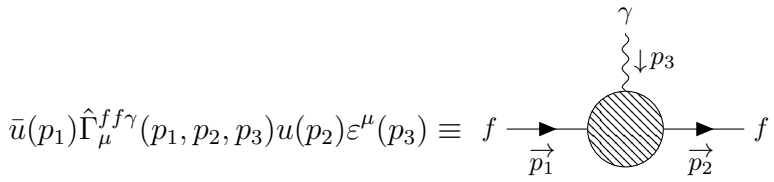

Figure 1.1: *The Feynman diagram of the $ff\gamma$ interaction for generic fermion flavor, f, defining the function $\hat{\Gamma}^{ff\gamma}_\mu$. Here the "blob" vertex represents bare one-loop corrections to the vertex, as well as all contributions from counterterms, including wavefunction counterterms.*

while the fermionic mass and field normalization counterterms are

$$\begin{aligned}
\delta m_f &= \frac{m_f}{2}\widetilde{\mathrm{Re}}\Big(\Sigma^L_f(m_f^2)+\Sigma^R_f(m_f^2)+\Sigma^S_f(m_f^2)+\Sigma^{S*}_f(m_f^2)\Big)\,,\\
\delta Z^L_f &= \widetilde{\mathrm{Re}}\Sigma^L_f(m_f^2)+\Sigma^S_f(m_f^2)-\Sigma^{S*}_f(m_f^2)\\
&\quad - m_f^2\frac{\partial}{\partial k^2}\left(\Sigma^L_f(m_f^2)+\Sigma^R_f(m_f^2)+\Sigma^S_f(m_f^2)+\Sigma^{S*}_f(m_f^2)\right)\,,\\
\delta Z^R_f &= \widetilde{\mathrm{Re}}\Sigma^R_f(m_f^2)\\
&\quad - m_f^2\frac{\partial}{\partial k^2}\left(\Sigma^L_f(m_f^2)+\Sigma^R_f(m_f^2)+\Sigma^S_f(m_f^2)+\Sigma^{S*}_f(m_f^2)\right)\,.
\end{aligned} \tag{1.2.18}$$

We note here that throughout this work we often consider δM rather than δM^2 for boson mass counterterms. These quantities are related via the simple relation

$$\delta M = \frac{1}{2M}\delta M^2\,, \tag{1.2.19}$$

for some boson of mass M. We must also consider the counterterm for the electric charge. The on-shell counterterm is derived by considering the three-point interaction between a photon and two charged fermions in the Thompson limit, i.e. the limit of vanishing photon momentum. The enforced condition is that in the Thompson limit the one-loop renormalized coupling of charged fermions to the photon should be equal to the measured electric charge. This condition may be written as

$$\overline{u}(p)\hat{\Gamma}^{ff\gamma}_\mu(p,p,0)u(p)\Big|_{p^2=m_f^2} = -iQ_f e\bar{u}(p)\gamma_\mu u(p)\,, \tag{1.2.20}$$

where the function $\hat{\Gamma}^{ff\gamma}_\mu$ is defined in Fig. 1.1. Making use of SM Ward identities allows us to write the form of the electric charge counterterm in the SM in terms of the two point functions defined in Eq. 1.2.12 as

$$\frac{\delta e}{e} = \frac{1}{2}\frac{\partial\Sigma^{AA}_T(k^2)}{\partial k^2}\Big|_{k^2=0} - \frac{v_f-a_f}{Q_f}\frac{\Sigma^{AZ}_T(0)}{M_Z^2}\,. \tag{1.2.21}$$

Physically, the γZ two-point function enters due to the ability of the photon to mix into a Z-boson at the one-loop level before coupling to the fermion, and it is also for this reason that we find the vector coupling, v_f, and axial-vector coupling, a_f, of the Z-boson enters the expression in Eq. 1.2.21. Charge universality guarantees that the final form of the electric charge counterterm is independent of the fermion considered in this derivation. In the SM we can make use of the relation $v_f - a_f = -Q_f s_w/c_w$ in Eq. 1.2.21, which explicitly shows the charge universality of the electric charge counterterm.

With the result of Eq. 1.2.21 at hand, we find that in the SM the entirety of the counterterm calculation procedure can be achieved by the calculation of a finite set of bare two-point functions.

1.2.3 Tadpole Renormalization

We begin by considering the Higgs doublet after SSB such that it has acquired a vev, which we now denote $\tilde{v}$, where we have a priori made no claims about the form of $\tilde{v}$

$$H = \frac{1}{\sqrt{2}} \begin{pmatrix} 0 \\ \tilde{v} + h \end{pmatrix} , \tag{1.2.22}$$

and where $\tilde{v}$ permits a perturbative expansion

$$\tilde{v} = v_0 + v_1 + \dots . \tag{1.2.23}$$

Importantly, we do not yet make any link between the value of $\tilde{v}$ and the parameters of the Higgs potential, λ and μ, from Eq. 1.1.10. The linear terms in h arising from the Higgs potential in Eq. 1.1.10 imply that at LO the vacuum may absorb the Higgs as shown in Diagram (1) in Fig. 1.2 and given by

$$T_0 \sim \langle h|(-\mu^2 v_0 + \lambda v_0^3)h|0\rangle , \tag{1.2.24}$$

where we have utilized the expansion in Eq. 1.2.23, and where at LO we need not be concerned with whether these are bare or renormalized quantities. The absorption of Higgs by the vacuum is a feature that we do not desire in our theory, and so, wishing to remove this LO absorption, we impose that the expression in Eq. 1.2.24 should vanish, i.e. $T_0 = 0$. Imposing this relation simultaneously enforces that the LO expansion of the Higgs vev, v_0, takes the form

$$v_0 = \sqrt{\frac{\mu^2}{\lambda}} , \tag{1.2.25}$$

which is the same as that seen in Eq. 1.1.12.

Figure 1.2: *Diagrams representing the one-point function, $h \to 0$, for (1): the LO absorption of the Higgs by the vacuum, and (2): the NLO absorption of the Higgs by the vacuum. These are known as tadpole diagrams.*

The procedure outlined above only ensures that tadpoles are eliminated from our theory at LO. The tadpole function also receives corrections at NLO, represented by Diagram (2) in Fig. 1.2. Due to the anomalously large corrections that tadpoles introduce at NLO[1] it is desirable to remove tadpoles at each order in perturbation theory. In fact, the true position of the vev of the Higgs doublet (which we denote v) receives perturbative quantum corrections, and any non-vanishing tadpole contributions in our calculations are present due to the form of the vev in the Higgs doublet differing from the true minima of the Higgs potential, v. To remove tadpoles at NLO we write the linear term in h of Higgs potential as

$$\begin{aligned} V(H)_{\text{lin.}} &= \left(- \left(\mu^{(0)}\right)^2 \tilde{v}^{(0)} + \lambda^{(0)} \left(\tilde{v}^{(0)}\right)^3 \right) h, \\ &= t^{(0)} h \,, \\ &= (t + \delta t) h \,, \end{aligned} \tag{1.2.26}$$

where in the second line of Eq. 1.2.26 we combined the bare terms into a single bare term, $t^{(0)}$, and in the third line of Eq. 1.2.26 we have expanded this into the sum of a renormalized quantity and a counterterm. Defining the bare tadpole function $T^{(0)}$ to be the sum of all one-loop contributions to the Higgs one-point function, we can define δt by imposing that that renormalized tadpole function $\hat{T}$ is

$$\hat{T} = T^{(0)} + \delta t = 0 \,. \tag{1.2.27}$$

This condition is the on-shell tadpole renormalization condition, equivalent to simply defining $\delta t = -T^{(0)}$. As the condition in Eq. 1.2.27 guarantees the absence of tadpoles at NLO, and because t and $\tilde{v}$ are linked from Eq. 1.2.26, we can conclude that the condition in Eq. 1.2.27 also places $\tilde{v}$ at the position of the true vev up to NLO, i.e. $\tilde{v} = v$. A consequence of tadpoles being entirely removed via Eq. 1.2.27 is that, for the calculation of any matrix element, tadpoles do not need to be included

[1] For example, corrections to the Higgs one-point function arising due to top-quark loops scale as $m_t^4/(m_H^2 v^2)$, inducing sizeable contributions.

in any contributing diagrams. Instead, the effects of these tadpole corrections are included in the renormalization of bare parameters defined in terms of the bare Higgs vev, such as $M_W^{(0)} = \frac{1}{2} g_2^{(0)} \tilde{v}^{(0)}$. However, we note here that tadpoles are gauge-dependent quantities. We see from Eq. 1.2.26 that the counterterm of $\tilde{v}$ (which with the condition in Eq. 1.2.27 we have established to be the true vev, v) must be some function of δt and therefore gauge dependent due to the relation in Eq. 1.2.27. When defined in this way, the particle masses of the theory are now all a function of $\tilde{v}$, resulting in all mass counterterms in the theory being gauge dependent. In a physical renormalization scheme, such as a purely on-shell scheme, the correspondence between parameters in our Lagrangian and observable quantities guarantees that any gauge-dependence present in mass counterterms drops out in the calculation of observables. However, in some scenarios it is beneficial to renormalize some quantities in the on-shell scheme while others are renormalized in the $\overline{\text{MS}}$ scheme. In this case, adopting the tadpole renormalization as described above would produce gauge-dependent results when calculating observable quantities.

We wish to implement some scheme of tadpole renormalization that results in gauge-independent counterterms for all parameters of the theory. Such a scheme was introduced by Fleischer and Jegerlehner and is known as the *Fleischer-Jegerlehner (FJ) tadpole scheme* [36–38]. This scheme allows us to preserve the definitions of m_H, M_W, M_Z, and m_f as a function of the LO Higgs vev, v_0, as defined throughout Eqs. 1.1.15, 1.1.25 and 1.1.39, which allows for gauge-independent definitions of the corresponding counterterms, while also renormalizing tadpoles in a consistent manner. To begin, we split the combination $\tilde{v} + h$ in the Higgs doublet of Eq. 1.2.22 as

$$\tilde{v} + h = v_0 + \Delta v + h \,. \tag{1.2.28}$$

We now insist that v_0 plays no part in the tadpole renormalization, and that the tadpoles should be entirely renormalized by the shift Δv, such that this shift cancels the tadpole contributions. As Δv is simply some constant value and not defined by the bare parameters of the theory, it consequently does not require a renormalization counterterm. Next, we consider the terms in the Higgs potential of Eq. 1.1.10 which are linear in $h\Delta v$

$$\begin{aligned} V(H)_{h\Delta v \text{ lin.}} &= 2\Delta v \lambda^{(0)} \left(v_0^{(0)}\right)^2 h^{(0)} \,, \\ &\equiv \delta t \, h^{(0)} \,. \end{aligned} \tag{1.2.29}$$

where we have recast Δv as a tadpole counterterm in the second line. We can then implement our aforementioned desire that the tadpoles are entirely renormalized by

Δv by solving Eq. 1.2.29 for Δv and making use of $\left(m_H^{(0)}\right)^2 = 2\lambda^{(0)}\left(v_0^{(0)}\right)^2$

$$\begin{aligned}\Delta v &= \frac{\delta t}{\left(m_H^{(0)}\right)^2}\,, \\ &= \frac{\delta t}{m_H^2} + \text{NNLO terms}\,, \\ &= -\frac{T^{(0)}}{m_H^2}\,, \end{aligned} \tag{1.2.30}$$

where we have enforced the tadpole renormalization condition in Eq. 1.2.27. The form of Δv is therefore determined by the bare NLO tadpole function. We may now replace Δv in our Lagrangian according to Eq. 1.2.30 to construct terms in the counterterm Lagrangian proportional to δt which allows us to remove the explicit tadpole contributions.

We now recognize that we are able to shift the Higgs field by any constant quantity, and in doing so we are guaranteed that the result of any S-matrix elements will not change. We therefore shift the Higgs field according to

$$h \to h - \Delta v\,, \tag{1.2.31}$$

where in doing so we have removed any explicit tadpole renormalization, but kept the definitions of m_H, M_W, M_Z and m_f from Eqs. 1.1.15, 1.1.25 and 1.1.39. However, from the S-matrix invariance we must therefore conclude that this scheme is equivalent to the scheme featuring the shift found in Eq. 1.2.28 where tadpoles are explicitly renormalized. Therefore a scheme in which the Higgs vev takes the LO value v_0, and where particle masses are defined according to Eqs. 1.1.15, 1.1.25 and 1.1.39 but where tadpoles are not explicitly renormalized is equivalent to the FJ tadpole scheme. This allows us to renormalize tadpoles in a consistent manner by simply including them at the appropriate order in perturbation theory in diagrams contributing to a particular process and setting the vev to v_0 from Eq. 1.2.25.

While we have examined two particular tadpole renormalization schemes, we note that there are a selection of schemes available, such as the β_h and β_t[1] scheme [39], and the scheme outlined in [40]. Throughout this work we will favor the FJ tadpole scheme for its advantages in regards to producing gauge-independent counterterms.

[1]The β_t scheme is equivalent to the FJ tadpole scheme.

1.3 IR Divergences

In QFTs we may also encounter infinities that are not UV, but IR in origin. Such divergences can be classified as either *colinear* or *soft*. For the calculations outlined in Part II, colinear divergences will be of little concern, and so here we focus on soft divergences. As discussed Section 1.2.1, conversely to UV divergences where a divergence occurs in a loop integral as the loop momenta tends to infinity, soft divergences may occur at the amplitude level in loop integrals which diverge as the loop momenta tends to zero. As we have seen in Section 1.2.2, in the on-shell scheme we can fully UV renormalize the SM by incorporating the UV poles from two-point functions into our counterterms. However, we find that in the SM none of these two-point functions contain poles which are IR in origin, and thus cannot be used to cancel any IR poles which emerge in the bare matrix element for a given process.

The *KLN theorem* shows that perturbatively in any finite energy window the SM is IR finite [41, 42]. Soft divergences are therefore removed by considering additional processes that involve the emission of additional massless particles. In the soft limit we recover a process which is indistinguishable from the original process under consideration. At NLO we need only consider the additional emission of a single massless particle. Such processes are often referred to as having *final-state radiation*. The KLN theorem then guarantees that the soft IR divergences present in these final-state-radiation diagrams cancel the soft IR divergences present in the loop integrals, again removing the dependence on the regulator ε. The dependence on the IR regulator for final-state-radiation diagrams emerges when performing the necessary phase-space integration in $d = 4 - 2\varepsilon$ dimensions, as described in Appendix B. Again, the divergent nature of the integral over phase space is apparent due to the emergence of $1/\varepsilon$ poles after the phase-space integration, and the cancellation of such poles against the IR poles which emerge in IR-divergent loop integrals allows us to safely take the limit $\varepsilon \to 0$ without any divergences. Therefore, an interesting feature is that while UV divergences may be removed at the level of the amplitude, IR divergences are instead removed only at the level of the observable. We also note that the constant factors that accompany $1/\varepsilon$ arising from IR-divergent loop integrals (as discussed at the end of Section 1.2.1) cancel against equivalent terms arising from the IR-divergent phase-space integral.

1.4 The Renormalization Group

A feature of loop corrections in QFTs is the emergence of the *running* of parameters renormalized in the $\overline{\text{MS}}$ scheme within the theory, that is, the observed values of

parameters changing as we vary the renormalization scale, μ. Here we explore how this running emerges, and the consequences of this running within the SM. In Section 1.4.1 we explore the running of the SM couplings, α and α_s, while in Section 1.4.2 we explore the running of the SM fermion masses. Finally, in section Section 1.4.3 we discuss the invariance of observables with respect to μ.

1.4.1 Running Gauge Couplings

Firstly, we consider the electromagnetic coupling constant, e. In the on-shell scheme e is defined in correspondence with a physical observable, and therefore does not vary with the renormalization scale μ. Consider, however, e renormalized in the $\overline{\text{MS}}$ scheme, which as discussed in Section 1.2.2, causes e to become a function of, and thus run with the varying of μ. We may write the bare electromagnetic coupling constant and its corresponding counterterm in $d = 4 - 2\varepsilon$ dimensions as

$$e^{(0)} = \mu^{\varepsilon} Z_e(\mu) e(\mu)\,, \tag{1.4.1}$$

where μ is the renormalization scale first seen in Section 1.2.1, and Z_e is the electric charge renormalization constant seen in Eq. 1.2.10. We recognize that the bare Lagrangian, and the parameters thereof, are necessarily independent of the renormalization scale, μ, a property which must be preserved when re-expressing the Lagrangian in terms of renormalized parameters and renormalization constants. Taking advantage of this property we may take the derivative of Eq. 1.4.1 with respect to μ to get (where we drop the arguments of e and Z_e)

$$\mu \frac{de^{(0)}}{d\mu} = 0 = \varepsilon \mu^{\varepsilon} Z_e e + \mu^{1+\varepsilon} \frac{dZ_e}{d\mu} e + \mu^{1+\varepsilon} Z_e \frac{de}{d\mu}\,. \tag{1.4.2}$$

which we may rewrite as

$$\begin{aligned} 0 &= \mu^{\varepsilon} e \frac{dZ_e}{d\ln(\mu)} + \mu^{\varepsilon} Z_e \left[\varepsilon e + \frac{de}{d\ln(\mu)} \right], \\ \Rightarrow 0 &= \alpha \frac{dZ_e}{d\ln(\mu)} + Z_e \left[\alpha\varepsilon + \frac{1}{2} \frac{d\alpha}{d\ln(\mu)} \right], \end{aligned} \tag{1.4.3}$$

where in the second line of Eq. 1.4.3 we have re-expressed the first line in terms of the fine-structure constant, $\alpha = e^2/4\pi$. We may rewrite Eq. 1.4.3 as

$$\frac{d\alpha}{d\ln(\mu)} \equiv \beta(\alpha)\,, \tag{1.4.4}$$

where $\beta(\alpha)$ is the QED *beta function* and may be determined order-by-order in α by calculating Z_e to increasingly higher orders. Equations of the type seen in Eq. 1.4.4

are known as renormalization-group (RG) equations. Written as an expansion in α we may therefore generically write this beta function as

$$\beta(\alpha) = -2\alpha(\mu)\left(\frac{\alpha}{4\pi}\beta_0(\alpha) + \left(\frac{\alpha(\mu)}{4\pi}\right)^2\beta_1(\alpha) + \dots\right). \tag{1.4.5}$$

Here, $\beta_0(\alpha)$ is the LO QED beta function. The decoupling theorem [43] guarantees that for a theory defined in a physical renormalization scheme, heavy degrees of freedom (that being with mass M where $\mu \lesssim M$) decouple from the theory. However, the $\overline{\text{MS}}$ scheme is not a physical renormalization scheme, and so this decoupling must be implemented "by hand". The result is that the LO QED beta function valid for scales $\mu \lesssim m_t$ is given by

$$\beta_0(\alpha) = -\frac{4}{3}\left[N_g Q_l^2 + N_c\left((N_g-1)Q_u^2 + N_g Q_d^2\right)\right], \tag{1.4.6}$$

where N_g is the number of generations, Q_l, Q_u, and Q_d are the charges of leptons, up-type quarks, and down-type quarks respectively, and where the decoupling of the heavy top quark is apparent from the $(N_g - 1)$ term.

Solving Eq. 1.4.4 to LO in the expansion we find

$$\alpha(\mu) = \frac{\alpha(\mu_0)}{1 - \alpha(\mu_0)\frac{\beta_0(\alpha)}{2\pi}\ln\left(\frac{\mu_0}{\mu}\right)}, \tag{1.4.7}$$

which allows us to calculate α at some scale, μ, given a measurement of α at some reference scale, μ_0. We could in principle have included higher-order corrections in α to our expression in Eq. 1.4.7, thus making this solution only an approximate solution, in this case known as the *leading log* approximation. An important feature of this running is that for QED the LO beta function in Eq. 1.4.6 takes a negative value; as a result we find that as we increase the scale μ, the value of $\alpha(\mu)$ increases. The processes considered in this work occur at a scale far below the breakdown of perturbative QED and so this property is of no cause for concern.

Next, we consider the strong coupling constant, g_3. The renormalization procedure for this parameter was not included in Section 1.2 as the explicit renormalization of this parameter does not play a role in the the processes considered in this thesis. However, this parameter plays an important role in the calculations considered in Part II of this thesis due to the evolution of this parameter with respect to the renormalization scale. Similarly to what was seen for QED, we may write the bare strong coupling constant as a function of the renormalized strong coupling constant and its corresponding counterterm in $d = 4 - 2\varepsilon$ dimensions as

$$g_3^{(0)} = \mu^{\varepsilon} Z_g(\mu) g_3(\mu), \tag{1.4.8}$$

where g_3 is the renormalized strong coupling constant and Z_g is the strong coupling renormalization constant. Again, we recognize the μ-independence of Eq. 1.4.8, and so take the derivative of this equation and rewrite this in terms of the strong fine-structure constant using $\alpha_s = g_3^2/4\pi$ to define

$$\frac{d\alpha_s}{d\ln(\mu)} \equiv \beta(\alpha_s)\,, \tag{1.4.9}$$

where $\beta(\alpha_s)$ is the QCD beta function, again permitting an expansion as

$$\beta(\alpha_s) = -2\alpha_s(\mu)\left(\frac{\alpha_s(\mu)}{4\pi}\beta_0(\alpha_s) + \left(\frac{\alpha_s(\mu)}{4\pi}\right)^2\beta_1(\alpha_s) + \dots\right). \tag{1.4.10}$$

We find from the calculation of Z_g that $\beta_0(\alpha_s)$ takes the form

$$\beta_0(\alpha_s) = \frac{11}{3}N_c - \frac{2}{3}n_l\,, \tag{1.4.11}$$

where we have again implemented the decoupling by hand such that n_l is the number of light quarks, this being $n_l = 5$ for $\mu \lesssim m_t$. Solving Eq. 1.4.10 for α_s to leading order gives

$$\alpha_s(\mu) = \frac{\alpha_s(\mu_0)}{1 - \alpha_s(\mu_0)\frac{\beta_0(\alpha_s)}{2\pi}\ln\left(\frac{\mu_0}{\mu}\right)}\,. \tag{1.4.12}$$

An important property of the QCD beta function is that in the SM with $n_l = 5$ the beta function takes a positive value, with the consequence being that $\alpha_s(\mu)$ decreases with increasing μ, increasing the applicability of perturbation theory at higher scales. Conversely, α_s grows with decreasing μ, such that at low energies perturbation theory breaks down and colored objects are highly confined. This important property, known as *asymptotic freedom*, is unique to QCD within the SM and allows for the binding of quarks into color-singlet objects such as hadrons [44,45].

1.4.2 Running Fermion Masses

A natural extension of the techniques explored in Section 1.4.1 is to apply them to the $\overline{\text{MS}}$ renormalized masses of the SM. As an example, we consider the running of a generic quark, denoted as q, the results of which are easily extended to the leptons of the SM. Again we use the property of the μ-independence of the bare parameters of the SM Lagrangian to write

$$\mu\frac{dm_q^{(0)}}{d\mu} = 0 = \mu\frac{dZ_{m_q}}{d\mu}m_q + \mu Z_{m_q}\frac{dm_q}{d\mu}\,, \tag{1.4.13}$$

where Z_{m_q} is the mass renormalization constant defined in Eq. 1.2.10. Similarly to how we defined the beta functions of QED and QCD we may also define the *anomalous dimension* of the quark mass as

$$\gamma_{m_q} \equiv \frac{1}{m_q}\frac{dm_q}{d\ln(\mu)}\,. \tag{1.4.14}$$

Due to quarks allowing for QED and QCD corrections, γ_{m_q} permits an expansion in both α and α_s

$$\gamma_{m_q} = \alpha(\mu)\gamma^{0,\gamma}_{m_q} + \alpha_s(\mu)\gamma^{0,g}_{m_q} + \alpha^2(\mu)\gamma^{1,\gamma}_{m_q} + \alpha_s^2(\mu)\gamma^{1,g}_{m_q} + \dots\,. \tag{1.4.15}$$

At leading order we find

$$\gamma^{0,\gamma}_{m_q} = -\frac{3}{2\pi}Q_q^2\,, \quad \gamma^{0,g}_{m_q} = -\frac{3}{2\pi}C_F\,, \tag{1.4.16}$$

where Q_q is the electric charge of the quark. We are free to drop the subscript of m_q on $\gamma^{0,g}_{m_q}$ due to the coupling of gluons and quarks being independent of the quark flavor. Neglecting QED corrections, we find that solving Eq. 1.4.14 with only the leading QCD corrections (which in this case are by far the most dominant) gives

$$m_q(\mu) = m_q(\mu_0)\left(\frac{\alpha_s(\mu_0)}{\alpha_s(\mu)}\right)^{2\pi\frac{\gamma^{0,g}}{\beta_0(\alpha_s)}}\,, \tag{1.4.17}$$

which is the running of the quark mass m_q in leading-log QCD. Again, this equation allows us to find the quark mass at some scale μ given a measurement of the mass at some other scale μ_0. We also find that Eq. 1.4.17 can be easily adapted to apply to leptons of type ℓ (which only receive QED corrections to the running at LO) with the replacements $q \to \ell$, $\gamma^{0,g} \to \gamma^{0,\gamma}_{m_\ell}$, $\alpha_s \to \alpha$, and $\beta_0(\alpha_s) \to \beta_0(\alpha)$.

1.4.3 Observable Invariance

Consider a observable, such as a decay rate or cross section, that is a function of the fine structure constant, α, the QCD coupling constant, α_s, and some mass, m. It must be true that to all orders in perturbation theory this observable is unchanged when we renormalize the aforementioned parameters in the on-shell scheme vs. when we renormalize these parameters in the $\overline{\text{MS}}$ scheme [46], summarized as

$$\mathcal{O} = \mathcal{O}^{\text{o.s}}(\alpha, \alpha_s, m, ...) = \overline{\mathcal{O}}\,(\alpha(\mu), \alpha_s(\mu), m(\mu), ...)\,, \tag{1.4.18}$$

where $\mathcal{O}$ represents some observable, $\mathcal{O}^{\text{o.s}}$ represents that observable with all parameters renormalized in the on-shell scheme, and $\overline{\mathcal{O}}$ represents the observable with the parameters α, α_s, and m renormalized in the $\overline{\text{MS}}$ scheme. As a result we may

write

$$\frac{d\mathcal{O}}{d\ln(\mu)} = \frac{d\alpha(\mu)}{d\ln(\mu)}\frac{\partial\overline{\mathcal{O}}}{d\alpha(\mu)} + \frac{d\alpha_s(\mu)}{d\ln(\mu)}\frac{\partial\overline{\mathcal{O}}}{d\alpha_s(\mu)} + \frac{dm(\mu)}{d\ln(\mu)}\frac{\partial\overline{\mathcal{O}}}{dm(\mu)} = 0\,. \tag{1.4.19}$$

The expression in Eq. 1.4.19 generalizes in an obvious way for additional observables renormalized in the $\overline{\text{MS}}$ scheme. We will take advantage of relations such as that in Eq. 1.4.19 in Section 4.6.2. We also note that, up to some some order, n, in perturbation theory, the quantities $\mathcal{O}^{\text{o.s}}$ and $\overline{\mathcal{O}}$ should be equal, with any differences occurring at order $n+1$. We are also able to take advantage of this property to sidestep issues that we might find in some particular renormalization scheme. For example, in the on-shell scheme we might find we have logarithms of two largely separated scales, leading to an anomalously large correction from such logarithms. In the $\overline{\text{MS}}$ scheme we may set our renormalization scale, μ, such that large logarithms are removed, but with the equivalence of the two schemes at the level of the observable we conclude that the large logarithms in the on-shell results are resummed in the definition of the $\overline{\text{MS}}$ renormalized parameters.

1.5 Gauge Fixing and Ghosts

As we have seen throughout Sections 1.1.1 to 1.1.3, we have a freedom in choosing a gauge in which to define our theory, with the result of such calculations of any observable quantity necessarily being independent of any particular gauge choice. As we shall see, however, this gauge freedom also amounts to a redundancy in our description of physics. As a result, we must be careful to ensure that we do not include multiple configurations of the same physical system (related by a gauge transformation) in any prediction relating to an observable quantity.

In Section 1.5.1 we demonstrate the necessity of gauge fixing, and how this may be implemented, while in Section 1.5.2 we demonstrate how the introduction of so-called *ghost* fields allow us to simplify calculations when using a gauge-fixed Lagrangian. While we keep the discussions in Sections 1.5.1 and 1.5.2 brief, a fully detailed version of the topics explored here in the context of the dimension-6 SMEFT can be found in Section 3.6, where the SM derivations are recovered in the limit $\Lambda_{\text{NP}} \to \infty$.

1.5.1 Gauge Fixing

As an example, consider the generating functional, $\mathcal{Z}$, for a free gauge theory

$$\mathcal{Z} = \int \mathcal{D}A \exp\left[i\int d^4x \left(-\frac{1}{4}F^a_{\mu\nu}F^{\mu\nu,a}\right)\right]\,, \tag{1.5.1}$$

with the gauge field invariant under the gauge transformations of Eq. 1.1.8. We see from Eq. 1.1.8 that there are an infinite number of physically equivalent gauge choices that exist for any particular gauge field. In performing the path integral of this generating functional we are also integrating over this infinite number of equivalent configurations. It should be of no surprise that as a consequence, due to the integration over these infinite physically equivalent states, the generating functional of Eq. 1.5.1 diverges. The solution to this problem is therefore that we must implement a method to ensure that we are performing the integral having made a particular choice of gauge. A method for implementing this was proposed by Faddeev and Popov [47]. The gauge can be fixed by introducing a gauge-fixing functional, G, and imposing that $G = 0$, similarly to the methods of a Lagrange multiplier. This ultimately results in the gauge-fixed functional for a Lagrangian with a gauge field taking the form

$$\mathcal{Z} = C \int \mathcal{D}\{\mathcal{K}\} \exp\left[i \int d^4x \left(\mathcal{L}(\{\mathcal{K}\}) - \frac{1}{2}(G)^2\right)\right] \det\left(\frac{\delta G}{\delta \alpha}\right) , \tag{1.5.2}$$

where α is the continuous parameter defining the gauge transformation of the set of fields $\{\mathcal{K}\}$ in the theory defined by the Lagrangian $\mathcal{L}$.

While an infinite set of gauge choices exists, we can take advantage of this freedom to make a choice that produces a desirable effect on the interactions or particles contained within a theory. Such choices are often made to make calculations easier, or to highlight a particular aspect of the theory. A common choice is the set of R_ξ gauges in the SM, which comprises an infinite set of gauge choices parameterized by the continuous parameter ξ and which is designed to remove the non-physical gauge- and Goldstone-boson mixing terms which appear in a non-gauge-fixed Lagrangian. These mixing terms take the form

$$\mathcal{L}_{\text{SM}} \supset (\partial\chi_i) A^a_\mu (gT)^a_{ij} \phi_{0j} \, , \tag{1.5.3}$$

where ϕ_0 is given below Eq. 1.1.19, A^a_μ is from Eq. 1.1.18, χ_i are the Goldstone bosons parameterized in terms of the fields in Eq. 1.1.14 such that

$$\chi_1 = \frac{1}{\sqrt{2}}(\phi^+ + \phi^-) \, , \quad \chi_2 = \frac{i}{\sqrt{2}}(\phi^+ - \phi^-) \, , \quad \chi_3 = \phi^0 \, , \quad \chi_4 = h \, , \tag{1.5.4}$$

and where T are the real antisymmetric representation matrices of the $SU(2) \times U(1)$ gauge group, defined in terms of the matrices introduced in Section 1.1.2 as $T^a = -i\tau^a = -i\frac{1}{2}\sigma^a$, where we now also introduce $\sigma^4 = \mathbf{1}_{2\times 2}$ and where similarly to $(g\tau)^a$, $(gT)^a$ is defined as

$$(gT)^a = (g_2 T^1, \, g_2 T^2, \, g_2 T^3, \, g_1 T^4) \, . \tag{1.5.5}$$

The set of R_ξ gauges are then defined by the gauge-fixing functional

$$G^a = \frac{1}{\sqrt{\xi}}\left(\partial^\mu A^a_\mu - \xi(gF)^a_i\chi_i\right), \tag{1.5.6}$$

where we have additionally defined the commonly occurring quantity $(gF)^a_i$ as

$$(gF)^a_i \equiv (gT)^a_{ij}\phi_{0j} = \frac{v}{2}\begin{pmatrix} g_2 & 0 & 0 & 0 \\ 0 & g_2 & 0 & 0 \\ 0 & 0 & g_2 & 0 \\ 0 & 0 & -g_1 & 0 \end{pmatrix}. \tag{1.5.7}$$

We can see that the $(G)^2$ term in Eq. 1.5.2 exactly cancels the gauge- and Goldstone-boson mixing term of Eq. 1.5.3 with the choice of $\xi = 1$, known as *Feynman gauge*. Another consequence of the gauge choice defined by Eq. 1.5.6 is that the $(G)^2$ term in Eq. 1.5.2 also introduces a mass matrix for the Goldstone bosons, supplying mass to these previously massless bosons. This mass matrix takes the form

$$(M^2_G)_{ij} = \xi(gF)^a_i(gF)^a_j, \tag{1.5.8}$$

which we see gives the Goldstone bosons a linear dependence of the R_ξ gauge parameter, ξ, but for the choice $\xi = 1$ gives a mass matrix with eigenvalues identical to that found for the gauge bosons in Eq. 1.1.20, and so gives an equivalence of gauge- and Goldstone-boson masses.

While several common choices for the parameter ξ exist, we make use of the choices $\xi = 1$, known a Feynman gauge, and $\xi \to \infty$, known as unitary gauge, which was introduced in Section 1.1.2. We note here that the G^2 term in Eq. 1.5.2 also introduces new kinetic terms for the gauge fields. This does not affect the canonical normalization of these fields, but the propagators for these fields now become a function of the parameter ξ. It is also clear that for the mass matrix in Eq. 1.5.8 in the limit of $\xi \to \infty$ (unitary gauge), the Goldstone bosons become infinitely massive and so decouple from the theory. We also note that we are free to not choose a particular value of ξ and instead keep it as a free parameter in any calculation, with the result being that the calculation of any physically observable quantity should be independent of ξ.

1.5.2 The Ghost Lagrangian

One potential complication of the gauge-fixing procedure outlined in Section 1.5.1 is the calculation of the determinant of Eq. 1.5.2. We are able to simplify the calculation of this determinant through the introduction of ghost fields. Using the

identity

$$\det(A) = \int \mathcal{D}c\mathcal{D}\bar{c}\exp(-\bar{c}Ac)\,, \tag{1.5.9}$$

where c and $\bar{c}$ are *Grassmann variables*, defined by the properties

$$\begin{aligned} c\bar{c} &= -\bar{c}c\,, \\ \int dc(A+Bc) &= B\,. \end{aligned} \tag{1.5.10}$$

We may then use the gauge transformations of the gauge and scalar fields to find the form of the determinant in terms of an integral over Grassmann variables

$$\det\left(\frac{\delta G^a}{\delta\alpha^b}\right) = \int \mathcal{D}c\mathcal{D}\bar{c}\exp\left\{i\bar{c}^a\left[-(\partial_\mu D^\mu)^{ab} - \xi(gF)^a_i\left((gF)^a_i + (gT)^a_{ij}\chi_j\right)\right]c^b\right\}\,, \tag{1.5.11}$$

where we have also introduced a factor of i multiplying the argument of the exponential. This introduction of i is valid, having used the property $\det(cA) = c^n\det(A)$ for an $n\times n$ matrix, A, and that $\delta G/\delta\alpha$ is a 4-dimensional matrix.

We see that with the interpretation of the fields c and $\bar{c}$ as scalars under Lorentz transformations, the argument of the exponential in Eq. 1.5.11 takes the form of a Lagrangian for fermionic scalar fields, so-called ghost fields

$$\mathcal{L}_{\text{ghost}} = \bar{c}^a\left[-(\partial_\mu D^\mu)^{ab} - \xi(gF)^a_i\left((gF)^a_i + (gT)^a_{ij}\chi_j\right)\right]c^b\,. \tag{1.5.12}$$

We see from Eq. 1.5.12 that these fictitious ghost fields have a mass matrix of the form

$$(m^2_{\text{ghost}})^{ab} = \xi(gF)^a_i(gF)^b_i\,, \tag{1.5.13}$$

which is identical to the form of the mass matrix found for gauge bosons in Eq. 1.1.20 with an additional linear factor of ξ. Clearly the choice of $\xi = 1$ gives the ghost fields identical masses to those found for the gauge bosons, while again the gauge choice $\xi\to\infty$ makes these fields infinitely massive and thus decouple from the theory. As previously mentioned, an advantage of introducing this ghost Lagrangian is that it allows us to account for the determinant in the gauge-fixed generating functional in Eq. 1.5.2. Therefore, we can completely implement gauge fixing by simply including terms generated by $(G)^2$ in Eq. 1.5.2 and by including ghost and their interactions on any internal lines as specified by Eq. 1.5.12.

Chapter 2

Effective Field Theories

In this chapter we introduce the notion of an *effective field theory* (EFT). This topic is first introduced in a general way in Section 2.1 by means of two examples, and then some general properties of EFTs are explored. In Section 2.2.1 we introduce the *Standard Model Effective Field Theory* (SMEFT), while in Section 2.3 we show how to transform this theory into the mass basis, as will be necessary for the calculations performed in Part II.

2.1 Effective Field Theories

An EFT is some approximate description of a high-energy theory valid only below a cut-off, where new heavy particles have been *integrated out*. The high-energy physics is then captured by parameters known as *Wilson coefficients* (WC) which describe some *effective coupling*. The problems present in the SM have broadly lead to the belief that it is an EFT, that is, it is valid only up to some cut-off in energy scale. Above this cut-off some new, currently unknown theory of particles and their interactions would be the appropriate description of nature. We discuss this latter point further in Part II.

2.1.1 Introduction to Effective Field Theories

To demonstrate the basic principles and properties of EFTs, we begin by borrowing a simple example from [48]. We define a field theory in $d = 0$ dimensions which couples two real fields, ϕ and χ, with masses m and M respectively with the action

$$S = \frac{m^2}{2}\phi^2 + \frac{M^2}{2}\chi^2 + \frac{\lambda}{4}\phi^2\chi^2\,, \tag{2.1.1}$$

which has no integration over spacetime due to the theory being defined in $d = 0$ dimensions. The generating functional of this theory is

$$\mathcal{Z} = \int_{-\infty}^{\infty} d\phi d\chi \exp\{-S\} \ . \tag{2.1.2}$$

We see that we may easily compute the integral over one of the fields, with the integral taking the form of a Gaussian integral. Choosing to integrate out χ[1] we find that the generating functional now takes the form

$$\mathcal{Z} = \int_{-\infty}^{\infty} d\phi \exp\left\{\ln\left[e^{-\frac{m^2}{2}\phi^2}\sqrt{\frac{2\pi}{M^2+\lambda\phi^2/2}}\right]\right\} \equiv \int_{-\infty}^{\infty} d\phi \exp\{-S_{\text{Eff.}}\} \ , \tag{2.1.3}$$

where we have now defined the *effective action*, $S_{\text{Eff.}}$. Working now in the limit $M \gg m$ we can expand this effective action as

$$S_{\text{Eff.}} = \frac{m^2\phi^2}{2} + \frac{\lambda\phi^2}{4M^2} - \frac{\lambda^2\phi^4}{16M^4} + \frac{\lambda^3\phi^6}{48M^6} + \dots \ . \tag{2.1.4}$$

From Eq. 2.1.4 we can see the consequences of integrating over the heavy field, χ, (a process known as integrating out the heavy field): the mass of ϕ has been shifted by a finite amount and we have generated an action which now only results in self interactions of the lighter field, ϕ. In fact, there is an infinite series of ϕ self-interaction terms, each generating couplings between an increasing number of ϕ fields, which are suppressed by increasing powers of the heavy mass, M. This is a typical result of integrating out a heavy field in a theory to produce an EFT, a *tower* of *effective operators* emerge, with increasingly smaller couplings. Often, one reframes an effective action in terms of *Wilson coefficients* as

$$\begin{aligned} S_{\text{Eff.}} &= \frac{m_{\text{Eff.}}^2\phi^2}{2} + C_1\phi^4 + C_2\phi^6 + \dots \ , \\ m_{\text{Eff.}} = m^2 + \frac{\lambda}{2M^2} \ , &\quad C_1 = -\frac{\lambda^2}{16M^4} \ , \quad C_2 = \frac{\lambda^3}{48M^6} \ , \end{aligned} \tag{2.1.5}$$

where we have written the mass term in terms of an effective mass, and where C_i are the Wilson coefficients. Practically, for using an effective action to calculate observables we must take only a finite number of the effective operators, i.e. we must *truncate* the tower of effective operators at some power in the heavy scale.

An example that is more pertinent to the study of the fields of the SM in an EFT context is that of the 4-Fermi theory of weak decays [49]. Here we consider interactions occurring at scales far below the mass of the weak gauge bosons and

[1] A consequence of integrating over χ is that we are now restricted to calculating amplitudes with only ϕ as the external field.

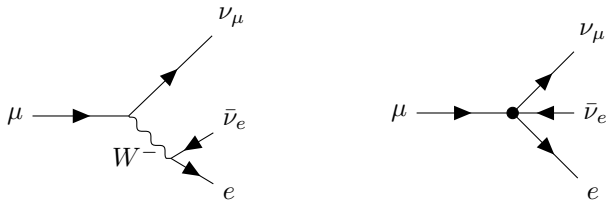

Figure 2.1: *LO diagrams of $\mu \to e\nu_\mu\bar{\nu}_e$ from the Lagrangians in Eq. 2.1.6. Here, (1) is the LO diagram for this process from the Lagrangian on the top line of Eq. 2.1.6, while (2) is the LO diagram for this process from the Lagrangian on the last line of Eq. 2.1.6. We see that the internal W propagator in (1) is contracted to a point in (2) to form and effective vertex, here represented by a dot.*

can therefore integrate out the weak gauge bosons. The example of integrating out the heavy fields in this instance is distinctly more complex than the $d = 0$ real scalar field example at the beginning of Section 2.1.1, although the process is well understood [50]. In this instance, after integrating out the heavy W- and Z-bosons (and truncating the resulting tower of operators to include only the LO term) we can replace the gauge boson-fermion interaction part of the weak Lagrangian (which we denote $\mathcal{L}_{\mathrm{W}}$) with an effective Lagrangian in which there are no weak gauge bosons

$$\begin{aligned}\mathcal{L}_{\mathrm{W}} &= -\frac{g_2}{2\sqrt{2}}\left(J^\mu W_\mu + J^{\dagger\mu}W_\mu^\dagger\right) - \frac{g_2}{2c_w}J_n^\mu Z_\mu \\ &\to -\frac{G_F}{\sqrt{2}}\left(J^\mu J_\mu^\dagger + J_n^\mu J_{n\mu}\right)\,, \end{aligned} \tag{2.1.6}$$

where (considering only lepton interactions for simplicity)

$$\begin{aligned} J^\mu &= 2\bar{\nu}_e\gamma^\mu P_L e\,, \\ J_n^\mu &= \bar{\nu}_e\gamma^\mu\nu_e - \bar{e}(P_L - 2s_w)e\,, \end{aligned} \tag{2.1.7}$$

and where G_F is known as the *Fermi constant* and at LO is given by

$$\frac{G_F}{\sqrt{2}} = \frac{g_2^2}{8M_W^2}\,. \tag{2.1.8}$$

We see now that the effective Lagrangian in Eq. 2.1.6 is built up of terms of the form $\sim G_F(\bar{\psi}\psi)(\bar{\psi}\psi)$ for fermionic fields, ψ, and that the weak gauge bosons are no longer present in the theory. These so-called *four-fermion* interactions do not exist in the SM and constitute effective interactions, with the corresponding Wilson coefficients being some function of G_F. The LO diagrams for muon decay from both Lagrangians in Eq. 2.1.6 are given in Fig. 2.1 as an example of the difference between the "full" and effective Lagrangian at the same order in perturbation theory. The

corresponding amplitudes are (in Feynman gauge)

$$\begin{aligned} i\mathcal{M}_{\text{Full}} &= i\left(\frac{g_2}{\sqrt{2}}\right)^2 \left(\bar{u}_e \gamma_\mu P_L v_{\nu_e}\right) \left(\frac{g^{\mu\nu}}{k^2 - M_W^2}\right) \left(\bar{u}_{\nu_\mu} \gamma_\nu P_L u_\mu\right) , \\ i\mathcal{M}_{\text{4-Fermi}} &= -i4\frac{G_F}{\sqrt{2}} \left(\bar{u}_e \gamma_\mu P_L v_{\nu_e}\right) \left(\bar{u}_{\nu_\mu} \gamma^\mu P_L u_\mu\right) . \end{aligned} \tag{2.1.9}$$

Considering the W propagator in the top line of Eq. 2.1.9 to be occurring at low momentum transfer compared to the mass of the W-boson we find we can expand the propagator as

$$\frac{1}{k^2 - M_W^2} = -\frac{1}{M_W^2}\left(1 + \frac{k^2}{M_W^2} + \frac{k^4}{M_W^4} + \dots\right) . \tag{2.1.10}$$

Using the LO expansion of the W propagator in $\mathcal{M}_{\text{Full}}$ we recover $\mathcal{M}_{\text{4-Fermi}}$. This process of expansion in the small parameter and matching is equivalent to the process of integrating out the heavy W fields and also demonstrates that the range of applicability of 4-Fermi theory is at scales $k^2 \ll M_W^2$. We could, of course, choose to keep terms beyond LO from the expansion in Eq. 2.1.10; choosing to keep n terms in this expansion we find that 4-Fermi theory is accurate to the full theory to an accuracy of $(k^2/M_W^2)^n$. This ratio of k^2/M_W^2 constitutes a *power counting* parameter – that is a parameter that allows us to keep track of the accuracy of our EFT calculation in relation to the full theory.

Further, we find that these effective operators are of mass dimension 6, a feature not found in the SM where all terms are generated by operators of mass dimension 4 and lower. Examining Eq. 2.1.8, we also recover another feature of EFTs previously discussed, that being that the Wilson coefficients are suppressed by the scale of the heavy physics, in this case the W boson mass, M_W. This also ensures that the combination of the operator and the Wilson coefficient are of mass dimension 4 – a requirement such that the action is dimensionless in 4-dimensional spacetime.

Presented in this way, the two examples here constitute *top-down* EFTs. In the case of a top-down EFT the full theory is known at all scales and the effective theory is derived from this by integrating out the heavy degrees of freedom. This generates an effective Lagrangian which is valid up to scales below that of the heavy scale of the full theory, and relations between the effective couplings and the couplings of the full theory. Conversely, one may also consider the case of a *bottom-up* EFT, where the full theory is not known, and the physics resulting from the unknown high-scale theory is described by effective operators with Wilson coefficients of unknown values, which must be measured experimentally. In fact, 4-Fermi theory was first proposed as a bottom-up EFT, with the value of G_F first being measured experimentally

before the emergence of electroweak theory, which allowed the parameterization of G_F in terms of more fundamental parameters.

2.1.2 Operator Running and Mixing

A feature of an EFT with multiple operators is that we observe the mixing of these operators between scales. This mixing can be understood from the perspective of the operators themselves, or from the corresponding Wilson coefficients; we choose the Wilson coefficient perspective. In this way, a Wilson coefficient at one scale potentially mixes into multiple coefficients at a different scale. This behavior is summarized as

$$\dot{C}_i \equiv \frac{dC_i}{d\ln(\mu)} = 16\pi^2 \gamma_{ij} C_j \,, \tag{2.1.11}$$

where γ_{ij} is the anomalous dimension matrix.

In the renormalization of EFTs at NLO we observe that we must also renormalize the Wilson coefficients themselves. In the $\overline{\text{MS}}$ scheme (as is appropriate for bottom-up EFTs) we can therefore define our renormalization constants for the Wilson coefficients according to

$$C_i^{(0)} = \mu^{2\varepsilon}[Z_c(\mu)]_{ij} C_j(\mu) = \mu^{2\varepsilon}\left(\delta_{ij} + [\delta Z_c(\mu)]_{ij}\right) C_j(\mu) = \mu^{2\varepsilon}\left(C_i(\mu) + \delta C_i(\mu)\right) \,, \tag{2.1.12}$$

where the renormalization constant matrix, Z_c, (and its corresponding expansion) accounts for the potential Wilson coefficient mixing. Similarly, δC_i may be a function of multiple Wilson coefficients. Using that the bare Wilson coefficient has no μ dependence we may write (suppressing the μ-dependent arguments)

$$\frac{dC_i^{(0)}}{d\ln(\mu)} = 0 = \frac{d(\mu^{2\varepsilon}[Z_c]_{ij})}{d\ln(\mu)} C_j + \mu^{2\varepsilon}[Z_c]_{ij}\dot{C}_j \,, \tag{2.1.13}$$

from which we may recover that

$$\gamma_{ij} = \frac{1}{16\pi^2}\mu^{-2\varepsilon}[Z_c^{-1}]_{ik}\frac{d(\mu^{2\varepsilon}[Z_c]_{kj})}{d\ln(\mu)} \,. \tag{2.1.14}$$

In the $\overline{\text{MS}}$ scheme, each term in the counterterms are accompanied by a UV pole, allowing us to write

$$\mu^{2\varepsilon}[\delta Z_c]_{ij} = \frac{A_{ij}}{\varepsilon} + 2A_{ij}\ln(\mu) + \mathcal{O}(\varepsilon) \,, \tag{2.1.15}$$

where A_{ij} is some unspecified constant. From Eq. 2.1.15 it is clear that we may

extract the form of the A_{ij} piece as

$$\begin{aligned} A_{ij} &= \frac{1}{2}\frac{d(\mu^{2\varepsilon}[Z_c]_{ij})}{d\ln(\mu)} \\ &= \frac{1}{2}[Z_c^{-1}]_{ik}\frac{d(\mu^{2\varepsilon}[Z_c]_{kj})}{d\ln(\mu)} + \text{NNLO terms} \\ &= \frac{1}{2}\mu^{2\varepsilon}\gamma_{ij} \\ &= \frac{1}{2}\gamma_{ij} + \mathcal{O}(\varepsilon)\,. \end{aligned} \tag{2.1.16}$$

We can therefore entirely reconstruct the pole structure of the Wilson coefficient counterterm, δC_i, from the Wilson coefficient anomalous dimension

$$\delta C_i = \frac{1}{2\varepsilon}\gamma_{ij}C_j = \frac{1}{16\pi^2}\frac{1}{2\varepsilon}\dot{C}_i\,. \tag{2.1.17}$$

2.1.3 Minimal Flavor Violation

The SM Lagrangian explored throughout Chapter 1 has the fermion content of two $SU(2)$ doublets and three $SU(2)$ singlets which (almost) exhibits a large global symmetry under the group $\mathcal{G}_f = U(3)^5$, i.e. under the transformations

$$\begin{gathered} q \to U_q q\,, \quad u \to U_u u\,, \quad d \to U_d d\,, \\ l \to U_l l\,, \quad e \to U_e e\,. \end{gathered} \tag{2.1.18}$$

We state that the SM *almost* exhibits a symmetry under these transformations as the Yukawa interactions in Eq. 1.1.34 break this symmetry. Applying the transformation in Eq. 2.1.3, the Yukawa interactions of Eq. 1.1.34 become

$$\begin{aligned} \mathcal{L}_{\text{yuk.}} \to -U_l^{\dagger\,mi}Y_e^{ij}{U_e}^{jn}\bar{l}_m H e_n - U_q^{\dagger\,mi}Y_d^{ij}{U_d}^{jn}\bar{q}_m H d_n \\ - U_q^{\dagger\,mi}Y_u^{ij}{U_u}^{jn}\bar{q}_m \tilde{H} u_n + \text{h.c.}\,, \end{aligned} \tag{2.1.19}$$

demonstrating the breaking of the symmetry under $\mathcal{G}_f$. From Eq. 2.1.19 we see that we can restore the Yukawa Lagrangian's invariance under the symmetry group $\mathcal{G}_f$ by treating the Yukawa matrices as *spurions* – constant fields that transform under the group $\mathcal{G}_f$ as

$$Y_e \to U_l Y_e U_e^\dagger\,, \quad Y_d \to U_q Y_d U_d^\dagger\,, \quad Y_u \to U_q Y_u U_u^\dagger\,, \tag{2.1.20}$$

such that the Lagrangian in 2.1.19 takes the same form as that seen in Eq. 1.1.34. In the context of EFTs, the Minimal Flavor Violation (MFV) hypothesis is that the source of symmetry breaking of the group $\mathcal{G}_f$ in any additional higher-dimensional operators proceeds in the same way as for the Yukawa interaction, i.e. when treating

the Yukawa matrices as spurions any additional higher-dimensional operators must be invariant under the symmetry group $\mathcal{G}_f$ [51–53]. Of course, we are by no means compelled to enforce MFV in effective operators, however, in EFTs with a large number of operators, such as in the dimension-6 SMEFT, enforcing MFV can reduce the total number of operators contributing to an observable, and as we shall see, can also provide scenarios in which to test the MFV hypothesis.

In principle, one may enforce MFV when constructing operators of a bottom-up EFT, incorporating the Yukawa matrices into the operators themselves. In some scenarios however, such as that which we will explore in Section 2.2.2, where the form of the operators are already defined, MFV can instead be imposed by placing restrictions on the form of the corresponding Wilson coefficients.

2.2 The Standard Model Effective Field Theory

Following from our discussion of bottom-up EFTs in Section 2.1.1, we now turn to a particular example of such an EFT, the SMEFT. In Section 2.2.1 we give a general introduction to the SMEFT, and in Section 2.1.3 we discuss MFV, which was first introduced in Section 2.1.3, but here discussed in the context of the SMEFT.

2.2.1 Introduction to the SMEFT

The SMEFT is a bottom-up EFT where higher dimensional operators are constructed with few assumptions made about the physics above the cut-off, except that any new particles have a mass of approximately the scale of the cut-off, Λ_{NP}, or above, and obey fundamental principles such as Poincaré invariance. Specifically, the SMEFT consists of adding to the SM Lagrangian all possible operators that can be built from SM fields obeying Poincaré and SM gauge symmetries. This guarantees that the corresponding physics that the SMEFT aims to describe also respects these symmetries or a larger symmetry group which is broken to the symmetry group of the SM. The SMEFT also assumes that the Higgs and Goldstone bosons are arranged into an $SU(2)$ doublet, such as that introduced in Eq. 1.1.14. As a result, the SMEFT describes all beyond Standard Model (BSM) physics compatible with the aforementioned assumptions without any bias towards a particular UV completion of such physics. Drawing on the examples described throughout Section 2.1.1, all Wilson coefficients must be suppressed by the correct power of the *new physics* (NP) scale such that the combination of the operator and Wilson coefficient remains dimensionless. Specifically, an operator of dimension n must have a corresponding Wilson coefficient of dimensions $4 - n$. We may therefore write our SMEFT

Lagrangian as

$$\mathcal{L}_{\text{SMEFT}} = \mathcal{L}_{\text{SM}} + \sum_{k=1} \mathcal{L}^{(k+4)} \,, \tag{2.2.1}$$

where $\mathcal{L}^{(n)}$ represents the Lagrangian comprising all operators of mass dimension $n > 4$. We further split each $\mathcal{L}^{(n)}$ into a sum of Wilson coefficients and operators as

$$\mathcal{L}^{(n)} = \sum_i C_i^{(n)} Q_i^{(n)} = \sum_i \frac{\widetilde{C}_i^{(n)}}{\Lambda_{\text{NP}}^{n-4}} Q_i^{(n)} \,, \tag{2.2.2}$$

where on the right of Eq. 2.2.2 we have explicitly separated out the factor of Λ_{NP} from the Wilson coefficient such that the Wilson coefficient with the tilde is dimensionless.

With each $\mathcal{L}^{(n)}$ of increasing n containing Wilson coefficients with increasing inverse powers of Λ_{NP} suppressing the effects of the corresponding operators, it is natural to first consider the leading (and therefore potentially dominant) term in this expansion in Λ_{NP}, these being the operators within $\mathcal{L}^{(5)}$. At this mass dimension for one fermion generation there is only one operator, often referred to as the *Weinberg operator* [54]

$$Q_{rs}^{\nu\nu} = \varepsilon_{ij}\varepsilon_{mn} H^i H^m l_r^{jT} l_s^{nC} \,. \tag{2.2.3}$$

This lepton-number-violating operator can generate neutrino masses, however, placing experimental constraints from measured neutrino masses on Λ_{NP} with $C_{\nu\nu} \sim 1$ gives that $\Lambda_{\text{NP}} \geqslant 10^{13}$ TeV. Conversely, with $\Lambda_{\text{NP}} \sim 1$ TeV gives $C_{\nu\nu} \leqslant 10^{-13}$. From an experimental standpoint, in the first scenario such an energy range is far beyond the projected energy scales of any current or future collider, while in the latter scenario the projected size of the Wilson coefficient is far beyond the precision of any current or future collider.

Naturally, we next consider the dimension-6 SMEFT Lagrangian, $\mathcal{L}^{(6)}$. Here, the Wilson coefficients are suppressed by two inverse powers of the new physics scale Λ_{NP}. We could in principle write down a vast set of operators satisfying the assumptions imposed by the SMEFT, however, it is found that many of these operators may be related by the equations of motion (EoM) of the corresponding fields. The result is that two apparently distinct operators are, in fact, equivalent. To illustrate this, we consider the simple example of a real scalar field, h, with a 4-point self-interaction augmented with the addition of two dimension-6 operators suppressed by the NP scale. The Lagrangian for this theory is given by

$$\mathcal{L} = \frac{1}{2}(\partial_\mu h)(\partial^\mu h) - \frac{1}{2}m^2 h^2 + \frac{\lambda}{4}h^4 + Q_1 + Q_2 \,, \tag{2.2.4}$$

where

$$Q_1 = \frac{\tilde{C}_1}{\Lambda_{\rm NP}^2} h^3 \partial^2 h \,,$$
$$Q_2 = \frac{\tilde{C}_2}{\Lambda_{\rm NP}^2} h^6 \,. \tag{2.2.5}$$

The corresponding EoM for h is thus given by

$$\partial^2 h = -m^2 h + \lambda h^3 + \mathcal{O}(\Lambda_{\rm NP}^{-2}) \,, \tag{2.2.6}$$

where terms in the EoM resulting from dimension-6 operators are contained within $\mathcal{O}(\Lambda_{\rm NP}^{-2})$. Using the EoM in Eq. 2.2.6 in the operator Q_1 we find

$$Q_1 = \lambda \frac{\tilde{C}_1}{\tilde{C}_2} Q_2 - \frac{\tilde{C}_2}{\Lambda_{\rm NP}^2} m^2 h^4 + \mathcal{O}(\Lambda_{\rm NP}^{-4}) \,. \tag{2.2.7}$$

From the above equation we see that the operators Q_1 and Q_2 are related by the EoM and are therefore not independent. Using this form of Q_1 in the Lagrangian in Eq. 2.2.4 we find that it now takes the form

$$\mathcal{L} = \frac{1}{2}(\partial_\mu h)(\partial^\mu h) - \frac{1}{2} m^2 h^2 + \frac{\lambda'}{4} h^4 + \eta Q_2 \,, \tag{2.2.8}$$

where

$$\lambda' = \lambda - 4m^2 \frac{\tilde{C}_2}{\Lambda_{\rm NP}^2} \,,$$
$$\eta = 1 + \lambda \frac{\tilde{C}_1}{\tilde{C}_2} \,. \tag{2.2.9}$$

Comparing the Lagrangians in Eq. 2.2.4 and Eq. 2.2.8 we see that they are equivalent up to the removal of Q_1 and a rescaling of the Wilson coefficient of Q_2 and coupling constant λ. As a result we see that the operator Q_1 was entirely redundant to the theory, such that including it in Eq. 2.2.4 constituted using an *over-complete basis*. This example demonstrates the importance of a *minimal basis* of effective operators. We also see that while keeping a consistent power counting in $\Lambda_{\rm NP}$, from Eq. 2.2.7 we only need the EoM from the dimension-4 components of the Lagrangian in Eq. 2.2.4. This is because using dimension-6 components of the EoM to transform a dimension-6 operator leads to dimension-8 effects, which we drop. This effect clearly carries over to the SMEFT, where we only require the SM EoMs to relate operators appearing at dimension-6. Similar redundancies to those seen in the example above can in general also be derived by performing integration by parts on operators involving derivatives.

The first attempt to characterize a minimal basis for the dimension-6 SMEFT was

performed by Buchmüller and Wyler in [55], who compiled a basis of 80 operators. Over the next several years it was found that their proposed basis was overcomplete and operators could be entirely removed using techniques similar to those outlined in the previous example. The earliest successful characterization of the dimension-6 SMEFT operators in a minimal basis was first described in [56]. The basis proposed here, now commonly referred to as the *Warsaw basis* is the basis of choice for the calculations performed throughout this work, and the corresponding operators are listed in Table A.1 in Appendix A. In total, this basis comprises of 59 independent lepton- and baryon-number conserving operators (and an additional four lepton- and baryon-number violating operators, which we do not consider) for a single fermion generation. This number increases to 2499 independent operators when allowing for full fermion flavor structure. This basis splits operators into groups according to the field content of the operators, for example, class 1 contains operators built entirely from field strength tensors (and dual tensors), class 2 contains operators build solely from Higgs doublets, class 3 contains operators built from Higgs doublets and covariant derivatives, etc. When compiling a basis of such operators, there is a large degree of freedom when choosing a minimal basis, and the Warsaw basis outlined here is by no means the only choice. Additional other basis choices also exist, for example, the SILH basis [57] and the Higgs basis [58].

Beyond dimension-6 there is the set of lepton- and baryon-number violating dimension-7 operators [59, 60], followed by the large set of dimension-8 operators[1] [61, 62] and beyond. Due to the increasing suppression of such operators by increasing powers of Λ_{NP}, we neglect the effects of operators beyond dimension-6 throughout this work.

2.2.2 Minimal Flavor Violation in the SMEFT

As stated, in an MFV scenario higher-dimensional operators must be invariant under the symmetry group $\mathcal{G}_f$ when Yukawa matrices are treated as spurions. In principle, this can be implemented by simply including the appropriate Yukawa matrices into the form of a higher-dimensional operator. For the SMEFT, in particular in the Warsaw basis where the form of the operators are already defined, we must be more careful. The consequences of enforcing MFV in the context of the dimension-6 SMEFT have been explored in [63]. Here, the SMEFT operators in Table A.1 have MFV imposed via restrictions placed on the form of the corresponding Wilson coefficients. In particular, it is recognized that the Wilson coefficients of fermion flavor independent operators of classes 1-4 can only be a function of the *flavor*

[1] Allowing for full flavor structure in a minimal basis, in total there are 36971 dimension-8 operators.

invariants

$$\mathrm{Tr}\left[f(Y_eY_e^\dagger)\right] \ , \quad \mathrm{Tr}\left[f(Y_dY_d^\dagger, Y_uY_u^\dagger)\right] \ , \tag{2.2.10}$$

where the function, f, may be different for each operator. Imposing MFV, the class-5 operators have Wilson coefficients which take the form

$$\begin{aligned} C_{\substack{eH \\ rs}} &= \left[Y_eG_{eH}(Y_eY_e^\dagger)\right]_{rs} \ , \\ C_{\substack{uH \\ rs}} &= \left[Y_uG_{uH}(Y_dY_d^\dagger, Y_uY_u^\dagger)\right]_{rs} \ , \\ C_{\substack{dH \\ rs}} &= \left[Y_dG_{dH}(Y_dY_d^\dagger, Y_uY_u^\dagger)\right]_{rs} \ , \end{aligned} \tag{2.2.11}$$

where the G_i are functions unique to each Wilson coefficient. Similarly, we see that the class-6 operators have the same fermionic structure as the class-5 operators (with the addition of $\sigma^{\mu\nu}$ placed between the fermionic components) and so the structures of the class-6 Wilson coefficients in MFV follow analogously to those seen in Eq. 2.2.11. For class-7 operators, under MFV the Wilson coefficients must take the following form

$$\begin{aligned} C^{(1,3)}_{\substack{Hl \\ rs}} &= \left[G^{(1,3)}_{Hl}(Y_eY_e^\dagger)\right]_{rs} \ , \\ C_{\substack{He \\ rs}} &= H_{He}\delta_{rs} + \left[Y_e^\dagger G_{He}(Y_eY_e^\dagger)Y_e\right]_{rs} \ , \\ C^{(1,3)}_{\substack{Hq \\ rs}} &= \left[G^{(1,3)}_{Hq}(Y_dY_d^\dagger, Y_uY_u^\dagger)\right]_{rs} \ , \\ C_{\substack{Hu \\ rs}} &= H_{Hu}\delta_{rs} + \left[Y_u^\dagger G_{Hu}(Y_dY_d^\dagger, Y_uY_u^\dagger)Y_u\right]_{rs} \ , \\ C_{\substack{Hd \\ rs}} &= H_{Hd}\delta_{rs} + \left[Y_d^\dagger G_{Hd}(Y_dY_d^\dagger, Y_uY_u^\dagger)Y_d\right]_{rs} \ , \\ C_{\substack{Hud \\ rs}} &= \left[Y_u^\dagger G_{Hud}(Y_dY_d^\dagger, Y_uY_u^\dagger)Y_d\right]_{rs} \ , \end{aligned} \tag{2.2.12}$$

where the H_i are constants. Class 8 contains the entire set of four-fermion operators within the SMEFT, where the fermionic structure of these operators can be built entirely from the fermionic structure of the operators in the flavor-dependent lower classes: classes 5, 6, and 7. For example, the class-8 operator $Q^{(1)}_{quqd}$ is built from the fermion structure contained within the class-5 operators Q_{uH} and Q_{dH}. As a result, the structure of the class-8 operator's Wilson coefficients can also be built from a combination of the structures contained throughout Eqs. 2.2.11 and 2.2.12.

2.3 The SMEFT in the Mass Basis

For the purposes of performing calculations within the SMEFT at energy scales accessible to colliders in a way that allows us to make a connection between our

Lagrangian and any observables, we must consider the SMEFT in the mass basis after EWSB. Here we review the ways in which the additional dimension-6 operators alter many of the tree-level relations of the SM, how we address these changes, and how the dimension-6 SMEFT Lagrangian can be rewritten to more closely resemble that of the SM. Of course, the latter of these changes is not strictly necessary, but as we will see, this parity with the SM will be useful for calculational purposes. In this section we closely follow the discussion of [63].

2.3.1 The Higgs Doublet, Vacuum Expectation Value, and Mass

The class-2 operator Q_H is a function of only the gauge-invariant object $H^\dagger H$ and therefore shifts the position of the LO vev found in the SM. Including dimension-6 effects with the SM Higgs potential in Eq. 1.1.10, the Higgs potential now takes the form

$$V(H) = \lambda\left(H^\dagger H - \frac{v_0^2}{2}\right)^2 + C_H(H^\dagger H)^3\,, \tag{2.3.1}$$

where we have rewritten the SM part of this potential in comparison with Eq. 1.1.10 to emphasize the position of the SM vev. Calculating the position of the Higgs vev given the potential in Eq. 2.3.1 one finds that the LO vev is shifted by dimension-6 corrections from the SM value, v_0, according to

$$\langle H_0^\dagger H_0\rangle \equiv \frac{1}{2}v_T^2 = \frac{v_0^2}{2}\left(1 + \frac{3v_0 C_H}{4\lambda}\right)\,. \tag{2.3.2}$$

It is now the quantity v_T which represents the LO vev of the Higgs doublet. The quantity v_0 is now simply some combination of SM parameters and no longer represents the position of the Higgs vev at LO.

As previously stated, class 3 introduces operators that involve combinations of the gauge-invariant quantity $H^\dagger H$ and derivative terms. As a result, these terms contribute to the kinetic terms of fields found in the Higgs doublet, these being the Higgs field for unitary gauge, and additionally for the neutral and charged Goldstone bosons the R_ξ gauges. Working in R_ξ gauge, the kinetic terms for the fields in the Higgs doublet in the dimension-6 SMEFT thus have the form

$$\begin{aligned}\mathcal{L}_{H,kin.}^{\text{D6 SMEFT}} &= \frac{1}{2}(\partial_\mu h)(\partial^\mu h) + \frac{1}{2}(\partial_\mu \phi^0)(\partial^\mu \phi^0) + (\partial_\mu \phi^-)(\partial^\mu \phi^+) \\ &\quad - v_T^2 C_{H\Box}(\partial_\mu h)(\partial^\mu h) + \frac{v_T^2}{4}C_{HD}(\partial_\mu h)(\partial^\mu h) + \frac{v_T^2}{4}C_{HD}(\partial_\mu \phi^0)(\partial^\mu \phi^0)\,.\end{aligned} \tag{2.3.3}$$

Firstly, we note that in Eq. 2.3.3 the charged Goldstone bosons, $\phi^{\pm}$, retain their canonical normalization, and so no further changes need to be made. For the Higgs field, h, and the neutral Goldstone boson, ϕ^0, to retain canonical normalization, and therefore retain the form of their propagators found in the SM, we must make the following field redefinitions

$$\begin{aligned} h &\to \left(1 + v_T^2 C_{H\Box} - \frac{v_T^2}{4} C_{HD}\right) h\,, \\ \phi^0 &\to \left(1 - \frac{v_T^2}{4} C_{HD}\right) \phi^0\,. \end{aligned} \tag{2.3.4}$$

As a result, the Higgs doublet is written in R_ξ gauge as

$$H(x) = \frac{1}{\sqrt{2}} \begin{pmatrix} -\sqrt{2} i \phi^+(x) \\ \left[1 + C_{H,\text{kin}}\right] h(x) + i \left[1 - \frac{v_T^2}{4} C_{HD}\right] \phi^0(x) + v_T \end{pmatrix}, \tag{2.3.5}$$

where we have defined

$$C_{H,\text{kin}} \equiv \left(C_{H\Box} - \frac{1}{4} C_{HD}\right) v_T^2\,. \tag{2.3.6}$$

As in the SM, the unitary gauge form of the Higgs doublet can be recovered from Eq. 2.3.5 by performing a gauge transformation that removes the charged and neutral Goldstone bosons, equivalent to setting these fields to zero in Eq. 2.3.5. We also note here that as the fields in the Higgs doublet have been scaled by constant quantities as specified by Eq. 2.3.4, these rescalings have no effect on the position of the vev of the Higgs potential. As a result, the form of the vev in Eq. 2.3.2 is still valid.

Finally, using the form of the Higgs doublet in Eq. 2.3.5 in the dimension-6 SMEFT Lagrangian, and considering terms proportional to h^2 we may find that the Higgs mass now takes the form

$$m_H^2 = 2\lambda v_T^2 \left(1 - \frac{3 v_T^2}{2\lambda} C_H + 2 C_{H,\text{kin}}\right), \tag{2.3.7}$$

and so receives shifts due to dimension-6 SMEFT Wilson coefficients as compared to the SM result in Eq. 1.1.15.

2.3.2 Gauge Fields

In Section 1.1.2 we reviewed the process of defining the mass basis of the gauge bosons in the SM. In the dimension-6 SMEFT, operators introduce additional $\mathcal{O}(\Lambda_{\text{NP}}^{-2})$ effects to this definition. Taking the notation for the $SU(2) \times U(1)$ covariant derivative defined in Eq. 1.1.17 we extend this to include the full symmetry group of the SM, i.e. we also include pieces related to the $SU(3)$ gauge group so that the covariant

derivative of the full SM now reads

$$D_\mu = \partial_\mu - i(g\tau)^a A^a_\mu - ig_3 T^A G^A_\mu \,, \tag{2.3.8}$$

where again $A^a_\mu = (W^1_\mu, W^2_\mu, W^3_\mu, B_\mu)$, and the generators are denoted $(g\tau)^a = (g_2\tau^1, g_2\tau^2, g_2\tau^3, g_1 Y)$, where $\tau^I = \sigma^I/2$ with σ^I the Pauli matrices, T^A the Gell-Mann matrices, and Y the hypercharge. Examining the form of the class-4 operators Q_{HW}, Q_{HB}, Q_{HWB} and Q_{HG} we find that they generate additional kinetic terms for the gauge fields B_μ, W^I_μ and G^A_μ respectively. Considering such kinetic terms arising from both the SM and the dimension-6 SMEFT we have

$$\begin{aligned}\mathcal{L}_{\text{Gauge,kin.}} = &-\frac{1}{4}B_{\mu\nu}B^{\mu\nu} - \frac{1}{4}W^I_{\mu\nu}W^{I,\mu\nu} - \frac{1}{4}G^A_{\mu\nu}G^{A,\mu\nu} \\ &+ \frac{v_T^2}{2}C_{HB}B_{\mu\nu}B^{\mu\nu} + \frac{v_T^2}{2}C_{HW}W^I_{\mu\nu}W^{I,\mu\nu} + \frac{v_T^2}{2}C_{HG}G^A_{\mu\nu}G^{A,\mu\nu} \\ &- \frac{v_T^2}{2}C_{HWB}W^3_{\mu\nu}B^{\mu\nu} \,,\end{aligned} \tag{2.3.9}$$

where clearly the canonical normalization of these terms present in the SM is no longer apparent. We can begin to restore the canonical normalization by making linear shifts in the gauge fields, which we choose to be

$$\begin{aligned}B_\mu &= \left(1 + v_T^2 C_{HB}\right)\mathcal{B}_\mu \,, \\ W^I_\mu &= \left(1 + v_T^2 C_{HW}\right)\mathcal{W}^I_\mu \,, \\ G^A_\mu &= \left(1 + v_T^2 C_{HG}\right)\mathcal{G}^A_\mu \,,\end{aligned} \tag{2.3.10}$$

which ensures the correct canonical normalization of the gluon fields. Clearly, these shifts will also affect the form of the covariant derivative in Eq. 2.3.8. We note however, that by defining new "barred" couplings as

$$\begin{aligned}\bar{g}_1 &= (1 + v_T^2 C_{HB})g_1 \,, \\ \bar{g}_2 &= (1 + v_T^2 C_{HW})g_2 \,, \\ \bar{g}_3 &= (1 + v_T^2 C_{HG})g_3 \,,\end{aligned} \tag{2.3.11}$$

the combinations $g_1 B_\mu = \bar{g}_1 \mathcal{B}_\mu$, $g_2 W^I_\mu = \bar{g}_2 \mathcal{W}^I_\mu$, and $g_3 G^A_\mu = \bar{g}_3 \mathcal{G}^A_\mu$ remain unchanged.

As stated, the shifts in the gauge fields defined in Eq. 2.3.10 are sufficient for the canonical normalization of the gluon fields. This is apparent when we rewrite Eq. 2.3.9 in terms of the "calligraphic" gauge fields

$$\mathcal{L} = -\frac{1}{4}\mathcal{B}_{\mu\nu}\mathcal{B}^{\mu\nu} - \frac{1}{2}\mathcal{W}^I_{\mu\nu}\mathcal{W}^{I,\mu\nu} - \frac{1}{4}\mathcal{G}^A_{\mu\nu}\mathcal{G}^{A,\mu\nu} - \frac{v_T^2}{2}C_{HWB}\mathcal{W}^3_{\mu\nu}\mathcal{B}^{\mu\nu} \,. \tag{2.3.12}$$

In Eq. 2.3.12 we also see that there is a kinetic-type mixing term between $\mathcal{B}_\mu$ and $\mathcal{W}^3_\mu$.

For canonical normalization of these fields, this mixing term must also be removed. This term can be removed by a linear shift in these fields, which proceeds as

$$\mathcal{A}_\mu^a = M^{ab} A_\mu'^b \,, \tag{2.3.13}$$

where $A_\mu'^a = (W_\mu'^1, W_\mu'^2, W_\mu'^3, B_\mu')$ and

$$M = \begin{pmatrix} \mathbf{1}_{2\times2} & \mathbf{0}_{2\times2} \\ \mathbf{0}_{2\times2} & m \end{pmatrix}, \qquad m = \begin{pmatrix} 1 & -\frac{1}{2}v_T^2 C_{HWB} \\ -\frac{1}{2}v_T^2 C_{HWB} & 1 \end{pmatrix}, \tag{2.3.14}$$

such that the new "primed" gauge fields have diagonal and canonically normalized kinetic terms. Similarly to what we saw in Section 1.1.2, these gauge fields are not the physically observed gauge fields after EWSB. Again, we must rotate the gauge fields to the mass basis to recover the physically observed fields. In the dimension-6 SMEFT the mass terms of the primed gauge fields after making all of the above shifts are given by

$$\begin{aligned} \mathcal{L}_{\text{Gauge,mass}} = \frac{v_T^2}{8}\bar{g}_2 \left[(W_\mu'^1)^2 + (W_\mu'^2)^2\right] + \left(\frac{v_T^2}{8} + \frac{v_T^4}{16}C_{HD}\right)\left(\bar{g}_2 W_\mu'^3 - \bar{g}_1 B_\mu'\right)^2 \\ + \left(\bar{g}_2 W_\mu'^3 - \bar{g}_1 B_\mu'\right)\left(v_T^2 C_{HWB} W'^{3,\mu} - v_T^2 C_{HWB} B'^\mu\right) . \end{aligned} \tag{2.3.15}$$

We can obtain the above expression in the mass basis with massive W- and Z-bosons, and a massless photon, where also the charged $W^\pm$ bosons have the correct electric charges by the rotation

$$A_\mu'^a = R^{ab}\tilde{A}_\mu^b \,, \tag{2.3.16}$$

where $\tilde{A}_\mu^a$ comprises the physical gauge fields as $\tilde{A}_\mu = (\mathcal{W}_\mu^+, \mathcal{W}_\mu^-, \mathcal{Z}_\mu, \mathcal{A}_\mu)$, and R is given by

$$R = \begin{pmatrix} \frac{1}{\sqrt{2}} & \frac{1}{\sqrt{2}} & 0 & 0 \\ \frac{i}{\sqrt{2}} & -\frac{i}{\sqrt{2}} & 0 & 0 \\ 0 & 0 & \bar{c}_w & \bar{s}_w \\ 0 & 0 & -\bar{s}_w & \bar{c}_w \end{pmatrix}, \tag{2.3.17}$$

where

$$\begin{aligned} \bar{s}_w &= \frac{\bar{g}_1}{\sqrt{\bar{g}_1^2 + \bar{g}_2^2}}\left[1 + \frac{v_T^2}{2}\frac{\bar{g}_2}{\bar{g}_1}\frac{\bar{g}_2^2 - \bar{g}_1^2}{\bar{g}_1^2 + \bar{g}_2^2}C_{HWB}\right], \\ \bar{c}_w &= \frac{\bar{g}_2}{\sqrt{\bar{g}_1^2 + \bar{g}_2^2}}\left[1 - \frac{v_T^2}{2}\frac{\bar{g}_2}{\bar{g}_1}\frac{\bar{g}_2^2 - \bar{g}_1^2}{\bar{g}_1^2 + \bar{g}_2^2}C_{HWB}\right]. \end{aligned} \tag{2.3.18}$$

Additionally, we can now find that the gauge boson masses in the SMEFT are given

by

$$\begin{aligned} M_A^2 &= 0\,, \\ M_W^2 &= \frac{\bar{g}_2^2 v_T^2}{4}\,, \\ M_Z^2 &= \frac{v_T^2}{4}(\bar{g}_1^2+\bar{g}_2^2) + \frac{v_T^4}{8}C_{HD}(\bar{g}_1^2+\bar{g}_2^2) + \frac{v_T^4}{4}\bar{g}_1\bar{g}_2 C_{HWB}\,. \end{aligned} \tag{2.3.19}$$

We find that in the limit of $\Lambda_{\rm NP} \to \infty$ the form of the gauge boson masses in Eq. 2.3.19 coincide with those in Eq. 1.1.25 after making use of the identities in Eq. 1.1.30, as expected. With this notation, the relation between the weak-basis fields $\mathcal{A}_\mu^a$ and the mass-basis fields $\tilde{A}_\mu^a$ is given by

$$\mathcal{A}_\mu^a = M^{ab} R^{bc} \tilde{A}_\mu^c\,. \tag{2.3.20}$$

In total, the manipulations throughout this section allow us to write the covariant derivative in the dimension-6 SMEFT as

$$D_\mu = \partial_\mu - i\frac{\bar{g}_w}{\sqrt{2}}\left[\mathcal{W}_\mu^+\tau^+ + \mathcal{W}_\mu^-\tau^-\right] - i\bar{g}_Z\left[T_f^3 - \bar{s}_w^2 Q_f\right]\mathcal{Z}_\mu - i\bar{e}Q_f\mathcal{A}_\mu - i\bar{g}_3 T^A \mathcal{G}_\mu^A\,, \tag{2.3.21}$$

where $\tau^\pm = (\tau^1 \pm i\tau^2)/\sqrt{2}$, $Q_f = \tau^3 + Y$ (the same definition as in the SM), and

$$\begin{aligned} \bar{e} &= \bar{g}_2\bar{s}_w - \frac{1}{2}\bar{c}_w\bar{g}_2 v_T^2 C_{HWB}\,, \\ \bar{g}_Z &= \frac{\bar{e}}{\bar{s}_w\bar{c}_w}\left[1 + \frac{\bar{g}_1^2+\bar{g}_2^2}{2\bar{g}_1+\bar{g}_2} v_T^2 C_{HWB}\right]. \end{aligned} \tag{2.3.22}$$

2.3.3 Yukawa sector

Additional to the changes outlined throughout Sections 2.3.1 and 2.3.2 we find that class-5 operators contribute to couplings between fermions and the fields in the Higgs doublet. As a result, the form of the fermion mass matrices and Yukawa-interactions terms are augmented by dimension-6 effects.

The relevant part of the SM+dimension-6 SMEFT Lagrangian is made up of the terms found in Eq. 1.1.34 plus the class-5 operators in Table A.1

$$\begin{aligned} \mathcal{L} \supset &- [Y_e]_{rs}\bar{l}^r H e^s - [Y_u]_{rs}\bar{q}^r \tilde{H} u^s - [Y_d]_{rs}\bar{q}^r H d^s \\ &+ \underset{rs}{C_{eH}}(H^\dagger H)(\bar{l}^{r,j} e^s H^j) + \underset{rs}{C_{uH}}(H^\dagger H)(\bar{q}^{r,j} u^s \tilde{H}^j) + \underset{rs}{C_{dH}}(H^\dagger H)(\bar{q}^{r,j} d^s H^j) + \text{h.c.}\,. \end{aligned} \tag{2.3.23}$$

Using the form of the Higgs doublet in Eq. 2.3.5 we first consider the fermion mass

terms in Eq. 2.3.23, given as

$$\begin{aligned}\mathcal{L}_{\text{fer. mass}} &= -\frac{v_T}{\sqrt{2}}\bar{e}_L^r\left([Y_e]_{rs} - \frac{v_T^2}{2}C_{\substack{eH\\rs}}\right)e_R^s - \frac{v_T}{\sqrt{2}}\bar{u}_L^r\left([Y_u]_{rs} - \frac{v_T^2}{2}C_{\substack{uH\\rs}}\right)u_R^s \\ &\quad - \frac{v_T}{\sqrt{2}}\bar{d}_L^r\left([Y_d]_{rs} - \frac{v_T^2}{2}C_{\substack{dH\\rs}}\right)d_R^s + \text{h.c.} \\ &\equiv -\frac{v_T}{\sqrt{2}}\bar{e}_L^r[\mathcal{M}_e]_{rs}e_R^s - \frac{v_T}{\sqrt{2}}\bar{u}_L^r[\mathcal{M}_u]_{rs}u_R^s - \frac{v_T}{\sqrt{2}}\bar{d}_L^r[\mathcal{M}_d]_{rs}d_R^s + \text{h.c.}\,, \end{aligned} \tag{2.3.24}$$

where we have defined the weak-basis fermion mass matrices, $[\mathcal{M}_f]$, as

$$[\mathcal{M}_f]_{rs} \equiv [Y_f]_{rs} - \frac{v_T^2}{2}C_{\substack{fH\\rs}}\,. \tag{2.3.25}$$

From Eq. 2.3.23, we can also separate the Yukawa-interaction terms[1]

$$\begin{aligned}\mathcal{L}_{\text{yuk.}} &= -\frac{1}{\sqrt{2}}h\bar{e}_L^r\left([Y_e]_{rs}\left[1 + C_{H,\text{kin}}\right] - \frac{3}{2}v_T^2C_{\substack{eH\\rs}}\right)e_R^s \\ &\quad - \frac{1}{\sqrt{2}}h\bar{u}_L^r\left([Y_u]_{rs}\left[1 + C_{H,\text{kin}}\right] - \frac{3}{2}v_T^2C_{\substack{uH\\rs}}\right)u_R^s \\ &\quad - \frac{1}{\sqrt{2}}h\bar{d}_L^r\left([Y_d]_{rs}\left[1 + C_{H,\text{kin}}\right] - \frac{3}{2}v_T^2C_{\substack{dH\\rs}}\right)d_R^s + \text{h.c.} \\ &\equiv -\frac{1}{\sqrt{2}}\bar{e}_L^r[\mathcal{Y}_e]_{rs}e_R^s - \frac{1}{\sqrt{2}}\bar{u}_L^r[\mathcal{Y}_u]_{rs}u_R^s - \frac{1}{\sqrt{2}}\bar{d}_L^r[\mathcal{Y}_d]_{rs}d_R^s + \text{h.c.}\,, \end{aligned} \tag{2.3.26}$$

where we have defined the effective Yukawa matrices

$$[\mathcal{Y}_f]_{rs} = [Y_f]_{rs}\left[1 + C_{H,\text{kin}}\right] - \frac{3}{2}v_T^2C_{\substack{fH\\rs}}\,. \tag{2.3.27}$$

Comparing the forms of Eq. 2.3.25 and Eq. 2.3.27 we see that, unlike as was seen for the SM in Section 1.1.3, the fermion mass matrices and Yukawa couplings are no longer proportional to each other, differing in the dimension-6 contribution. Upon transforming to the mass basis, this non-linearity introduces a large set of flavor-violating effects beyond those seen in the SM, such as hf_1f_2 couplings for $f_1 \neq f_2$.

We may again use the unitary rotation matrices in Eq. 1.1.37[2] to rotate the weak-basis fermion mass matrices, $[\mathcal{M}_f]$, to the mass basis. We find that the fermion

[1] We define the Yukawa-interaction terms to be those involving the coupling between two fermions (of any flavor) and one Higgs field.

[2] Note that, due to additional dimension-6 effects, the exact form of the unitary matrices in Eq. 1.1.37 required to rotate the fermion fields to the mass basis would not be the same as in the SM case. Instead, the rotation matrices S_f and K_f would be augmented with additional dimension-6 effects. As we do not report the exact form of S_f or K_f in Eq. 1.1.37 we do not change the notation of the equivalent dimension-6 SMEFT matrices, with it understood that they differ from the forms found in Eq. 1.1.37.

masses are now defined according to

$$
\begin{aligned}
[m_e]_{rs} &\equiv \frac{v_T}{\sqrt{2}}[S_e^\dagger]_{ri}[\mathcal{M}_e]_{ij}[K_e]_{js} = \frac{v_T}{\sqrt{2}}\left([N_e]_{rs} - \frac{v_T^2}{2}C^m_{eH\,rs}\right) = \mathrm{diag}(m_e,\, m_\mu,\, m_\tau)\,, \\
[m_u]_{rs} &\equiv \frac{v_T}{\sqrt{2}}[S_u^\dagger]_{ri}[\mathcal{M}_u]_{ij}[K_u]_{js} = \frac{v_T}{\sqrt{2}}\left([N_u]_{rs} - \frac{v_T^2}{2}C^m_{uH\,rs}\right) = \mathrm{diag}(m_u,\, m_c,\, m_t)\,, \\
[m_d]_{rs} &\equiv \frac{v_T}{\sqrt{2}}[S_d^\dagger]_{ri}[\mathcal{M}_d]_{ij}[K_d]_{js} = \frac{v_T}{\sqrt{2}}\left([N_d]_{rs} - \frac{v_T^2}{2}C^m_{dH\,rs}\right) = \mathrm{diag}(m_d,\, m_s,\, m_b)\,,
\end{aligned}
\tag{2.3.28}
$$

where $N_f = S_f^\dagger M_f K_f$, and where we have defined the mass-basis Wilson coefficients, distinguished by the superscript, m, according to

$$
C^m_{fH} \equiv S_f^\dagger C_{fH} K_f\,. \tag{2.3.29}
$$

The topic of mass-basis Wilson coefficients is something we will return to in Section 3.4.

Part II

Higgs Decay to Fermion Pairs at NLO in the SMEFT

Chapter 3

Preliminaries

In this chapter we introduce the main focus of this thesis, that being the calculation of the decay rate of $h \to f\bar{f}$ for $f \in \{b, c, \tau, \mu\}$ to NLO in the dimension-6 SMEFT. We first motivate the need for such a result in Section 3.1 and then discuss a number of general aspects of calculations in the dimension-6 SMEFT, these being the choice of input scheme in Section 3.2, the digital implementation of the dimension-6 SMEFT Lagrangian in Section 3.3, the chosen notation of the Wilson coefficients in Section 3.4, imposing MFV in the small-mass limit in Section 3.5, and gauge fixing in the dimension-6 SMEFT in Section 3.6. As the discussion of such topics are not necessarily unique to the calculation of $h \to f\bar{f}$, these discussions are separated from the discussion of the particulars of this calculation, which are given in Chapter 4.

3.1 Motivation

Over the past several decades, the SM has proven to be an incredibly powerful theoretical tool for making predictions within particle physics. Some of its most impressive contributions include the phenomenal precision of its prediction of the anomalous magnetic dipole moment of the electron [64] and its remarkable accuracy to the experimentally measured value [65], and the prediction of the top quark [26] and its eventual discovery [66], amongst many others. Despite the numerous successes, it is widely believed that the SM is incomplete due to its contention with several observed phenomena. For example, besides the lack of incorporating a quantum theory of gravity, the SM currently provides no explanation for the nature of dark matter, about which very little is known, but is estimated to account for approximately 24% of the energy density content of the universe, the existence of which can be inferred, for instance, through the measured rotation velocities of spiral galaxies. It also does not provide a mechanism for the experimentally

measured non-zero neutrino masses, nor does it provide adequate sources of CP violation necessary to create the observed matter-antimatter asymmetry, amongst other observations. Over many years, specific models have been built, such as supersymmetry, to try and explain some of these observations. Such models often introduce additional particles and interactions into the SM, and as a consequence usually generate experimentally verifiable predictions. Presently, none of these models has been successful in producing a prediction that has been verified with the necessary experimental precision to validate any of these models. This problem is compounded by measurements at collider experiments being unable to expose many significant deviations between experimental measurements and SM predictions.

In light of the lack of direct evidence supporting any particular BSM model, there has been much recent interest in precision measurements in an attempt to expose any potential discrepancies between experimental measurements and SM predictions. As it is able to avoid any commitment to a particular UV complete BSM theory, subject to the assumptions outlined in Section 2.2.1, the SMEFT, as introduced in Section 2.2.1, has become a popular tool to parameterize any such discrepancies. From the theory standpoint, calculations of observables in the dimension-6 SMEFT have received much recent interest [67–94]. In principle, this allows one to constrain dimension-6 SMEFT Wilson coefficients by utilizing a set of experimental measurements along with corresponding predictions in the dimension-6 SMEFT and performing some variety of fit. Currently, there are many fits available, adopting multiple methodologies, for some examples see [95–100], but such fits are not explored here. It is also possible to match the dimension-6 SMEFT to UV complete theories such that the Wilson coefficients of the SMEFT are recast as fundamental parameters of the UV complete theory. Such matching, along with constraints on the SMEFT operators therefore presents a systematic way to simultaneous test a spectrum of UV complete models.

In this work we focus on providing a set of predictions for observables within the dimension-6 SMEFT, at NLO in perturbation theory. In particular, we focus on the decay of the Higgs boson to fermion anti-fermion pairs. The predicted branching fractions of the Higgs into its various decay products in the SM is found in Fig. 3.1. Assuming that the measured branching fractions of the Higgs do not significantly vary from the predictions in Fig. 3.1, we see from that figure that by far the largest branching fraction of the Higgs is its decay into a bottom anti-bottom pair, at $\sim 58.2\%$. The decay into tau anti-tau pairs and charm anti-charm pairs then contribute $\sim 6.3\%$ and $\sim 2.9\%$ respectively, while the decay to a muon anti-muon pair constitutes $\sim 0.02\%$ of the total decay width. Decays into the remaining SM fermions are not shown in Fig. 3.1, and while they do constitute a theoretically

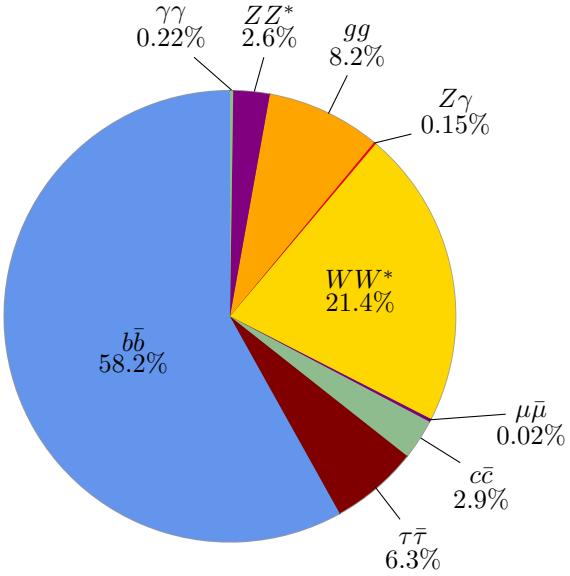

Figure 3.1: *The nine largest branching fractions predicted in the SM for a SM Higgs of mass* 125 *GeV. The segment for* $h \to \mu\bar{\mu}$ *has been enlarged by a factor of 10 for visibility. Values taken from [101].*

possible decay channel of the Higgs, their branching fractions are small enough that we may effectively consider them to be vanishing.

The discovery of the Higgs boson in 2012 was a triumph for the SM [102–104]. Since then its decay into a bottom anti-bottom pair has been observed [105, 106], as has the decay to a tau anti-tau pair [107, 108], both with an $\mathcal{O}(10\%)$ precision. Limits have also been placed on the decay into muon anti-muon pairs [109, 110], and charm anti-charm pairs [111, 112]. The relatively low precision of these measurements (and the infancy of Higgs measurements at the LHC in general) presently offers a great deal of room for NP in Higgs measurements. This, along with the projected percent level accuracy of measurements of the aforementioned decay modes (aside from decay to muon anti-muon pairs, where projections suggest somewhat worse precision) at future lepton colliders [113–117] serves as a great motivation to explore these decay modes within the SMEFT. While a LO analysis would be sufficient given the current precision of the measurements of these decay modes, the anticipated precision of future measurements necessitates a more precise calculation. Additionally, at the aforementioned order in perturbation theory, not only do we increase the precision of the predicted contributions from operators appearing at LO, but the dimension-6 SMEFT also introduces a plethora of new Wilson coefficients that do not appear at tree level, presenting an opportunity for the fitting of such coefficients. Finally, matching to a UV complete theory requires the running of Wilson coefficients measured at the scale of the experiment to the UV scale, Λ_{UV}, via the Wilson

coefficient anomalous dimensions. These anomalous dimensions potentially mix the Wilson coefficients at a particular scale into a number of coefficients at another scale, however, this effect is entirely ignored in a purely LO analysis.

3.2 Input Scheme

When calculating predictions for observable quantities we wish to write any results as a function of experimentally measurable parameters. For EW processes, one has a freedom in the choice of *input schemes* – that is, a choice of parameters in which a result may be expressed.[1] This is due to an over-completeness in the basis of potential input parameters. In the SM, at any particular order in perturbation theory, different input schemes produce different analytical and numerical results. These differences originate from the accuracy in experimental measurements of non-independent parameters, and from the limitations of relating non-independent parameters at all orders. In an ideal scenario where any parameter may be measured with infinite precision, and where non-independent parameters may be related to all orders in perturbation theory, these small differences in theoretical predictions would vanish. Some typical EW input schemes are $\{\alpha,\, M_W,\, M_Z\}$, $\{\alpha,\, M_Z,\, G_F\}$ and $\{G_F,\, M_W,\, M_Z\}$, where G_F is the Fermi constant introduced in Eq. 2.1.8. The Fermi constant and W-boson mass are not independent parameters, but are related at LO by Eq. 2.1.8. As discussed, it is also possible to calculate perturbative corrections to this relation. In this way it is clear how one may switch between the aforementioned input schemes at a particular order in perturbation theory. Ideally, one would like to choose an input scheme which minimizes NLO corrections; within the SM, such scheme choices have been studied in a systematic way [118]. Such a systematic study in the dimension-6 SMEFT is beyond the scope of this work. An example of a scheme that reduces the size of corrections in a particular scenario would be the use of G_F as an input parameter in processes involving W-bosons in the SM. In this case, the choice of G_F as an input parameter causes a cancellation of large-m_t corrections arising from the renormalization of s_w in the W-boson coupling [118]. We investigate the use of G_F as an input parameter for reducing large m_t-dependent corrections further in the context of the calculations performed here in the dimension-6 SMEFT in Section 4.4.2

In the case of the SMEFT, we induce a strong Wilson coefficient dependence in any choice of input scheme. As an example we again consider the decay $\mu \to e\nu_\mu\bar{\nu}_e$ first explored in Section 2.1.1, but now in the context of the dimension-6 SMEFT.

[1] This scheme dependence is eliminated in QCD scenarios, where the only possible choice of input parameters are the strong coupling constant and quark masses.

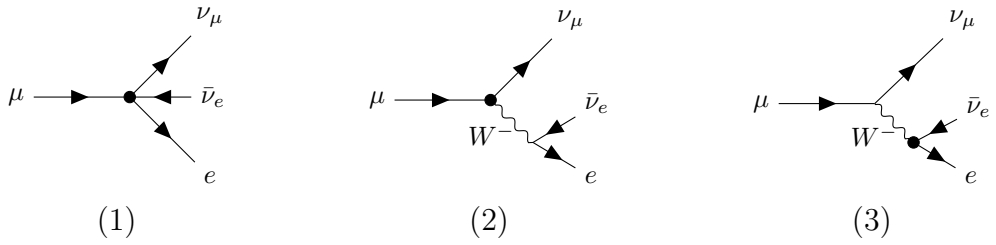

Figure 3.2: *LO diagrams of $\mu \to e\nu_\mu\bar{\nu}_e$ with effective operators (4-Fermi and dimension-6 SMEFT) represented by a dotted vertex. Diagram (1) contains the 4-Fermi contribution and contributions from the operators $Q_{\substack{ll\\2112}}$ and $Q_{\substack{ll\\1221}}$, diagram (2) contains contributions from $Q^{(3)}_{\substack{Hl\\22}}$ and diagram (3) contains contributions from $Q^{(3)}_{\substack{Hl\\11}}$. Each diagram has at most one dimension-6 effective operator insertion, consistent with $\mathcal{O}(\Lambda_{\rm NP}^{-2})$ calculations.*

The LO diagrams for this process to $\mathcal{O}(\Lambda_{\rm NP}^{-2})$ are shown in Fig. 3.2. Comparing the amplitudes for this process calculated in 4-Fermi theory and in the dimension-6 SMEFT we find a new LO expression for the Fermi constant

$$G_F = \frac{1}{\sqrt{2}v_T^2} + \frac{1}{\sqrt{2}}\left(C^{(3)}_{\substack{Hl\\11}} + C^{(3)}_{\substack{Hl\\22}}\right) + \frac{1}{2\sqrt{2}}\left(C_{\substack{ll\\2112}} + C_{\substack{ll\\1221}}\right). \tag{3.2.1}$$

Clearly, from the form of M_W in Eq. 2.3.19, we may use Eq. 3.2.1 to exchange either $M_W \leftrightarrow G_F$ or $\alpha \leftrightarrow G_F$ as input parameters, thus linking the three input schemes introduced at the start of this chapter. Unlike in the SM however, this change of input parameters also changes an expression's dependence on certain Wilson coefficients – for example, a dependence on the Wilson coefficients present in Eq. 3.2.1 may appear, where previously these coefficients were absent. Furthermore, at NLO this Wilson coefficient dependence on input scheme expands to a larger set of Wilson coefficients, although any new coefficients introduced at NLO are necessarily suppressed by an additional power of α. The first full calculation of G_F at NLO in the dimension-6 SMEFT was performed in [72], building on the large-m_t limit calculation in [119]. While one may in principle use expressions such as those found in Eq. 3.2.1 to convert between input schemes, often calculations are repeated from scratch to generate results in multiple input schemes, for example in [73].

Along with the aforementioned advantages of using G_F as an input parameter, historically, precision SM EW calculations were calculated with G_F as an input parameter due to the precision of the measurements of G_F. Presently, the measurements of M_W are sufficiently precise that using M_W as an input parameter in place of G_F is not the limiting factor it once was. While G_F remains the more precisely measured quantity,

the precision of the measurement of M_W is sufficient for the purposes explored here.[1]

Throughout this work, we use the $\{\alpha,\, M_W,\, M_Z\}$ input scheme. The full set of input parameters is

$$\alpha_s,\, \alpha,\, m_f,\, m_H,\, M_W,\, M_Z,\, V_{ij}, C_i\,. \tag{3.2.2}$$

We find that the input scheme outlined in Eq. 3.2.2 is particularly advantageous in the context of EW calculations within SMEFT – as we will see, this scheme minimizes the number of Wilson coefficients entering the Lagrangian shifts. In particular, it prevents four-fermion operators, such as those in Eq. 3.2.1 from appearing in the LO Higgs decay rate.

In Section 2.3 we defined the dimension-6 SMEFT Lagrangian in the mass basis where we introduced many quantities such as v_T and $\bar{g}$. To write the results of our calculations as a function of the input parameters in Eq. 3.2.2, it is therefore important to rewrite the dimension-6 Lagrangian as a function of the input parameters in Eq. 3.2.2. Firstly, we recognize that $\bar{e}$ in Eq. 2.3.22 is the value of the electric charge that one would measure experimentally, and so in terms of our input parameter, α, this is now given by

$$\alpha = \frac{\bar{e}^2}{4\pi}\,, \tag{3.2.3}$$

and similarly for the strong coupling constant

$$\alpha_s = \frac{\bar{g}_3^2}{4\pi}\,. \tag{3.2.4}$$

For the remainder of this thesis, we drop the bars on e and g_3 when discussing the variables defined by Eqs. 2.3.11 and 2.3.22, with it understood that these are simply the input parameters. We continue by defining a set of hatted variables

$$\hat{v}_T = \frac{2M_W \hat{s}_w}{e}\,, \qquad \hat{s}_w^2 = 1 - \frac{M_W^2}{M_Z^2}\,, \qquad \hat{c}_w^2 = 1 - \hat{s}_w^2\,, \tag{3.2.5}$$

such that these hatted quantities coincide with their SM definitions, in particular, $\hat{v}_T = v_0$. Manipulating the equations in Eqs. 2.3.18, 2.3.19 and 2.3.22 we can write v_T, defined in Eq. 2.3.2, as a function of our input parameters in Eq. 3.2.2 as

$$v_T = \hat{v}_T \left[1 - \hat{v}_T^2 \left(C_{HWB} + \frac{\hat{c}_w}{4\hat{s}_w} C_{HD}\right)\right]\,. \tag{3.2.6}$$

Written in this way, in terms of the hatted counterpart, it is clear that in the limit $\Lambda_{\rm NP} \to \infty$ the expression for v_T returns to the SM definition. A feature we also

[1] The current PDG values are $G_F = 1.1663787(6)^{-5}\,\text{GeV}^{-2}$ and $M_W = 80.379 \pm 0.012$ GeV [23].

highlight in Eq. 3.2.6 is that up to $\mathcal{O}(\Lambda_{\rm NP}^{-2})$ Wilson coefficients can only multiply input parameters from Eq. 3.2.2, or hatted quantities.

We continue by considering the expression in Eq. 2.3.7. We may use this equation to express the Lagrangian parameter λ in terms of the parameters in Eq. 3.2.2 as

$$\lambda = \frac{m_H^2}{2\hat{v}_T^2}\left[1 - C_{H,\text{kin1}} + 2\hat{v}_T^2\frac{\hat{c}_w}{\hat{s}_w}\left(C_{HWB} + \frac{\hat{c}_w}{4\hat{s}_w}C_{HD} + \frac{3\hat{v}_T^4}{m_H^2}C_H\right)\right]. \tag{3.2.7}$$

Next, we may also express the quantities $\bar{g}_1$ and $\bar{g}_2$ from Eq. 2.3.11 as

$$\begin{aligned}\bar{g}_1 &= \frac{e}{\hat{c}_w}\left(1 - \frac{\hat{v}_T^2}{4}C_{HD}\right),\\ \bar{g}_2 &= \frac{e}{\hat{s}_w}\left(1 + \hat{v}_T^2\frac{\hat{c}_w}{\hat{s}_w}\left[C_{HWB} + \frac{\hat{c}_w}{4\hat{s}_w}C_{HD}\right]\right).\end{aligned} \tag{3.2.8}$$

This further allows us to write the dimension-6 weak rotation angles, $\bar{c}_w$ and $\bar{s}_w$, from Eq. 2.3.18 as

$$\begin{aligned}\bar{c}_w &= \hat{c}_w\left(1 + \frac{\hat{v}_T^2}{4}C_{HD} + \frac{\hat{s}_w\hat{v}_T^2}{2\hat{c}_w}C_{HWB}\right),\\ \bar{s}_w &= \hat{s}_w\left(1 - \frac{\hat{c}_w^2\hat{v}_T^2}{4\hat{s}_w^2}C_{HD} - \frac{\hat{c}_w\hat{v}_T^2}{2\hat{s}_w}C_{HWB}\right).\end{aligned} \tag{3.2.9}$$

The rotation in Eq. 2.3.20 thus takes the form

$$\begin{pmatrix}\mathcal{W}_\mu^3\\ \mathcal{B}_\mu\end{pmatrix} = \begin{pmatrix}\hat{c}_w + \frac{1}{4}\hat{c}_w\hat{v}_T^2\left(C_{HD} + 4\frac{\hat{s}_w}{\hat{c}_w}C_{HWB}\right) & \hat{s}_w - \frac{\hat{c}_w^2\hat{v}_T^2}{4\hat{s}_w}\left(C_{HD} + 4\frac{\hat{s}_w}{\hat{c}_w}C_{HWB}\right)\\ -\hat{s}_w + \frac{\hat{c}_w^2\hat{v}_T^2}{4\hat{s}_w}C_{HD} & \hat{c}_w + \frac{\hat{c}_w\hat{v}_T^2}{4}C_{HD}\end{pmatrix}\begin{pmatrix}\mathcal{Z}_\mu\\ \mathcal{A}_\mu\end{pmatrix}, \tag{3.2.10}$$

and the dimension-6 SMEFT covariant derivative in Eq. 2.3.21 takes the form

$$\begin{aligned}D_\mu = \partial_\mu - i\frac{e}{\hat{s}_w}&\left[1 + \frac{\hat{c}_w^2\hat{v}_T^2}{4\hat{s}_w^2}C_{HD} + \frac{\hat{c}_w\hat{v}_T^2}{\hat{s}_w}C_{HWB}\right]\left(\mathcal{W}_\mu^+\tau^+ + \mathcal{W}_\mu^-\tau^-\right)\\ &- i\left[\frac{e}{\hat{c}_w\hat{s}_w}\left(1 + \frac{(2\hat{c}_w^2 - 1)\hat{v}_T^2}{4\hat{s}_w^2}C_{HD} + \frac{\hat{c}_w\hat{v}_T^2}{\hat{s}_w}C_{HWB}\right)\left(\tau^3 - \hat{s}_w^2 Q\right)\right.\\ &\left. + e\left(\frac{\hat{c}_w\hat{v}_T^2}{2\hat{s}_w}C_{HD} + \hat{v}_T^2 C_{HWB}\right)Q_f\right]\mathcal{Z}_\mu - ieQ_f\mathcal{A}_\mu\,.\end{aligned} \tag{3.2.11}$$

3.3 Lagrangian Implementation

The large set of operators of the dimension-6 SMEFT in Table A.1 introduces an enormous number of possible interactions beyond those seen in the SM. For the full set of possible interactions see [120]. A consequence of this is that at NLO the already large number of diagrams contributing to the process $h \to f\bar{f}$ in the

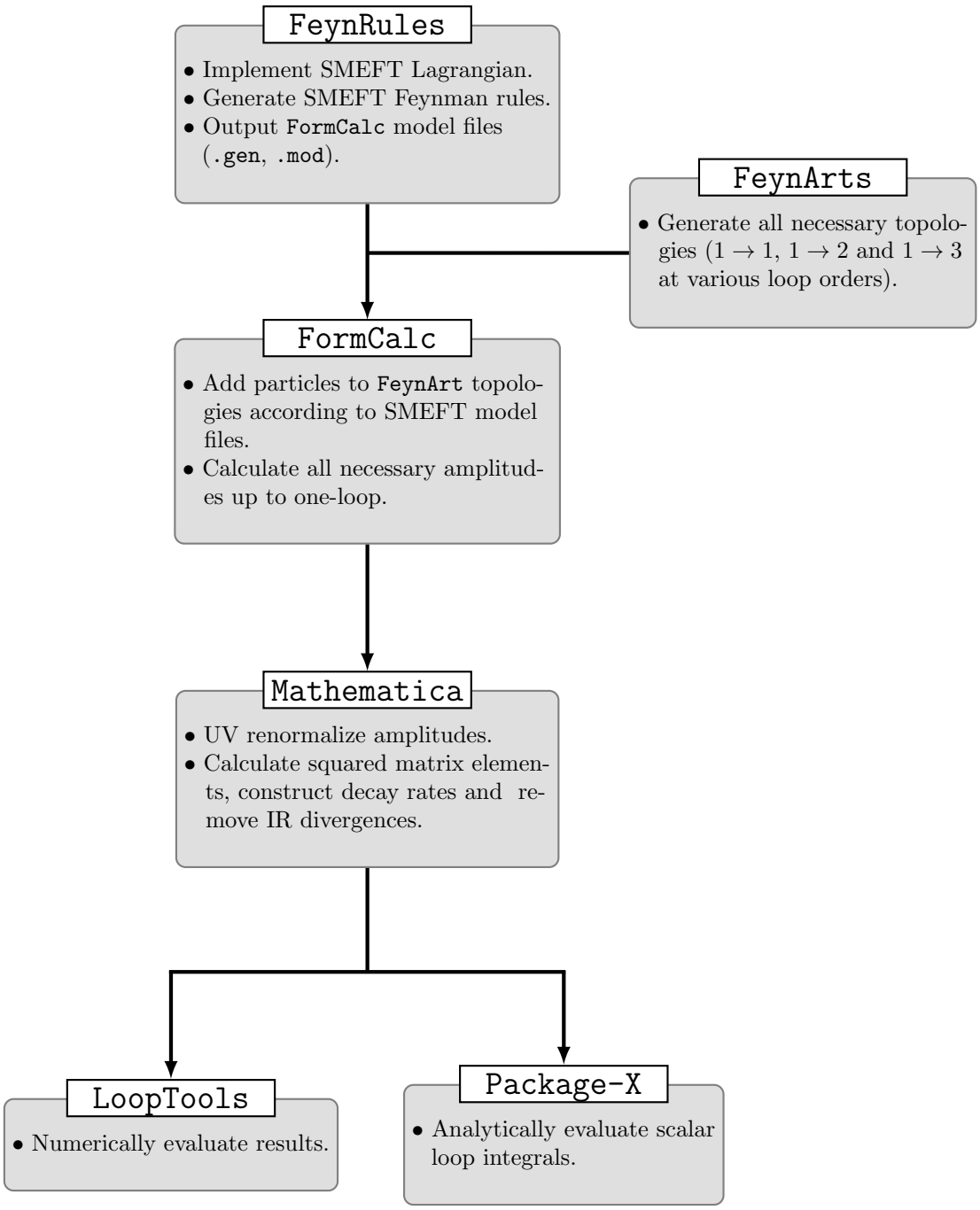

Figure 3.3: *A diagram demonstrating the workflow and implementation of* `Mathematica` *and the packages* `FeynRules`, `FormCalc`, `FeynArts`, `LoopTools`, *and* `Package-X` *used to renormalize, and numerically and analytically evaluate the processes considered in this work.*

SM is increased dramatically. We therefore implement the dimension-6 SMEFT Lagrangian electronically and automate the calculation of the necessary diagrams. To do this, we break the dimension-6 SMEFT Lagrangian into the 8 classes of Table A.1, and implement the Lagrangian for each class using the `Mathematica` [121] package `FeynRules` [122]. The only exception to this are the class-8 operators, the calculations for which were performed by hand. `FeynRules` allows the user to write any valid[1] Lagrangian, and automate the generation of Feynman rules, as well as generate output files of these rules for use in other packages. We use `FeynRules` to output `FormCalc` [123] model files. `FormCalc` is a `Mathematica` package which automates the analytical calculation of amplitudes in d-dimensions up to and including the one-loop level. At one-loop these amplitudes are written as a function of the tensoral loop-integral functions introduced in Section 1.2.1, with the option of automatically reducing these to the set of scalar loop integrals. To generate the necessary topologies we use `FeynArts` [124]. After outputting the results for the necessary diagrams, the calculations to produce UV- and IR-finite decay rates were then performed in `Mathematica` notebooks. The output of these calculations were then evaluated numerically using `LoopTools` [123], and the necessary scalar one-loop integrals were generated using `Package-X`[2] [125] which were then numerically cross-checked against the `LoopTools` results. A flowchart demonstrating this sequence of automation is seen in Fig. 3.3.

3.4 Wilson Coefficient Notation

The dimension-6 SMEFT operators in Table A.1 are defined in the weak basis, however, the physical decay rates and on-shell renormalization conditions are defined in the mass basis. Therefore, to connect calculations, such as those performed in this work, to experimental measurements in a consistent manner, we must also be able to connect the Wilson coefficients and corresponding operators of Table A.1 to an equivalent mass basis. In this way, we wish to express such mass-basis operators entirely from measurable parameters. For the operators of classes 1-4, which are exclusively built from bosonic fields, this connection is trivial as the Higgs doublet can simply be replaced by its post-SSB counterpart, and the rotation of the weak-basis gauge fields to their mass-basis counterparts proceeds via experimentally measurable quantities. As such, the Wilson coefficients in the mass basis and weak basis for

[1] By valid we mean Lagrangians which obey the usual mathematical constraints placed on Lagrangians in QFT, e.g. that they should be scalar quantities etc.

[2] The exception to this are the derivative two-point scalar integrals, $\frac{\partial}{\partial k^2} B_0(k^2, m_2^2, m_3^2)|_{k^2 \to m_1^2} \equiv B_0'(m_1^2, m_2^2, m_3^2)$, which were calculated by hand.

classes 1-4 are related by

$$C^{w}_{(1-4)} \equiv C^{m}_{(1-4)}\,, \tag{3.4.1}$$

where the superscripts w and m denote the weak and mass basis respectively.

The operators throughout classes 5-8 of Table A.1 are functions of fermionic fields. As seen throughout Section 1.1.3, the rotation of the weak-basis fields to the mass-basis fields requires the rotation via unitary matrices, which are not individually measurable quantities. As such, we must absorb these unitary matrices into the definitions of the mass-basis Wilson coefficients themselves. As an example, we consider the class-5 operator Q_{uH}, which is defined in the weak basis in Table A.1. The explicit form of this term, which we denote by $\mathcal{L}_{uH}$, is

$$\mathcal{L}_{uH} = \underset{rs}{C^{w}_{uH}}(H^\dagger H)(\bar{q}^{w}_{r} u^{w}_{s} \tilde{H})\,, \tag{3.4.2}$$

where we have also introduced a superscript, w, on the fermionic fields to distinguish them from the mass basis fermions, which we will denote with an m superscript. Applying the rotation of the fermion fields to the mass basis, according to the transformations in Eq. 1.1.37, we find that the fields in Eq. 3.4.2 become

$$\begin{aligned} u^{w}_{R} &= K_u u^{m}_{R}\,, \\ q^{w}_{L} &= \begin{pmatrix} S_u u^{m}_{L} \\ S_d d^{m}_{L} \end{pmatrix}\,, \end{aligned} \tag{3.4.3}$$

such that the operator in Eq. 3.4.2 becomes

$$\mathcal{L}_{uH} = \underset{rs}{C^{w}_{uH}}(H^\dagger H)\left((\bar{u}^{m}_{L} S^\dagger_u,\, \bar{d}^{m}_{L} S^\dagger_d)_r [K_u]_{si} u^{m}_{R_i} \tilde{H}\right)\,. \tag{3.4.4}$$

Here, we recognize that we have a freedom in defining the mass-basis Wilson coefficient. We may choose

$$\underset{rs}{C^{m}_{uH}} \equiv [S^\dagger_u]_{ri} \underset{ij}{C^{w}_{uH}} [K_u]_{jr}\,, \tag{3.4.5}$$

such that Eq. 3.4.2 takes the form

$$\mathcal{L}_{uH} = \underset{rs}{C^{m}_{uH}}(H^\dagger H)\left((\bar{u}^{m}_{L},\, \bar{d}^{m}_{L} V^\dagger)_r u^{m}_{R_s} \tilde{H}\right)\,, \tag{3.4.6}$$

or we may choose

$$\underset{rs}{C^{m}_{uH}} \equiv [S^\dagger_d]_{ri} \underset{ij}{C^{w}_{uH}} [K_u]_{jr}\,, \tag{3.4.7}$$

such that Eq. 3.4.2 takes the form

$$\mathcal{L}_{uH} = \underset{rs}{C^{m}_{uH}}(H^\dagger H)\left((\bar{u}^{m}_{L} V,\, \bar{d}^{m}_{L})_r u^{m}_{R_s} \tilde{H}\right)\,. \tag{3.4.8}$$

In both choices outlined in Eq. 3.4.5 and Eq. 3.4.7 we have satisfied the requirement that the mass-basis operator should be built from observable, mass-basis quantities, however we have also identified a freedom in the definition of the mass basis. When considering dimension-6 SMEFT in full generality, this choice is one which must be specified.[1] However, for the calculations considered here, we impose the approximation common to EW calculations of $V_{ij} \approx \delta_{ij}$. We will explore the implications of this approximation within the context of the calculations outlined in this work in Section 4.3.1, but for now we see that within this approximation the two possible choices of mass-basis Wilson coefficients seen in Eq. 3.4.5 and Eq. 3.4.7 are equivalent and would lead to an identical form of the mass-basis operator, specifically

$$\mathcal{L}_{uH} = \underset{rs}{C^m_{uH}}(H^\dagger H)\left(\bar{q}^m_r u^m_s \tilde{H}\right) . \tag{3.4.9}$$

As such, with this approximation in place, we are able to specify a unique form of the mass-basis operator without committing to a particular definition of the mass-basis Wilson coefficient in terms of its weak-basis counterpart. Further, examining the form of the mass-basis operator in Eq. 3.4.9, we see that it is analogous to its weak-basis counterpart in Eq. 3.4.2, with the straightforward replacement of the weak-basis Wilson coefficient and fermion fields with their mass-basis counterparts. This pattern holds in general for the operators throughout classes 5-8: with the diagonal CKM approximation, the mass-basis operators are identical to the weak-basis operators upon the replacement of weak-basis Wilson coefficients and operators by their mass-basis counterparts, without the need to specify the particular definition of the mass-basis Wilson coefficients in terms of the weak-basis Wilson coefficients.

To check that our abstention from a particular choice of mass-basis Wilson coefficients does not have any effects anywhere else in the full dimension-6 SMEFT Lagrangian, we again briefly consider the Yukawa couplings in the dimension-6 SMEFT, first discussed in Section 2.3.3. There, we defined our mass-basis Wilson coefficients analogously to Eq. 3.4.5 to convert our Wilson coefficients to the mass basis. Had we instead chosen to define the mass-basis Wilson coefficients similarly to Eq. 3.4.7 we would now find that, for example, the expression for $[m_u]$ in Eq. 2.3.28 would now read

$$[m_u]_{rs} \equiv \frac{v_T}{\sqrt{2}}[S^\dagger_u]_{ri}[\mathcal{M}_u]_{ij}[K_u]_{js} = \frac{v_T}{\sqrt{2}}\left([M_u]_{rs} - \frac{v_T^2}{2}V_{ri}\underset{is}{C^m_{uH}}\right) = \text{diag}(m_u,\, m_c,\, m_t)\,, \tag{3.4.10}$$

where there is an introduction of the CKM matrix where previously there was none. Within the approximation of $V_{ij} \approx \delta_{ij}$ the expression in Eq. 3.4.10 is the same as

[1] For an example of one particular choice, see [120].

that found in Eq. 2.3.28, and so again we are free to not specify a particular choice for the form of the mass-basis Wilson coefficients.

In quoting analytic and numerical results in the remainder of this thesis, we always work with mass-basis quantities, and for simplicity drop the superscripts m on the fields and Wilson coefficients. Moreover, within our approximations, $h \to f\bar{f}$ decay is sensitive to a group of generation-diagonal operators involving right-handed fermion fields. For these, we use the shorthand notation where, e.g. $C_{cH} \equiv C_{\substack{uH \\ 22}}$, thus allowing us to suppress flavor indices. In fact, the only Wilson coefficients appearing in our calculation which require explicit flavor indices are the class-7 quantities $C_{Hl}^{(1,3)}$ and $C_{Hq}^{(1,3)}$, in addition to the coefficients of the class-8 four-fermion operators.

3.5 MFV and the Small-Mass Limit

With the exception of the top quark, Higgs couplings to fermions in the SM are suppressed by small and hierarchical Yukawa couplings, a feature not inherited by generic SMEFT interactions. In order to avoid pushing the UV scale of the effective theory to values far above the TeV scale to avoid flavor constraints, one often considers the SMEFT Wilson coefficients to be constrained by MFV, which we first outlined in general in Section 2.1.3, and in the context of the dimension-6 SMEFT in Section 2.2.2. In the calculation of the decay rate of $h \to f\bar{f}$ presented in Chapter 4, we often consider the small-mass limit. In this limit we keep leading order terms in the expansion about the light-fermion masses, which we define as all SM fermions except for the top quark. More details of this expansion may be found in Section 4.1. It is in this small-mass limit that we study the MFV scenario.

As we saw in Section 2.1.3, imposing MFV in the SMEFT constrains the flavor indices of the Wilson coefficients to be carried by certain combinations of Yukawa matrices. Upon rotation to the mass basis, Yukawa couplings are converted to powers of the fermion masses, which for light fermions can be expanded in the small-mass limit. As an explicit example we consider this expansion for the class-5 Wilson coefficients, starting with C_{uH}. MFV implies that the weak-basis coefficient takes the form seen in Eq. 2.2.11

$$C_{\substack{uH \\ rs}}^{w} = \left[Y_u G_{uH} \left(Y_d Y_d^\dagger, Y_u Y_u^\dagger \right) \right]_{rs} , \tag{3.5.1}$$

where the function G_{uH} is regular in the limit that its arguments go to zero, but otherwise arbitrary. In the approximation where the CKM matrix is the unit matrix, the MFV scaling for the mass basis coefficient is obtained by making the replacement

$Y_u \to M_u$, where M_u are the mass-basis Yukawas, defined as

$$[M_f]_{ij} = \sqrt{2}\frac{[m_f]_{ij}}{\hat{v}_T}\,, \tag{3.5.2}$$

where the $[m_f]_{ij}$ were defined in Eq. 2.3.28. The mass-basis Yukawas are diagonal matrices and their elements vanish in the small-mass limit, with the exception of $[M_u]_{33}$ which is proportional to the top-quark mass and thus order one in that limit. Therefore, to leading order in the small-mass limit, we can write

$$\left[G_{uH}\left(Y_d Y_d^\dagger, Y_u Y_u^\dagger\right)\right]_{ks} \approx \delta_{ks} G_{uH}(0,0) + \delta_{k3}\delta_{s3}\sum_{k=1}^{\infty}\frac{y_t^{2k}}{k!}\left(\frac{d^k}{(dy_t^2)^k}G_{uH}(0,y_t^2)\Big|_{y_t\to 0}\right)\,, \tag{3.5.3}$$

where $y_t^2 = 2m_t^2/\hat{v}_T^2$. It follows that the expansion of the mass-basis coefficient C_{uH} in the small-mass limit within MFV is given by

$$C_{uH}\underset{rs}{} \approx [M_u]_{rk}\left[\mathcal{C}^1_{uH}\underset{ks}{} + \mathcal{O}\left(\frac{m^2}{\hat{v}_T^2}\right)\right]\,, \tag{3.5.4}$$

where the superscript j on the calligraphic Wilson coefficients $\mathcal{C}_i^j$ indicates that they multiply j explicit powers of mass-basis Yukawa matrices and where m is any light-fermion mass. The explicit expression for $\mathcal{C}^1_{uH}$ can be read off by matching Eq. 3.5.4 with Eq. 3.5.3. Similar statements hold for the MFV version of C_{dH} in the small-mass limit, which can be obtained from the C_{uH} result by the replacement $u \to d$.

For the corresponding leptonic operator the MFV expression is

$$C^w_{eH}\underset{rs}{} = \left[Y_e G_{eH}\left(Y_e Y_e^\dagger\right)\right]_{rs}\,. \tag{3.5.5}$$

All elements of the mass-basis Yukawa coupling M_e vanish in the small-mass limit, so the mass-basis coefficient is given by

$$C_{eH}\underset{rs}{} \approx [M_e]_{rs}\left[\mathcal{C}^1_{eH} + \mathcal{O}\left(\frac{m^2}{\hat{v}_T^2}\right)\right]\,, \tag{3.5.6}$$

where $\mathcal{C}^1_{eH} = G_{eH}(0)$ carries no flavor indices and is thus universal, in contrast to the quark cases.

It is a straightforward exercise to obtain analogous results for the other Wilson coefficients in MFV in the small-mass limit. For our analysis in Section 4.7, the important point is whether, after factoring out j overall Yukawa factors, the calligraphic Wilson coefficients, $\mathcal{C}_i^j$, are flavor universal (as in the case of $i = eH$), or flavor non-universal due to contributions from top-quark Yukawas (as in the case of

$i = dH, uH$). The flavor-universal cases used in Section 4.7 are

$$\begin{aligned} C_{\substack{eH\\pr}} &\approx [M_e]_{pr}\mathcal{C}^1_{eH}\,, & C_{\substack{Hd\\pr}} &\approx \delta_{pr}\mathcal{C}^0_{Hd}\,,\\ C_{\substack{eF\\pr}} &\approx [M_e]_{pr}\mathcal{C}^1_{eF}\,, & C_{\substack{He\\pr}} &\approx \delta_{pr}\mathcal{C}^0_{He}\,,\\ C^{(1,3)}_{\substack{H\ell\\pr}} &\approx \delta_{pr}\mathcal{C}^{(1,3),0}_{H\ell}\,, & C_{\substack{le\\prst}} &\approx \delta_{pr}\delta_{st}\mathcal{C}^0_{le}\,, \end{aligned} \tag{3.5.7}$$

where F is any gauge field appearing in the class-6 operators. The flavor non-universal cases are

$$\begin{aligned} C_{\substack{uH\\pr}} &\approx [M_u]_{pr}\mathcal{C}^1_{\substack{uH\\pr}}\,, & C_{\substack{Hud\\pr}} &\approx [M_u]_{pr}[M_d]_{pr}\mathcal{C}^2_{\substack{Hud\\pr}}\,,\\ C_{\substack{dH\\pr}} &\approx [M_d]_{pr}\mathcal{C}^1_{\substack{dH\\pr}}\,, & C^{(1,8)}_{\substack{qu\\prst}} &\approx \delta_{pr}\delta_{st}\mathcal{C}^{(1,8),0}_{\substack{qu\\prst}}\,,\\ C_{\substack{uF\\pr}} &\approx [M_u]_{pr}\mathcal{C}^1_{\substack{uF\\pr}}\,, & C^{(1,8)}_{\substack{qd\\prst}} &\approx \delta_{st}\delta_{pr}\mathcal{C}^{(1,8),0}_{\substack{qd\\pr}}\,,\\ C_{\substack{dF\\pr}} &\approx [M_d]_{pr}\mathcal{C}^1_{\substack{dF\\pr}}\,, & C_{\substack{ledq\\prst}} &\approx [M_e]_{pr}[M_d]_{st}\mathcal{C}^2_{\substack{ledq\\st}}\,,\\ C^{(1,3)}_{\substack{Hq\\pr}} &\approx \delta_{pr}\mathcal{C}^{(1,3),0}_{\substack{Hq\\pr}}\,, & C^{(1,8)}_{\substack{quqd\\prst}} &\approx [M_u]_{pr}[M_d]_{st}\mathcal{C}^{(1,8),2}_{\substack{quqd\\prst}}\,,\\ C_{\substack{Hu\\pr}} &\approx \delta_{pr}\mathcal{C}^0_{\substack{Hu\\pr}}\,, & C^{(1,3)}_{\substack{lequ\\prst}} &\approx [M_e]_{pr}[M_u]_{st}\mathcal{C}^{(1,3),2}_{\substack{lequ\\st}}\,, \end{aligned} \tag{3.5.8}$$

where there is no implied summation on repeated indices on the right-hand side of the approximations. The notation of Eq. 3.5.8 makes it clear that the calligraphic coefficients are flavor diagonal in the pairs of indices pr and st. We note that while the Wilson coefficients $C^{(1,8)}_{qd}$, C_{ledq} and $C^{(1,3)}_{lequ}$ carry four flavor indices, their corresponding small-mass MFV expansion functions, $\mathcal{C}_i$, are a function of (and therefore only carry) two flavor indices.

An important aspect of the flavor non-universal Wilson coefficients in Eq. 3.5.8 is that in several cases there is some redundancy in the notation such that two Wilson coefficients carrying different flavor indices may indeed be the same. As an example, we consider the Wilson coefficient $C^{(1,3)}_{Hq}$. Following the procedure outlined earlier in this section we find that in the small-mass limit after imposing MFV

$$C^{(1,3)}_{\substack{Hq\\pr}} \approx \delta_{pr}G^{(1,3)}_{Hq}(0,0) + \delta_{p3}\delta_{r3}\sum_{k=1}^{\infty}\frac{y_t^{2k}}{k!}\left(\frac{d^k}{(dy_t^2)^k}G^{(1,3)}_{Hq}(0,y_t^2)\bigg|_{y_t\to 0}\right). \tag{3.5.9}$$

Considering separately the cases of $pr = \{11, 22, 33\}$ we therefore find

$$\begin{aligned} C^{(1,3)}_{\substack{Hq\\11}} &\approx G^{(1,3)}_{Hq}(0,0) \equiv \mathcal{C}^{(1,3),0}_{\substack{Hq\\11}}\,,\\ C^{(1,3)}_{\substack{Hq\\22}} &\approx G^{(1,3)}_{Hq}(0,0) \equiv \mathcal{C}^{(1,3),0}_{\substack{Hq\\22}}\,,\\ C^{(1,3)}_{\substack{Hq\\33}} &\approx G^{(1,3)}_{Hq}(0,0) + \sum_{k=1}^{\infty}\frac{y_t^{2k}}{k!}\left(\frac{d^k}{(dy_t^2)^k}G^{(1,3)}_{Hq}(0,y_t^2)\bigg|_{y_t\to 0}\right) \equiv \mathcal{C}^{(1,3),0}_{\substack{Hq\\33}}\,. \end{aligned} \tag{3.5.10}$$

From Eq. 3.5.10, we see that the object $\mathcal{C}_{\substack{Hq \\ ks}}^{(1,3),0}$ is flavor-diagonal, but non-universal in the sense that $\mathcal{C}_{\substack{Hq \\ 11}}^{(1,3),0} = \mathcal{C}_{\substack{Hq \\ 22}}^{(1,3),0} \neq \mathcal{C}_{\substack{Hq \\ 33}}^{(1,3),0}$. This property carries over to a number of other flavor-dependent Wilson coefficients, and we will indicate in this work where such properties are used.

As discussed in Section 2.2.2, all the SMEFT coefficients can also depend on Yukawas through functions of flavor invariants such as

$$\mathrm{Tr}\left(Y_e Y_e^\dagger\right), \quad \mathrm{Tr}\left(Y_d Y_d^\dagger\right), \quad \mathrm{Tr}\left(Y_u Y_u^\dagger\right). \tag{3.5.11}$$

In the small-mass limit these are either constants, or functions of y_t^2. They can thus be absorbed into the definitions of the $\mathcal{C}_i^j$ above. For consistency of notation, we make explicit that Wilson coefficients in classes 1-4 depend on the above invariants and should also be expanded in the small-mass limit. Since those Wilson coefficients carry no flavor indices, this amounts to a change of notation $C_i \to \mathcal{C}_i^0$, where the superscript indicates that the small-mass limit has been taken in the flavor invariants on which the coefficients can depend.

3.6 Gauge Fixing in the Dimension-6 SMEFT

The techniques of gauge fixing, and the motivation for doing so in a QFT, specifically the SM, were first presented in Section 1.5. This necessity of gauge fixing also applies to the dimension-6 SMEFT. The topic of gauge fixing in the dimension-6 SMEFT has been previously discussed in [120, 126, 127]. Here, we present our own implementation, which extends the techniques presented in Section 1.5 to include dimension-6 corrections.

We begin by again considering the SM. We parameterize the Higgs doublet in terms of real scalar fields as

$$H = \frac{1}{\sqrt{2}} \begin{pmatrix} -i(\phi_1 - i\phi_2) \\ \phi_4 + i\phi_3 \end{pmatrix}, \tag{3.6.1}$$

and use the real representation of the generators, $T^a = -i\tau^a$, where the τ^a were defined above Eq. 1.1.21. Following the notation of Section 1.5.1, we expand each ϕ_i about its LO vacuum expectation value, denoted $\langle \phi_i \rangle = \phi_{0_i}$ as

$$\phi_i = \phi_{0_i} + \chi_i, \tag{3.6.2}$$

where $\chi_{i\neq 4}$ are the Goldstone bosons, χ_4 is related to the physical Higgs boson, h, and $\phi_{0_i} = \delta_{i4} v_T/\sqrt{2} = (0,1)^T v_T/\sqrt{2}$. In R_ξ gauge one aims to remove the Goldstone-

gauge boson mixing terms, which in the SM take the form

$$\mathcal{L} \supset (\partial^\mu \chi_i) A^a_\mu (gT)^a_{ij} \phi_{0_j} \,, \tag{3.6.3}$$

where $(gT)^a$ is defined in Eq. 1.5.5. The $i = 4$ component in Eq. 3.6.3 gives no contribution to the Lagrangian.

We now consider the inclusion of the dimension-6 SMEFT. We begin by defining the canonically-normalized fields of the Higgs doublet in Eq. 2.3.5 in terms of those in Eq. 3.6.2 via the transformation

$$\chi_i = X_{ij}\chi'_j \,, \qquad X = \begin{pmatrix} 1 & 0 & 0 & 0 \\ 0 & 1 & 0 & 0 \\ 0 & 0 & 1 - \frac{1}{4}\hat{v}_T^2 C_{HD} & 0 \\ 0 & 0 & 0 & 1 + C_{H,\text{kin}} \end{pmatrix} , \tag{3.6.4}$$

such that the χ'_i are related to the fields in Eq. 2.3.5 by

$$\chi'_1 = \frac{1}{\sqrt{2}}(\phi^+ + \phi^-) \,, \quad \chi'_2 = \frac{i}{\sqrt{2}}(\phi^+ - \phi^-) \,, \quad \chi'_3 = \phi^0 \,, \quad \chi'_4 = h \,. \tag{3.6.5}$$

Moreover, we replace the gauge fields and couplings as in Eq. 2.3.10, Eq. 2.3.11 and Eq. 2.3.13 such that all the Goldstone-gauge mixing terms of the SMEFT Lagrangian may be written

$$\begin{aligned} \mathcal{L} &\supset (X_{ik}\partial^\mu \chi'_k) A'^a_\mu (\bar{g}T')^a_{ij} \phi_{0_j} + \frac{1}{2} v_T^2 C_{HD} (\partial^\mu \chi'_3) A'^a_\mu (\bar{g}T')^a_{3j} \phi_{0_j} \\ &= (\partial^\mu \chi'_i) A'^a_\mu (\bar{g}\mathcal{F})^a_i \,, \end{aligned} \tag{3.6.6}$$

where the second term on the first line of Eq. 3.6.6 is the contribution arising from the explicit presence of the $C_{HD}Q_{HD}$ term in the dimension-6 SMEFT Lagrangian. In Eq. 3.6.6 we have also introduced the object $(\bar{g}T)^a$, which is defined similarly to $(gT)^a$ in Eq. 1.5.5, but with all instances of the gauge couplings replaced as $g_i \to \bar{g}_i$, and further defined "primed" generators

$$\begin{aligned} (\bar{g}T')^a &= M^{ab}(\bar{g}T)^b \\ &= \left(\bar{g}_2 T^1, \, \bar{g}_2 T^2, \, \bar{g}_2 T^3 - \frac{1}{2}\bar{g}_1 v_T^2 C_{HWB} T^4, \, \bar{g}_1 T^4 - \frac{1}{2}\bar{g}_2 v_T^2 C_{HWB} T^3 \right) , \end{aligned} \tag{3.6.7}$$

where M^{ab} is given in Eq. 2.3.14. Eq. 3.6.6 also introduces the object

$$\begin{aligned} (\bar{g}\mathcal{F})^a_i &= X_{ij}(\bar{g}T')^a_{jk}\phi_{0_k} + \delta_{i3}\frac{v_T^2}{2} C_{HD} (\bar{g}T')^a_{3k} \phi_{0_k} \\ &= (X^{-1})_{ij} (\bar{g}T')^a_{jk} \phi_{0_k} \,, \end{aligned} \tag{3.6.8}$$

where in the final line we have used that X has only diagonal elements, $X_{11} = X_{22} =$

$(X^{-1})_{11} = (X^{-1})_{22} = 1$, $(1 + \frac{\hat{v}_T^2}{2} C_{HD}) X_{33} = (X^{-1})_{33}$ and that the X_{44} component gives no contribution. In order to calculate the matrix $(\bar{g}\mathcal{F})^a_i$ we use, for example, that $(\bar{g}T')^1\phi_0$ equals $\bar{g}_2 v_T/2$ times a unit vector in the ϕ^1 direction. One finds

$$(\bar{g}\mathcal{F})^a_i = \frac{v_T}{2} \begin{pmatrix} \bar{g}_2 & 0 & 0 & 0 \\ 0 & \bar{g}_2 & 0 & 0 \\ 0 & 0 & \bar{g}_2(1 + \frac{\hat{v}_T^2}{4} C_{HD}) + \bar{g}_1 \frac{\hat{v}_T^2}{2} C_{HWB} & 0 \\ 0 & 0 & -\bar{g}_1(1 + \frac{\hat{v}_T^2}{4} C_{HD}) - \bar{g}_2 \frac{\hat{v}_T^2}{2} C_{HWB} & 0 \end{pmatrix} . \tag{3.6.9}$$

We follow the Faddeev-Popov gauge-fixing procedure outlined in Section 1.5.2 such that the SMEFT gauge-fixed generating functional $\mathcal{Z}$ takes the form

$$\mathcal{Z} = C \int \mathcal{D}A' \mathcal{D}\chi' \exp\left[i \int d^4x \left(\mathcal{L}\left[A', \chi', ...\right] - \frac{1}{2}(G)^2 \right) \right] \det\left(\frac{\delta G}{\delta(\alpha'/\bar{g})} \right) , \tag{3.6.10}$$

where G^a is the gauge-fixing functional and the object $(\alpha'/\bar{g})^b$ is defined later in this section. Note that in comparison with Eq. 1.5.2, Eq. 3.6.10 the functional derivative in the determinant is with respect to the object $(\alpha'/\bar{g})$, rather than α, however this change is valid due to the freedom in rescaling α. Given the form of the Goldstone-gauge mixing terms in Eq. 3.6.6, we choose the gauge-fixing functional in Eq. 3.6.10 to be

$$G^a = \frac{1}{\sqrt{\xi}} \left(\partial^\mu A'^a_\mu - \xi(\bar{g}\mathcal{F})^a_i \chi'_i \right) , \tag{3.6.11}$$

which defines the R_ξ gauges in the SMEFT.[1] We see that the form of the gauge-fixing functional in Eq. 3.6.11 resembles that of the R_ξ gauges in the SM in Eq. 1.5.6 with the gauge fields replaced by their primed counterparts and F replaced with $\mathcal{F}$. The Goldstone-gauge boson mixing terms in Eq. 3.6.6 are then removed by the $-\frac{1}{2}(G)^2$ term in Eq. 3.6.10.

Interactions of SM particles with ghost fields arise through the functional determinant in Eq. 3.6.10, for which we must determine the variation of G^a under arbitrary gauge transformations. The gauge transformation of the scalar fields may be written

$$\delta\phi_i = -\alpha^a T^a_{ij} \phi_j \equiv -\left(\frac{\alpha}{\bar{g}}\right)^a (\bar{g}T)^a_{ij} \phi_j \equiv -\left(\frac{\alpha'}{\bar{g}}\right)^a (\bar{g}T')^a_{ij} \phi_j \, , \tag{3.6.12}$$

where the second relation defines the object $(\alpha/\bar{g})^a$ to be

$$\left(\frac{\alpha}{\bar{g}}\right)^a = \left(\frac{\alpha^1}{\bar{g}_2}, \frac{\alpha^2}{\bar{g}_2}, \frac{\alpha^3}{\bar{g}_2}, \frac{\alpha^4}{\bar{g}_1} \right) , \tag{3.6.13}$$

[1] Note that in principle we can have a different ξ for each of the physical gauge fields.

and the third relation in Eq. 3.6.12 defines the object $(\alpha'/\bar{g})^a$ as

$$\left(\frac{\alpha}{\bar{g}}\right)^a = M^{ab}\left(\frac{\alpha'}{\bar{g}}\right)^b . \tag{3.6.14}$$

We may use Eq. 3.6.4 and Eq. 3.6.12 to find the gauge transformation of χ_i':

$$\begin{aligned}\delta\chi_i' = (X^{-1})_{ij}\delta\chi_j &= -\left(\frac{\alpha'}{\bar{g}}\right)^a (X^{-1})_{ij}(\bar{g}T')^a_{jk}(\phi_{0_k} + X_{kl}\chi_l') \\ &\equiv -\left(\frac{\alpha'}{\bar{g}}\right)^a \left((\bar{g}\mathcal{F})^a_i + (\bar{g}\mathcal{T})^a_{ij}\chi_j'\right) ,\end{aligned} \tag{3.6.15}$$

where we have defined the object $(\bar{g}\mathcal{T})^a_{ij} \equiv (X^{-1})_{ik}(\bar{g}T')^a_{kl}X_{lj}$. Explicitly $(\bar{g}\mathcal{T})^a_{ij}$ acts on χ_i' as (for brevity and as no other terms enter our calculation in Chapter 4, we give only the Higgs contributions to this term)

$$(\bar{g}\mathcal{T})^a_{ij}\chi_j' \supset \frac{h}{2}\begin{pmatrix} \bar{g}_2(1+C_{H,\mathrm{kin}}) & 0 & 0 & 0 \\ 0 & \bar{g}_2(1+C_{H,\mathrm{kin}}) & 0 & 0 \\ 0 & 0 & \bar{g}_2(1+\hat{v}_T^2 C_{H\Box}) + \bar{g}_1\frac{\hat{v}_T^2}{2}C_{HWB} & 0 \\ 0 & 0 & -\bar{g}_1(1+\hat{v}_T^2 C_{H\Box}) - \bar{g}_2\frac{\hat{v}_T^2}{2}C_{HWB} & 0 \end{pmatrix} . \tag{3.6.16}$$

We may similarly write the transformation of the unprimed gauge fields as

$$\delta A^a_\mu = \partial_\mu\left(\frac{\alpha}{\bar{g}}\right)^a - f^{abc}\alpha^b A^c_\mu \equiv \partial_\mu\left(\frac{\alpha}{\bar{g}}\right)^a - \bar{g}_2 f^{abc}\left(\frac{\alpha}{\bar{g}}\right)^b A^c_\mu . \tag{3.6.17}$$

The object $f^{abc} = \epsilon^{abc}$ if $a, b, c \in 1, 2, 3$ and vanishes otherwise, which we have used to replace $\alpha^b \to \bar{g}_2(\alpha/\bar{g})^b$ in the above equation. The form of $\delta A'^a_\mu$ in terms of the object $(\alpha'/\bar{g})^a$ is then found using Eq. 2.3.13, Eq. 3.6.14 and Eq. 3.6.17

$$\delta A'^a_\mu = (M^{-1})^{ab}\delta A^b_\mu = \partial_\mu\left(\frac{\alpha'}{\bar{g}}\right)^a - \bar{g}_2(M^{-1})^{ab}f^{bcd}M^{cc'}\left(\frac{\alpha'}{\bar{g}}\right)^{c'} A^d_\mu . \tag{3.6.18}$$

We can now calculate the functional derivatives needed to evaluate Eq. 3.6.10 using the results in Eq. 3.6.15 and Eq. 3.6.18. First, one has

$$\frac{\delta A'^a_\mu}{\delta(\alpha'/\bar{g})^b} \equiv \mathcal{M}^{ab}_\mu = \delta^{ab}\partial_\mu - \bar{g}_2(M^{-1})^{ab'}f^{b'cd}A^d_\mu M^{cb} , \tag{3.6.19}$$

(note that the gauge fields here are the unprimed gauge fields), where the explicit result is

$$\mathcal{M}^{ab}_\mu = \bar{g}_2\begin{pmatrix} \frac{1}{\bar{g}_2}\partial_\mu & W^3_\mu & -W^2_\mu & \frac{1}{2}\hat{v}_T^2 C_{HWB}W^2_\mu \\ -W^3_\mu & \frac{1}{\bar{g}_2}\partial_\mu & W^1_\mu & -\frac{1}{2}\hat{v}_T^2 C_{HWB}W^1_\mu \\ W^2_\mu & -W^1_\mu & \frac{1}{\bar{g}_2}\partial_\mu & 0 \\ \frac{1}{2}\hat{v}_T^2 C_{HWB}W^2_\mu & -\frac{1}{2}\hat{v}_T^2 C_{HWB}W^1_\mu & 0 & \frac{1}{\bar{g}_2}\partial_\mu \end{pmatrix} . \tag{3.6.20}$$

From Eq. 3.6.19 and Eq. 3.6.15, the variation of the gauge-fixing functional, G^a in Eq. 3.6.11 is

$$\frac{\delta G^a}{\delta(\alpha'/\bar{g})^b} = \frac{1}{\sqrt{\xi}}\left(\partial^\mu \mathcal{M}_\mu^{ab} + \xi(\bar{g}\mathcal{F})_i^a\left((\bar{g}\mathcal{F})_i^b + (\bar{g}\mathcal{T})_{ij}^b\chi_j'\right)\right). \tag{3.6.21}$$

Following the procedure outlined at the beginning of Section 1.5.2, the ghost Lagrangian is then

$$\mathcal{L}_{\text{ghost}} = \overline{c}^a\left[-\left(\partial^\mu \mathcal{M}_\mu^{ab}\right) - \xi(\bar{g}\mathcal{F})_i^a\left((\bar{g}\mathcal{F})_i^b + (\bar{g}\mathcal{T})_{ij}^b\chi_j'\right)\right]c^b. \tag{3.6.22}$$

The ghost fields in Eq. 3.6.22 are given by $c^a = (c_{W^1}, c_{W^2}, c_{W^3}, c_B)$, and similarly for the fields in $\overline{c}^a$. Comparing Eq. 3.6.22 with its equivalent form in the SM found in Eq. 1.5.12, we recover the SM result in the limit $\Lambda_{\text{NP}} \to \infty$, as expected. In fact, the form of Eq. 3.6.22 is reminiscent of the SM form in Eq. 1.5.12, which is recovered by the simple substitutions

$$\begin{aligned} \mathcal{M}_\mu^{ab} &\to D_\mu^{ab}, & \chi' &\to \chi, \\ (\bar{g}\mathcal{T})_{ij}^a &\to (gT)_{ij}^a, & (\bar{g}\mathcal{F})_i^a &\to (gF)_i^a. \end{aligned} \tag{3.6.23}$$

We must now find the form of the Lagrangian in Eq. 3.6.22 in the mass basis. The form of the ghost mass matrix in Eq. 3.6.22 is

$$(m_{\text{ghost}}^2)^{ab} = \xi(\bar{g}\mathcal{F})_i^a(\bar{g}\mathcal{F})_i^b, \tag{3.6.24}$$

which is diagonalized by the matrix R in Eq. 2.3.17 such that

$$(m_{D,\text{ghost}}^2)^{ab} \equiv (R^{-1})^{ac}(m_{\text{ghost}}^2)^{cd}R^{db} = \text{diag}(M_W, M_W, M_Z, 0). \tag{3.6.25}$$

The ghosts in the mass basis, denoted u^a and $\overline{u}^a$, are thus related to those in the weak basis by

$$c^a = R^{ab}u^b, \qquad \overline{c}^a = \overline{u}^b(R^{-1})^{ba}, \tag{3.6.26}$$

where $u^a = (u_{W^+}, u_{W^-}, u_Z, u_A)$, and similarly for $\overline{u}^a$. With the gauge fields A_μ written in terms of the mass basis as described in Eq. 2.3.20, the ghost Lagrangian in the mass basis is therefore

$$\begin{aligned} \mathcal{L}_{\text{ghost}} = \overline{u}^a\Big[&-\left((R^{-1})^{ac}\partial^\mu \mathcal{M}_\mu^{cd}R^{db}\right) \\ &- \xi\left((m_{D,\text{ghost}}^2)^{ab} + (R^{-1})^{ac}(\bar{g}\mathcal{F})_i^c(\bar{g}\mathcal{T})_{ij}^d\chi_j'R^{db}\right)\Big]u^b. \end{aligned} \tag{3.6.27}$$

Although our derivation is rather different, we find that the Feynman rules produced by the Lagrangian in Eq. 3.6.27 exactly match those found in [120], which were instead derived by taking advantage of BRST invariance.

Chapter 4

$h \to f\bar{f}$ at NLO in the SMEFT

In this chapter we present the calculational techniques and results for the decay rate of $h \to f\bar{f}$ for $f \in \{b, c, \tau, \mu\}$ up to NLO in the dimension-6 SMEFT. While aspects of the calculation that apply generally to calculations in the dimension-6 SMEFT have been discussed in Chapter 3, the topics discussed here are of particular relevance to the aforementioned Higgs decay mode. The NLO SM result was first calculated in [128], and partial results exist for the NLO dimension-6 SMEFT results. The results in the large-m_t limit, and a subset of the four-fermion operator results for the decay modes $h \to b\bar{b}$ and $h \to \tau\bar{\tau}$ were calculated in [119] using the $\{G_F, M_W, M_Z\}$ input scheme. The QCD corrections to $h \to b\bar{b}$ were calculated in [129]. In this work we recover these results as a subset of the full corrections to the corresponding decay modes. We begin by outlining the calculation and setting up the necessary notation in Section 4.1, followed by the LO results in Section 4.2. This is followed by discussions of the NLO calculation of this decay mode, including discussions of some approximations made, and other topics of relevance throughout Sections 4.3.1 to 4.3.4. In Section 4.4 we present a subset of the analytic results that are relevant to later discussions. In Section 4.5 we discuss sources of enhanced NLO corrections, and how to avoid these, followed by the presentation and discussion of the numerical results and scale uncertainties in Section 4.6. Finally, we present numerical results for ratios of decay rates in Section 4.7 and discuss the advantages of considering such ratios.

4.1 Outline of the Calculation

In this section we aim to outline the calculation of the decay rate $h \to f\bar{f}$ up to NLO in the dimension-6 SMEFT. To this end, it is useful to break the decay rate

up into LO and NLO components as

$$\Gamma(h \to f\bar{f}) \equiv \Gamma_f = \Gamma_f^{(0)} + \Gamma_f^{(1)}\,, \tag{4.1.1}$$

where the subscript f denotes the flavor of the final-state fermion pair, and where the superscripts (0) and (1) denote the LO and NLO contributions to the decay rate respectively. As we do not include contributions of $\mathcal{O}(\hat{v}_T^4/\Lambda_{\rm NP}^4)$ and above, we may further split the decay rate up as

$$\begin{aligned}\Gamma_f^{(0)} &= \Gamma_f^{(4,0)} + \Gamma_f^{(6,0)}\,,\\ \Gamma_f^{(1)} &= \Gamma_f^{(4,1)} + \Gamma_f^{(6,1)}\,.\end{aligned} \tag{4.1.2}$$

Here the superscript (i,j) refers to the dimension-i contribution at j-th order in perturbation theory. As such, each term contributing to $\Gamma_f^{(6,j)}$ is a function of exactly one Wilson coefficient.

It is useful to our later analysis to further break up the NLO corrections as

$$\begin{aligned}\Gamma_f^{(i,1)} &= \Gamma_{f,(g,\gamma)}^{(i,1)} + \Gamma_{f,(\text{weak})}^{(i,1)}\,,\\ &= \Gamma_{f,(g,\gamma)}^{(i,1)} + \Gamma_{f,(t)}^{(i,1)} + \Gamma_{f,(\text{rem.})}^{(i,1)}\,.\end{aligned} \tag{4.1.3}$$

Here, $\Gamma_{f,(g,\gamma)}^{(i,1)}$ includes all diagrams with photon or gluon corrections, and real emission of gluons and photons. Similarly, $\Gamma_{f,(\text{weak})}^{(i,1)}$ includes the remaining weak corrections. In the second line of Eq. 4.1.3 we have further broken $\Gamma_{f,(\text{weak})}^{(i,1)}$ down into two pieces. The first of these, $\Gamma_{f,(t)}^{(i,1)}$ contains the virtual weak corrections in the large-m_t limit (which we define further in Section 4.4.2), while $\Gamma_{f,(\text{rem.})}^{(i,1)}$ contains the remaining corrections that do not fall into either of the other categories.

To produce the decay rates outlined earlier in this section, we must calculate both the UV-renormalized virtual corrections to the LO decay rate, as well as the decay rate including the real emission of photons and gluons at the same order in α and α_s. Together, these components form a UV- and IR-finite decay rate. This is summarized as

$$\Gamma_f = \int \frac{d\phi_2}{2m_H} \sum_s \left|\mathcal{M}_{h\to f\bar{f}}\right|^2 + \int \frac{d\phi_3}{2m_H} \sum_{s,\lambda} \left|\mathcal{M}_{h\to f\bar{f}(g,\gamma)}\right|^2\,, \tag{4.1.4}$$

where the summation is performed over final-state spins and polarizations (where applicable) and where $d\phi_i$ is the differential Lorentz-invariant phase-space measure for an i-body final-state process. Details on the evaluation of these integrals is given in Appendix B. While both terms in Eq. 4.1.4 are individually UV-finite, it is only in the sum of the two terms in Eq. 4.1.4 that we arrive at a fully UV- and IR-finite decay rate. In this way, the calculation performed here really corresponds to the

calculation of the decay rate $h \to f\bar{f}(A)$, for $A = g$, γ. For brevity, we will generally refer to the decay mode simply as $h \to f\bar{f}$.

This work involves the calculation of a large number of $1 \to 1$, $1 \to 2$, and $1 \to 3$ diagrams at various loop orders. While calculating the renormalized matrix element, we see that for some subsets of corrections, such as the QED-QCD corrections, the results for $h \to f\bar{f}$ may be inferred for all f after the calculation of this decay mode for a particular process, as we shall see in Sections 4.4.1 and 4.4.2. However, for most subsets of NLO corrections, owing to the differences in representations of the SM symmetry group seen in Table 1.3 (aside from the pair τ and μ), we generally find that the results for one particular process cannot be inferred from the results of another. As a result, we calculate from scratch all the necessary one-loop amplitudes for each process. As noted, the exception to this is the process $h \to \mu\bar{\mu}$, the results for which may be inferred from the results of $h \to \tau\bar{\tau}$.

There are a small number of simplifying assumptions that we make throughout this calculation. The first is the diagonal CKM approximation. This approximation states that the form of the CKM matrix introduced in Section 1.1.3 is well approximated by $V_{ij} \approx \delta_{ij}$. Such an approximation is standard in SM EW calculations, and the consequences of this approximation in the context of the calculations performed here are explored in Section 4.3.1. The second assumption is that the first generation fermions (e, u and d) are massless.

In the calculation outlined throughout this chapter we have performed numerous cross-checks. Firstly, we have performed all the calculations in both unitary and Feynman gauge, and verified that the results in both gauges are equal. This confirms that the results we obtain are gauge invariant, and helps verify that the form of the result is correct. Further, we have verified the UV finiteness of our result. Finally, we have verified that the IR poles present in both terms of Eq. 4.1.4 cancel in the sum of the two-body and three-body final-state decay rates.

Throughout this work we will also often refer to what we call *the small-mass limit*, which we have already touched on in Section 3.5. In this limit we suppose that all fermions (besides the top quark) have masses much less than the EW bosons (besides the photon), and in taking this limit we retain only LO terms in the expansion in light-fermion masses. We find that not only does this limit produce far simpler analytical results whilst maintaining a high degree of accuracy to the full result, but also provides some theoretical advantages over the full-mass-dependent result when we introduce decoupling constants in Section 4.5.2.

4.2 LO Calculation

We begin by considering the process $h \to f\bar{f}$ at LO within the dimension-6 SMEFT. While throughout this chapter we typically consider $f \in \{b, c, \tau, \mu\}$, at LO in the dimension-6 SMEFT the results for all fermions are analogous. For this reason, the results presented in this section apply to all massive SM fermions (except for the top quark), where the result for a specific fermion is achieved with the corresponding replacement of f, where f represents a generic fermion.

For this process, the LO diagrams appear at zeroth loop order. As was outlined in Section 1.2, we therefore currently need not be concerned with UV divergences. There is only one diagram that contributes to $h \to f\bar{f}$ at LO, which is shown in Fig. 4.1. We may write the amplitude of this process in the form

$$i\mathcal{M}^{(0)} = -i\bar{u}(p_f)\left(\mathcal{M}_L^{(0)}P_L + \mathcal{M}_L^{(0)*}P_R\right)v(p_{\bar{f}})\,, \tag{4.2.1}$$

where, analogously to Eq. 4.1.1, the superscript (0) represents that this amplitude occurs at zeroth loop order. We also note that for this process the left- and right-handed components of the amplitude are related via complex conjugation, i.e. $\mathcal{M}_R^{(0)} = \mathcal{M}_L^{(0)*}$; a relation we have already used in Eq. 4.2.1. In the SM this is due to the Higgs coupling equally to left- and right-handed fermions. In the dimension-6 SMEFT it is possible for the Higgs to couple differently to LH and RH fermions, for example, via off-diagonal elements of the class-5 operators seen in Table A.1. This property does not affect the LO results and we are free to use that $\mathcal{M}_R^{(0)} = \mathcal{M}_L^{(0)*}$ for the LO SMEFT amplitude. At NLO in the dimension-6 SMEFT we must be more careful when using $\mathcal{M}_R = \mathcal{M}_L$, so we examine some operators that potentially spoil this relation in Section 4.3.1. At LO however, this allows us to simplify the calculation by only having to calculate the components of the amplitude proportional to P_L. We further split up $\mathcal{M}_L^{(0)}$ into its SM and dimension-6 components analogously to Eq. 4.1.2 as

$$\mathcal{M}_L^{(0)} = \mathcal{M}_L^{(4,0)} + \mathcal{M}_L^{(6,0)}\,. \tag{4.2.2}$$

Adopting the input scheme outlined in Section 3.2 we find

$$\begin{aligned}\mathcal{M}_L^{(4,0)} &= \frac{m_f}{\hat{v}_T}\,,\\ \mathcal{M}_L^{(6,0)} &= m_f\hat{v}_T\left[C_{H\Box} - \frac{C_{HD}}{4}\left(1 - \frac{\hat{c}_w^2}{\hat{s}_w^2}\right) + \frac{\hat{c}_w}{\hat{s}_w}C_{HWB} - \frac{\hat{v}_T}{m_f}\frac{C_{fH}^*}{\sqrt{2}}\right]\,.\end{aligned} \tag{4.2.3}$$

Despite the fact that the only SMEFT operators that directly generates the hff vertex in Fig. 4.1 are the set of class-5 operators C_{fH} of Table A.1, we see the emergence of three other Wilson coefficients in Eq. 4.2.3. These are a result of both

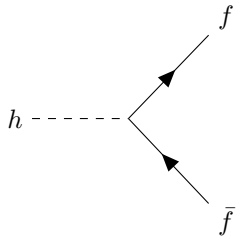

Figure 4.1: *The only Feynman diagram contributing to $h \to f\bar{f}$ at LO. In this diagram there is no visual distinction in the vertex to signify a SM or dimension-6 contribution, with it understood that both contributions are included.*

the shifts in the Higgs doublet required to ensure canonical normalization as outlined in Section 2.3.1, and due to the replacement of v_T according to Eq. 3.2.6 to satisfy our choice of input scheme.

To complete our analysis of this decay mode at LO, we must also calculate the squared amplitude and perform the integral over phase space to find the LO decay rate. The squared matrix element takes the form

$$|\mathcal{M}_L^{(0)}|^2 = |\mathcal{M}_L^{(4,0)}|^2 + \mathcal{M}_L^{(4,0)}\mathcal{M}_L^{(6,0)*} + \mathcal{M}_L^{(6,0)}\mathcal{M}_L^{(4,0)*} + \mathcal{O}\left(\frac{\hat{v}_T^4}{\Lambda_{\rm NP}^4}\right), \tag{4.2.4}$$

where the first term contributes to the SM decay rate, the second and third terms contribute to the dimension-6 decay rate, and where we have been careful to neglect the cross term between dimension-6 amplitudes which contributes at $\mathcal{O}(\hat{v}_T^4/\Lambda_{\rm NP}^4)$ (formally, a dimension-8 contribution) and is thus ignored here. Details of the phase-space integral for a $1 \to 2$ process may be found in Appendix B.1. We find that the component contributions to the LO decay rate are

$$\begin{aligned}
\Gamma_f^{(4,0)} &= \frac{N_c^f m_H m_f^2 \beta_f^3}{8\pi \hat{v}_T^2}\,, \\
\Gamma_f^{(6,0)} &= 2\Gamma_f^{(4,0)}\left[C_{H\Box} - \frac{C_{HD}}{4}\left(1 - \frac{\hat{c}_w^2}{\hat{s}_w^2}\right) + \frac{\hat{c}_w}{\hat{s}_w}C_{HWB} - \frac{\hat{v}_T}{m_f}\frac{\mathrm{Re}(C_{fH})}{\sqrt{2}}\right]\hat{v}_T^2\,,
\end{aligned} \tag{4.2.5}$$

where N_c^f is a color factor such that $N_c^f = N_c = 3$ for quarks, and $N_c^f = 1$ for leptons, and where

$$\beta_f = \sqrt{1 - \frac{4m_f^2}{m_H^2}}\,, \quad \text{for } f \neq t\,, \tag{4.2.6}$$

is a kinematic function arising from the phase-space integration.[1] Note that the function in Eq. 4.2.6 applies only to the light fermions, and we later define a similar

[1] Specifically, this function is related to the absolute velocity of the outgoing fermion in the rest frame of the decaying Higgs as $v_f = m_H\beta_f/2$.

term for top quarks. The dimension-6 result is proportional to the SM result; this is a result of the cross terms of the SM and dimension-6 amplitudes, i.e. the second and third terms of Eq. 4.2.4. Together, the equations in Eq. 4.2.5 constitute all the results of this decay mode at LO up to and including $\mathcal{O}\left(\hat{v}_T^2/\Lambda_{\rm NP}^2\right)$.

4.3 NLO Calculation

In this section we discuss several technical aspects of the calculation of $h \to f\bar{f}$ at NLO in the dimension-6 SMEFT. We begin by considering the appropriateness of the diagonal CKM approximation for these decay modes in both the SM and the dimension-6 SMEFT in Section 4.3.1, and then discuss the construction of the one-loop counterterm for these processes in Section 4.3.2. We then consider several technical complications for the renormalization of these decay modes in the dimension-6 SMEFT throughout Sections 4.3.3 to 4.3.5. Finally, we discuss the construction of the NLO decay rate in Section 4.3.6.

4.3.1 Diagonal CKM Approximation

Before proceeding further with our discussion of the calculation of the decay rate for the process $h \to f\bar{f}$ we consider an effect that first emerges at NLO for this process, that being the introduction of CKM-matrix elements, first discussed in Section 1.1.3.

While the inclusion of CKM elements beyond the approximation $V_{ij} \approx \delta_{ij}$ can be of paramount importance, for example in flavor physics, we explore the consequences of such an approximation within the processes considered here. We can observe the accuracy of this approximation by considering the form of the Wolfenstein parameterization seen in Eq. 1.1.43. Considering the process $h \to f\bar{f}$ at NLO in the SM, while the majority of contributing diagrams are not a function of CKM elements, for those that are it is always the product of two CKM elements. Restricting this to the processes considered here, $f \in \{b,\, c,\, \tau,\, \mu\}$, the minimum off-diagonal CKM suppression in the SM at NLO with our approximation of vanishing first-generation fermion masses is brought to $\lambda^4 \approx 2 \times 10^{-3}$ for both $h \to b\bar{b}$ and $h \to c\bar{c}$. Therefore, within the SM, applying the diagonal CKM approximation for this process only neglects terms which are highly suppressed.

From the above discussion, we see that the diagonal CKM approximation is accurate within the SM. Before proceeding further with the corresponding calculations in the dimension-6 SMEFT it is important to check that this approximation is still accurate.

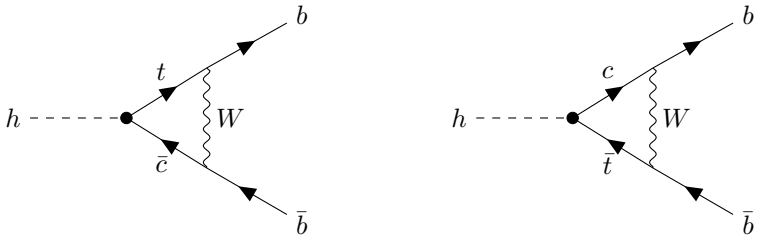

Figure 4.2: *The two diagrams with minimum off-diagonal CKM suppression for the process $h \to b\bar{b}$. Here, the "blob" vertex represents the effective vertex generated only by the operators $Q_{\substack{uH \\ 32}}$, $Q_{\substack{uH \\ 23}}$, and their hermitian conjugates.*

We first consider $h \to b\bar{b}$, and for simplicity we work in unitary gauge.[1] Here we find that the minimum possible CKM suppression would arise from the diagrams seen in Fig. 4.2. As seen in these diagrams, unlike in the SM, the dimension-6 SMEFT generates couplings between the Higgs and fermion pairs of different flavor, in this case a *htc* coupling. In the case of the diagrams seen in Fig. 4.2, this allows for the generation of amplitudes which are a function of only a single off-diagonal CKM element (rather than two as required in the SM), in this case arising from the *Wcb* vertex. We find that diagrams of the form seen in Fig. 4.2 would enter the decay rate and scale as

$$\Gamma_{b,\text{CKM-min}} \sim \lambda^2 \left(\text{Re}\left(C_{\substack{uH \\ 23}} \right) + \text{Re}\left(C_{\substack{uH \\ 32}} \right) \right) , \tag{4.3.1}$$

where $\Gamma_{b,\text{CKM-min}}$ represents contributions to the decay rate from diagrams which give the minimum possible off-diagonal CKM suppression (i.e. the diagrams in Fig. 4.2). We consider the factor of $\lambda^2 \approx 0.05$ to be an appreciably large enough suppression that we adopt the diagonal CKM approximation when considering $h \to b\bar{b}$.

We next turn our attention to the process $h \to c\bar{c}$. Similarly to the approach taken above when considering $h \to b\bar{b}$, in unitary gauge we consider the diagrams that would lead to the minimum off-diagonal CKM suppression, which are found in Fig. 4.3. We again find that these diagrams are a function of only a single off-diagonal CKM element, and enter the decay rate for this process as

$$\Gamma_{c,\text{CKM-min}} \sim \lambda \left(1 - \frac{\lambda^2}{2} \right) \left(\text{Re}\left(C_{\substack{dH \\ 12}} \right) + \text{Re}\left(C_{\substack{dH \\ 21}} \right) \right) . \tag{4.3.2}$$

Here, the off-diagonal CKM element results in a smaller suppression, and therefore a larger overall correction than that seen in the $h \to b\bar{b}$ case, being approximately given

[1] In R_ξ gauge, along with the contributions in Figs. 4.2 and 4.3 we also get similar contributions from diagrams where we replace W with the charged Goldstone boson, ϕ, in Figs. 4.2 and 4.3.

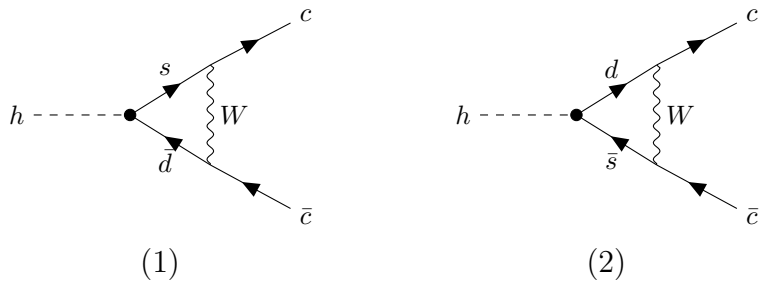

Figure 4.3: *The two diagrams with minimum off-diagonal CKM suppression for the process $h \to c\bar{c}$. Here, the "blob" vertex represents the effective vertex generated only by the operators $Q_{\substack{dH \\ 12}}$, $Q_{\substack{dH \\ 21}}$, and their hermitian conjugates.*

by $\lambda(1-\lambda^2/2) \approx 0.21$. In this instance it is therefore possible that the diagonal CKM approximation may not be appropriate. To estimate the size of the contributions that would be neglected in the diagonal CKM approximation, we calculate in full the contributions to the decay rate from the diagrams in Fig. 4.3, with all parameters renormalized in the $\overline{\text{MS}}$ scheme. Using the inputs found in Table 4.2[1] we numerically find at $\mu = m_H$

$$\begin{aligned}\frac{\Gamma_{c,\text{CKM-min}}}{\Gamma_c^{(4,0)}} &= \frac{\hat{v}_T^2}{\Lambda^2}(-4\times10^{-5})|V_{cd}||V_{cs}|\,\text{Re}\left(C_{\substack{dH \\ 12}}\right) \\ &= \frac{\hat{v}_T^2}{\Lambda^2}(9\times10^{-6})\,\text{Re}\left(C_{\substack{dH \\ 12}}\right)\,, \end{aligned} \tag{4.3.3}$$

where we have normalized the results by the LO SM results. Looking ahead, comparing the result in Eq. 4.3.3 to the results in Eq. 4.6.7 we see that the result in Eq. 4.3.3 constitutes a tiny NLO correction.[2] With this in mind, and considering that we expect this correction to be the largest of those that are a function of off-diagonal CKM elements, we conclude that the diagonal CKM approximation is also suitable for the process $h \to c\bar{c}$. Furthermore, considering the analytic form of the expression producing Eq. 4.3.3, we find that the decay rate scales at LO in the small-mass limit as $\sim m_c^2 m_s$.[3] We find that every other term in the small-mass limit scales as either $\sim m_c$ or $\sim m_c^2$, and so $\Gamma_{c,\text{CKM-min}}$ is suppressed by an additional power of light-fermion mass, explaining its small numerical size.

Finally, considering Higgs decay to lepton anti-lepton pair, it is clear that at NLO

[1] The values in this table include on-shell parameter values. We note however that the numerical differences between on-shell parameter values and $\overline{\text{MS}}$ parameter values at $\mu = 125$ GeV are sufficiently small enough that they do not affect the conclusions of this illustrative analysis.

[2] In fact, it is smaller than even the smallest corrections observed when using the diagonal CKM approximation by approximately an order of magnitude.

[3] One factor of m_c is from the tree-level $h \to c\bar{c}$ amplitude, while the additional factors of m_c and m_s are due to these fields requiring chirality flips to ensure the correct handedness to interact with the W-boson, and the correct handedness of the final-state particles.

there are no contributions from CKM elements to any diagrams contributing to the decay rate, and so the diagonal CKM approximation may be applied without neglecting any terms. Furthermore, analogous reasoning to that presented throughout this section tells us that with the diagonal CKM approximation, only diagonal elements of the non-class-8 operators in Table A.1 contribute to the processes considered here. This allows us to use the relation $\mathcal{M}_R = \mathcal{M}_L^*$, introduced in Section 4.2, at NLO in the dimension-6 SMEFT.

4.3.2 The One-Loop Counterterm

We first described the principle of UV renormalization of one-loop amplitudes in Section 1.2.2. The techniques described throughout that section carry over analogously to the dimension-6 SMEFT, where we now must include dimension-6 operator contributions such that our results are now a function of Wilson coefficients. In summary, we are required to take the mass-basis dimension-6 SMEFT in our chosen input scheme, described throughout Section 2.3 and Section 3.2, and replace the bare input parameters with renormalized parameters and counterterms. These replacements, which also apply to the dimension-6 SMEFT, are given by Eqs. 1.2.9 and 1.2.10, and the Wilson coefficient replacements can be found in Eq. 2.1.12. We must then calculate all resulting diagrams at NLO in perturbation theory, these being the bare one-loop diagrams and tree-level counterterm diagrams, where the counterterms are evaluated after calculating a set of two-point functions. The NLO corrections may therefore be split as

$$\mathcal{M}_f^{(1)} = \mathcal{M}_f^{(1),\text{bare}} + \mathcal{M}_f^{\text{C.T.}}\,, \tag{4.3.4}$$

where $\mathcal{M}^{(1),\text{bare}}$ contains the set of bare one-loop diagrams, and $\mathcal{M}^{\text{C.T.}}$ contains all diagrams with counterterm insertions. The diagrams contributing to $\mathcal{M}_f^{(1),\text{bare}}$ are too numerous to report in this thesis in full, however, we give some subsets of diagrams in Section 4.4.3 and Appendices C.1 and C.2. We also note that all diagrams in unitary gauge also contribute in Feynman gauge (albeit with differing analytical contributions), however, in Feynman gauge there are also contributions from diagrams with ghost fields and Goldstone bosons on the internal lines. The diagrams contributing to $\mathcal{M}_f^{\text{C.T.}}$ can be found in Fig. 4.4. Analogously to Eq. 4.2.1, we may split our counterterm amplitude into left- and right-handed components as

$$i\mathcal{M}_f^{\text{C.T.}} = -i\bar{u}(p_f)\left(\delta\mathcal{M}_{f,L}P_L + \delta\mathcal{M}_{f,L}^* P_R\right) v(p_{\bar{f}})\,, \tag{4.3.5}$$

where we have carried over the property of $\mathcal{M}_R = \mathcal{M}_L^*$ to the counterterms. Similarly to what we saw in Section 4.2 we can actually describe all light fermion flavors

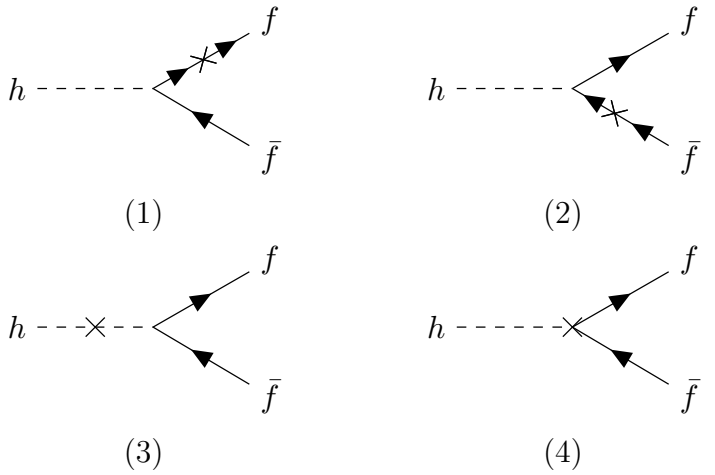

Figure 4.4: *The four counterterm diagrams contributing to the process $h \to f\bar{f}$ at NLO. Here, a cross represents a counterterm insertion. Diagrams (1-3) represent wavefunction renormalization counterterms, while Diagram (4) represents a vertex counterterm. The counterterms include both SM and dimension-6 SMEFT contributions.*

simultaneously in the construction of the matrix element counterterm, again representing all light fermions flavors generically with f. Note however, that although all fermions may be treated in this way generally, the specific form of each individual counterterm, for example δm_f, may differ. We split our matrix element counterterm into a SM and dimension-6 component according to

$$\delta\mathcal{M}_{f,L} = \frac{1}{16\pi^2}\left(\delta\mathcal{M}^{(4)}_{f,L} + \delta\mathcal{M}^{(6)}_{f,L}\right), \tag{4.3.6}$$

and similarly for the constituent counterterms

$$\delta Z = \frac{1}{16\pi^2}\left(\delta Z^{(4)} + \delta Z^{(6)}\right), \tag{4.3.7}$$

where Z denotes any parameter requiring renormalization. Note that as the Wilson coefficient counterterms, δC_i, contain only dimension-6 contributions we do not distinguish these with a (6) superscript. We then find that the dimension-4 contribution to the matrix element counterterm is

$$\delta\mathcal{M}^{(4)}_{f,L} = \frac{m_f}{\hat{v}_T}\left(\frac{\delta m_f^{(4)}}{m_f} - \frac{\delta\hat{v}_T^{(4)}}{\hat{v}_T} + \frac{1}{2}\delta Z_h^{(4)} + \frac{1}{2}\delta Z_f^{(4),L} + \frac{1}{2}\delta Z_f^{(4),R*}\right), \tag{4.3.8}$$

while the dimension-6 matrix element counterterm is given by

$$\begin{aligned}\delta\mathcal{M}^{(6)}_{f,L} =& \frac{m_f}{\hat{v}_T}\left(\frac{\delta m_f^{(6)}}{m_f} - \frac{\delta\hat{v}_T^{(6)}}{\hat{v}_T} + \frac{1}{2}\delta Z_h^{(6)} + \frac{1}{2}\delta Z_f^{(6),L} + \frac{1}{2}\delta Z_f^{(6),R*}\right)\\ &+ \mathcal{M}^{(6,0)}_{f,L}\left(\frac{\delta m_f^{(4)}}{m_f} + \frac{\delta\hat{v}_T^{(4)}}{\hat{v}_T} + \frac{1}{2}\delta Z_h^{(4)} + \frac{1}{2}\delta Z_f^{(4),L} + \frac{1}{2}\delta Z_f^{(4),R*}\right)\end{aligned}$$

$$- \frac{\hat{v}_T^2}{\sqrt{2}} C_{fH}^* \left(\frac{\delta \hat{v}_T^{(4)}}{\hat{v}_T} - \frac{\delta m_f^{(4)}}{m_f} \right) + m_f \hat{v}_T \left[C_{HWB} + \frac{\hat{c}_w}{2\hat{s}_w} C_{HD} \right] \delta \left(\frac{\hat{c}_w}{\hat{s}_w} \right)^{(4)}$$
$$+ m_f \hat{v}_T \left(\delta C_{H\Box} - \frac{\delta C_{HD}}{4} \left(1 - \frac{\hat{c}_w^2}{\hat{s}_w^2} \right) + \frac{\hat{c}_w}{\hat{s}_w} \delta C_{HWB} - \frac{\hat{v}_T}{m_b} \frac{\delta C_{fH}^*}{\sqrt{2}} \right) , \quad (4.3.9)$$

where we have defined

$$\frac{\delta \hat{v}_T}{\hat{v}_T} \equiv \frac{\delta M_W}{M_W} + \frac{\delta \hat{s}_w}{\hat{s}_w} - \frac{\delta e}{e} , \quad (4.3.10)$$

and also made use of the definitions of $\hat{c}_w$ and $\hat{s}_w$ in Eq. 3.2.5 to find

$$\frac{\delta \hat{s}_w}{\hat{s}_w} = - \frac{\hat{c}_w^2}{\hat{s}_w^2} \left(\frac{\delta M_W}{M_W} - \frac{\delta M_Z}{M_Z} \right) , \quad \delta \left(\frac{\hat{c}_w}{\hat{s}_w} \right)^{(4)} = - \frac{1}{\hat{c}_w \hat{s}_w} \left(\frac{\delta \hat{s}_w^{(4)}}{\hat{s}_w} \right) . \quad (4.3.11)$$

As the Wilson coefficient counterterms in Eq. 4.3.9 are those of a bottom-up EFT we are constrained to define these terms in the $\overline{\text{MS}}$ scheme only. As discussed in Section 2.1.2 we can recover the Wilson coefficient counterterms according to Eq. 2.1.17, which we rewrite here

$$\delta C_i = \frac{1}{2\varepsilon} \gamma_{ij} C_j = \frac{1}{16\pi^2} \frac{1}{2\varepsilon} \dot{C}_i . \quad (4.3.12)$$

The form of γ_{ij} were calculated in [63, 130, 131] and we make use of these results to find the form of δC_i.

Eqs. 4.3.8 and 4.3.9 are valid for counterterms defined in both the on-shell and $\overline{\text{MS}}$ schemes. In the on-shell scheme, the constituent counterterms, such as δm_f, are determined by calculating the functions found in Eqs. 1.2.16 to 1.2.18 using the appropriate two-point functions, as described throughout Section 1.2.2, which as we have noted equally applies to the dimension-6 SMEFT. The only exception is the electric charge counterterm which, in the form presented in Eq. 1.2.21, does not apply to the dimension-6 SMEFT, a point which is addressed in Section 4.3.3.

We will find throughout this work that is is useful for us to be flexible with which renormalization scheme we adopt for different parameters. Where necessary, we distinguish parameters in the on-shell scheme from those in the $\overline{\text{MS}}$ scheme through the notation

$$X^{\text{O.S.}} = X^{(0)} + \delta X^{\text{O.S.}} ,$$
$$\overline{X}(\mu) = X^{(0)} + \delta \overline{X}(\mu) , \quad (4.3.13)$$

where O.S. indicates the on-shell scheme and we have made the μ dependence in the $\overline{\text{MS}}$ parameter $\overline{X}(\mu)$ explicit. As discussed in Section 1.2.2, the counterterms in the two schemes have the same UV divergences, but differ in the finite parts: the UV-finite part is set to zero in the $\overline{\text{MS}}$ scheme, making the counterterms purely UV-divergent. We can therefore facilitate conversion between the $\overline{\text{MS}}$ and on-shell

schemes by writing

$$X = X^{(0)} \left(1 + \frac{\delta X^{\text{div.}}}{X} + c_X \frac{\delta X^{\text{O.S.,fin.}}}{X}\right), \tag{4.3.14}$$

where the notation splits the counterterm into UV-divergent ($\delta X^{\text{div.}}$) and UV-finite ($\delta X^{\text{fin.}}$) pieces. Results in the on-shell scheme are picked out by setting $c_X = 1$, while $c_X = 0$ picks out the $\overline{\text{MS}}$ scheme. This notation allows us to suppress the extra labels in Eq. 4.3.13 and refer instead to a generic quantity X, with the understanding that the renormalization scheme can be specified by adjusting the value of c_X and the numerical value of X appropriately.

4.3.3 Electric Charge Renormalization

The dimension-4 and dimension-6 one-loop counterterms found in Eq. 4.3.8 and Eq. 4.3.9 respectively are functions of the electric charge counterterm through the object $\delta\hat{v}_T$. We have seen the form of the electric charge counterterm in the SM in Eq. 1.2.21. Adapting this equation to the notation adopted throughout this section it takes the form

$$\frac{\delta e^{(4)}}{e} = \frac{1}{2}\frac{\partial \Sigma_T^{AA(4)}(k^2)}{\partial k^2}\bigg|_{k^2=0} - \frac{(v_f^{(4)} - a_f^{(4)})}{Q_f}\frac{\Sigma_T^{AZ(4)}(0)}{M_Z^2}, \tag{4.3.15}$$

where again, the (4) superscript refers to dimension-4 contributions. As we saw in Section 1.2.2, although the electric charge counterterm is a vertex counterterm, we may express it as a function of two-point functions (as in Eq. 4.3.15) by taking advantage of the Ward identities of the SM. We note again here that $v_f^{(4)} - a_f^{(4)} = Q_f \hat{s}_w/\hat{c}_w$, such that Eq. 4.3.15 is independent of the fermion flavor used to derive this expression.

To renormalize $h \to f\bar{f}$ in the dimension-6 SMEFT we similarly need an expression for the dimension-6 component of the electric charge counterterm, $\delta e^{(6)}$. We begin by considering a naïve extension of Eq. 1.2.21 to $\mathcal{O}(\hat{v}_T^2/\Lambda_{\text{NP}}^2)$. Such an expression takes the form

$$\frac{\delta e^{(6)}}{e} = \frac{1}{2}\frac{\partial \Sigma_T^{AA(6)}(k^2)}{\partial k^2}\bigg|_{k^2=0} - \frac{(v_f^{(4)} - a_f^{(4)})}{Q_f}\frac{\Sigma_T^{AZ(6)}(0)}{M_Z^2} - \frac{(v_f^{(6)} - a_f^{(6)})}{Q_f}\frac{\Sigma_T^{AZ(4)}(0)}{M_Z^2}. \tag{4.3.16}$$

Next we consider the contributions to $(v_f^{(6)} - a_f^{(6)})$ from the class-7 operators C_{Hf}.

For these operators we find

$$v^{(6)}_{f,C_{Hf}} = -a^{(6)}_{f,C_{Hf}} = C_{Hf}\frac{\hat{v}_T^2}{4\hat{c}_w\hat{s}_w}\,, \tag{4.3.17}$$

such that

$$\left(v^{(6)}_{f,C_{Hf}} - a^{(6)}_{f,C_{Hf}}\right) = C_{Hf}\frac{\hat{v}_T^2}{2\hat{c}_w\hat{s}_w}\,. \tag{4.3.18}$$

The results in Eq. 4.3.17 are due to the class-7 operator C_{Hf} producing a coupling between the Z-boson and right-handed fermions (without a similar such coupling to left-handed fermions), producing vector and axial-vector couplings of equal magnitude but opposite sign – a feature not observed in the SM. We also encounter a problem due to these results, this being that Eq. 4.3.18 implies that the electric charge counterterm is dependent on the fermion flavor used to calculate the counterterm through the Wilson coefficient C_{Hf}. Such a result is clearly incompatible with charge universality.

Instead, we may determine the correct form of the dimension-6 electric charge counterterm by renormalizing the $ff\gamma$ vertex directly. By explicit calculation, we find that this counterterm, which is built from three-point functions, may also be written similarly to the expression in Eq. 4.3.15, that is, as a sum of the $A-A$ and $A-Z$ two-point functions

$$\frac{\delta e^{(6)}}{e} = \frac{1}{2}\frac{\partial\Sigma_T^{AA(6)}(k^2)}{\partial k^2}\bigg|_{k^2=0} + \frac{1}{M_Z^2}\left(\frac{\hat{s}_w}{\hat{c}_w}\Sigma_T^{AZ(6)}(0) - \frac{\hat{v}_T^2}{4\hat{c}_w\hat{s}_w}C_{HD}\Sigma_T^{AZ(4)}(0)\right)\,, \tag{4.3.19}$$

such that in the dimension-6 SMEFT, like for the SM, all constituent counterterms in the matrix element counterterm of Eq. 4.3.9 can be constructed by considering only two-point functions. Fortunately, we find that the expression in Eq. 4.3.19 is also independent of fermion flavor, f. An important check on this expression is that the UV poles in the NLO decay amplitude cancel once it is used, which we have verified. Rather than inferring the form of the electric charge counterterm in Eq. 4.3.19 from three-point functions, as was done here, it should be possible to find its form in a similar way to the expression in Eq. 4.3.15 by using the dimension-6 SMEFT EW Ward identities, which were recently described in [132], although such a derivation is not the focus, and therefore not explored in this work.

4.3.4 Higgs-Z Mixing

A subset of the dimension-6 SMEFT operators of Table A.1 are associated with complex Wilson coefficients, specifically, the operators of classes 5, 6 and select

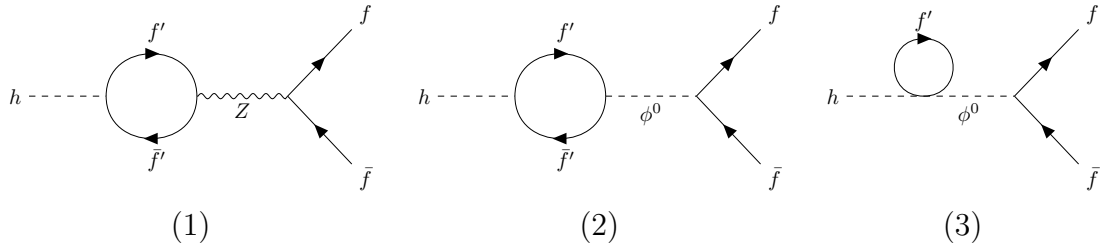

Figure 4.5: *Diagrams contributing to $h \to f\bar{f}$ from Higgs mixing to (1) Z-boson (R_ξ gauge and unitary gauge), and (2,3) neutral Goldstone boson (R_ξ gauge only). The loops get contributions from all massive SM fermions, denoted by f' to distinguish them from the final-state fermions, f.*

operators of classes 7 and 8. While the imaginary components of these Wilson coefficients are absent from the expressions for decay rates and other observables (a necessity of measurable quantities), they appear at the amplitude level in NLO calculations, and introduce complications to the renormalization process that are absent in the SM. Of particular importance to the process $h \to f\bar{f}$ considered here is the mixing of the Higgs, h, with the longitudinal component of the Z-boson (in both R_ξ and unitary gauge), and with the neutral Goldstone boson, ϕ^0, (only in R_ξ gauge) at the one-loop level. As we explored in Section 1.1.2, the Higgs, h, and neutral Goldstone boson, ϕ^0, are the real and imaginary parts of the neutral component of the complex Higgs doublet respectively, after EWSB. As such, any mixing between the two fields must be mediated by a complex coupling, a feature which is absent in the mass-basis SM. In the dimension-6 SMEFT, however, such a complex coupling exists due to the class-5 operators of Table A.1. As a result, there is a purely imaginary contribution to the NLO amplitude of $h \to f\bar{f}$ from the diagrams shown in Fig. 4.5. The sum of these diagrams yields a gauge-invariant result proportional to

$$\eta_5 = \frac{\sqrt{2}}{\hat{v}_T} \operatorname{Im}\left[N_c \sum_{d_i} m_{d_i} C_{d_i H} - N_c \sum_{u_i} m_{u_i} C_{u_i H} + \sum_{\ell_i} m_{\ell_i} C_{\ell_i H} \right], \tag{4.3.20}$$

where the summations represent a sum over down-type, up-type and leptonic fermions. The loop integrals multiplying η_5 contain UV divergences, which are exactly canceled by a corresponding term also proportional to η_5 in the Wilson coefficient counterterm δC_{fH} in Eq. 4.3.9. We note that although the diagrams in Fig. 4.5 are essential to the UV renormalization of the process $h \to f\bar{f}$ at the amplitude level, their purely-imaginary contribution ultimately results in their cancellation upon squaring the full matrix elements, and therefore does not contribute to the decay rate.

While in the unbroken phase it is unambiguous that the η_5 term arises from mixing

of real and imaginary parts of the complex Higgs doublet, in the broken phase the exact origin (but not the result itself) depends on the gauge: in unitary gauge it is due entirely to Higgs mixing with the longitudinal component of the Z-boson, while in R_ξ gauge it is due to the sum of graphs containing Z and neutral Goldstone bosons.

4.3.5 Tadpoles

As discussed in Section 1.2.3, tadpole renormalization forms an important component of NLO calculations, especially if one is concerned with gauge-invariant counterterms and retaining gauge invariance in processes where not all parameters are renormalized in the on-shell scheme – two properties which we wish to preserve in this work. To summarize the results of Section 1.2.3, we can consistently renormalize tadpole corrections, while also ensuring that counterterms relating to observable quantities are gauge invariant by employing the FJ tadpole scheme. Additionally, we saw that the FJ tadpole scheme was equivalent to a scheme where tadpoles are not explicitly renormalized and where the real part of the lower component of the Higgs doublet takes the form of the Higgs field plus the LO Higgs vev, which in the dimension-6 SMEFT is given by $h + v_T$. Taking advantage of this equivalence means that we can easily calculate amplitudes with consistently renormalized tadpoles and gauge-invariant counterterms by simply including tadpole corrections in all diagrams at the appropriate order in perturbation theory.

As discussed in Section 1.2.3, while tadpole corrections to individual terms cancel between one another in a renormalized amplitude when employing a purely on-shell scheme, in a scheme in which some parameters are renormalized in the $\overline{\text{MS}}$ scheme, it is only the UV-divergent components of the tadpoles that cancel between terms. Therefore, in a such a hybrid renormalization scheme, some finite components of tadpoles remain and must be included in NLO corrections to arrive at a gauge-invariant result.

As shown in [38], the FJ tadpole scheme applies to extensions of the SM without any essential complications. We therefore use this scheme for our NLO calculations within the dimension-6 SMEFT, specifically by applying the equivalent scheme in which tadpoles are not renormalized. This latter approach is particularly convenient as we do not need to explicitly include tadpole counterterms in the already lengthy expression for the matrix element counterterms in Eqs. 4.3.8 and 4.3.9. We therefore only need to include tadpole topologies in all n-point amplitudes that enter our calculation up to mass dimension 6.

Within the SM, for the processes $h \to f\bar{f}$, tadpole contributions appear only in the two-point functions required for the calculation of counterterms, as seen in

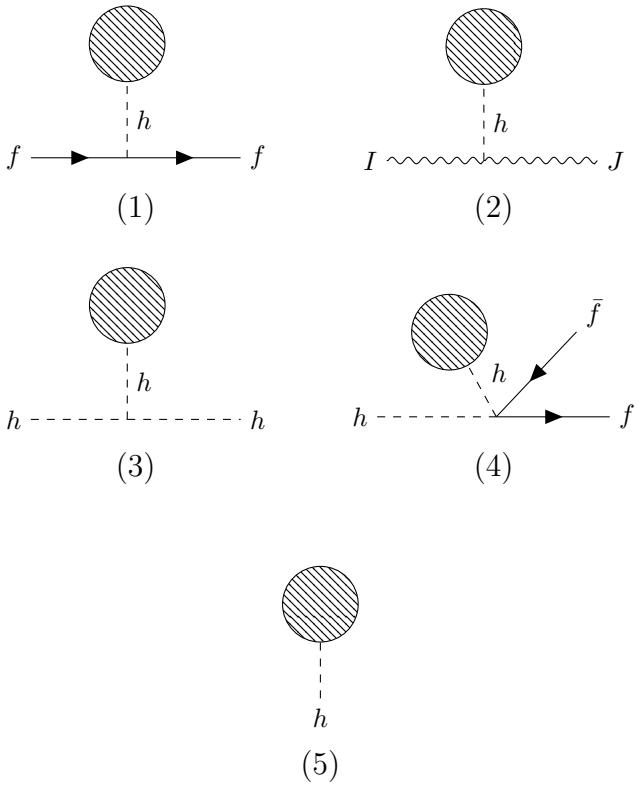

Figure 4.6: *NLO tadpole diagrams which appear in our calculations. The "blob" vertex represents all bare one-loop contributions. In addition to contributions to two-point functions of (1) the fermion, f, (2) vector bosons, where $IJ = \gamma\gamma, \gamma Z, WW, ZZ$, and (3) the Higgs, the contributions to the $h \to f\bar{f}$ matrix element shown in (4) appear through the dimension-6 operator Q_{fH} and its hermitian conjugate. In each case the diagram factorizes into the product of the tadpole function in (5), a Higgs propagator, a Higgs coupling to the tree-level diagram, and the tree-level diagram itself.*

Diagrams (1-3) of Fig. 4.6. In the dimension-6 SMEFT, tadpole contributions enter not only in the two-point functions, but also in the bare matrix elements through the diagram seen in Diagram (4) of Fig. 4.6. The tadpole function, shown diagrammatically in Diagram (5) of Fig. 4.6 is the dimension-6 extension of the tadpole function first explored in Section 1.2.3, such that it contains both SM and dimension-6 contributions. Diagrams (1-4) of Fig. 4.6 may be written as a product of the tadpole function in Diagram (5) of Fig. 4.6 and the corresponding tree-level diagram, provided we also include the necessary Higgs coupling and propagator. We may split the result of the tadpole function as

$$T = T^{(4)} + T^{(6)}\,, \tag{4.3.21}$$

where the superscripts (4) and (6) represent the SM and dimension-6 contributions

respectively. In unitary gauge we find

$$T^{(4)}_{\text{un.}} = \frac{1}{32\pi^2\hat{v}_T}\Bigg\{6\left(1-\frac{2\varepsilon}{3}\right)\left[2M_W^2A_0(M_W^2)+M_Z^2A_0(M_Z^2)\right] + 3m_H^2A_0(m_H^2) - 8\sum_f N_c^f m_f^2 A_0(m_f^2)\Bigg\}, \tag{4.3.22}$$

while in Feynman gauge

$$T^{(4)}_{\text{Feyn.}} = T^{(4)}_{\text{un.}} + \frac{m_H^2}{32\pi^2\hat{v}_T}\left[2A_0(M_W^2)+A_0(M_Z^2)\right], \tag{4.3.23}$$

where f refers to quarks (q) or charged leptons (l), where again $N_c^q = 3$, $N_c^l = 1$, and where A_0 is the scalar loop function introduced in Section 1.2.1

$$A_0(M^2) = M^2\left(\frac{1}{\varepsilon}+\ln\left(\frac{\mu^2}{M^2}\right)+1\right). \tag{4.3.24}$$

For the dimension-6 contribution, in unitary gauge we find

$$\begin{aligned} T^{(6)}_{\text{un.}} = \frac{\hat{v}_T}{32\pi^2}\Bigg\{ &\left(-6C_H\hat{v}_T^2 + 4C_{H,\text{kin}}\frac{m_H^2}{\hat{v}_T^2}\right)A_0(m_H^2) + (24-16\varepsilon)C_{HW}M_W^2A_0(M_W^2) \\ &+ (3-2\varepsilon)\left[C_{HD}+4(C_{HW}\hat{c}_w^2 + C_{HB}\hat{s}_w^2 + \hat{c}_w\hat{s}_wC_{HWB})\right]M_Z^2A_0(M_Z^2) \\ &+ \sum_f N_c^f 2\sqrt{2}\hat{v}_T m_f(C_{fH}+C_{fH}^*)A_0(m_f^2)\Bigg\} \\ &+ \left[C_{H,\text{kin}} + \hat{v}_T^2\frac{\hat{c}_w}{\hat{s}_w}\left(C_{HWB}+\frac{\hat{c}_w}{4\hat{s}_w}C_{HD}\right)\right]T^{(4)}_{\text{un.}}, \end{aligned} \tag{4.3.25}$$

and in Feynman gauge

$$\begin{aligned} T^{(6)}_{\text{Feyn.}} = T^{(6)}_{\text{un.}} &- \frac{m_H^2\hat{v}_T}{16\pi^2}\left(\frac{2}{\hat{v}_T^2}C_{H,\text{kin}}A_0(M_W^2) + C_{H\Box}A_0(M_Z^2)\right) \\ &+ \left[C_{H,\text{kin}} + \hat{v}_T^2\frac{\hat{c}_w}{\hat{s}_w}\left(C_{HWB}+\frac{\hat{c}_w}{4\hat{s}_w}C_{HD}\right)\right](T^{(4)}_{\text{Feyn.}} - T^{(4)}_{\text{un.}}), \end{aligned} \tag{4.3.26}$$

where $C_{H,\text{kin}}$ is defined in Eq. 2.3.6. The results throughout Eqs. 4.3.23 and 4.3.26 clearly demonstrate that tadpoles are gauge-dependent quantities in both the SM and the dimension-6 SMEFT.

An interesting feature of the SMEFT is that, in contrast to the SM, tadpole diagrams contribute to electric charge renormalization through the $\gamma\gamma$ two-point function. These contributions are proportional to the $h\gamma\gamma$ coupling in the SMEFT, which is induced by class-4 operators and involves the combination of Wilson coefficients

$$c_{h\gamma\gamma} = C_{HB}\hat{c}_w^2 + C_{HW}\hat{s}_w^2 - C_{HWB}\hat{c}_w\hat{s}_w. \tag{4.3.27}$$

Direct calculation in unitary gauge of the piece of the electric charge counterterm as described in section Section 4.3.3 yields the result

$$\frac{\delta e_4^{(6)}}{e} = \frac{1}{16\pi^2}\left[c_{h\gamma\gamma}A_0(m_H^2) + 4\hat{c}_w\hat{s}_w C_{HWB}\left(4M_W^2 - 3A_0(M_W^2)\right)\right] - 2c_{h\gamma\gamma}\frac{\hat{v}_T}{m_H^2}T^{(4)}_{\text{un.}}\,, \tag{4.3.28}$$

where the subscript 4 indicates restriction to class-4 operators of Table A.1. The term proportional to the SM tadpole function $T^{(4)}_{\text{un.}}$ arises through diagrams of the type shown in Diagram (2) of Fig. 4.6 with $IJ = \gamma\gamma$. In Feynman gauge the division into tadpole and the remaining contributions instead reads

$$\begin{aligned}\frac{\delta e_4^{(6)}}{e} = \frac{1}{16\pi^2}\Big[&c_{h\gamma\gamma}\left(A_0(m_H^2) + 2A_0(M_W^2) + A_0(M_Z^2)\right)\\ &+4\hat{c}_w\hat{s}_w C_{HWB}\left(4M_W^2 - 3A_0(M_W^2)\right)\Big] - 2c_{h\gamma\gamma}\frac{\hat{v}_T}{m_H^2}T^{(4)}_{\text{Feyn.}}\,.\end{aligned} \tag{4.3.29}$$

Comparing Eq. 4.3.28 with Eq. 4.3.29 while making use of Eq. 4.3.23 shows that these expressions are identical.

This example illustrates the general feature that parameter counterterms are gauge invariant only after including tadpoles. The same is true of the sum of bare matrix elements and wavefunction renormalization factors, which is also a gauge-invariant object. The mechanism through which tadpoles ensure this gauge invariance is non-trivial. For instance, in contrast to the SM, tadpoles contribute directly to bare matrix elements through diagrams of the type shown in Diagram (4) of Fig. 4.6. They also contribute to wavefunction renormalization of the fermion field, f. Evaluating the tadpole contribution to the fermion self-energy shown in Diagram (1) of Fig. 4.6 and using it to extract the wavefunction renormalization factor using the form of the expression for δZ_f^L in Eq. 1.2.9, we find

$$\delta Z^L_{f,\text{tad.}} = -\frac{i\sqrt{2}\hat{v}_T^2}{m_H^2 m_f}\text{Im}(C_{fH})T^{(4)}\,, \tag{4.3.30}$$

where T is the tadpole function in the chosen gauge. While this purely-imaginary contribution drops out of the NLO decay rate, it is needed to ensure gauge invariance of the sum of the NLO matrix element and the wavefunction renormalization factors, and also plays a role in the cancellation of tadpoles in the on-shell scheme.

These examples illustrate that while the treatment of tadpoles in the SMEFT is conceptually the same as in the SM, the exact structure of tadpoles in the diagrammatic calculations is more involved. We have calculated all tadpole contributions to the bare matrix elements and counterterms appearing in the $h \to f\bar{f}$ decay amplitude at NLO in unitary gauge and in Feynman gauge, and confirmed that the gauge

dependence in the tadpole functions cancels against that in other diagrams, such that the counterterms for mass and electric charge renormalization, as well as the sum of the bare matrix element and the wavefunction renormalization factors, are separately gauge invariant. We have also confirmed that tadpoles completely cancel when all parameters are renormalized in the on-shell scheme.

4.3.6 The NLO Decay Rate

In Section 4.1 we saw that the calculation of the decay rate at NLO involves the squaring and integrating over phase space of the matrix elements of $h \to f\bar{f}$ and $h \to f\bar{f}(g,\gamma)$ calculated at the same order in perturbation theory. For the virtual NLO corrections we again must first calculate the squared matrix element

$$\begin{aligned}|\mathcal{M}_{f,L}|^{2,(1)} = {} & \mathcal{M}_{f,L}^{(4,0)}\mathcal{M}_{f,L}^{(4,1)*} + \mathcal{M}_{f,L}^{(4,1)}\mathcal{M}_{f,L}^{(4,0)*} \\ & + \mathcal{M}_{f,L}^{(4,0)}\mathcal{M}_{f,L}^{(6,1)*} + \mathcal{M}_{f,L}^{(4,1)}\mathcal{M}_{f,L}^{(6,0)*} + \mathcal{M}_{f,L}^{(6,0)}\mathcal{M}_{f,L}^{(4,1)*} + \mathcal{M}_{f,L}^{(6,1)}\mathcal{M}_{f,L}^{(4,0)*} \\ & + \mathcal{O}\left(\frac{\hat{v}_T^4}{\Lambda_{\rm NP}^4}\right), \end{aligned} \tag{4.3.31}$$

where $|\mathcal{M}_{f,L}|^{2,(1)}$ represents only the NLO components of $|\mathcal{M}_{f,L}|^2$. In Eq. 4.3.31 we have again been careful to only keep terms at NLO in the perturbative expansion parameter, and of mass dimension 6, such that each term in Eq. 4.3.31 is a function of exactly one Wilson coefficient.

Similarly we must find the squared matrix element of the corresponding process with a real emission of a single photon or gluon

$$\begin{aligned}|\mathcal{M}_{h\to f\bar{f}(g,\gamma)}|^2 = {} & \mathcal{M}_{h\to f\bar{f}(g,\gamma)}^{(4,0)}\mathcal{M}_{h\to f\bar{f}(g,\gamma)}^{(4,0)*} + \mathcal{M}_{h\to f\bar{f}(g,\gamma)}^{(4,0)}\mathcal{M}_{h\to f\bar{f}(g,\gamma)}^{(6,0)*} \\ & + \mathcal{M}_{h\to f\bar{f}(g,\gamma)}^{(4,0)*}\mathcal{M}_{h\to f\bar{f}(g,\gamma)}^{(6,0)} + \mathcal{O}\left(\frac{\hat{v}_T^4}{\Lambda_{\rm NP}^4}\right), \end{aligned} \tag{4.3.32}$$

where, like in the $h \to f\bar{f}$ case, $\mathcal{M}_{h\to f\bar{f}(g,\gamma)}^{(i,j)}$ denotes dimension-i component at jth order in perturbation theory. Note however, using QED as an example, that for $h \to f\bar{f}$ at LO in perturbation theory the matrix element is of order $\alpha^{1/2}$, and at NLO in perturbation theory is of order $\alpha^{3/2}$, whereas for $h \to f\bar{f}\gamma$, LO in perturbation theory is of order α. Therefore, the terms in Eq. 4.3.31 and Eq. 4.3.32 occur at the same order in the expansion of α.

With these squared matrix elements now calculated, finally we must sum over final-state spins and polarizations (where applicable) and calculate the corresponding 2-body and 3-body phase-space integrals, details of which can be found in Appendix B.

4.4 Select Analytic Results

In this section we examine a subset of the results of the NLO calculation. The results for the LO calculation are reported in Eq. 4.2.5. The results presented in this section are chosen to highlight theoretical aspects of the calculation that have not been addressed thus far, and in the case of the results reported in Sections 4.4.1 and 4.4.2, to examine sources of NLO enhancements, which we address in Section 4.5.1.

To simplify the results reported in this section we split the real, finite parts of the on-shell counterterms related to fermion mass and electric charge renormalization into contributions from QED-QCD corrections, large-m_t corrections, and remaining corrections (a split introduced in Section 4.1) according to

$$\begin{aligned}\frac{\mathrm{Re}\left(\delta m_f^{(i),\mathrm{O.S.,fin.}}\right)}{m_f} &= \delta f^{(i)}_{(g,\gamma)} + \delta f^{(i)}_{(t)} + \delta f^{(i)}_{(\mathrm{rem.})}\,,\\ \frac{\mathrm{Re}\left(\delta e^{(i),\mathrm{O.S.,fin.}}\right)}{e} &= \delta e^{(i)}_{(g,\gamma)} + \delta e^{(i)}_{(t)} + \delta^{(i)}_{(\mathrm{rem.})}\,,\end{aligned} \tag{4.4.1}$$

where the superscript i refers to dimension-i contributions. We note that contributions to the top line of Eq. 4.4.1 vary according to the fermion flavor, while charge universality ensures that contributions to the bottom line of Eq. 4.4.1 are the same for each process considered here.

Finally, the decay rates reported in this section are observable quantities and therefore are necessarily entirely real. To simplify notation, throughout this section, and for the remainder of this work, all Wilson coefficients are assumed to be only the real components, i.e. $C_i = \mathrm{Re}\,(C_i)$.

4.4.1 QED-QCD Results and IR Renormalization

In this section we report the QED-QCD results. As noted in Section 4.1, the QED-QCD results are defined to be those originating from any virtual-correction diagram with a photon or gluon on an internal line, or any real-emission diagram with a photon or gluon in the final state. As we will see in Section 4.5.1, not only do these results constitute large NLO corrections to processes involving final-state quarks due to large QCD corrections, but large logarithmic corrections will motivate us to carefully consider our choice of renormalization scheme in Section 4.5.1. Additionally, IR poles emerge from some virtual-correction diagrams featuring the exchange of a photon or gluon, and from diagrams with final-state radiation. In the latter case, IR poles emerge specifically in the soft-radiation limit, that being when the momentum of the final-state radiation particle approaches zero. In such a scenario the process

with final-state radiation is indistinguishable from the corresponding process without final-state radiation.

There is only a small set of diagrams contributing to this subset of the NLO corrections; the diagrams are reported in Appendix C.1, where the QED diagrams can be found in Fig. C.1, while the QCD diagrams can be found in Fig. C.2. Note that corrections from photon and gluon two-point functions are not present due to our definition of QED-QCD corresponding to diagrams with photons or gluons only on internal lines. From direct calculation, we find that diagrams that lead to IR poles are only those that are "SM like", by which we mean the diagrams take the same form as the diagrams found in the SM, but with a single dimension-6 operator insertion. For both QED and QCD this amounts to Diagrams (v1), (r1), and (r2) in Figs. C.1 and C.2. The details of how to calculate the phase-space integrals for 3-body final-state diagrams is outlined in Appendix B.2.1, while details on how to separate the IR pole in such calculations is outlined in Appendix B.2.2. An interesting feature of computing phase-space integrals in $d = 4 - 2\varepsilon$ dimensions is the necessary shift in the definitions of the couplings, first seen in Eq. 1.2.4. This shift results in additional $\mathcal{O}(\varepsilon)$ terms multiplying the $1/\varepsilon$ IR poles to produce numerically significant additional finite terms. As UV poles only exist in the virtual corrections, which are removed at the level of the amplitude, analogous finite pieces due to UV poles do not exist.

Comparing the diagrams across Figs. C.1 and C.2, we observe a great deal of similarity between the QED and QCD contributions. In fact, the QCD results may be entirely inferred from a subset of the QED results by making the necessary changes in coupling constants etc. There are, however, diagrams contributing to the QED corrections which have no analogue in QCD, these being the diagrams containing a $h\gamma Z$ vertex seen in Diagrams (v5), (v6) and (r5) of Fig. C.1.

We now report the QED-QCD results for the processes considered here. In fact, besides the subset of processes $h \to f\bar{f}$ where $f \in \{b, c, \tau, \mu\}$, these results extend to all massive SM fermion flavors, except for $f = t$. We have additionally verified the UV and IR finiteness of the results after summing all contributions from the diagrams found in Figs. C.1 and C.2. Here, for brevity, and for reasons that will become clear in Section 4.5.2, we report these results in the small-mass limit, while keeping leading-order pieces in the light-fermion masses, m_f, in this limit. The QED-QCD results with full fermion mass dependence can be found in Appendix E.1. As noted in Section 4.3.2 we are able to renormalize all input parameters except the Wilson coefficients in the on-shell scheme, and the strong coupling constant is necessarily the $\overline{\text{MS}}$ parameter. For brevity, we simply refer to decay rates calculated in this way as the *on-shell scheme decay rates*. We write the results in such a way

that it is easy for the reader to convert between this scheme, and a scheme in which the light-fermion masses and electric charge are renormalized in the $\overline{\text{MS}}$ scheme. We refer to this latter scheme where the electric charge and light-fermion masses (as well as the Wilson coefficients) are renormalized in the $\overline{\text{MS}}$ scheme as *the hybrid renormalization scheme*.

Before presenting these results we introduce some notation. For the decay rates we distinguish between the on-shell scheme and the hybrid renormalization scheme as follows: the decay rate without a bar, Γ, represents the on-shell scheme decay rate, while the decay rate with a bar, $\overline{\Gamma}$, represents the hybrid renormalization scheme decay rate. As discussed at the end of Section 4.3.2, where the quantities α and m_f occur we suppress the explicit notation denoting whether these parameters are on-shell or $\overline{\text{MS}}$ renormalized. For NLO corrections, the renormalization scheme of these parameters is implied through the choice of c_X. For the LO results, the choice of $X^{\text{o.s}}$ or $\overline{X}$ for $X \in \{m_f,\, \alpha\}$ is implicit through the presence (or lack thereof) of a bar on the corresponding decay rate.

The NLO QED-QCD corrections in the SM may be written

$$\Gamma^{(4,1)}_{f,(g,\gamma)} = \overline{\Gamma}^{(4,1)}_{f,(g,\gamma)} + 2c_{m_f}\Gamma^{(4,0)}_f \delta f^{(4)}_{(g,\gamma)}\,, \tag{4.4.2}$$

where here and throughout this section $\Gamma^{(i,0)}_f$ are the small-mass limit versions of Eq. 4.2.5, found by replacing in $\beta_f \to 1$ in that equation. We also find the $\delta f^{(4)}_{(g,\gamma)}$ in Eq. 4.4.2 takes the form

$$\delta f^{(4)}_{(g,\gamma)} = \left(\frac{\delta_{f,q} C_F \alpha_s + Q_f^2 \alpha}{\pi}\right)\left[1 + \frac{3}{4}\ln\left(\frac{\mu^2}{m_f^2}\right)\right]\,, \tag{4.4.3}$$

where $\delta_{f,q} = 1$ if f is a quark, and $\delta_{f,q} = 0$ if f is a lepton. Similarly, the dimension-6 SMEFT results take the form

$$\Gamma^{(6,1)}_{f,(g,\gamma)} = \overline{\Gamma}^{(6,1)}_{f,(g,\gamma)} + 2c_{m_f}\Gamma^{(4,0)}_f \delta f^{(4)}_{(g,\gamma)}\left(\frac{C_{fH}\hat{v}_T^2}{\sqrt{2}}\frac{\hat{v}_T}{m_f} + \frac{\Gamma^{(6,0)}_f}{\Gamma^{(4,0)}_f}\right)\,, \tag{4.4.4}$$

where we have also used that $\delta f^{(6)}_{g,\gamma} = 0$ in the small-mass limit, contrary to what is seen for full mass dependent results in Eq. E.1.4. The main results of this section are then

$$\overline{\Gamma}^{(4,1)}_{f,(g,\gamma)} = \overline{\Gamma}^{(4,0)}_f \left(\frac{\delta_{f,q} C_F \alpha_s + Q_f^2 \alpha}{\pi}\right)\left[\frac{17}{4} + \frac{3}{2}\ln\left(\frac{\mu^2}{m_H^2}\right)\right]\,,$$

$$\begin{aligned}\overline{\Gamma}^{(6,1)}_{f,(g,\gamma)} &= \overline{\Gamma}^{(6,0)}_f \frac{\overline{\Gamma}^{(4,1)}_{f,(g,\gamma)}}{\overline{\Gamma}^{(4,0)}_f} + \frac{\hat{v}_T^2}{\pi}\overline{\Gamma}^{(4,0)}_f \\ &\times \left\{ \frac{m_H^2}{\sqrt{2}\hat{v}_T m_f}\left(\delta_{f,q}\frac{C_F}{g_s}\alpha_s C_{fG} + \frac{Q_f}{e}\alpha\left(C_{fB}\hat{c}_w + 2T_f^3 C_{fW}\hat{s}_w\right)\right)\right. \\ &+ \left(\delta_{f,q}C_F\alpha_s C_{HG} + Q_f^2\alpha\, c_{h\gamma\gamma}\right)\left[19 - \pi^2 + \ln^2\left(\frac{m_f^2}{m_H^2}\right) + 6\ln\left(\frac{\mu^2}{m_H^2}\right)\right] \\ &\left. + c_{h\gamma Z}\, v_f Q_f \alpha\, F_{h\gamma Z}\left(\frac{M_Z^2}{m_H^2}, \frac{\mu^2}{m_H^2}, \frac{m_f^2}{m_H^2}\right)\right\}, \end{aligned} \tag{4.4.5}$$

where $v_f = (T_f^3 - 2Q_f\hat{s}_w^2)/(2\hat{s}_w\hat{c}_w)$ is the vector coupling of f to the Z-boson, T_f^3 is the weak isospin of fermion,[1] $c_{h\gamma\gamma}$ was defined in Eq. 4.3.27, and where

$$c_{h\gamma Z} = 2\left(C_{HB} - C_{HW}\right)\hat{c}_w\hat{s}_w + C_{HWB}\left(\hat{c}_w^2 - \hat{s}_w^2\right), \tag{4.4.6}$$

is the combination of Wilson coefficients entering the $h\gamma Z$ dimension-6 SMEFT vertex, seen in Diagrams (v5), (v6) and (r5) of Fig. C.1. In Eq. 4.4.5 we also introduce the function $F_{h\gamma Z}$ which accompanies the vertex function $c_{h\gamma Z}$ and in the small-mass limit is given by

$$\begin{aligned}F_{h\gamma Z}\left(z, \hat{\mu}^2, 0\right) = -12 + 4z - \frac{4}{3}\pi^2\bar{z}^2 + \left(3 + 2z + 2\bar{z}^2\ln(\bar{z})\right)\ln(z) \\ + 4\bar{z}^2\mathrm{Li}_2(z) - 6\ln(\hat{\mu}^2), \end{aligned} \tag{4.4.7}$$

where

$$\bar{z} = 1 - z\,. \tag{4.4.8}$$

An interesting feature of Eq. 4.4.5 is the double logarithm in the ratio m_f^2/m_H^2 multiplying C_{HG} and $c_{h\gamma\gamma}$. In the SM, logarithms of this type first appear at NNLO, and are related to diagrams where the Higgs couples to a top-quark loop which in the large-m_t limit can be shrunk to an effective hAA vertex, where $A = \gamma, g$, multiplied by an m_t-dependent matching coefficient. These SM corrections, not only the logarithms but also the finite parts, are thus proportional to the SMEFT corrections given above (see for instance Eq. (8) of [133]). As noted already in [134], these double logarithms cancel against corresponding terms in the $h \to AA$ decay rate, such that total Higgs decay width remains finite in the limit of vanishing fermion masses. In a less inclusive quantity such as $h \to ff$, they introduce sizeable flavor-dependent contributions to the decay rate, even though they multiply flavor-universal Wilson coefficients. We return to this issue when studying ratios of decay rates in Section 4.7.

[1] These weak isospins differ between up-type quarks, down-type quarks and leptons as $T_u^3 = \frac{1}{2}$, $T_d^3 = T_\ell^3 = -\frac{1}{2}$.

4.4.2 Large-m_t Results and Input Scheme Revisited

In this section we report the results of the calculation in the large-m_t limit. In this limit we report the LO terms in m_t. Like in the QED-QCD case in Section 4.4.1 we may report these results in a single equation for all massive fermion flavors of the SM, except for $f = t$.

As in the QED-QCD results in Section 4.4.1, we write these results in such a way that it is simple to convert between the on-shell scheme and the hybrid renormalization scheme. We also retain the general notation used throughout Section 4.4.1. To emphasize the cancellation of tadpole corrections in the on shell scheme we write the results in such a way that we give the full form of the on-shell results, rather than the hybrid renormalization scheme results. We note that, again, throughout this section we use that $\Gamma_f^{(i,0)}$ are the small-mass limit versions of Eq. 4.2.5. With this in mind, the SM result may be written

$$\overline{\Gamma}_{f,(t)}^{(4,1)} = \Gamma_{f,(t)}^{(4,1)} - 2\bar{c}_{m_f}\delta f_t^{(4)}\Gamma_f^{(4,0)}\,, \tag{4.4.9}$$

where $\bar{c}_X \equiv 1 - c_X$ for $X \in \{m_f, e\}$, such that the choice $\bar{c}_X = 1$ picks out the hybrid renormalization scheme results. The dimension-6 SMEFT results are

$$\overline{\Gamma}_{f,(t)}^{(6,1)} = \Gamma_{f,(t)}^{(6,1)} - 2\Gamma_f^{(4,0)}\left(\bar{c}_{m_f}\left[\delta f_t^{(6)} + \delta f_t^{(4)}\left(\frac{C_{fH}\hat{v}_T^2}{\sqrt{2}}\frac{\hat{v}_T}{m_f}\right) + \frac{\Gamma_f^{(6,0)}}{\Gamma_f^{(4,0)}}\right] + \bar{c}_e\delta e_t^{(6)}\right). \tag{4.4.10}$$

The SM and dimension-6 SMEFT results in the on-shell scheme are then given by

$$\begin{aligned}
\Gamma_{f,(t)}^{(4,1)} &= \Gamma_f^{(4,0)}\left(-6\delta_{f,b} + N_c\frac{7-10\hat{c}_w^2}{3\hat{s}_w^2}\right)\frac{m_t^2}{16\pi^2\hat{v}_T^2}\,,\\
\Gamma_{f,(t)}^{(6,1)} &= \Gamma_f^{(6,0)}\frac{\Gamma_{f,(t)}^{(4,1)}}{\Gamma_f^{(4,0)}} - \frac{1}{2}\dot{\Gamma}_{f,(t)}^{(6,0)}\ln\left(\frac{\mu^2}{m_t^2}\right)\\
&\quad + \Gamma_f^{(4,0)}\frac{m_t^2}{16\pi^2}\left\{C_{H\Box}N_c\frac{2+4\hat{c}_w^2}{3\hat{s}_w^2} - C_{HD}\left(\frac{3\hat{c}_w^2}{\hat{s}_w^2}\delta_{f,b} + N_c\frac{1+2\hat{c}_w^4}{6\hat{s}_w^4}\right)\right.\\
&\quad + C_{HWB}\frac{\hat{c}_w}{\hat{s}_w}\left(-12\delta_{f,b} + N_c\frac{5-8\hat{c}_w^2}{3\hat{s}_w^2}\right) + \frac{C_{fH}}{\sqrt{2}}\frac{\hat{v}_T}{m_b}\left(-\frac{17}{2}\delta_{f,b} + 3N_c\frac{1-2\hat{c}_w^2}{\hat{s}_w^2}\right)\\
&\quad \left. + 2C_{Hq}^{(3)}\left(-\delta_{f,b} + N_c\frac{1-2\hat{c}_w^2}{\hat{s}_w^2}\right)\right\}.
\end{aligned} \tag{4.4.11}$$

In Eq. 4.4.11 we have introduced $\delta_{f,b}$, where $\delta_{f,b} = 1$ for $f = b$ and $\delta_{f,b} = 0$ otherwise. The presence of $\delta_{f,b}$ demonstrates the asymmetry that exists between results for $h \to b\bar{b}$ and $h \to f\bar{f}$ for f being any of the remaining light fermions, in the large-m_t limit. The diagonal CKM matrix approximation, discussed in Section 4.3.1, prevents coupling between quarks of different generations; this result therefore gives

precedence to $h \to b\bar{b}$ which now receives a greater number contributing diagrams in the large-m_t limit when compared to Higgs decay to other fermion pairs. This greater number of diagrams contributing to $h \to b\bar{b}$ extends to both the bare matrix elements, and the two-point functions required for UV renormalization. For a diagram to contribute in the large-m_t limit it must feature a top-quark on an internal line. All such diagrams for the processes considered here are found in Appendix C.2. Diagrams that are unique to the process $h \to b\bar{b}$ are found in Fig. C.3, while those that apply to $h \to f\bar{f}$ for all light fermions, f, including $f = b$, are found in Fig. C.4. We see that all the diagrams in Fig. C.4 contain a closed top-quark loop, resulting in all non-$\delta_{f,b}$ terms in Eq. 4.4.11 being proportional to N_c. We also see in Eq. 4.4.11 that the μ-dependence is governed by

$$\dot{\Gamma}^{(6,0)}_{f,(t)} \equiv \Gamma^{(6,0)}_{f}\Big|_{C_i \to \dot{C}_{i,(t)}}, \quad \dot{C}_{i,(t)} \equiv \frac{dC_i}{d\ln(\mu)}\Big|_{m_t \to \infty}. \tag{4.4.12}$$

We again note that although what we call the on-shell decay rates have all SM parameters renormalized in the on-shell scheme, the Wilson coefficients are necessarily renormalized in the $\overline{\text{MS}}$ scheme. It is for this reason that we have explicit μ-dependent terms for the dimension-6 result in Eq. 4.4.11. The form of the $\dot{C}_{i,(t)}$ relevant to these results can be obtained from the results in [131] and read

$$\begin{aligned}
\dot{C}_{H\Box,(t)} &= 4\frac{m_t^2}{\hat{v}_T^2} N_c \left(C_{H\Box} + C^{(1)}_{\substack{Hq\\33}} - 3C^{(3)}_{\substack{Hq\\33}} - 2C_{Ht} \right), \\
\dot{C}_{HD,(t)} &= 8\frac{m_t^2}{\hat{v}_T^2} N_c \left(C_{HD} + 2C^{(1)}_{\substack{Hq\\33}} - 2C_{Ht} \right), \\
\dot{C}_{HWB,(t)} &= 4\frac{m_t^2}{\hat{v}_T^2} C_{HWB}, \\
\dot{C}_{bH,(t)} &= \frac{m_t^2}{\hat{v}_T^2} \Bigg(-4C_{bH} + 12\sqrt{2}\frac{m_b}{\hat{v}_T} C^{(3)}_{\substack{Hq\\33}} - 4\sqrt{2}\frac{m_t}{\hat{v}_T} C_{Htb} \\
&\qquad - 4\sqrt{2}\left((1+2N_c) C^{(1)}_{\substack{quqd\\3333}} + C^{(8)}_{\substack{quqd\\3333}} \right) - 2\frac{m_b}{m_t} C_{tH} \Bigg), \\
\dot{C}_{cH,(t)} &= 2\frac{m_t^2}{\hat{v}_T^2} \left(3N_c C_{cH} - 4\sqrt{2} N_c \frac{m_c}{\hat{v}_T} C^{(3)}_{\substack{Hq\\33}} + 9\sqrt{2}\frac{m_t}{\hat{v}_T} \left(C^{(1)}_{\substack{qu\\3333}} + C_F C^{(8)}_{\substack{qu\\3333}} \right) \right), \\
\dot{C}_{\tau H,(t)} &= 2\frac{m_t^2}{\hat{v}_T^2} \left(3C_{\tau H} - 4\sqrt{2}\frac{m_\tau}{\hat{v}_T} C^{(3)}_{\substack{Hq\\33}} + 8\sqrt{2}\frac{m_t}{\hat{v}_T} N_c C^{(1)}_{\substack{lequ\\3333}} \right), \\
\dot{C}_{\mu H,(t)} &= 2N_c \frac{m_t^2}{\hat{v}_T^2} \left(3C_{\mu H} + 4\frac{m_t}{\hat{v}_T} C^{(1)}_{\substack{lequ\\2233}} \right).
\end{aligned} \tag{4.4.13}$$

We also here report the forms of $\delta f^{(i)}_{(t)}$ and $\delta e^{(i)}_{(t)}$ defined in Eq. 4.4.1. It is convenient to further split these results into tadpole and non-tadpole contributions according

to

$$\delta f^{(i)}_{(t)} = \frac{m_t^2}{16\pi^2 \hat{v}_T^2}\left(\delta \hat{f}^{(i)}_{(t)} + \frac{m_t^2}{m_H^2}\delta \hat{f}^{(i)}_{(t),\text{tad.}}\right),$$
$$\delta e^{(i)}_{(t)} = \frac{m_t^2}{16\pi^2 \hat{v}_T^2}\left(\delta \hat{e}^{(i)}_{(t)} + \frac{m_t^2}{m_H^2}\delta \hat{e}^{(i)}_{(t),\text{tad.}}\right). \tag{4.4.14}$$

For the non-tadpole quantities we find

$$\begin{aligned}
\delta \hat{b}^{(4)}_{(t)} &= -\frac{5}{4} - \frac{3}{2}\ln\left(\frac{\mu^2}{m_t^2}\right), \\
\delta \hat{c}^{(4)}_{(t)} &= \delta \hat{\tau}^{(4)}_{(t)} = \delta \hat{\mu}^{(4)}_{(t)} = 0, \\
\delta \hat{b}^{(6)}_{(t)} &= \hat{v}_T^2 \Bigg\{ \delta \hat{b}^{(4)}_{(t)} \left(C_{HD}\frac{\hat{c}_w^2}{2\hat{s}_w^2} + 2C_{HWB}\frac{\hat{c}_w}{\hat{s}_w} + 2C^{(3)}_{\substack{Hq \\ 33}} \right) \\
&\quad + \frac{m_t}{m_b}\left[C_{Htb} + C^{(1)}_{\substack{quqd \\ 3333}}(1+2N_c) + C_F C^{(8)}_{\substack{quqd \\ 3333}} \right]\left(1 + \ln\left(\frac{\mu^2}{m_t^2}\right)\right) \Bigg\}, \\
\delta \hat{c}^{(6)}_{(t)} &= -2\hat{v}_T^2 \frac{m_t}{m_c}\left[C^{(1)}_{\substack{qu \\ 2332}} + C_F C^{(8)}_{\substack{qu \\ 2332}} \right]\left(1 + 2\ln\left(\frac{\mu^2}{m_t^2}\right)\right), \\
\delta \hat{\tau}^{(6)}_{(t)} &= -\hat{v}_T^2 \frac{m_t}{m_\tau} C^{(1)}_{\substack{lequ \\ 3333}}\left(1 + \ln\left(\frac{\mu^2}{m_t^2}\right)\right), \\
\delta \hat{\mu}^{(6)}_{(t)} &= -\hat{v}_T^2 \frac{m_t}{m_\mu} C^{(1)}_{\substack{lequ \\ 2233}}\left(1 + \ln\left(\frac{\mu^2}{m_t^2}\right)\right), \\
\delta \hat{e}^{(4)}_{(t)} &= \hat{e}^{(6)}_{(t)} = 0,
\end{aligned} \tag{4.4.15}$$

while the tadpole contributions read

$$\begin{aligned}
\delta \hat{f}^{(4)}_{(t),\text{tad.}} &= 4N_c\left(1 + \ln\left(\frac{\mu^2}{m_t^2}\right)\right), \\
\delta \hat{f}^{(6)}_{(t),\text{tad.}} &= 2\delta \hat{f}^{(4)}_{(t),\text{tad.}}\left[C_{H\Box} - \frac{C_{HD}}{4}\left(1 - \frac{\hat{c}_w^2}{\hat{s}_w^2}\right) + \frac{\hat{c}_w}{\hat{s}_w}C_{HWB} - \frac{\hat{v}_T}{m_f}\frac{C_{fH}}{2\sqrt{2}} \right]\hat{v}_T^2, \\
\delta \hat{e}^{(4)}_{(t),\text{tad.}} &= 0, \\
\delta \hat{e}^{(6)}_{(t),\text{tad.}} &= 8N_c c_{h\gamma\gamma}\hat{v}_T^2\left(1 + \ln\left(\frac{\mu^2}{m_t^2}\right)\right),
\end{aligned} \tag{4.4.16}$$

where $c_{h\gamma\gamma}$ was defined in Eq. 4.3.27. We see in Eq. 4.4.16 that the general form of $\delta f_{(t),\text{tad.}}$ is the same for all fermions, f, up to fermion masses and the flavor-dependent Wilson coefficient C_{fH}. From Fig. C.4 we see that this is a result of the form of the large-m_t tadpole corrections to the fermion mass counterterms being the same for all fermions, with no unique contributions to $h \to b\bar{b}$.

We conclude this section by revisiting the topic of input schemes, introduced in Section 3.2. In that section, we stated that in the SM the choice of G_F as an input parameter leads to the cancellation of terms scaling like m_t^2/M_W^2 in some particular

instances, and thus typically smaller NLO corrections. With the large-m_t corrections in our chosen input scheme, $\{\alpha,\, M_W,\, M_Z\}$, (which we refer to as the α input scheme) we investigate this feature in the dimension-6 SMEFT by comparing with the same results using the input scheme $\{G_F,\, M_W,\, M_Z\}$ (which we refer to as the G_F input scheme). Large-m_t results in the G_F input scheme can be found in [119] for the decay rates $h \to b\bar{b}$ and $h \to \tau\bar{\tau}$. The same reference also gives NLO dimension-6 SMEFT corrections to the Fermi constant G_F in the large-m_t limit, allowing us to cross-check the results found throughout this section, which we have performed. Numerically, using the values in Table 4.2,[1] $G_F = 1.17 \times 10^{-5}\text{GeV}^{-2}$, and setting $\mu = m_t$ we find in the SM for $h \to b\bar{b}$ (and normalizing results to the LO SM decay rate)

$$\begin{aligned} \frac{\Gamma^{(4,1),\alpha}_{b,(t)}}{\Gamma^{(4,0),\alpha}_{b,(t)}} &= -0.03\,, \\ \frac{\Gamma^{(4,1),G_F}_{b,(t)}}{\Gamma^{(4,0),G_F}_{b,(t)}} &= 0.0003\,, \end{aligned} \tag{4.4.17}$$

where the superscripts α and G_F denote results in the α and G_F input schemes respectively. For the remaining light fermions, $f\backslash b$,[2] we find

$$\begin{aligned} \frac{\Gamma^{(4,1),\alpha}_{f\backslash b,(t)}}{\Gamma^{(4,0),\alpha}_{f\backslash b,(t)}} &= -0.003\,, \\ \frac{\Gamma^{(4,1),G_F}_{f\backslash b,(t)}}{\Gamma^{(4,0),G_F}_{f\backslash b,(t)}} &= 0.007\,, \end{aligned} \tag{4.4.18}$$

where we have used that the G_F input scheme results for τ from [119] simply extend to all remaining light fermions $f\backslash b$. From Eq. 4.4.17 we see that indeed using the G_F input scheme reduces the size of the SM NLO corrections in the large-m_t limit when compared to the α input scheme for the decay mode $h \to b\bar{b}$. However, the opposite is true when we consider the Higgs decay to fermions pairs other than b-quarks, where the corrections are generally of the same order of magnitude.

To perform an analogous analysis for the results in the dimension-6 SMEFT we first define the dimensionless Wilson coefficients according to

$$\tilde{C}_i(\mu) \equiv \Lambda^2_{\text{NP}} C_i(\mu)\,, \tag{4.4.19}$$

[1] Similarly to the analysis performed in Section 4.3.1, the inputs in Table 4.2 are a mix of on-shell and $\overline{\text{MS}}$ parameters. Again, the differences in results from using a parameter renormalized in the incorrect scheme are small enough to ignore for the illustrative purposes of the analysis performed here.

[2] Extending the discussion earlier in this section, we can consider that $f\backslash b$ actually applies to all massive SM fermions except for the top and bottom quarks.

so that we may write our results with a symbolic factor of $\hat{v}_T^2/\Lambda_{\rm NP}^2 \approx 6\%$ when $\Lambda_{\rm NP} = 1$ TeV. Dropping the arguments of the Wilson coefficients, with it implicit that they are evaluated at the scale $\mu = m_t$, we find for final state $b\bar{b}$

$$\begin{aligned}
\frac{\Gamma^{(6,1),\alpha}_{b,(t)}}{\Gamma^{(4,0),\alpha}_{b,(t)}} &= \frac{\hat{v}_T^2}{\Lambda_{\rm NP}^2}\Bigg\{ -0.05\tilde{C}^{(3)}_{\substack{Hq\\33}} - 0.03\frac{\hat{v}_T}{m_b}\tilde{C}_{bH} + 0.01\tilde{C}_{H\Box} - 0.14\tilde{C}_{HD} - 0.22\tilde{C}_{HWB}\Bigg\}, \\
\frac{\Gamma^{(6,1),G_F}_{b,(t)}}{\Gamma^{(4,0),G_F}_{b,(t)}} &= \frac{\hat{v}_T^2}{\Lambda_{\rm NP}^2}\Bigg\{0.01\tilde{C}^{(3)}_{\substack{Hq\\33}} - 0.003\frac{\hat{v}_T}{m_b}\tilde{C}_{bH} + 0.01\tilde{C}_{H\Box} - 0.003\tilde{C}_{HD} - 0.0006\tilde{C}^{(3)}_{\substack{Hl\\11}} \\
&\qquad - 0.0006\tilde{C}^{(3)}_{\substack{Hl\\22}} + 0.01\tilde{C}^{(3)}_{\substack{lq\\1133}} + 0.01\tilde{C}^{(3)}_{\substack{lq\\2233}} + 0.003\tilde{C}_{\substack{ll\\1221}} + 0.003\tilde{C}_{\substack{ll\\2112}}\Bigg\},
\end{aligned} \tag{4.4.20}$$

while for the remaining light fermions, $f\backslash b$, we find

$$\begin{aligned}
\frac{\Gamma^{(6,1),\alpha}_{f\backslash b,(t)}}{\Gamma^{(4,0),\alpha}_{f\backslash b,(t)}} &= \frac{\hat{v}_T^2}{\Lambda_{\rm NP}^2}\Bigg\{ -0.04\tilde{C}^{(3)}_{\substack{Hq\\33}} - 0.01\frac{\hat{v}_T}{m_f}\tilde{C}_{fH} + 0.05\tilde{C}_{H\Box} - 0.09\tilde{C}_{HD} - 0.07\tilde{C}_{HWB}\Bigg\}, \\
\frac{\Gamma^{(6,1),G_F}_{f\backslash b,(t)}}{\Gamma^{(4,0),G_F}_{f\backslash b,(t)}} &= \frac{\hat{v}_T^2}{\Lambda_{\rm NP}^2}\Bigg\{0.02\tilde{C}^{(3)}_{\substack{Hq\\33}} - 0.003\frac{\hat{v}_T}{m_f}\tilde{C}_{fH} + 0.05\tilde{C}_{H\Box} - 0.01\tilde{C}_{HD} - 0.05\tilde{C}^{(3)}_{\substack{Hl\\11}} \\
&\qquad - 0.05\tilde{C}^{(3)}_{\substack{Hl\\22}} + 0.01\tilde{C}^{(3)}_{\substack{lq\\1133}} + 0.01\tilde{C}^{(3)}_{\substack{lq\\2233}} + 0.02\tilde{C}_{\substack{ll\\1221}} + 0.02\tilde{C}_{\substack{ll\\2112}}\Bigg\}.
\end{aligned} \tag{4.4.21}$$

Note that in Eqs. 4.4.20 and 4.4.21 we have factored out the symbolic quantity $\hat{v}_T/m_f$ from the coefficient of C_{fH}, which we discuss further in Section 4.6.

From studying the results in Eqs. 4.4.20 and 4.4.21 we see that, in general, the G_F input scheme leads to smaller NLO corrections, however, it suffers from the problem of introducing many more Wilson coefficients (10 in total in this example) than in the α input scheme case (where there are 5 in total).

From this analysis, despite that in the α input scheme the large-m_t NLO corrections are larger than those found in the G_F scheme, looking ahead to the LO numerical results in Eq. 4.6.2 we see that these corrections are not anomalously large in either renormalization scheme. Further, we see that the α input scheme also has the advantage of introducing far fewer Wilson coefficients into the NLO corrections. For these reasons we consider the α input scheme appropriate for the currently considered decay modes and continue to use it throughout the rest of our analysis.

4.4.3 Four-Fermion Results

Unlike the results found in Sections 4.4.1 and 4.4.2, the four-fermion results are not one of the subsets of results defined in Eq. 4.1.3, but are a subset of the results in

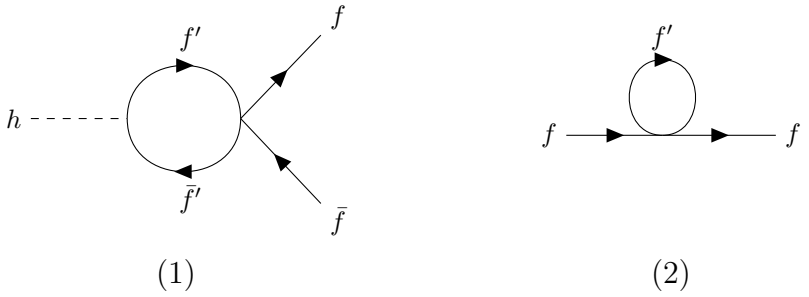

Figure 4.7: *Diagrams showing (1) the virtual corrections to the $h \to f\bar{f}$ matrix element due to four-fermion operators, and (2) the corrections to the fermion two-point function from four-fermion operators. Additionally f' can refer to any fermion, including being the same type as the final state fermion, f.*

$\Gamma^{(1)}_{f,\text{weak}}$, and are also a combination of select results in $\Gamma^{(1)}_{f,(t)}$ and $\Gamma^{(1)}_{f,(\text{rem.})}$. We list these results to better understand the scaling of terms in the decay rates in terms of powers of the fermion masses, which will become important to our numerical studies in Section 4.6.1. The four-fermion contributions are from only a small number of diagrams, which can be found in Fig. 4.7. As we see from this figure, there is only one generic diagram topology that contributes to the bare matrix element, and only one generic diagram topology that contributes to the fermion two-point function required for renormalization of the fermion field normalization and mass.

Similarly to the large-m_t results in Section 4.4.2, we write this decay rate as

$$\overline{\Gamma}^{(6,1)}_{f,(4\text{F})} = \Gamma^{(6,1)}_{f,(4\text{F})} - 2\Gamma^{(4,0)}_{f}\overline{c}_{m_f}\delta f^{(6)}_{(4\text{F})}\,, \tag{4.4.22}$$

where the subscript (4F) indicates the four-fermion contributions, which in this instance applies to the NLO decay rate and to δf defined in Eq. 4.4.1. As was the case in Section 4.4.1, we report the results in the small-mass limit, for brevity, and again for other reasons which will become clear in Section 4.5.2. Therefore, throughout this section, $\Gamma^{(i,0)}$ from Eq. 4.2.5 are defined to be in the small-mass limit also. For completeness, the four-fermion results while retaining full mass dependence may be found in Appendix E.2.

The results for $\delta f_{(4\text{F})}$ for each f under consideration here are

$$\begin{aligned}
\delta b^{(6)}_{(4\text{F})} &= \frac{1}{16\pi^2}\frac{m_t^3}{m_b}\left((1+2N_c)C^{(1)}_{\substack{quqd\\3333}} + C_F C^{(8)}_{\substack{quqd\\3333}}\right)\left[1+\ln\left(\frac{\mu^2}{m_t^2}\right)\right]\,,\\
\delta c^{(6)}_{(4\text{F})} &= -\frac{1}{16\pi^2}2\frac{m_t^3}{m_c}\left(C^{(1)}_{\substack{qu\\2332}} + C_F C^{(8)}_{\substack{qu\\2332}}\right)\left[1+2\ln\left(\frac{\mu^2}{m_t^2}\right)\right]\,,\\
\delta \tau^{(6)}_{(4\text{F})} &= -\frac{1}{16\pi^2}2N_c C_{\substack{lequ\\3333}}\frac{m_t^3}{m_\tau}\left[1+\ln\left(\frac{\mu^2}{m_t^2}\right)\right]\,,\\
\delta \mu^{(6)}_{(4\text{F})} &= -\frac{1}{16\pi^2}2N_c C_{\substack{lequ\\2233}}\frac{m_t^3}{m_\mu}\left[1+\ln\left(\frac{\mu^2}{m_t^2}\right)\right]\,.
\end{aligned} \tag{4.4.23}$$

Before presenting the decay rate we first introduce some functions used to simplify the result. In cases where top-quark loops contribute, the results involve the functions

$$F_{8S}\left(\frac{m_t^2}{m_H^2},\frac{\mu^2}{m_H^2}\right) = \beta_t^2\left(2\beta_t \text{arccot}\left(\beta_t\right) - \ln\left(\frac{\mu^2}{m_t^2}\right) - 2\right),$$
$$F_{8V}\left(\frac{m_t^2}{m_H^2},\frac{\mu^2}{m_H^2}\right) = \beta_t^2\left(-8\beta_t \text{arccot}\left(\beta_t\right) + 4\ln\left(\frac{\mu^2}{m_t^2}\right) + 6\right), \tag{4.4.24}$$

where

$$\beta_t \equiv \sqrt{\frac{4m_t^2}{m_H^2} - 1}\,. \tag{4.4.25}$$

Note that the form of β_t in Eq. 4.4.25 differs from the form of β_f for the light fermions in Eq. 4.2.6. Contributions from other fermions involve the real part of the above functions in the limit $m_t \to 0$, given by

$$F_{8S}\left(0,\frac{\mu^2}{m_H^2}\right) = 2 + \ln\left(\frac{\mu^2}{m_H^2}\right),$$
$$F_{8V}\left(0,\frac{\mu^2}{m_H^2}\right) = -6 - 4\ln\left(\frac{\mu^2}{m_H^2}\right). \tag{4.4.26}$$

The functions with subscripts $8V$ arise from four-fermion operators of the form $(\bar{L}L)(\bar{R}R)$ in Table A.1, whereas those with subscripts $8S$ arise from four-fermion operators of the form $(\bar{L}R)(\bar{R}L)$ or $(\bar{L}R)(\bar{L}R)$ given in the last row of that table. In terms of these functions, the result for $h \to b\bar{b}$ reads

$$\begin{aligned}\Gamma_{b,(4\text{F})} = \frac{m_H^2\Gamma_b^{(4,0)}}{16\pi^2}\Bigg\{ &\left[C^{(1)}_{\substack{qd\\3333}} + C_F C^{(8)}_{\substack{qd\\3333}} + \frac{m_s}{m_b}\left(C^{(1)}_{\substack{qd\\2332}} + C_F C^{(8)}_{\substack{qd\\2332}}\right)\right] F_{8V}\left(0,\frac{\mu^2}{m_H^2}\right)\\
&+ \frac{m_t}{m_b}\left[(1+2N_c)C^{(1)}_{\substack{quqd\\3333}} + C_F C^{(8)}_{\substack{quqd\\3333}}\right] F_{8S}\left(\frac{m_t^2}{m_H^2},\frac{\mu^2}{m_H^2}\right)\\
&+ \Bigg(\frac{m_c}{m_b}\left[C^{(1)}_{\substack{quqd\\3223}} + C_F C^{(8)}_{\substack{quqd\\3223}} + 2N_c C^{(1)}_{\substack{quqd\\2233}}\right] + 2\frac{m_\tau}{m_b}C_{\substack{ledq\\3333}}\\
&+ 2\frac{m_\mu}{m_b}C_{\substack{ledq\\2233}}\Bigg) F_{8S}\left(0,\frac{\mu^2}{m_H^2}\right)\Bigg\}.\end{aligned} \tag{4.4.27}$$

For $h \to c\bar{c}$ we find

$$\begin{aligned}\Gamma_{c,(4\text{F})} = \frac{m_H^2\Gamma_c^{(4,0)}}{16\pi^2}\Bigg\{ &\left[C^{(1)}_{\substack{qu\\2222}} + C_F C^{(8)}_{\substack{qu\\2222}}\right] F_{8V}\left(0,\frac{\mu^2}{m_H^2}\right)\\
&+ \frac{m_t}{m_c}\left[C^{(1)}_{\substack{qu\\2332}} + C_F C^{(8)}_{\substack{qu\\2332}}\right] F_{8V}\left(\frac{m_t^2}{m_H^2},\frac{\mu^2}{m_H^2}\right) + \Bigg(\frac{m_b}{m_c}\Bigg[C^{(1)}_{\substack{quqd\\3223}} + C_F C^{(8)}_{\substack{quqd\\3223}}\\
&+ 2N_c C^{(1)}_{\substack{quqd\\2233}}\Bigg] + \frac{m_s}{m_c}\left[(1+2N_c)C^{(1)}_{\substack{quqd\\2222}} + C_F C^{(8)}_{\substack{quqd\\2222}}\right] - 2\frac{m_\tau}{m_c}C^{(1)}_{\substack{lequ\\3322}}\\
&- 2\frac{m_\mu}{m_c}C^{(1)}_{\substack{lequ\\2222}}\Bigg) F_{8S}\left(0,\frac{\mu^2}{m_H^2}\right)\Bigg\}.\end{aligned} \tag{4.4.28}$$

To simplify the results in Eqs. 4.4.27 and 4.4.28, we have used relations such as $C^{(k)}_{\substack{qu\\2332}} = C^{(k)\dagger}_{\substack{qu\\3223}}$ (with $k = 1, 8$) which follow from the hermiticity of the SMEFT Lagrangian. There are similar flavor-indices degeneracies for a large number of flavor-dependent operators in Table A.1, and so we must choose a subset of Wilson coefficients in which to express our results; in this work we choose to follow the convention adopted by [135]. For $h \to \tau\bar{\tau}$ we find

$$\begin{aligned}\Gamma_{\tau,(4\mathrm{F})} = \frac{m_H^2 \Gamma_\tau^{(4,0)}}{16\pi^2}\Bigg\{ &\left[C_{\substack{le\\3333}} + \frac{m_\mu}{m_\tau} C_{\substack{le\\2332}}\right] F_{8V}\left(0, \frac{\mu^2}{m_H^2}\right) \\ &- 2N_c \frac{m_t}{m_\tau} C^{(1)}_{\substack{lequ\\3333}} F_{8S}\left(\frac{m_t^2}{m_H^2}, \frac{\mu^2}{m_H^2}\right) + 2N_c \Bigg[\frac{m_b}{m_\tau} C_{\substack{ledq\\3333}} - \frac{m_c}{m_\tau} C^{(1)}_{\substack{lequ\\3322}} \\ &+ \frac{m_s}{m_\tau} C_{\substack{ledq\\3322}}\Bigg] F_{8S}\left(0, \frac{\mu^2}{m_H^2}\right)\Bigg\}. \end{aligned} \tag{4.4.29}$$

Finally, for $h \to \mu\bar{\mu}$ we find

$$\begin{aligned}\Gamma_{\mu,(4\mathrm{F})} = \frac{m_H^2 \Gamma_\mu^{(4,0)}}{16\pi^2}\Bigg\{ &\left[C_{\substack{le\\2222}} + \frac{m_\tau}{m_\mu} C_{\substack{le\\2332}}\right] F_{8V}\left(0, \frac{\mu^2}{m_H^2}\right) \\ &- 2N_c \frac{m_t}{m_\mu} C^{(1)}_{\substack{lequ\\2233}} F_{8S}\left(\frac{m_t^2}{m_H^2}, \frac{\mu^2}{m_H^2}\right) + 2N_c \Bigg[\frac{m_b}{m_\mu} C_{\substack{ledq\\2233}} - \frac{m_c}{m_\mu} C^{(1)}_{\substack{lequ\\2222}} \\ &+ \frac{m_s}{m_\mu} C_{\substack{ledq\\2222}}\Bigg] F_{8S}\left(0, \frac{\mu^2}{m_H^2}\right)\Bigg\}. \end{aligned} \tag{4.4.30}$$

Across the results in Eqs. 4.4.27 to 4.4.30, we find that contributions from top-quark loops are enhanced by factors of m_t/m_f. If we impose MFV, the Wilson coefficients multiplying these contributions scale with an additional factor of $m_f/\hat{v}_T$, therefore removing this large enhancement. Further, we see from the results in Eq. 3.5.8 that for $h \to c\bar{c}$ after imposing MFV the top-loop contributions are entirely removed.

4.5 Enhanced NLO Corrections and Decoupling Relations

In this section we numerically examine some subsets of the results reported thus far. In particular, we have not yet committed to any particular renormalization scheme, instead choosing to write results in a way that allows us to easily switch between schemes for a subset of parameters appearing in the LO decay rate. The size of NLO perturbative corrections depend on the particular renormalization scheme one employs, and it is important to reduce the size of NLO corrections to ensure good convergence of the perturbative expansion. This makes the choice of renormaliza-

tion scheme an important one. In Section 4.5.1 we asses two sources of enhanced NLO corrections to the decay rate, while in Section 4.5.2 we introduce *decoupling relations* as a way to combine QCD and EW NLO corrections to the processes under consideration here while simultaneously removing parametrically-enhanced corrections.

4.5.1 Structure of the NLO Decay Rate

Thus far, our results have been reported with some degree of flexibility regarding the renormalization scheme – the results have been written such that it is easy for the reader to convert between the on-shell and $\overline{\text{MS}}$ schemes for the electric charge and final-state-pair masses. Here, we consider two sources of parametrically-large NLO corrections to the LO decay rate and how the choice of renormalization scheme affects these corrections.

We first consider the QED-QCD corrections reported in Section 4.4.1. It is easy to identify that the logarithm (and in particular the double logarithm) of the small ratio m_f/m_H in Eq. 4.4.5 could potentially lead to large NLO corrections. Keeping only these logarithmic corrections we have

$$\begin{aligned}\frac{\Gamma^{(1)}_{f,(g,\gamma)}}{\Gamma^{(4,0)}_f} \approx \ln^2\left(\frac{m_f^2}{m_H^2}\right)\frac{\hat{v}_T^2}{\pi}\left(\delta_{f,q}C_F\alpha_s C_{HG} + Q_f^2\alpha c_{h\gamma\gamma}\right) \\ + \; c_{m_f}\ln\left(\frac{m_f^2}{m_H^2}\right)\frac{3}{2}\left(\frac{\delta_{f,q}C_F\alpha_s + Q_f^2\alpha}{\pi}\right)\Bigg[1 + 2\hat{v}_T^2\Bigg(C_{H\Box} \\ - \frac{C_{HD}}{4}\left(1 - \frac{\hat{c}_w^2}{\hat{s}_w^2}\right) + \frac{\hat{c}_w}{\hat{s}_w}C_{HWB} - \frac{\hat{v}_T}{m_f}\frac{C_{fH}}{2\sqrt{2}}\Bigg)\Bigg],\end{aligned} \tag{4.5.1}$$

which upon evaluating numerically using the parameter values listed in Table 4.2 and using $\mu = m_H$ we find generically takes the form[1]

$$\begin{aligned}\frac{\Gamma^{(1)}_{f,(g,\gamma)}}{\Gamma^{(4,0)}_f} \approx \hat{v}_T^2\left(N^f_{HG}C_{HG} + N^f_{h\gamma\gamma}c_{h\gamma\gamma}\right) \\ + N^f_{\text{O.S.}}c_{m_f}\left[1 + 2\hat{v}_T^2\left(C_{H\Box} - \frac{C_{HD}}{4}\left(1 - \frac{\hat{c}_w^2}{\hat{s}_w^2}\right) + \frac{\hat{c}_w}{\hat{s}_w}C_{HWB} - \frac{\hat{v}_T}{m_f}\frac{C_{fH}}{2\sqrt{2}}\right)\right],\end{aligned} \tag{4.5.2}$$

[1]The values in Table 4.2 include the light-fermion masses and electromagnetic fine structure constant defined in the $\overline{\text{MS}}$ scheme, while the expression in Eq. 4.5.1 allows us to choose between the on-shell scheme and $\overline{\text{MS}}$ scheme for these quantities. Similarly to the analyses performed in Sections 4.3.1 and 4.4.2, the differences between the on-shell and $\overline{\text{MS}}$ inputs for these parameters is small enough that using the $\overline{\text{MS}}$ input values from Table 4.2 does not significantly affect the analysis performed here.

Final state, f	N^f_{HG}	$N^f_{h\gamma\gamma}$	$N^f_{\text{O.S.}}$
b	2.4	0.02	-0.5
c	4.6	0.11	-0.7
τ	0	0.18	-0.03
μ	0	0.51	-0.05

Table 4.1: *The numerical values of N^f_{HG}, $N^f_{h\gamma\gamma}$ and $N^f_{O.S.}$ defined in Eq. 4.5.2 for final state fermions $f \in \{b, c, \tau, \mu\}$.*

where the N_i^f are numerical values which differ for each final state, and are reported in Table 4.1.

Examining the values found in Table 4.1, we see that for processes involving final-state quarks, the NLO QED-QCD corrections are dominated by the double logarithmic term on the first line of Eq. 4.5.1, especially for the QCD component. As noted in Section 4.4.1 this term does not appear at NLO in the SM, and in the dimension-6 SMEFT is of IR origin and cannot be removed through a choice of renormalization scheme.[1] It would need to be treated with QCD resummation techniques which we do not explore here. For processes involving final-state leptons, we see from Table 4.1 that although the absence of QCD corrections reduces the overall size of contributions related to the double logarithmic term, the small fermion masses (particularly for the muon) still results in sizeable QED corrections. The single logarithmic term in the second and third lines of (4.5.1) arises from the finite part of the fermion mass renormalization counterterm in the on-shell scheme. For processes involving final-state quarks, although this correction is not as large as the double logarithmic term, it still contributes a sizeable correction of -50% and -70% to the LO result for b-quark and c-quark final states respectively. For processes involving final-state leptons, while these corrections are significantly smaller due to the absence of QCD, the NLO corrections of -3% and -5% for final-state tau anti-tau pair and muon anti-muon pair respectively are still large for QED corrections. These single logarithmic corrections can be removed from the explicit NLO correction and resummed by renormalizing the fermion masses in the $\overline{\text{MS}}$ scheme. We therefore conclude that to best avoid enhanced NLO corrections of QED-QCD origin, we should renormalize the fermion masses in the $\overline{\text{MS}}$ scheme, as is standard for SM calculations.

The second source of potentially large NLO corrections to the decay rate are weak corrections enhanced by powers of $m_t^2/\hat{v}_T^2$, which appear in the object $\Gamma^{(1)}_{f,(t)}$, intro-

[1] This contribution arises from the interference of the SM amplitude with dimension-6 amplitudes involving Hgg and $H\gamma\gamma$ vertices. These vertices do not contain a Yukawa coupling, so the fact that the contribution to the decay rate scales as m_f^2 is due to a chirality flip in the fermion propagator.

duced in Eq. 4.1.3. We have reported explicit SM and dimension-6 results for $\Gamma^{(1)}_{f,(t)}$ in Section 4.4.2, written in such a way that we may easily switch between the on-shell scheme, and the hybrid renormalization scheme in which the fermion mass, m_f, and the electric charge, e, are renormalized in the $\overline{\text{MS}}$ scheme. The results in Section 4.4.2 show that in the hybrid renormalization scheme the dominant contributions are due to tadpole corrections which scale as $m_t^4/(\hat{v}_T^2 m_H^2)$. As discussed throughout Sections 1.2.3 and 4.3.5, tadpole corrections cancel in a purely on-shell scheme, and so the dominant results in the on-shell scheme instead scale as $m_t^2/\hat{v}_T^2$. We now consider both the on-shell scheme, and the hybrid renormalization scheme numerically to examine the size of these dominant large-m_t NLO corrections. Keeping only leading order terms in the large-m_t limit, the hybrid renormalization scheme gives

$$\frac{\overline{\Gamma}^{(4,1)}_{f,(t)}}{\overline{\Gamma}^{(4,0)}_{f}} \approx -\frac{N_c}{2\pi^2}\frac{m_t^4}{m_H^2\hat{v}_T^2} \approx -0.15\,, \tag{4.5.3}$$

which is valid for all light fermions due to this term arising from universal tadpole corrections, and where we have used $\mu = m_t$. In the on-shell scheme we instead find

$$\begin{aligned}
\frac{\Gamma^{(4,1)}_{b,(t)}}{\Gamma^{(4,0)}_{b}} &\approx \frac{m_t^2}{16\pi^2\hat{v}_T^2}\left(-6 + N_c\frac{7-10\hat{c}_w^2}{3\hat{s}_w^2}\right) \approx -0.03\,,\\
\frac{\Gamma^{(4,1)}_{f\setminus b,(t)}}{\Gamma^{(4,0)}_{f\setminus b}} &\approx \frac{m_t^2}{16\pi^2\hat{v}_T^2}\left(N_c\frac{7-10\hat{c}_w^2}{3\hat{s}_w^2}\right) \approx -0.01\,.
\end{aligned} \tag{4.5.4}$$

In the SM, from Eqs. 4.5.3 and 4.5.4 we see that in the hybrid renormalization scheme, the large-m_t corrections constitute an approximately -15% correction to the LO decay rate, and thus anomalously large for a weak correction, while the purely on-shell result gives an approximately -3% correction for $h \to b\bar{b}$ and an approximately -1% correction for Higgs decay to all other light fermion pairs, in line with what one typically expects from weak corrections.

For the dimension-6 SMEFT, the equivalent contributions in the hybrid renormalization scheme read

$$\begin{aligned}
\frac{\overline{\Gamma}^{(6,1)}_{f,(t)}}{\overline{\Gamma}^{(4,0)}_{f}} &\approx \frac{N_c\hat{v}_T^2}{2\pi^2}\frac{m_t^4}{m_H^2\hat{v}_T^2}\bigg(-4C_{H\Box} + C_{HD}\left(1-\frac{\hat{c}_w^2}{\hat{s}_w^2}\right) - 2C_{HWB}\frac{\hat{c}_w}{\hat{s}_w}(2-\hat{s}_w^2)\\
&\quad - 2\hat{c}_w^2 C_{HB} - 2\hat{s}_w^2 C_{HW} + \sqrt{2}\frac{\hat{v}_T}{m_f}C_{fH}\bigg)\\
&\approx \frac{\hat{v}_T^2}{\Lambda^2_{\text{NP}}}\bigg(-0.59C_{H\Box} - 0.37C_{HD} - 0.99C_{HWB} - 0.23C_{HB}\\
&\quad - 0.07C_{HW} + 0.21\frac{m_f}{\hat{v}_T}C_{fH}\bigg)\,,
\end{aligned} \tag{4.5.5}$$

which again applies to all light-fermion final states. The result in the on-shell scheme differs for a final-state b-quark pair compared to all other final-state light-fermion pairs, and these results may be found in the first lines of Eq. 4.4.20 and Eq. 4.4.21 respectively. Comparing the results across Eqs. 4.4.20, 4.4.21 and 4.5.5 we see that, like in the SM, the on-shell scheme results are significantly smaller, typically by around a factor of between 2 and 10, depending on the Wilson coefficient. We therefore conclude that in the dimension-6 SMEFT, like in the SM, the large-m_t NLO corrections are relatively smaller in the on-shell renormalization scheme.

While we have not explicitly demonstrated so here, it is clear that the on-shell electric charge would result in large corrections also arising from logarithms involving the light-fermion masses. It is possible to remove these contributions at NLO via the choice of the effective on-shell fine structure constant, $\alpha(M_Z^2)$,[1] as an input parameter [118]. However, for our purposes these corrections are also removed with the choice of renormalizing this parameter in the $\overline{\text{MS}}$ scheme.

The conclusion we draw from the analysis seen throughout this section is that while QED-QCD corrections (and terms arising from the electric charge renormalization) are best behaved in the hybrid renormalization scheme, the EW corrections are best behaved in a purely on-shell scheme, where sizeable tadpole corrections from heavy particles, such as the top quark, completely cancel at the level of the renormalized amplitude. At least in the SM, an apparent compromise would be to use the $\overline{\text{MS}}$ scheme for all parameters appearing in the tree-level result, be it fermion masses, the electric charge, M_W or M_Z. This is however an imperfect solution, for although in that case no explicit tadpoles appear in the NLO corrections, they reappear in the RG equations. Moreover, in the SMEFT it is not possible to remove all explicit tadpole contributions in this manner, since in contrast to the SM they can also appear in the bare matrix element through contributions such as that shown in Diagram (4) of Fig. 4.6.

The resolution to this dilemma would be to renormalize the light-fermion masses and electric charge such that the QCD-QED corrections are treated in the $\overline{\text{MS}}$ scheme while weak corrections involving the top quark and heavy electroweak bosons are treated in the on-shell scheme. In that way contributions from potentially large tadpole corrections cancel, but logarithms of m_f/m_H can still be resummed in the $\overline{\text{MS}}$ scheme. At the technical level, the simplest way to implement such a scheme is to make use of so-called *decoupling relations*.

[1] The effective on-shell coupling, $\alpha(M_Z^2)$, is found from running the on-shell value of $\alpha(k^2 = 0)$ from $k^2 = 0$ to $k^2 = M_Z^2$ [118].

4.5.2 Decoupling Relations

In this section we describe decoupling relations which allow us to connect parameters renormalized in the $\overline{\text{MS}}$ scheme to those defined in a low-energy theory where the top quark and EW bosons are integrated out. A detailed discussion of this in the SM for the b-quark mass defined in the $\overline{\text{MS}}$ scheme can be found in [136]. Our low energy theory is therefore one in which the constituent particles are the leptons, five flavors of quark, photons and gluons. We hereafter refer to this theory simply as QED×QCD. Specifically, we wish to consider only SM effects, which we find is equivalent to neglecting terms that scale as m_f^2/M_W^2, where f is all fermions except for the top quark. This also offers the additional advantage of the RG running of these parameters being entirely due to the simpler SM anomalous dimensions.

We can write the decoupling relations between the $\overline{\text{MS}}$ renormalized parameters in our hybrid renormalization scheme with those defined in QED×QCD by

$$\begin{aligned} \overline{m}_f(\mu) &= \zeta_f(\mu, m_t, m_H, M_W, M_Z)\overline{m}_f^{(\ell)}(\mu)\,, \\ \overline{e}(\mu) &= \zeta_e(\mu, m_t, m_H, M_W, M_Z)\overline{e}^{(\ell)}(\mu)\,, \end{aligned} \tag{4.5.6}$$

where the parameters on the left-hand side are defined in the SM+dimension-6 SMEFT, while those on the right-hand side with superscript ℓ are defined in QED×QCD. As previously stated, the QED×QCD parameters have the advantage of obeying the usual SM RG equations

$$\begin{aligned} \frac{d\overline{m}_f^{(\ell)}(\mu)}{d\ln(\mu)} &= \gamma_f(\mu)\overline{m}_f^{(\ell)}(\mu)\,, \\ \frac{d\overline{e}^{(\ell)}(\mu)}{d\ln(\mu)} &= \gamma_e(\mu)\overline{e}^{(\ell)}(\mu)\,, \end{aligned} \tag{4.5.7}$$

where $\gamma_f(\mu)$ was given to LO in QED and QCD separately in Eq. 1.4.16, while the form of $\gamma_e(\mu)$ can be derived from the expressions found in Eqs. 1.4.4 to 1.4.6. In total, these expressions take the form

$$\begin{aligned} \gamma_f(\mu) &= -\frac{3}{2\pi}\left[\delta_{f,q}\alpha_s(\mu)C_F + \overline{\alpha}^{(\ell)}(\mu)Q_f^2\right]\,, \\ \gamma_e(\mu) &= \frac{\overline{\alpha}^{(\ell)}}{3\pi}\left[N_g Q_\ell^2 + N_c\left((N_g-1)Q_u^2 + N_g Q_d^2\right)\right]\,, \end{aligned} \tag{4.5.8}$$

where in the top line we have again included a factor of $\delta_{f,q}$ to emphasize that at LO only quarks receive QCD contributions to the RG running, and where $\overline{\alpha}^{(\ell)}(\mu) = [\overline{e}^{(\ell)}(\mu)]^2/(4\pi)$.

The ζ_i in Eq. 4.5.6 are decoupling constants and can be determined by the relations between the $\overline{\text{MS}}$ and on-shell parameters in the two theories. These take the form

$$\begin{aligned} m_f &= z_f^{-1}(\mu, m_f, m_t, m_H, M_W, M_Z)\overline{m}_f(\mu) = \left[z_f^{(\ell)}(\mu, m_f)\right]^{-1} \overline{m}_f^{(\ell)}(\mu)\,, \\ e &= z_e^{-1}(\mu, m_b, m_t, m_H, M_W, M_Z)\overline{e}(\mu) = \left[z_e^{(\ell)}(\mu, m_b)\right]^{-1} \overline{e}^{(\ell)}(\mu)\,, \end{aligned} \tag{4.5.9}$$

where we have used that the on-shell parameters, m_f and e, are defined through non-perturbative renormalization conditions, and therefore do not depend of the Lagrangian or particle content of each theory. The z_i and $z_i^{(\ell)}$ in Eq. 4.5.9 are constants connecting the $\overline{\text{MS}}$ parameters in each theory to the on-shell parameters and can be calculated at each order in perturbation theory. Using the fermion mass as an example, we begin by noting that in the full SM+dimension-6 SMEFT theory, these two parameters are related by (where for clarity of notation we drop the arguments of these functions)

$$m_f^{(0)} = m_f + \delta m_f = \overline{m}_f + \delta\overline{m}_f\,. \tag{4.5.10}$$

We therefore find

$$\begin{aligned} m_f &= \left(1 + \frac{\delta\overline{m}_f}{\overline{m}_f}\right)\left(1 - \frac{\delta m_f}{m_f}\right)\overline{m}_f\,, \\ &= \left(1 + \frac{\delta\overline{m}_f - \delta m_f}{\overline{m}_f}\right)\overline{m}_f\,, \end{aligned} \tag{4.5.11}$$

where in the second line we have substituted the equation from the first line into itself to remove the factor of m_f on the right-hand side, and kept terms up to and including NLO. Considering the quantity $\delta\overline{m}_f - \delta m_f$, we note that each counterterm necessarily contains the same pole structure, which cancels between these two terms, leaving only the finite pieces of the on-shell counterterm

$$m_f = \left(1 - \frac{\delta m_f^{\text{fin.}}}{\overline{m}_f}\right)\overline{m}_f\,, \tag{4.5.12}$$

where $\delta m_f^{\text{fin.}}$ contains the finite pieces of the on-shell counterterm of the full theory. We therefore find

$$z_f = 1 + \frac{\delta m_f^{\text{fin.}}}{\overline{m}_f}\,. \tag{4.5.13}$$

Similarly, we can relate the on-shell fermion mass to the $\overline{\text{MS}}$ renormalized mass in the five-flavor QED×QCD theory

$$m_f = \left(1 + \frac{\delta\overline{m}_f^{(\ell)} - \delta m_f^{(\ell)}}{\overline{m}_f^{(\ell)}}\right)\overline{m}_f^{(\ell)}\,. \tag{4.5.14}$$

Now considering the quantity $\delta\overline{m}_f^{(\ell)} - \delta m_f^{(\ell)}$, again each counterterm necessarily contains the same pole structure, but note that the remaining finite pieces only come from corrections in the five-flavor QED×QCD theory. This difference in counterterms is therefore equal to the finite parts of the QED×QCD pieces of the full theory, which we denote $\delta m_f^{\text{fin.}}\big|_{\text{QED}\times\text{QCD}}$. Therefore, we have the relation

$$m_f = \left(1 - \frac{\delta m_f^{\text{fin.}}\big|_{\text{QED}\times\text{QCD}}}{\overline{m}_f^{(\ell)}}\right)\overline{m}_f^{(\ell)}\,, \tag{4.5.15}$$

such that $z_f^{(\ell)}$ takes the form

$$z_f^{(\ell)} = 1 + \frac{\delta m_f^{\text{fin.}}\big|_{\text{QED}\times\text{QCD}}}{\overline{m}_f^{(\ell)}}\,. \tag{4.5.16}$$

Analogously, the forms of z_e and $z_e^{(\ell)}$ are given by

$$\begin{aligned} z_e &= 1 + \frac{\delta e^{\text{fin.}}}{\overline{e}}\,, \\ z_e^{(\ell)} &= 1 + \frac{\delta e^{\text{fin.}}\big|_{\text{QED}\times\text{QCD}}}{\overline{e}^{(\ell)}}\,. \end{aligned} \tag{4.5.17}$$

Making use of Eqs. 4.5.6 and 4.5.9 we see that the decoupling constants may be written in terms of z_i and $z_i^{(\ell)}$ as (restoring the arguments of these functions)

$$\zeta_i(\mu, m_t, m_H, M_W, M_Z) = \left.\frac{z_i(\mu, m_f, m_t, m_H, M_W, M_Z)}{z_i^{(\ell)}(\mu, m_f)}\right|_{m_f\to 0}\,, \tag{4.5.18}$$

where $i = e$, f, and where we have now enforced the small mass limit, $m_f \to 0$ in accordance with the description of QED×QCD at the beginning of this section. In terms of the renormalization constants, the decoupling constant for the fermion mass may be written

$$\begin{aligned} \zeta_f &= \left.\left(1 + \frac{\delta m_f^{\text{fin.}}}{\overline{m}_f}\right)\left(1 - \frac{\delta m_f^{\text{fin.}}\big|_{\text{QED}\times\text{QCD}}}{\overline{m}_f^{(\ell)}}\right)\right|_{m_f\to 0}\,, \\ &= 1 + \left.\frac{\delta m_f^{\text{fin.}} - \delta m_f^{\text{fin.}}\big|_{\text{QED}\times\text{QCD}}}{m_f}\right|_{m_f\to 0}\,, \end{aligned} \tag{4.5.19}$$

where in the second line we have made use of the fact that neglecting NNLO and higher order terms allows us to exchange both $\overline{m}_f$ and $\overline{m}_f^{(\ell)}$ for m_f. We see from Eq. 4.5.19 that the decoupling constant for the fermion mass is a function of the finite part of the corresponding renormalization constant, with the QED×QCD

contributions factored out. Similarly for the electric charge

$$\zeta_e = 1 + \left.\frac{\delta e^{\text{fin.}} - \delta e^{\text{fin.}}\big|_{\text{QED}\times\text{QCD}}}{e}\right|_{m_f\to 0} . \tag{4.5.20}$$

We may now write the decoupling constants, ζ_i, as a perturbative expansion as

$$\zeta_i = 1 + \zeta_i^{(4,1)} + \zeta_i^{(6,1)} , \tag{4.5.21}$$

where the superscript (i, j) refers to the dimension-i contribution at jth order in perturbation theory.

The expression for ζ_e is compact, and the SM contribution is

$$\zeta_e^{(4,1)} = \frac{\alpha}{\pi}\left[-\frac{1}{12} - \frac{7}{8}\ln\left(\frac{\mu^2}{M_W^2}\right) + \frac{N_c}{6}Q_t^2\ln\left(\frac{\mu^2}{m_t^2}\right)\right] , \tag{4.5.22}$$

while the dimension-6 SMEFT contribution is

$$\begin{aligned}\zeta_e^{(6,1)} =& \frac{\alpha}{\pi}\left[\sqrt{2}\hat{v}_T m_t N_c Q_t\left(\hat{c}_w\frac{C_{tB}}{e} + \hat{s}_w\frac{C_{tW}}{e}\right)\ln\left(\frac{\mu^2}{m_t^2}\right)\right. \\ &\left. + 9\frac{C_W}{e}\hat{s}_w M_W^2\ln\left(\frac{\mu^2}{M_W^2}\right)\right] + \left.\frac{\delta e_4^{(6)}}{e}\right|_{\text{fin.},\, m_f\to 0} ,\end{aligned} \tag{4.5.23}$$

where the final term is the UV-finite part of the class-4 electric charge counterterm from Eq. 4.3.29 in the small-mass limit. Decoupling constants for the final state fermion masses, m_f, for $f \in \{b,\, c,\, \tau,\, \mu\}$ are lengthy, and can be found in Appendix F.

As previously concluded, we wish to write our decay rate in terms of the QED×QCD renormalized parameters $\overline{m}_f^{(\ell)}$ and $\overline{e}^{(\ell)}$ in the $\overline{\text{MS}}$ scheme, while making use of decoupling constants to restore the finite top-quark and massive boson contributions such that we may resum the large QED-QCD corrections while simultaneously avoiding large tadpole corrections. In this way, we effectively renormalize QED-QCD corrections to $\overline{m}_f^{(\ell)}$ and $\overline{e}^{(\ell)}$ in the $\overline{\text{MS}}$ scheme, while renormalizing the remaining contributions in the on-shell scheme. We refer to this scheme as *the decoupled hybrid renormalization scheme*, where the aforementioned choice of input parameters is implied by this scheme choice. With this as our chosen scheme, it is simple to rewrite the form of our decay rates at each mass dimension and order in perturbation theory by making use of the decoupling constants. We denote the decay rate as $\overline{\Gamma}^{(\ell)}$ in the decoupled hybrid renormalization scheme. These decay rates may be written in terms of the decay rates with parameters $\overline{m}_f$ and $\overline{e}$ of the full theory by simply using the expression in Eq. 4.5.6 in the decay rate, $\overline{\Gamma}$, and expanding up to NLO. As the decoupling constants contribute at the one-loop level, at LO the decay rates are the same up to a simple replacement of the full theory parameters with the QED×QCD

parameters. At NLO we find

$$\begin{aligned}
\overline{\Gamma}_f^{(4,1),(\ell)} &= \left\{ \overline{\Gamma}_f^{(4,1)} + 2\overline{\Gamma}_f^{(4,0)} \left(\zeta_f^{(4,1)} + \zeta_e^{(4,1)} \right) \right\} \Bigg|_{P \to \overline{P}^{(\ell)}} , \\
\overline{\Gamma}_f^{(6,1),(\ell)} &= \left\{ \overline{\Gamma}_f^{(6,1)} + 2\overline{\Gamma}_f^{(4,0)} \left(\zeta_f^{(6,1)} + \zeta_e^{(6,1)} \right) + 2\overline{\Gamma}_f^{(6,0)} \zeta_f^{(4,1)} \right. \\
&\quad \left. + \sqrt{2} C_{fH} \frac{(\overline{v}^{(\ell)})^3}{\overline{m}_f^{(\ell)}} \overline{\Gamma}_f^{(4,0)} \left(\zeta_f^{(4,1)} + \zeta_e^{(4,1)} \right) \right\} \Bigg|_{P \to \overline{P}^{(\ell)}} ,
\end{aligned} \tag{4.5.24}$$

where we have suppressed the dependence on the $\overline{\text{MS}}$ renormalization scale, μ, and where we have introduced

$$P = \{m_f, \alpha\} , \quad \overline{P}^{(\ell)} = \{\overline{m}_f^{(\ell)}, \overline{\alpha}^{(\ell)}\} , \tag{4.5.25}$$

for $f \neq t$. The replacement in Eq. 4.5.24 makes it clear that (unlike in the on-shell scheme or hybrid renormalization scheme cases) in the decoupled hybrid renormalization scheme we intend to keep the explicit superscripts on the QED×QCD renormalized input parameters $\overline{m}_f^{(\ell)}$ and $\overline{\alpha}^{(\ell)}$. In Eq. 4.5.24 we have also introduced

$$\overline{v}^{(\ell)}(\mu) \equiv \frac{2 M_W \hat{s}_w}{\overline{e}^{(\ell)}(\mu)} . \tag{4.5.26}$$

Interestingly, the same results of Eq. 4.5.24 can be obtained by the replacements of the UV counterterms found in Eqs. 4.3.8 and 4.3.9 according to

$$\begin{aligned}
\frac{\delta m_f}{m_f} &\to \frac{\delta m_f}{m_f} + \zeta_f , \\
\frac{\delta e}{e} &\to \frac{\delta e}{e} + \zeta_f .
\end{aligned} \tag{4.5.27}$$

From this it is clear that evaluating the decay rate according to Eq. 4.5.24 is equivalent to using a new renormalization scheme.

As was seen in Eq. 4.1.3, we can again split our decay rate in the decoupled hybrid renormalization scheme into various contributions

$$\overline{\Gamma}_f^{(1),(\ell)} = \overline{\Gamma}_{f,(g,\gamma)}^{(1),(\ell)} + \overline{\Gamma}_{f,(t)}^{(1),(\ell)} + \overline{\Gamma}_{f,(\text{rem.})}^{(1),(\ell)} , \tag{4.5.28}$$

which again denote the QED-QCD, large-m_t, and remainder corrections. Fortunately, it is a simple process to convert the QED-QCD, large-m_t and four-fermion results already reported from their forms found in Sections 4.4.1, 4.4.2, and 4.4.3 respectively. For the QED-QCD results we can recover the results in the decoupled

hybrid renormalization scheme as

$$\overline{\Gamma}^{(1),(\ell)}_{f,(g,\gamma)} = \overline{\Gamma}^{(1)}_{f,(g,\gamma)}\Big|_{P\to\overline{P}^{(\ell)}}, \tag{4.5.29}$$

where $\overline{\Gamma}^{(1)}_{f,(g,\gamma)}$ was defined in Eq. 4.4.5. The large-m_t results can be converted to the decoupled hybrid renormalization scheme using

$$\overline{\Gamma}^{(1),(\ell)}_{f,(t)} = \Gamma^{(1)}_{f,(t)}\Big|_{P\to\overline{P}^{(\ell)}}, \tag{4.5.30}$$

where $\Gamma^{(1)}_{f,(t)}$ is found in Eq. 4.4.11. We can also apply this conversion to the four-fermion operator results in Section 4.4.3 by

$$\overline{\Gamma}^{(6,1),(\ell)}_{f,(4\mathrm{F})} = \Gamma^{(6,1)}_{f,(4\mathrm{F})}\Big|_{P\to\overline{P}^{(\ell)}}, \tag{4.5.31}$$

where $\Gamma^{(6,1)}_{f,(4\mathrm{F})}$ are found throughout Eqs. 4.4.27 to 4.4.30.

4.6 Numerical Results

The full analytic results of the calculations performed here are lengthy, and so are not reported analytically in this work, but can be found in electronic form in the computer files of the arXiv submissions on which this thesis is based [1, 2]. In this section we report the numerical results of the full NLO dimension-6 SMEFT decay rate in the decoupled hybrid renormalization scheme defined in Eq. 4.5.24 for $h \to f\bar{f}$ where $f \in \{b, c, \tau, \mu\}$. We report these results in the small-mass limit, $m_f \to 0$, while keeping leading order terms in m_f. We report results in this limit due to the decoupling constants in Eqs. 4.5.19 and 4.5.20 being defined in the small-mass limit, and therefore only completely cancel against the large tadpole corrections of the decay rate in this same limit. We note, however, that in the full mass dependent results with the decoupling constants defined according to Eqs. 4.5.19 and 4.5.20 that the large tadpole corrections mostly cancel, with the remaining uncanceled tadpoles being suppressed by powers of light-fermion masses and are numerically negligible. For the process $h \to b\bar{b}$ (the most massive final-state fermion pair), the numerical difference between the full mass dependent result and the small-mass limit result is small. Terms in the small-mass limit result that scale as m_b^2 are highly accurate, differing from the full-mass results by only around 0.6%. Terms in the small-mass limit result that scale as m_b (which correspond to operators with non-trivial MFV scalings proportional to the b-quark Yukawa, such as C_{bH}) are accurate within approximately $1\% - 3\%$. For the general process $h \to f\bar{f}$, the dominant

α_s	0.1	M_W	80.4 GeV
$\overline{e}^{(\ell)}(m_H)$	$\sqrt{4\pi/128}$	$\overline{m}_b^{(\ell)}(m_H)$	3.0 GeV
$\overline{v}^{(\ell)}(m_H)$	240 GeV	$\overline{m}_\tau^{(\ell)}(m_H)$	1.7 GeV
m_t	173 GeV	$\overline{m}_c^{(\ell)}(m_H)$	0.7 GeV
m_H	125 GeV	$\overline{m}_\mu^{(\ell)}(m_H)$	0.1 GeV
M_Z	91.2 GeV	–	–

Table 4.2: *Input parameters employed throughout the numerical analysis, where we have also listed the derived quantity $\overline{v}^{(\ell)}(m_H) \equiv 2M_W \hat{s}_w/\overline{e}^{(\ell)}(m_H)$ for convenience. The origins of these values can be found in the body of the text.*

corrections to this limit scale as m_f^2/M_W^2, so for processes producing less massive final-state fermions, the difference between the small-mass limit results and the full mass dependent results are even smaller.

In Section 4.6.1 we report the values at the default choice of $\mu = m_H$, and then perform a study of perturbative uncertainties due to scale variations in Section 4.6.2. The input parameters needed in these analyses are listed in Table 4.2.

4.6.1 Results at $\mu = m_H$

It is convenient to normalize all results to the LO decay rate at $\mu = m_H$, and therefore define the ratios

$$\Delta_f^{(i,j)}(\mu) \equiv \frac{\overline{\Gamma}^{(i,j),(\ell)}(\mu)}{\overline{\Gamma}_f^{(4,0),(\ell)}(m_H)}\,, \tag{4.6.1}$$

where in analogy with Eq. 4.1.2 the superscript (i,j) denotes the dimension-i contribution at jth order in perturbation theory. We extend such definitions to the complete LO and NLO corrections as

$$\begin{aligned}\Delta_f^{\rm LO}(\mu) &\equiv \Delta_f^{(4,0)}(\mu) + \Delta_f^{(6,0)}(\mu)\,,\\ \Delta_f^{\rm NLO}(\mu) &\equiv \Delta_f^{\rm LO}(\mu) + \Delta_f^{(4,1)}(\mu) + \Delta_f^{(6,1)}(\mu)\,.\end{aligned} \tag{4.6.2}$$

We also make use of the dimensionless Wilson coefficients defined in Eq. 4.4.19.

The input values used throughout this analysis are found in Table 4.2. For the on-shell masses, m_t, m_H, M_Z, and M_W, we take the PDG values listed in [23]. For $\alpha_s(m_H)$ we take the "world average" value of $\alpha_s(M_Z) = 0.11$ from [23] and use the result of Eq. 1.4.7 to run this value to $\mu = m_H$ where we find that within the accuracy

we provide this value does not change. For $\overline{\alpha}^{(\ell)}(m_H)$ we note that this is related to the effective on-shell coupling $\alpha(M_Z^2)$ introduced in Section 4.5.1 according to

$$\frac{\overline{\alpha}^{(\ell)}(M_Z^2)}{\alpha(M_Z^2)} = 1 + \frac{100\alpha}{27\pi}\,, \tag{4.6.3}$$

where $\alpha(M_Z^2) \approx 1/129$ and $\alpha \approx 1/137$ [23]. This allows us to recover a value for $\overline{\alpha}^{(\ell)}(M_Z^2)$ which we can then RG evolve to $\mu = m_H$. For $\overline{m}_b^{(\ell)}(m_H)$ we take the PDG value of $\overline{m}_b(\overline{m}_b) = 4.18$ GeV and use Eq. 1.4.17 to run this value to $\mu = m_H$. For $\overline{m}_c^{(\ell)}$ we do not take the PDG value as this quantity is reported at $\overline{m}_c(\overline{m}_c)$, a low enough scale that we risk inaccurate results trying to apply perturbatively calculated RG equations at a potentially non-perturbative scale. Instead we take the value in [101] of $\overline{m}_c(3\text{GeV}) = 0.986$, and again RG evolve this value to $\mu = m_H$ using Eq. 1.4.17. Finally, for $\overline{m}_\tau^{(\ell)}(m_H)$ and $\overline{m}_\mu^{(\ell)}(m_H)$ we take the on-shell PDG values of $m_\tau = 1.78$ GeV and $m_\mu = 0.106$ GeV and convert these to the QED×QCD $\overline{\text{MS}}$ scheme according to

$$\begin{aligned}
\overline{m}_\tau^{(\ell)}(m_\tau) &= m_\tau + \delta m_\tau^{\text{fin.}}(m_\tau)\Big|_{\text{QED}} = 1.77\,\text{GeV}\,,\\
\overline{m}_\mu^{(\ell)}(m_\tau) &= m_\mu + \delta m_\mu^{\text{fin.}}(m_\mu)\Big|_{\text{QED}} = 0.105\,\text{GeV}\,,
\end{aligned} \tag{4.6.4}$$

and then RG evolve these values in the same way as for $\overline{m}_b^{(\ell)}$ and $\overline{m}_c^{(\ell)}$ to $\mu = m_H$. Note that, unlike for the quark masses, we can RG evolve values of the lepton masses measured at arbitrarily low scales. This is because at NLO lepton masses receive only QED corrections, which are perturbative at low scales; see Section 1.4.

We now report the numerical values of the decay rates, suppressing the arguments of the $\overline{\text{MS}}$ renormalized quantities, $\overline{m}_f^{(\ell)}(m_H)$, $\overline{e}^{(\ell)}(m_H)$ and $\tilde{C}_i(m_H)$.[1] We find the LO result

$$\Delta_f^{\text{LO}}(m_H) = 1 + \frac{(\overline{v}^{(\ell)})^2}{\Lambda_{\text{NP}}^2}\left[3.74\tilde{C}_{HWB} + 2.00\tilde{C}_{H\Box} - 1.41\frac{\overline{v}^{(\ell)}}{\overline{m}_f^{(\ell)}}\tilde{C}_{fH} + 1.24\tilde{C}_{HD}\right]. \tag{4.6.5}$$

Firstly we note that the result in Eq. 4.6.5 applies to all processes considered here (and also for all massive fermions of the SM, except the top quark) with the simple replacement of f with the fermion flavor of choice. We find in Eq. 4.6.5 (as we also saw in Eqs. 4.4.20 and 4.4.21) that the contribution from $\tilde{C}_{fH}$ is enhanced by a factor of $\overline{v}^{(\ell)}/\overline{m}_f^{(\ell)}$ compared to the other contributions, which we choose to factor out symbolically. We do this to highlight that this contribution to the decay rate scales as m_f rather than as m_f^2 as in the SM, and so that the numerical factor

[1] We also suppress the argument of the derived quantity $\overline{v}^{(\ell)}(m_H)$.

multiplying this Wilson coefficient is finite in the limit $m_f \to 0$. In a theory that respects MFV, this enhancement factor would be compensated for by an implicit scaling of the Wilson coefficient itself (which for this particular example can be seen from Eq. 2.2.11) such that the overall contribution scales as m_f^2. While we do not necessarily advocate MFV, we choose to write our results in such a way that they are free from large numerical factors multiplying dimension-6 Wilson coefficients. At NLO this effect additionally affects a number of coefficients. For the class-6 coefficients $C_{f(B,W)}$ and C_{fG} we also factor out $1/\overline{e}^{(\ell)}$ and $1/g_3$ respectively. This is because in these operators, gauge bosons couple through the field strength tensor rather than through covariant derivatives, so separating these factors ensures that the numerical prefactors to these Wilson coefficients scale with the same powers of $\overline{\alpha}^{(\ell)}$ and α_s as in the SM.

The NLO corrections depend on the fermion flavor, f, therefore all results cannot be reported in a single equation, like for the LO results in Eq. 4.6.5. For $f = b$ we find

$$\begin{aligned}
\Delta_b^{\rm NLO}(m_H) = 1.13 + \frac{(\bar{v}^{(\ell)})^2}{\Lambda_{\rm NP}^2}\Bigg\{ & 4.16\tilde{C}_{HWB} + 2.75\tilde{C}_{HG} + 2.40\tilde{C}_{H\Box} - 1.73\frac{\bar{v}^{(\ell)}}{\overline{m}_b^{(\ell)}}\tilde{C}_{bH} \\
& + 1.33\tilde{C}_{HD} - 0.12\tilde{C}^{(3)}_{\substack{Hq\\33}} + \Bigg[- 7.9\tilde{C}_{Ht} + 5.8\tilde{C}^{(1)}_{\substack{Hq\\33}} + 4.4\frac{m_t}{\overline{m}_b^{(\ell)}}\tilde{C}^{(1)}_{\substack{quqd\\3333}} - 3.1\tilde{C}_{tH} \\
& + 2.7\tilde{C}_{HW} + 2.4\tilde{C}_H + 2.0\frac{\overline{m}_c^{(\ell)}}{\overline{m}_b^{(\ell)}}\tilde{C}^{(1)}_{\substack{quqd\\2233}} - 1.9\frac{\bar{v}^{(\ell)}}{\overline{e}^{(\ell)}\,\overline{m}_b^{(\ell)}}\tilde{C}_{bW} - 1.3\Bigg(\tilde{C}^{(8)}_{\substack{qd\\3333}} \\
& + \frac{\overline{m}_s^{(\ell)}}{\overline{m}_b^{(\ell)}}\tilde{C}^{(8)}_{\substack{qd\\2332}}\Bigg) - 1.3\frac{\tilde{C}_{tW}}{\overline{e}^{(\ell)}} - 1.0\Bigg(\tilde{C}^{(1)}_{\substack{qd\\3333}} + \frac{\overline{m}_s^{(\ell)}}{\overline{m}_b^{(\ell)}}\tilde{C}^{(1)}_{\substack{qd\\2332}}\Bigg)\Bigg] \times 10^{-2} + \Bigg[- 9\Bigg(\frac{\tilde{C}_{tB}}{\overline{e}^{(\ell)}} \\
& + \tilde{C}^{(3)}_{\substack{Hq\\22}} + \tilde{C}^{(3)}_{\substack{Hq\\11}} - \tilde{C}_{HB} + \tilde{C}_{Hu} + \tilde{C}_{Hc}\Bigg) + 8\frac{\bar{v}^{(\ell)}}{g_3\overline{m}_b^{(\ell)}}\tilde{C}_{bG} + 8\frac{m_t}{\overline{m}_b^{(\ell)}}\tilde{C}^{(8)}_{\substack{quqd\\3333}} \\
& + 7\Bigg(\frac{\overline{m}_\tau^{(\ell)}}{\overline{m}_b^{(\ell)}}\tilde{C}_{\substack{ledq\\3333}} + \frac{\overline{m}_\mu^{(\ell)}}{\overline{m}_b^{(\ell)}}\tilde{C}_{\substack{ledq\\2233}}\Bigg) - 7\tilde{C}_W + 4\Bigg(\tilde{C}^{(1)}_{\substack{Hl\\33}} + \tilde{C}^{(1)}_{\substack{Hl\\22}} - \tilde{C}^{(1)}_{\substack{Hq\\22}} + \tilde{C}^{(1)}_{\substack{Hl\\11}} - \tilde{C}^{(1)}_{\substack{Hq\\11}} \\
& + \tilde{C}_{H\tau} + \tilde{C}_{H\mu} + \tilde{C}_{He} + \tilde{C}_{Hs} + \tilde{C}_{Hd} - \frac{\bar{v}^{(\ell)}}{\overline{m}_b^{(\ell)}}\tilde{C}_{Htb} + 4\frac{\overline{m}_c^{(\ell)}}{\overline{m}_b^{(\ell)}}\tilde{C}^{(8)}_{\substack{quqd\\3223}}\Bigg) - 3\Bigg(\tilde{C}^{(3)}_{\substack{Hl\\33}} \\
& + \tilde{C}^{(3)}_{\substack{Hl\\22}} + \tilde{C}^{(3)}_{\substack{Hl\\11}} - \frac{\overline{m}_c^{(\ell)}}{\overline{m}_b^{(\ell)}}\tilde{C}^{(1)}_{\substack{quqd\\3223}}\Bigg) + 2\tilde{C}_{Hb}\Bigg] \times 10^{-3} - 4\times 10^{-5}\frac{\bar{v}^{(\ell)}}{\overline{e}^{(\ell)}\,\overline{m}_b^{(\ell)}}\tilde{C}_{bB}\Bigg\}.
\end{aligned} \tag{4.6.6}$$

While the (in general) unknown size of the Wilson coefficients means we can't know the exact size of each contribution we can make some general statements. Firstly, with $\overline{v}^{(\ell)}/\overline{m}_b^{(\ell)} \approx 80$ we see that by far the coefficients potentially offering the largest contributions are from those that carry a non-trivial scaling with $\overline{m}_b^{(\ell)}$ in MFV. Higgs decays therefore offer an interesting test of MFV, a topic which we will explore further

in Section 4.7. This aside, we see from Eq. 4.6.6 that by far the next largest NLO contribution is from the operator Q_{HG}. This operator contributes QCD corrections seen in Eq. 4.4.5 and is enhanced by the double logarithm of the small ratio $\overline{m}_b^{(\ell)}/m_H$, as described in Section 4.5.1. For operators not appearing at LO, only $\tilde{C}^{(1)}_{\substack{Hq\\33}}$, $\tilde{C}^{(3)}_{\substack{Hq\\33}}$ and $\tilde{C}_{Ht}$ contribute at the $\mathcal{O}(10\%)$ level,[1] primarily due to these operators permitting the large-m_t corrections seen throughout Section 4.4.2, which scale as $m_t^2/(\overline{v}^{(\ell)})^2$. There are 19 operators that contribute at the greater than 1% level, 15 of which first appear at NLO. In total, there are 44 new operators that first contribute at NLO.

For $f = c$ we have

$$\begin{aligned}
\Delta_c^{\rm NLO}(m_H) = 1.16 + \frac{(\overline{v}^{(\ell)})^2}{\Lambda_{\rm NP}^2}\Bigg\{ & 4.95\tilde{C}_{HG} + 4.31\tilde{C}_{HWB} + 2.46\tilde{C}_{H\Box} - 1.75\frac{\overline{v}^{(\ell)}}{\overline{m}_c^{(\ell)}}\tilde{C}_{cH} \\
& + 1.41\tilde{C}_{HD} + \Bigg[9.4\tilde{C}_{HB} - 8.9\tilde{C}^{(3)}_{\substack{Hq\\33}} - 7.9\tilde{C}_{Ht} - 6.3\frac{m_t}{\overline{m}_c^{(\ell)}}\tilde{C}^{(8)}_{\substack{qu\\2332}} + 5.4\tilde{C}_{HW} \\
& + 5.2\tilde{C}^{(1)}_{\substack{Hq\\33}} - 4.8\frac{m_t}{\overline{m}_c^{(\ell)}}\tilde{C}^{(1)}_{\substack{qu\\2332}} - 4.6\tilde{C}_{tH} + 2.4\tilde{C}_H + 2.4\frac{\overline{m}_s^{(\ell)}}{\overline{m}_c^{(\ell)}}\tilde{C}^{(1)}_{\substack{quqd\\2222}} + 2.0\frac{\overline{m}_b^{(\ell)}}{\overline{m}_c^{(\ell)}}\tilde{C}^{(1)}_{\substack{quqd\\2233}} \\
& - 1.3\tilde{C}^{(8)}_{\substack{qu\\2222}} - 1.0\tilde{C}^{(1)}_{\substack{qu\\2222}} + 1.0\tilde{C}^{(3)}_{\substack{Hq\\22}} - 1.0\tilde{C}^{(1)}_{\substack{Hq\\22}}\Bigg] \times 10^{-2} + \Bigg[-9\Bigg(\frac{\tilde{C}_{tB}}{\overline{e}^{(\ell)}} + \tilde{C}^{(3)}_{\substack{Hq\\11}} \\
& + \tilde{C}_{Hu}\Bigg) + 8\frac{\overline{v}^{(\ell)}}{\overline{m}_c^{(\ell)}}\frac{\tilde{C}_{cG}}{g_3} - 7\frac{\overline{m}_\tau^{(\ell)}}{\overline{m}_c^{(\ell)}}\tilde{C}^{(1)}_{\substack{lequ\\3322}} - 7\frac{\overline{m}_\mu^{(\ell)}}{\overline{m}_c^{(\ell)}}\tilde{C}^{(1)}_{\substack{lequ\\2222}} - 7\tilde{C}_W - 5\tilde{C}_{Hc} \\
& + 4\Bigg(\frac{\overline{m}_b^{(\ell)}}{\overline{m}_c^{(\ell)}}\tilde{C}^{(8)}_{\substack{quqd\\3223}} + \frac{\overline{m}_s^{(\ell)}}{\overline{m}_c^{(\ell)}}\tilde{C}^{(8)}_{\substack{quqd\\2222}} + \tilde{C}^{(1)}_{\substack{Hl\\11}} + \tilde{C}^{(1)}_{\substack{Hl\\22}} + \tilde{C}^{(1)}_{\substack{Hl\\33}} - \tilde{C}^{(1)}_{\substack{Hq\\11}} + \tilde{C}_{He} + \tilde{C}_{H\mu} + \tilde{C}_{H\tau} \\
& + \tilde{C}_{Hd} + \tilde{C}_{Hs} + \tilde{C}_{Hb}\Bigg) - 3\Bigg(-\frac{\overline{m}_b^{(\ell)}}{\overline{m}_c^{(\ell)}}\tilde{C}^{(1)}_{\substack{quqd\\3223}} + \tilde{C}^{(3)}_{\substack{Hl\\11}} + \tilde{C}^{(3)}_{\substack{Hl\\22}} + \tilde{C}^{(3)}_{\substack{Hl\\33}}\Bigg) + 2\frac{\tilde{C}_{tW}}{\overline{e}^{(\ell)}} \\
& + \frac{\overline{v}^{(\ell)}}{\overline{m}_c^{(\ell)}}\frac{\tilde{C}_{cW}}{\overline{e}^{(\ell)}}\Bigg] \times 10^{-3} + (2\times 10^{-4})\frac{\overline{v}^{(\ell)}}{\overline{m}_c^{(\ell)}}\frac{\tilde{C}_{cB}}{\overline{e}}\Bigg\}. \qquad (4.6.7)
\end{aligned}$$

The results in Eq. 4.6.7 broadly follow that which was seen in Eq. 4.6.6. Again, we find that the operator Q_{HG} generates the largest NLO contribution from operators with trivial MFV scalings in $\overline{m}_c^{(\ell)}$. This is again due primarily to the double logarithm seen in Eq. 4.4.5 of the small ratio $\overline{m}_c^{(\ell)}/m_H$ from QCD corrections. With this ratio being even smaller than the corresponding ratio in the $h \to b\bar{b}$ results in Eq. 4.6.7, we now see that the NLO contribution from Q_{HG} is larger even than the contributions from Wilson coefficients that first appear at LO. The analogous QED double logarithm is also correspondingly larger such that the operators generating this logarithm, Q_{HWB}, Q_{HB}, and Q_{HW} now all contribute at the $\mathcal{O}(10\%)$ level, unlike in the $h \to b\bar{b}$ case.

[1] By $\mathcal{O}(10\%)$ corrections we mean in units of $(\overline{v}^{(\ell)})^2/\Lambda_{\rm NP}^2$. For the remainder of this work we will not specify this explicitly.

In this case we also have 20 Wilson coefficients contributing at the greater than 1% level, with 16 of these first appearing at NLO, and 43 new Wilson coefficients appearing at NLO.

For $f = \tau$ we have

$$\begin{aligned}\Delta_\tau^{\rm NLO}(m_H) = 0.98 + \frac{(\overline{v}^{(\ell)})^2}{\Lambda_{\rm NP}^2}\Bigg\{ & 3.63\tilde{C}_{HWB} + 2.11\tilde{C}_{H\Box} - 1.50\frac{\overline{v}^{(\ell)}}{\overline{m}_\tau^{(\ell)}}\tilde{C}_{\tau H} + 1.20\tilde{C}_{HD} \\ & + 0.16\tilde{C}_{HB} + \Bigg[- 9.0\tilde{C}^{(3)}_{\substack{Hq \\ 33}} - 7.9\tilde{C}_{Ht} + 6.8\tilde{C}_{HW} + 5.2\tilde{C}^{(1)}_{\substack{Hq \\ 33}} - 4.6\tilde{C}_{tH} \\ & - 3.8\frac{m_t}{\overline{m}_\tau^{(\ell)}}\tilde{C}^{(1)}_{\substack{lequ \\ 3333}} + 2.4\tilde{C}_H + 2.0\left(\frac{\overline{m}_b^{(\ell)}}{\overline{m}_\tau^{(\ell)}}\tilde{C}_{\substack{ledq \\ 3333}} - \frac{\overline{m}_c^{(\ell)}}{\overline{m}_\tau^{(\ell)}}\tilde{C}^{(1)}_{\substack{lequ \\ 3322}} + \frac{\overline{m}_s^{(\ell)}}{\overline{m}_\tau^{(\ell)}}\tilde{C}_{\substack{ledq \\ 3322}}\right) \\ & + 1.5\tilde{C}^{(3)}_{\substack{Hl \\ 33}} - 1.0\left(\tilde{C}_{\substack{le \\ 3333}} + \frac{\overline{m}_\mu^{(\ell)}}{\overline{m}_\tau^{(\ell)}}\tilde{C}_{\substack{le \\ 2332}}\right)\Bigg] \times 10^{-2} + \Bigg[- 9\left(\frac{\tilde{C}_{tB}}{\overline{e}^{(\ell)}} + \tilde{C}^{(3)}_{\substack{Hq \\ 11}} + \tilde{C}^{(3)}_{\substack{Hq \\ 22}}\right. \\ & \left. - \tilde{C}^{(1)}_{\substack{Hl \\ 33}} + \tilde{C}_{Hu} + \tilde{C}_{Hc}\right) - 7\tilde{C}_W + 4\left(\tilde{C}^{(1)}_{\substack{Hl \\ 11}} + \tilde{C}^{(1)}_{\substack{Hl \\ 22}} + \tilde{C}_{He} + \tilde{C}_{H\mu} - \tilde{C}^{(1)}_{\substack{Hq \\ 11}} - \tilde{C}^{(1)}_{\substack{Hq \\ 22}}\right. \\ & \left. + \tilde{C}_{Hd} + \tilde{C}_{Hs} + \tilde{C}_{Hb}\right) - 3\left(\tilde{C}^{(3)}_{\substack{Hl \\ 11}} + \tilde{C}^{(3)}_{\substack{Hq \\ 22}}\right) + 2\frac{\tilde{C}_{tW}}{\overline{e}^{(\ell)}} + \frac{\overline{v}^{(\ell)}}{\overline{m}_\tau^{(\ell)}}\frac{\tilde{C}_{\tau W}}{\overline{e}^{(\ell)}}\Bigg] \times 10^{-3} \\ & + (4 \times 10^{-4})\left(\tilde{C}_{H\tau} - \frac{\overline{v}^{(\ell)}}{\overline{m}_\tau^{(\ell)}}\frac{\tilde{C}_{\tau B}}{\overline{e}^{(\ell)}}\right)\Bigg\}. \end{aligned} \tag{4.6.8}$$

Without QCD, the corrections to $h \to \tau\bar{\tau}$ in Eq. 4.6.8 are generally milder, the largest of which (aside from operators with non-trivial MFV scalings in $\overline{m}_\tau^{(\ell)}$) being generated by Q_{HB}. This is again due to the double logarithm in Eq. 4.4.5, this time of the ratio $\overline{m}_\tau^{(\ell)}/m_H$. Here, there are fewer operators contributing at the greater than 1% level (in this case 18) compared to both $h \to b\bar{b}$ and $h \to c\bar{c}$, and 36 operators contribute for the first time at NLO.

The results for $f = \mu$ are very similar to those for $f = \tau$. For this reason, while the results for $h \to \mu\bar{\mu}$ will form an important part of Section 4.7, they do little to serve the forthcoming discussion of the above results, and so we relegate the numerical results for $h \to \mu\bar{\mu}$ to Appendix D.1. The only feature we point out is that the QED double logarithm is now in the ratio $\overline{m}_\mu^{(\ell)}/m_H$. As $\overline{m}_\mu^{(\ell)}$ is the smallest final-state mass in Table 4.2, it correspondingly produces the largest QED NLO corrections to the LO decay rate from the Wilson coefficients contributing to this double logarithmic term. This changes the numerical coefficients to $\tilde{C}_{HWB}$, $\tilde{C}_{HW}$ and $\tilde{C}_{HB}$ to 3.49, 0.14 and 0.41 respectively.

Considering this set of results generally, besides operators with non-trivial MFV scalings in $\overline{m}_f^{(\ell)}$, an operator generally only gives a significant contribution to the decay rate if involves QCD or large-m_t corrections. To illustrate the relative importance

$h \to b\bar{b}$	SM	$\tilde{C}_{HWB}$	$\tilde{C}_{H\Box}$	$\frac{\overline{v}^{(\ell)}}{\overline{m}_f^{(\ell)}}\tilde{C}_{fH}$	$\tilde{C}_{HD}$
NLO QED-QCD	18.2%	17.9 %	18.2%	18.2%	18.2%
NLO large-m_t	-3.1%	-4.6%	3.2%	3.3%	-9.0%
NLO remainder	-2.2%	-1.9%	-1.2%	0.6%	-2.0%
NLO correction	12.9%	11.3%	20.2%	22.3%	7.1%
$h \to c\bar{c}$					
NLO QED-QCD	18.5%	17.0 %	18.5%	18.5%	18.5%
NLO large-m_t	-1.1%	-0.7%	5.1%	4.4%	-4.4%
NLO remainder	-1.7%	-1.0%	-0.7%	0.9%	-0.8 %
NLO correction	15.7%	15.3 %	22.9 %	23.8%	13.3%
$h \to \tau\bar{\tau}$					
NLO QED	1.1%	-1.3 %	1.1%	1.1%	1.1%
NLO large-m_t	-1.1%	-0.7%	5.1%	4.4%	-4.4%
NLO remainder	-1.7%	-0.9%	-0.7%	0.8%	-0.6%
NLO correction	-1.7%	-2.9%	5.5%	6.3%	-3.9%

Table 4.3: *Size of NLO corrections to different terms in LO decay rate, split into QED(-QCD), large-m_t, and remainder corrections define in Eq. 4.1.3 for $h \to b\bar{b}$ (top), $h \to c\bar{c}$ (middle) and $h \to \tau\bar{\tau}$ (bottom). Equivalent results for $h \to \mu\bar{\mu}$ are found in Table D.1 in Appendix D.1. Weak corrections, defined in Eq. 4.1.3 are the sum of the large-m_t and remainder corrections.*

of these two effects we show in Table 4.3 the contributions of these two subsets of corrections to the corresponding contributions to the LO decay rate, as well as the contribution of the remaining corrections, according to the split defined in Eq. 4.1.3. Specifically, for the dimension-6 operators, the numbers in Table 4.3 show the NLO correction from $\tilde{C}_i$ to $\overline{\Gamma}_f^{(1),(\ell)}$ divided by its contribution to $\overline{\Gamma}_f^{(0),(\ell)}$.

There are two interesting effects to highlight in Table 4.3 which apply to all processes considered here. Firstly, we see that, aside from C_{HWB}, the QED-QCD corrections are of the same size for all Wilson coefficients appearing in the LO decay rate. This is a result of the cross terms of the LO SMEFT amplitude and NLO QED-QCD SM amplitude, and the fact that in QED-QCD these coefficients only contribute to the hff vertex in the "SM-like" diagrams seen in Diagrams (v1,r1-3) of Figs. C.1 and C.2. The result of these two effects can be seen in Eq. 4.4.5 where the LO SMEFT decay rate multiplies the NLO SM QED-QCD decay rate, leading to the pattern seen in Table 4.3. Conversely, C_{HWB} also contributes to Diagrams (v4-6,r4-5) of Fig. C.1, giving additional contributions and this explaining why it does not fit the trend seen for the other Wilson coefficients appearing at LO. We also observe that there is a distinct lack of correlation for the large-m_t corrections in Table 4.3, with the corrections for each coefficient varying both in size and magnitude. There

are two sources for this lack of correlation. Firstly, considering the form of the LO SMEFT result in Eq. 4.2.5, we see that each Wilson coefficient is multiplied by a unique prefactor, each of which is some function of $\hat{c}_w$, $\hat{s}_w$, and $\hat{v}_T$, which get NLO corrections of various sizes and magnitudes. For example, in Feynman gauge and ignoring tadpoles (which as discussed in Section 4.3.5 cancel in the NLO decay rate) we find these terms get finite large-m_t corrections in the SM given by[1]

$$\begin{aligned}
\hat{s}_w &\to \hat{s}_w + \delta\hat{s}^{(4)}_{w,(t)} = \hat{s}_w(1 - 0.020)\,, \\
\hat{c}_w &\to \hat{c}_w + \delta\hat{c}^{(4)}_{w,(t)} = \hat{c}_w(1 + 0.0057)\,, \\
\hat{v}_T &\to \hat{v}_T + \delta\hat{v}^{(4)}_{T,(t)} = \hat{v}_T(1 - 0.028)\,,
\end{aligned} \tag{4.6.9}$$

where $\delta X^{(4)}_{(t)}$ are the finite large-m_t NLO corrections to X in the SM. The second source producing a lack of correlation of the large-m_t results is from the fact that, unlike the QED-QCD case, each of the Wilson coefficients appearing at LO do not enter a shared set of NLO diagrams. For example, of the Wilson coefficients appearing at LO, Diagram (sf1) of Fig. C.4 gets contributions from only C_{HWB} and C_{HD}. Together, these two effects account for the lack of correlation found in the large-m_t results of Table 4.3.

For Higgs decay to quark pairs, we see that while QCD effects are dominant, the large-m_t corrections are non-negligible and in some cases even the remaining corrections are not necessarily negligible, and have a strong dependence on the Wilson coefficient. Therefore, for Higgs decay to quark pairs, approximating the NLO corrections in the dimension-6 SMEFT by multiplying the tree-level result by a universal K-factor derived from the SM QCD corrections would be a poor estimate of the full calculation performed here. Furthermore, while it is true that the large-m_t corrections generally make up the bulk of the EW corrections, in some cases the remainder corrections are larger than the large-m_t ones.

For Higgs decay to leptons, in the absence of QCD corrections we see that the large-m_t corrections are generally the most significant, although there is again a strong Wilson coefficient dependence on this. In terms of the size of their relative correction to the NLO decay rate, Table 4.3 shows that the EW remainder corrections are more important for Higgs decay to leptons than for Higgs decay to quarks. For example, considering $\tilde{C}_{HWB}$, the EW remainder corrections to $h \to b\bar{b}$ constitute -17% of the overall correction for $h \to b\bar{b}$, but $+31\%$ to the overall correction for $h \to \tau\bar{\tau}$.

The conclusions we can draw from this are, firstly, for Higgs decay to quarks it is not enough to only calculate the QED-QCD corrections to obtain accurate predictions,

[1] Note that, as discussed in Section 4.3.5, when ignoring tadpole contributions the results in Eq. 4.6.9 are gauge dependent.

and in many cases the addition of large-m_t corrections are not sufficient. As we do not know a priori which Wilson coefficients in particular will be most affected by this previous statement, we believe it is therefore necessary to calculate the full set of strong and EW corrections to obtain accurate results. For Higgs decay to lepton pairs, despite the overall corrections being milder, the remainder corrections constitute a larger contribution to the NLO corrections as a whole, and so the necessity of calculating the full set of corrections is only amplified.

4.6.2 Scale Uncertainties

From our analyses thus far, there are two obvious questions to address: can the size of the NLO corrections be reliably estimated through the scale variations of the LO result, and what is the residual uncertainty beyond NLO? In this section we address these questions through studies involving the variation of the unphysical renormalization scale, μ.

Typically in perturbation theory these questions are addressed by considering varying the unphysical renormalization scale, μ, up and down by a factor of two, and considering the change in the decay rate to be a measure of the uncertainty due to uncalculated, higher order corrections. While in the SM most parameters are measured with a high degree of precision, in the dimension-6 SMEFT the study of measurements of Wilson coefficients are still in their infancy, and as such, most Wilson coefficients are not measured with a high precision. Consequently, we give the results of this section as a function of the Wilson coefficients measured at a fixed scale, which we choose to be $\mu = m_H$. We therefore need to relate the Wilson coefficients at some scale, $C_i(\mu)$, to those at $C_i(m_H)$. This is achieved with the RG equations for the dimension-6 SMEFT Wilson coefficients in [63, 130, 131]. In this section we make use of the electronic implementation of the anomalous dimensions in `DsixTools` [135].

For the analysis performed here, we must make use of the RG equations for all $\overline{\text{MS}}$ renormalized parameters in this calculation, these being the light-fermion masses, $\overline{m}_f^{(\ell)}$, the electromagnetic fine-structure constant, $\overline{\alpha}^{(\ell)}$, the Wilson coefficients, C_i, and the strong coupling constant, α_s, which although is not renormalized in this calculation, has no on-shell definition and thus also varies with renormalization scale. We can simplify the analysis here by taking advantage of the fact that when varying the unphysical renormalization scale, μ, by factors of 2 we have $\mu \sim m_H$ and so we may use fixed-order results for the RG equations, rather than the exact results in Eqs. 1.4.7, 1.4.12 and 1.4.17. The anomalous dimensions for the dimension-6 SMEFT Wilson coefficients are known only to the one-loop level, and so we also

use only the one-loop results for the running of the necessary SM parameters. The solutions of the RG equations to NLO at fixed order are

$$\begin{aligned} C_i(\mu_C) &= C_i(m_H) + \ln\left(\frac{\mu_C}{m_H}\right)\dot{C}_i(m_H)\,, \\ \overline{m}_f^{(\ell)}(\mu_R) &= \overline{m}_f^{(\ell)}(m_H)\left[1+\gamma_f(m_H)\ln\left(\frac{\mu_R}{m_H}\right)\right], \\ \overline{\alpha}^{(\ell)}(\mu_R) &= \overline{\alpha}^{(\ell)}(m_H)\left[1+2\gamma_e(m_H)\ln\left(\frac{\mu_R}{m_H}\right)\right], \\ \alpha_s(\mu_R) &= \alpha_s(m_H)\left[1-2\gamma_g(m_H)\ln\left(\frac{\mu_R}{m_H}\right)\right], \end{aligned} \tag{4.6.10}$$

where γ_e and γ_f were reported in Eq. 4.5.8 and the form of γ_g may be deduced from the relations in Eqs. 1.4.11 and 1.4.12 and is

$$\gamma_g(\mu_R) = \frac{\alpha_s(\mu_R)}{4\pi}\left(\frac{11}{3}N_c - \frac{2}{3}n_l\right), \tag{4.6.11}$$

where again, n_l is the number of light quarks, i.e. those with mass approximately less than the scale under consideration, which for our purposes is $n_l = 5$.

We have written Eq. 4.6.10 in such a way as to emphasize that we may have different renormalization scales, μ_C and μ_R, for the Wilson coefficients and SM parameters, respectively. In fact, we could introduce a separate renormalization scale for each $\overline{\text{MS}}$ parameter, but that option is not explored here. Until this point we have used $\mu = \mu_C = \mu_R$, but in our scale variation analysis it will be informative to separate these scales and vary them independently. In the SM, the absence of Wilson coefficients results in all renormalization scales being $\mu = \mu_R$. For the LO SMEFT result it is simple to construct the dependence on μ_R and μ_C by simply making all SM parameters a function of μ_R and all Wilson coefficients a function of μ_C

$$\overline{\Gamma}_f^{(6,0),(\ell)}(\mu_R,\mu_C) = \overline{\Gamma}_\ell^{(6,0),(\ell)}(\mu_C)\Big|_{\overline{p}(\mu_C)\to\overline{p}(\mu_R)}, \tag{4.6.12}$$

where $\overline{p}(\mu) \in \{\overline{\alpha}^{(\ell)}(\mu),\, \overline{m}_f^{(\ell)}(\mu),\, \alpha_s(\mu)\}$ are the $\overline{\text{MS}}$ renormalized parameters appearing in the calculation and where we have defined $\overline{\Gamma}_f^{(6,i),(\ell)}(\mu) \equiv \overline{\Gamma}_f^{(6,i),(\ell)}(\mu,\mu)$. For the NLO SMEFT results however, the calculation of loop integrals introduces additional μ terms, where it is not immediately obvious if these μ are μ_R or μ_C. Fortunately we can reconstruct this dependence. We can write our NLO SMEFT results with the correct dependence on these two scales generically as

$$\overline{\Gamma}_f^{(6,1),(\ell)}(\mu_R,\mu_C) = A(\mu_R,\mu_C)\ln(\mu_R) + B(\mu_R,\mu_C)\ln(\mu_C) + C(\mu_R,\mu_C)\,, \tag{4.6.13}$$

where A, B, and C are some generic functions of the parameters of the calculation. Setting all scales in the NLO SMEFT result to μ_C in Eq. 4.6.13 this expression takes the form

$$\overline{\Gamma}_f^{(6,1),(\ell)}(\mu_C) = \Big[A(\mu_C,\mu_C) + B(\mu_C,\mu_C)\Big]\ln(\mu_C) + C(\mu_C,\mu_C)\,. \tag{4.6.14}$$

We see that we can restore the explicit μ_R dependence in Eq. 4.6.14 by subtracting out the the $A(\mu_C,\mu_C)$ piece, and adding it back in with the correct μ_R dependence

$$\overline{\Gamma}_f^{(6,1),(\ell)}(\mu_R,\mu_C) = \Bigg\{\overline{\Gamma}_f^{(6,1),(\ell)}(\mu_C) - A(\mu_C,\mu_C)\left[\ln\left(\frac{\mu_C}{m_H}\right) - \ln\left(\frac{\mu_R}{m_H}\right)\right]\Bigg\}\Bigg|_{\overline{p}(\mu_C)\to\overline{p}(\mu_R)}\,. \tag{4.6.15}$$

We can construct the form of $A(\mu_R,\mu_C)$ by taking advantage of observable invariance, discussed in Section 1.4.3. Using that our LO+NLO decay rate should be independent of both renormalization scales, μ_C and μ_R, up to terms of NNLO and higher we may write (ignoring SM terms)

$$\frac{d}{d\ln(\mu_R)}\overline{\Gamma}_f^{(6,0),(\ell)}(\mu_R,\mu_C) + \frac{d}{d\ln(\mu_R)}\overline{\Gamma}_f^{(6,1),(\ell)}(\mu_R,\mu_C) = 0\,, \tag{4.6.16}$$

which, keeping only NLO terms, gives

$$A(\mu_R,\mu_C) = -\frac{d}{d\ln(\mu_R)}\overline{\Gamma}_f^{(6,0),(\ell)}(\mu_R,\mu_C)\,. \tag{4.6.17}$$

Using the expressions in Eq. 4.5.7 and the LO SMEFT result in Eq. 4.2.5 it is simple to calculate the form of $A(\mu_R,\mu_C)$. Therefore, from Eq. 4.6.15 we find the NLO SMEFT results is a function of the two scales, μ_C and μ_R, according to

$$\overline{\Gamma}_f^{(6,1),(\ell)}(\mu_R,\mu_C) = \Bigg\{\overline{\Gamma}_f^{(6,1),(\ell)}(\mu_C) + 2\left[\ln\left(\frac{\mu_C}{m_H}\right) - \ln\left(\frac{\mu_R}{m_H}\right)\right]\Bigg(\gamma_f(\mu_C)\overline{\Gamma}_f^{(6,0),(\ell)}(\mu_C) + \frac{C_{fH}(\mu_C)}{\sqrt{2}}\frac{(\overline{v}^{(\ell)}(\mu_C))^3}{\overline{m}_f^{(\ell)}(\mu_C)}\overline{\Gamma}_f^{(4,0),(\ell)}(\mu_C)\big[\gamma_f(\mu_C)+\gamma_e(\mu_C)\big]\Bigg)\Bigg\}\Bigg|_{\overline{p}(\mu_C)\to\overline{p}(\mu_R)}\,. \tag{4.6.18}$$

There are many methods we might apply to obtain estimates for the residual uncertainties, some of which are discussed at the end of this section. In the method adopted here we vary one scale, for example μ_C, up and down about its default value of m_H by a factor of 2 while holding the the other scale fixed at $\mu_R = m_H$. We then vary μ_R up and down by a factor of 2 while holding μ_C fixed. For the upper uncertainty we add the maximum of the results of the procedure just outlined in

quadrature, while for the lower uncertainty we add the minimum of the results of this procedure in quadrature. In summary, writing the decay rate including uncertainty bands as $\Gamma_f^{(i,j)+\delta_+^{(i,j)}}_{-\delta_-^{(i,j)}}$, we can obtain the values of these upper and lower uncertainty limits by first defining

$$D_f^{(i,j)}(\mu_R, \mu_C) = \Gamma_f^{(i,j)}(\mu_C, \mu_R) - \Gamma_f^{(i,j)}(m_H)\,, \tag{4.6.19}$$

such that $\delta_\pm^{(i,j)}$ are given by

$$\begin{aligned}
\delta_+^{(i,j)} = \Bigg\{ &\left[\max\left(D_f^{(i,j)}\left(\frac{m_H}{2}, m_H\right),\, D_f^{(i,j)}\left(2m_H, m_H\right),\, 0\right)\right]^2 \\
&+ \left[\max\left(D_f^{(i,j)}\left(m_H, \frac{m_H}{2}\right),\, D_f^{(i,j)}\left(m_H, 2m_H\right),\, 0\right)\right]^2 \Bigg\}^{\frac{1}{2}}, \\
\delta_-^{(i,j)} = \Bigg\{ &\left[\min\left(D_f^{(i,j)}\left(\frac{m_H}{2}, m_H\right),\, D_f^{(i,j)}\left(2m_H, m_H\right),\, 0\right)\right]^2 \\
&+ \left[\min\left(D_f^{(i,j)}\left(m_H, \frac{m_H}{2}\right),\, D_f^{(i,j)}\left(m_H, 2m_H\right),\, 0\right)\right]^2 \Bigg\}^{\frac{1}{2}},
\end{aligned} \tag{4.6.20}$$

where the max and min functions return the largest and smallest value of their arguments respectively. Each of these functions also carries 0 as an argument; this allows us to avoid scenarios in which, for example, the scale variations only serve to reduce the size of the decay rate such that the max functions simply pick out the least negative result of these variations which then erroneously result in a non-zero upper uncertainty.

We write the results of this analysis similarly to the form of the results found in Section 4.6.1, that is, making use of the expressions in Eq. 4.6.2 to give the upper and lower uncertainty bands normalized to the SM LO result. In this way we may define $\Delta_f(\mu_R, \mu_C)$ in analogy with Eq. 4.6.18. We report the results for each process considered here separately. For $f = b$ we find the LO uncertainties

$$\begin{aligned}
\Delta_b^{\rm LO}(m_H, m_H) = (1 \pm 0.08) + \frac{(\bar{v}^{(\ell)})^2}{\Lambda_{\rm NP}^2}\Bigg\{ &\\
&(3.74 \pm 0.36)\tilde{C}_{HWB} + (2.00 \pm 0.21)\tilde{C}_{H\Box} - (1.41 \pm 0.07)\frac{\bar{v}^{(\ell)}}{\overline{m}_b^{(\ell)}}\tilde{C}_{bH} \\
&+ (1.24 \pm 0.14)\tilde{C}_{HD} \pm 0.35\tilde{C}_{HG} \pm 0.19\tilde{C}^{(1)}_{\substack{Hq\\33}} \pm 0.18\tilde{C}_{Ht} \pm 0.11\tilde{C}^{(3)}_{Hq} \\
&\pm 0.11\frac{m_t}{\overline{m}_b^{(\ell)}}\tilde{C}^{(1)}_{\substack{quqd\\3333}} + \ldots \Bigg\},
\end{aligned} \tag{4.6.21}$$

while at NLO we find

$$\begin{aligned}\Delta_b^{\rm NLO}(m_H,m_H) = 1.13^{+0.01}_{-0.04} + \frac{(\bar{v}^{(\ell)})^2}{\Lambda^2_{\rm NP}}\Big\{ \\ \left(4.16^{+0.05}_{-0.14}\right)\tilde{C}_{HWB} + \left(2.75^{+0.49}_{-0.48}\right)\tilde{C}_{HG} + \left(2.40^{+0.04}_{-0.09}\right)\tilde{C}_{H\Box} \\ + \left(-1.73^{+0.04}_{-0.03}\right)\frac{\bar{v}^{(\ell)}}{\overline{m}_b^{(\ell)}}\tilde{C}_{bH} + \left(1.33^{+0.01}_{-0.04}\right)\tilde{C}_{HD} + \left(-0.12^{+0.04}_{-0.01}\right)\tilde{C}^{(3)}_{\substack{Hq\\33}} \\ + \left(-0.08^{+0.05}_{-0.01}\right)\tilde{C}_{Ht} + \left(0.06^{+0.00}_{-0.05}\right)\tilde{C}^{(1)}_{\substack{Hq\\33}} + \left(0.04^{+0.03}_{-0.01}\right)\frac{m_t}{\overline{m}_b^{(\ell)}}\tilde{C}^{(1)}_{\substack{quqd\\3333}} \\ + \left(0.00^{+0.07}_{-0.04}\right)\frac{\tilde{C}_{tG}}{g_3} + \ldots\Big\}, \end{aligned} \tag{4.6.22}$$

where the ellipses in the final lines of Eqs. 4.6.21 and 4.6.22 indicate terms that in total contribute less than a 5% correction when on the extreme values of the uncertainties. By this, we mean that for a term of the form x^{+y}_{-z} we neglect terms where both $|x+y|$ and $|x-z|$ give a less than 5% contribution. We follow this same convention for the remaining scale uncertainties we report. For $f = c$ we find the LO results

$$\begin{aligned}\Delta_c^{\rm LO}(m_H,m_H) = (1\pm 0.08) + \frac{(\overline{v}^{(\ell)})^2}{\Lambda^2_{\rm NP}}\Big\{ \\ (3.74^{+0.37}_{-0.36})\tilde{C}_{HWB} + (2.00^{+0.22}_{-0.21})\tilde{C}_{H\Box} + (-1.41\pm 0.07)\frac{\overline{v}^{(\ell)}}{\overline{m}_c^{(\ell)}}\tilde{C}_{cH} + (1.24^{+0.15}_{-0.14})\tilde{C}_{HD} \\ \pm 0.35\tilde{C}_{HG} \pm 0.19\tilde{C}^{(1)}_{\substack{Hq\\33}} \pm 0.18\tilde{C}_{Ht} \pm 0.05\tilde{C}_{tH} \pm 0.05\tilde{C}^{(3)}_{\substack{Hq\\33}} + \ldots\Big\}, \end{aligned} \tag{4.6.23}$$

while at NLO we have

$$\begin{aligned}\Delta_c^{\rm NLO}(m_H,m_H) = (1.16^{+0.02}_{-0.04}) + \frac{(\overline{v}^{(\ell)})^2}{\Lambda^2_{\rm NP}}\Big\{(4.95^{+0.89}_{-0.84})\tilde{C}_{HG} + (4.31^{+0.06}_{-0.15})\tilde{C}_{HWB} \\ + (2.46^{+0.05}_{-0.10})\tilde{C}_{H\Box} + (-1.75^{+0.04}_{-0.03})\frac{\overline{v}^{(\ell)}}{\overline{m}_c^{(\ell)}}\tilde{C}_{cH} + (1.41^{+0.02}_{-0.05})\tilde{C}_{HD} + (0.00^{+0.12}_{-0.08})\frac{\tilde{C}_{tG}}{g_3} \\ + (0.09^{+0.01}_{-0.01})\tilde{C}_{HB} + (-0.09^{+0.03}_{-0.01})\tilde{C}^{(3)}_{\substack{Hq\\33}} + (-0.08^{+0.06}_{-0.01})\tilde{C}_{Ht} \\ + (-0.06^{+0.08}_{-0.08})\frac{m_t}{\overline{m}_c^{(\ell)}}\tilde{C}^{(8)}_{\substack{qu\\2332}} + (0.05^{+0.01}_{-0.01})\tilde{C}_{HW} + (0.05^{+0.01}_{-0.06})\tilde{C}^{(1)}_{\substack{Hq\\33}} \\ + (-0.05^{+0.06}_{-0.06})\frac{m_t}{\overline{m}_c^{(\ell)}}\tilde{C}^{(1)}_{\substack{qu\\2332}} + (-0.05^{+0.02}_{-0.02})\tilde{C}_{tH} + \ldots\Big\}. \end{aligned} \tag{4.6.24}$$

The features of the scale uncertainties for $h \to b\bar{b}$ and $h \to c\bar{c}$ are generally similar and so we discuss both of these here. We see in both cases that the scale uncertainties associated with NLO corrections are much smaller than those associated with the LO result, indicating a good convergence of the perturbative series. We also observe that the size of the NLO corrections due to a particular dimension-6 operator generally

sit between the uncertainty bands of the LO result, showing that the size of the NLO corrections are well estimated by the variation of the LO result. There are two clear exceptions to this. The first are the Wilson coefficients appearing at LO, and the SM, where the NLO corrections generally sit outside the uncertainty bands of the LO result. This is primarily a result of the NLO QCD corrections in the SM being larger than what one obtains from the scale variation of $\overline{m}_b^{(\ell)}$ and $\overline{m}_c^{(\ell)}$. This effect is therefore transferred to the Wilson coefficients that appear at LO in the dimension-6 SMEFT through the interference of the NLO SM and LO SMEFT amplitudes. The second exception is from $\tilde{C}_{HG}$, where the variation of the LO result badly estimates the size of the NLO correction, where we even find that the uncertainty in the NLO results is larger than that found in the LO case. This, however, is unsurprising as the size of the NLO correction is a result of the double logarithm $\sim \ln^2(\overline{m}_f^{(\ell)}/\overline{v}^{(\ell)})$ (for $f = b, c$) in Eq. 4.4.5, and is unrelated to the RG running. We also find that the RG running of $\tilde{C}_{HG}$ in the NLO result produces scale uncertainties for the operator $\tilde{C}_{tG}$ that are larger than the size of most NLO corrections. This is because the running of $\tilde{C}_{HG}$ in the NLO result produces terms proportional to $\alpha_s^2 \ln^2(\overline{m}_f^{(\ell)}/\overline{v}^{(\ell)})$, which are numerically comparable to most NLO corrections for other Wilson coefficients. Considering that for both $h \to b\bar{b}$ and $h \to c\bar{c}$, $\tilde{C}_{HG}$ receives large NNLO corrections $\sim \alpha_s^2 \ln^4(\overline{m}_f^{(\ell)}/\overline{v}^{(\ell)})$, a more reliable prediction of these processes would involve a resummation of the logarithmic terms. While techniques for such a resummation exist for the virtual $h \to AA$ for $A = g, \gamma$ [137–140], it is not clear how to translate them to the inclusive $h \to f\bar{f}$ decay rate, which receives double-logarithmic corrections from both real and virtual contributions.

The results for $f = \tau$ at LO are

$$\begin{aligned}\Delta_\tau^{\rm LO}(m_H, m_H) = (1^{+0.002}_{-0.003}) + \frac{(\overline{v}^{(\ell)})^2}{\Lambda^2_{\rm NP}}\Big\{ \\ (3.74 \pm 0.14)\tilde{C}_{HWB} + (2.00 \pm 0.12)\tilde{C}_{H\Box} - (1.41 \pm 0.06)\frac{\overline{v}^{(\ell)}}{\overline{m}_\tau^{(\ell)}}\tilde{C}_{\tau H} \\ + (1.24 \pm 0.09)\tilde{C}_{HD} \pm 0.19\tilde{C}^{(1)}_{\substack{Hq \\ 33}} \pm 0.18\tilde{C}_{Ht} \pm 0.09\frac{m_t}{\overline{m}_\tau^{(\ell)}}\tilde{C}^{(1)}_{\substack{lequ \\ 3333}} \\ \pm 0.05\tilde{C}_{tH} \pm 0.05\tilde{C}^{(3)}_{\substack{Hq \\ 33}} + \dots \Big\}, \end{aligned} \tag{4.6.25}$$

while at NLO we find

$$\begin{aligned}\Delta_\tau^{\rm NLO}(m_H, m_H) = (0.98^{+0.0001}_{-0.0002}) + \frac{(\overline{v}^{(\ell)})^2}{\Lambda^2_{\rm NP}}\Big\{ \\ (3.62^{+0.00}_{-0.01})\tilde{C}_{HWB} + (2.11^{+0.00}_{-0.02})\tilde{C}_{H\Box} + (-1.50^{+0.01}_{-0.00})\frac{\overline{v}^{(\ell)}}{\overline{m}_\tau^{(\ell)}}\tilde{C}_{\tau H} + (1.20^{+0.00}_{-0.01})\tilde{C}_{HD}\end{aligned}$$

$$+ (0.16^{+0.00}_{-0.00})\tilde{C}_{HB} + (-0.09^{+0.02}_{-0.00})\tilde{C}^{(3)}_{\substack{Hq\\33}} + (-0.08^{+0.03}_{-0.00})\tilde{C}_{Ht} + (0.07^{+0.00}_{-0.00})\tilde{C}_{HW}$$
$$+ (0.05^{+0.00}_{-0.03})\tilde{C}^{(1)}_{\substack{Hq\\33}} + (-0.05^{+0.01}_{-0.00})\tilde{C}_{tH} + \dots \Big\} . \quad (4.6.26)$$

The results for $f = \mu$ are very similar for the results for $f = \tau$ in Eqs. 4.6.25 and 4.6.26 and so are instead reported in Appendix D.2. Again, the results in Eqs. 4.6.25 and 4.6.26 show that, in general, the uncertainties are significantly reduced in the NLO result, and that the NLO results are within the uncertainty estimates of the LO result, again indicating excellent convergence of the perturbative series. There are two exceptions to this. The first of these is the SM result where we see that the uncertainty bands of the LO and NLO results show no overlap. Unlike in the Higgs decay to quarks instance, where this was caused by large NLO QCD corrections to the decay rate, the effect here is primarily due to the small size of the uncertainty bands for both the LO and NLO results. The small size of these uncertainty bands is primarily a result of correlations between the running of $\overline{m}_\tau^{(\ell)}$ and $\overline{v}^{(\ell)}$ which results in the ratio $\overline{m}_\tau^{(\ell)}(\mu_R)/\overline{v}^{(\ell)}(\mu_R)$ being more stable under scale variations than either the numerator or denominator alone. We could help to alleviate this problem by introducing separate renormalization scales for both $\overline{m}_\tau^{(\ell)}$ and $\overline{\alpha}^{(\ell)}$ separately, as discussed at the beginning of this section, but this option is not explored here. The second instance where NLO corrections are not accurately estimated through variation of the LO results are for the coefficients $\tilde{C}_{HW}$ and $\tilde{C}_{HB}$. Like in the previously discussed case of $\tilde{C}_{HG}$ for the Higgs decay to quark anti-quark pair, the size of these NLO corrections are due to the large double logarithm $\sim \ln^2(\overline{m}_\tau^{(\ell)}/m_H)$ from Eq. 4.4.5 and is therefore again inaccessible to an RG analysis.

The uncertainties obtained throughout this section are only estimates, and as stated above Eq. 4.6.19, there are many methods of obtaining such estimates that one might choose to apply. We now briefly consider a second, simpler such method and compare it to the method adopted above. In this second method we let $\mu_R = \mu_C = \mu$, and again vary the unphysical renormalization scale about $\mu = m_H$ by factors of two. We first consider the LO results, where analytic expressions for the uncertainties obtained in this way are simple. Denoting the uncertainty in the LO results as $\delta\overline{\Gamma}_f^{(i,0),(\ell)}$ we find for the LO SM and dimension-6 SMEFT

$$\delta\overline{\Gamma}_f^{(4,0),(\ell)} = \pm 2\ln(2)\overline{\Gamma}_f^{(4,0),(\ell)}\left(\gamma_f + \gamma_e\right) ,$$
$$\delta\overline{\Gamma}_f^{(6,0),(\ell)} = \pm 2\ln(2)\Bigg[\gamma_f\overline{\Gamma}_f^{(6,0),(\ell)} + \frac{C_{fH}(\overline{v}^{(\ell)})^2}{\sqrt{2}}\frac{\overline{v}^{(\ell)}}{\overline{m}_f^{(\ell)}}\overline{\Gamma}_f^{(4,0),(\ell)}\left(\gamma_f + \gamma_e\right)$$
$$+ \frac{1}{2}\overline{\Gamma}_f^{(6,0),(\ell)}\Big|_{C_i\to\dot{C}_i}\Bigg] , \quad (4.6.27)$$

where we have dropped the arguments of all scale-dependent quantities, with the understanding that these are all evaluated at $\mu = m_H$. As they lack any μ_C dependence, the SM scale uncertainties found with this method match those found using the quadrature method. Additionally, compared to the results found in Eq. 4.6.21, 4.6.23, and 4.6.25, this method only changes the uncertainties for Wilson coefficients already appearing at LO. With this in mind we find

$$\begin{aligned}
\delta\overline{\Gamma}_b^{(6,0),(\ell)} &= \frac{(\overline{v}^{(\ell)})^2}{\Lambda_{\rm NP}^2}\left\{ \pm 0.20\tilde{C}_{HWB} \pm 0.06\tilde{C}_{H\Box} \pm 0.08\frac{\overline{v}^{(\ell)}}{\overline{m}_b^{(\ell)}}\tilde{C}_{bH} \pm 0.02\tilde{C}_{HD} + \dots \right\}, \\
\delta\overline{\Gamma}_c^{(6,0),(\ell)} &= \frac{(\overline{v}^{(\ell)})^2}{\Lambda_{\rm NP}^2}\left\{ \pm 0.20\tilde{C}_{HWB} \pm 0.07\tilde{C}_{H\Box} \pm 0.08\frac{\overline{v}^{(\ell)}}{\overline{m}_c^{(\ell)}}\tilde{C}_{cH} \pm 0.02\tilde{C}_{HD} + \dots \right\}, \\
\delta\overline{\Gamma}_\tau^{(6,0),(\ell)} &= \frac{(\overline{v}^{(\ell)})^2}{\Lambda_{\rm NP}^2}\left\{ \pm 0.12\tilde{C}_{HWB} \pm 0.10\tilde{C}_{H\Box} \pm 0.05\frac{\overline{v}^{(\ell)}}{\overline{m}_\tau^{(\ell)}}\tilde{C}_{\tau H} \pm 0.08\tilde{C}_{HD} + \dots \right\}, \\
\delta\overline{\Gamma}_\mu^{(6,0),(\ell)} &= \frac{(\overline{v}^{(\ell)})^2}{\Lambda_{\rm NP}^2}\left\{ \pm 0.12\tilde{C}_{HWB} \pm 0.004\tilde{C}_{H\Box} \pm 0.05\frac{\overline{v}^{(\ell)}}{\overline{m}_\mu^{(\ell)}}\tilde{C}_{\mu H} \pm 0.08\tilde{C}_{HD} + \dots \right\},
\end{aligned} \tag{4.6.28}$$

where the ellipses represent coefficients not appearing in the LO result which are unaffected by this alternative analysis. We see that for all processes, the uncertainties obtained in this way for the operator $\tilde{C}_{fH}$ closely match the values obtained using the quadrature method, and for processes involving decay into final state lepton anti-lepton pair, this is also true for $\tilde{C}_{HWB}$. However, we see that for the majority of cases the uncertainties are artificially small to assign to LO process, with the smallest of these being 0.4% for the coefficient $\tilde{C}_{H\Box}$ for the process $h \to \mu\bar{\mu}$. We conclude that such a method of obtaining uncertainties, while reliable for the SM and some dimension-6 SMEFT Wilson coefficients, can also lead to unreliable estimates. Therefore, we do not consider pursuing this method of uncertainty estimates any further.

4.7 Ratios of Decay Rates

As discussed in Section 3.1, while measurements of the decay of the Higgs into all four processes considered here exist, these measurements are very limited, especially in the cases of $h \to c\bar{c}$ and $h \to \mu\bar{\mu}$. However, at future lepton colliders it is expected that all four processes considered here will be measured with good precision. This motivates us to consider not only the predictions for the decay rates themselves, but also to look at calculating ratios of decay rates.

In the SM it is clear that the ratio of decay rates of Higgs to fermion anti-fermion

pairs causes the (either partial or exact) cancellation of flavor universal counterterms. To illustrate this, consider the ratio of the left-handed component of the renormalized NLO SM amplitude for the Higgs decay to distinct fermion pairs, f_1 and f_2, in the small-mass limit

$$\begin{aligned}\frac{\mathcal{M}_{L,f_1}^{(4,1)}}{\mathcal{M}_{L,f_2}^{(4,1)}} &= \frac{\mathcal{M}_{L,f_1}^{(4,1),\text{bare}} + \delta\mathcal{M}_{L,f_1}^{(4)}}{\mathcal{M}_{L,f_2}^{(4,1),\text{bare}} + \delta\mathcal{M}_{L,f_2}^{(4)}} \\ &= \frac{1}{\mathcal{M}_{L,f_2}^{(4,1),\text{bare}}}\Bigg\{\mathcal{M}_{L,f_1}^{(4,1),\text{bare}} + \frac{m_{f_1}}{\hat{v}_T}\left[\frac{1}{2}\delta Z_h^{(4)} - \frac{\delta\hat{v}_T^{(4)}}{\hat{v}_T}\right]\left(1 - \frac{\mathcal{M}_{L,f_1}^{(4,1),\text{bare}}}{\mathcal{M}_{L,f_2}^{(4,1),\text{bare}}}\frac{m_{f_2}}{m_{f_1}}\right) \\ &\quad + \frac{m_{f_1}}{\hat{v}_T}\left(\frac{\delta m_{f_1}^{(4)}}{m_{f_1}} + \frac{1}{2}\delta Z_{f_1}^{(4)} - \frac{\mathcal{M}_{L,f_1}^{(4,1),\text{bare}}}{\mathcal{M}_{L,f_2}^{(4,1),\text{bare}}}\frac{m_{f_2}}{m_{f_1}}\left[\frac{\delta m_{f_2}^{(4)}}{m_{f_2}} + \frac{1}{2}\delta Z_{f_2}^{(4)}\right]\right)\Bigg\}, \quad (4.7.1)\end{aligned}$$

where we have used the expression for the SM one-loop counterterm from Eq. 4.3.8 and where we have defined

$$\delta Z_f \equiv \delta Z_f^L + \delta Z_f^{R*}\,. \quad (4.7.2)$$

From Eq. 4.7.1 we find that the terms in the curved parenthesis (...) contain the difference of terms that are potentially similar in size. In fact, in the small-mass limit, for final states of the same charges under the SM symmetry group the terms in curved parenthesis exactly cancel. This is because in this instance we find

$$\begin{aligned}\frac{\mathcal{M}_{L,f_1}^{(4,1),\text{bare}}}{\mathcal{M}_{L,f_2}^{(4,1),\text{bare}}} &= \frac{m_{f_1}}{m_{f_2}}\,, \\ \frac{\delta m_{f_1}}{m_{f_1}} &= \frac{\delta m_{f_2}}{m_{f_2}}\,, \\ \delta Z_{f_1} &= \delta Z_{f_2}\,. \quad (4.7.3)\end{aligned}$$

As a result we also find

$$\frac{m_{f_2}^2}{m_{f_1}^2}\frac{\Gamma_{f_1}^{(4,1)}}{\Gamma_{f_2}^{(4,1)}} = 1\,. \quad (4.7.4)$$

Alternatively, if the two final-state fermion pairs under consideration do not have the same charges under the SM symmetry group this cancellation is only approximate and we instead find that the ratio in Eq. 4.7.4 would be only approximately equal to 1. Given these cancellations, the ratios of the decay rate in the SM are more stable under perturbative corrections than the decay rates themselves.

The arguments outlined in this section also carry over to the SMEFT where we find the cancellation of many flavor-universal dimension-6 Wilson coefficients in these ratios. To a large extent, these ratios also cause the cancellation of input-scheme-

dependent terms, overall reducing the input scheme dependence when considering ratios of decay rates. Finally, as we shall shortly see, the ratios of decay rates offer stringent tests of MFV, as well as probes of the hgg and $h\gamma\gamma$ couplings found in the dimension-6 SMEFT.

As established, the ratios in which we find the greatest cancellation of terms in the ratios of decay rates are those where the final-state fermion pairs of the two processes have the same charges under the SM symmetry group. Lepton colliders should be able to measure the tau to muon decay rate ratio, and so we focus on this as a concrete possibility. First we define the ratio of these decay rates as

$$R_{\tau/\mu} = \frac{(\overline{m}_\mu^{(\ell)})^2}{(\overline{m}_\tau^{(\ell)})^2}\frac{\overline{\Gamma}_\tau^{(\ell)}}{\overline{\Gamma}_\mu^{(\ell)}}\,. \tag{4.7.5}$$

As established earlier in this section, in the SM we find in the small-mass limit, and ignoring terms suppressed by powers of $(\overline{m}_\ell^{(\ell)})^2/m_H^2$ that $R_{\tau/\mu} = 1$. In the SMEFT, keeping up to and including $\mathcal{O}((\overline{v}^{(\ell)})^2/\Lambda_{\rm NP}^2)$ terms we find at the scale $\mu = m_H$

$$\begin{aligned}
R_{\tau/\mu} - 1 &= \Delta_\tau^{\rm NLO}(m_H) - \Delta_\mu^{\rm NLO}(m_H) - \Delta_\tau^{(4,1)}\left(\Delta_\tau^{(6,0)} - \Delta_\mu^{(6,0)}\right) \\
&= \frac{(\overline{v}^{(\ell)})^2}{\Lambda_{\rm NP}^2}\Bigg\{ -1.53\left(\frac{\overline{v}^{(\ell)}}{\overline{m}_\tau^{(\ell)}}\tilde{C}_{\tau H} - \frac{\overline{v}^{(\ell)}}{\overline{m}_\mu^{(\ell)}}\tilde{C}_{\mu H}\right) - 0.25\tilde{C}_{HB} + 0.13\tilde{C}_{HWB} \\
&+ \Bigg[-7.2\tilde{C}_{HW} - 3.8\left(\frac{m_t}{\overline{m}_\tau^{(\ell)}}\tilde{C}^{(1)}_{\substack{lequ\\3333}} - \frac{m_t}{\overline{m}_\mu^{(\ell)}}\tilde{C}^{(1)}_{\substack{lequ\\2233}}\right) + 2.0\left(\frac{\overline{m}_b^{(\ell)}}{\overline{m}_\tau^{(\ell)}}\tilde{C}_{\substack{ledq\\3333}}\right. \\
&\left. - \frac{\overline{m}_b^{(\ell)}}{\overline{m}_\mu^{(\ell)}}\tilde{C}_{\substack{ledq\\2233}} + \frac{\overline{m}_s^{(\ell)}}{\overline{m}_\tau^{(\ell)}}\tilde{C}_{\substack{ledq\\3322}} - \frac{\overline{m}_s^{(\ell)}}{\overline{m}_\mu^{(\ell)}}\tilde{C}_{\substack{ledq\\2222}} - \frac{\overline{m}_c^{(\ell)}}{\overline{m}_\tau^{(\ell)}}\tilde{C}^{(1)}_{\substack{lequ\\3322}} + \frac{\overline{m}_c^{(\ell)}}{\overline{m}_\mu^{(\ell)}}\tilde{C}^{(1)}_{\substack{lequ\\2222}}\right) \\
&+ 1.8\left(\tilde{C}^{(3)}_{\substack{Hl\\33}} - \tilde{C}^{(3)}_{\substack{Hl\\22}}\right) - 1.0\left(\left(\frac{\overline{m}_\mu^{(\ell)}}{\overline{m}_\tau^{(\ell)}} - \frac{\overline{m}_\tau^{(\ell)}}{\overline{m}_\mu^{(\ell)}}\right)\tilde{C}_{\substack{le\\2332}} + \tilde{C}_{\substack{le\\3333}} - \tilde{C}_{\substack{le\\2222}}\right)\Bigg] \times 10^{-2} \\
&+ \left[4\left(\tilde{C}^{(1)}_{\substack{Hl\\33}} - \tilde{C}^{(1)}_{\substack{Hl\\22}} - \tilde{C}_{H\tau} + \tilde{C}_{H\mu}\right) + \left(\frac{\overline{v}^{(\ell)}}{\overline{m}_\tau^{(\ell)}}\frac{\tilde{C}_{\tau W}}{\overline{e}^{(\ell)}} - \frac{\overline{v}^{(\ell)}}{\overline{m}_\mu^{(\ell)}}\frac{\tilde{C}_{\mu W}}{\overline{e}^{(\ell)}}\right)\right] \times 10^{-3} \\
&- (4\times 10^{-4})\left(\frac{\overline{v}^{(\ell)}}{\overline{m}_\tau^{(\ell)}}\frac{\tilde{C}_{\tau B}}{\overline{e}^{(\ell)}} - \frac{\overline{v}^{(\ell)}}{\overline{m}_\mu^{(\ell)}}\frac{\tilde{C}_{\mu B}}{\overline{e}^{(\ell)}}\right)\Bigg\}\,,
\end{aligned} \tag{4.7.6}$$

where in the top line of Eq. 4.7.6 we have used that $\Delta_\tau^{(4,1)} = \Delta_\mu^{(4,1)}$ to simplify this expression. While the sum $\overline{\Gamma}_\tau^{(\ell)} + \overline{\Gamma}_\mu^{(\ell)}$ is a function of 48 Wilson coefficients, the above ratio, $R_{\tau/\mu}$, is a function of only 26, a reduction of 22. This is a result of almost all coefficients whose corresponding operator is not a function of a fermion field canceling in this ratio. The only exception to this are the flavor universal coefficients C_{HW}, C_{HB} and C_{HWB}, the coefficients to which are a function of fermion masses and thus do not cancel in the ratio $R_{\tau/\mu}$.

The ratio in Eq. 4.7.6 is simplified further if some universality is assumed for the generation-dependent Wilson coefficients. As an example we study the ratio $R_{\tau/\mu}$ while also implementing MFV, which we first discussed in general in Section 2.1.3 and in the context of the SMEFT in Section 2.2.2. Specifically, in correspondence with the results here being presented in the small-mass limit, we use the same limit for the MFV Wilson coefficients, which we developed in Section 3.5. As discussed in Section 3.5, the flavor-space indices of the Wilson coefficients are then carried by powers of the Yukawa matrices, which are expanded in the small-mass limit to produce the equations found in Eqs. 3.5.7 and 3.5.8. After taking the MFV limit, and dropping terms suppressed by powers of $\overline{m}_f^{(\ell)}/m_H$ we find

$$\begin{aligned}\left[R_{\tau/\mu}-1\right]_{\text{MFV}} &= \frac{\overline{\alpha}^{(\ell)}(\overline{v}^{(\ell)})^2}{\pi}\mathcal{C}_{h\gamma\gamma}\left(\ln^2\left(\frac{(\overline{m}_\tau^{(\ell)})^2}{m_H^2}\right)-\ln^2\left(\frac{(\overline{m}_\mu^{(\ell)})^2}{m_H^2}\right)\right)\\ &= \frac{(\overline{v}^{(\ell)})^2}{\Lambda_{\text{NP}}^2}\left(-0.25\tilde{\mathcal{C}}_{HB}^0+0.13\tilde{\mathcal{C}}_{HWB}^0-0.072\tilde{\mathcal{C}}_{HW}^0\right), \qquad (4.7.7)\end{aligned}$$

where the form of $\mathcal{C}_{h\gamma\gamma}$ is found by replacing the Wilson coefficients in $c_{h\gamma\gamma}$ from Eq. 4.3.27 with the small-mass limit MFV counterparts to give

$$\mathcal{C}_{h\gamma\gamma}=\mathcal{C}_{HB}^0\hat{c}_w^2+\mathcal{C}_{HW}^0\hat{s}_w^2-\mathcal{C}_{HWB}^0\hat{c}_w\hat{s}_w\,. \qquad (4.7.8)$$

In Eq. 4.7.7 we have also given the analytic form of the ratio $R_{\tau/\mu}$ to demonstrate that the remaining terms are a result of the double logarithms arising from the $h\gamma\gamma$ coupling found in Eq. 4.4.5. It is clear that imposing MFV brings the number of Wilson coefficients in the ratio $R_{\tau/\mu}$ down to only three. Comparing Eq. 4.7.6 and Eq. 4.7.7 we see that with a generic flavor structure it is possible to have a significant deviation from the SM result in $\overline{\Gamma}_\tau^{(\ell)}$, $\overline{\Gamma}_\mu^{(\ell)}$, and $R_{\tau/\mu}$ simultaneously, while in an MFV scenario any deviations from the SM due to modified fermion couplings in the decay rates would not propagate to the ratio $R_{\tau/\mu}$. From this we see that measuring the ratio $R_{\tau/\mu}$ offers an interesting test of MFV, and an independent constraint on the Wilson coefficients in Eq. 4.7.7. As an estimate, we take the values for the Wilson coefficients appearing in Eq. 4.7.7 from a recent global fit [100]. We take the 95% confidence level limits for the relevant coefficients from this reference where a global fit over 19 Wilson coefficients is performed, marginalized over all coefficients which finds $C_{HB}\approx[-0.5,0.5]$, $C_{HW}\approx[-1.5,1.5]$, and $C_{HWB}\approx[-0.125,+0.125]$. Using these values in such a way as to maximize Eq. 4.7.7 we find

$$\left[R_{\tau/\mu}-1\right]_{\text{MFV}}\approx[-0.25,+0.25]\frac{(\overline{v}^{(\ell)})^2}{\Lambda_{\text{NP}}^2}\,. \qquad (4.7.9)$$

Using the estimate stated in Section 4.6.1 of $(\overline{v}^{(\ell)})^2/\Lambda^2\approx 6\%$, we see that this

corresponds to a $\sim 1.4\%$ possible deviation from the SM result.

As a second example, we consider the ratio of decay rate of $h \to c\bar{c}$ and $h \to b\bar{b}$ defined as

$$R_{c/b} = \frac{(\overline{m}_b^{(\ell)})^2}{(\overline{m}_c^{(\ell)})^2} \frac{\overline{\Gamma}_c^{(\ell)}}{\overline{\Gamma}_b^{(\ell)}} \,. \tag{4.7.10}$$

As discussed at the beginning of this section, due to the differences in charges under the SM gauge group leading to different couplings of these fermions to gauge bosons, we do not expect the cancellation between terms in this ratio to be as exact as was seen for $R_{\tau/\mu}$. However, we do find that QCD corrections to the SM result (and therefore also flavor-universal contributions from "SM-like" QCD diagrams) cancel in the ratio, so deviations from unitary in the SM component of $R_{c/b}$ are due to SM EW effects. The ratio in Eq. 4.7.10 for generic flavor structure takes the form

$$\begin{aligned}
R_{c/b} - 1 &= \Delta_c^{\rm NLO} - \Delta_b^{\rm NLO} - \Delta_c^{(4,1)}\Delta_b^{(6,0)} - \Delta_b^{(4,1)}\Delta_c^{(6,0)} + 2\Delta_b^{(4,1)}\Delta_b^{(6,0)} \\
&= 0.03 + \frac{(\overline{v}^{(\ell)})^2}{\Lambda_{\rm NP}^2}\Bigg\{ 2.20\tilde{C}_{HG} - 1.57\frac{\overline{v}^{(\ell)}}{\overline{m}_c^{(\ell)}}\tilde{C}_{cH} + 1.59\frac{\overline{v}^{(\ell)}}{\overline{m}_b^{(\ell)}}\tilde{C}_{bH} + \Bigg[8.5\tilde{C}_{HB} \\
&\quad - 6.3\frac{m_t}{\overline{m}_c^{(\ell)}}\tilde{C}^{(8)}_{\substack{qu\\2332}} - 4.8\frac{m_t}{\overline{m}_c^{(\ell)}}\tilde{C}^{(1)}_{\substack{qu\\2332}} - 4.4\frac{m_t}{\overline{m}_b^{(\ell)}}\tilde{C}^{(1)}_{\substack{quqd\\3333}} + 4.4\tilde{C}_{HWB} + 4.2\tilde{C}_{HD} \\
&\quad + 2.7\tilde{C}_{HW} + 2.6\tilde{C}^{(3)}_{\substack{Hq\\33}} + 2.4\frac{\overline{m}_s^{(\ell)}}{\overline{m}_c^{(\ell)}}\tilde{C}^{(1)}_{\substack{quqd\\2222}} + 2.0\left(\frac{\overline{m}_b^{(\ell)}}{\overline{m}_c^{(\ell)}} - \frac{\overline{m}_c^{(\ell)}}{\overline{m}_b^{(\ell)}}\right)\tilde{C}^{(1)}_{\substack{quqd\\2233}} + 1.9\tilde{C}^{(3)}_{\substack{Hq\\22}} \\
&\quad + 1.9\frac{\overline{v}^{(\ell)}}{\overline{m}_b^{(\ell)}}\frac{\tilde{C}_{bW}}{\overline{e}^{(\ell)}} - 1.5\tilde{C}_{tH} + 1.5\frac{\tilde{C}_{tW}}{\overline{e}^{(\ell)}} - 1.3\left(\tilde{C}^{(8)}_{\substack{qu\\2222}} - \tilde{C}^{(8)}_{\substack{qd\\3333}} - \frac{\overline{m}_s^{(\ell)}}{\overline{m}_b^{(\ell)}}\tilde{C}^{(8)}_{\substack{qd\\2332}}\right) \\
&\quad - 1.0\left(\tilde{C}^{(1)}_{\substack{qu\\2222}} - \tilde{C}^{(1)}_{\substack{qd\\3333}} - \frac{\overline{m}_s^{(\ell)}}{\overline{m}_b^{(\ell)}}\tilde{C}^{(1)}_{\substack{qd\\2332}}\right)\Bigg] \times 10^{-2} + \Bigg[8\left(\frac{\overline{v}^{(\ell)}}{\overline{m}_c^{(\ell)}}\frac{\tilde{C}_{cG}}{g_3} - \frac{\overline{v}^{(\ell)}}{\overline{m}_b^{(\ell)}}\frac{\tilde{C}_{bG}}{g_3}\right) \\
&\quad - 8\frac{m_t}{\overline{m}_b^{(\ell)}}\tilde{C}^{(8)}_{\substack{quqd\\3333}} - 7\left(\frac{\overline{m}_\tau^{(\ell)}}{\overline{m}_c^{(\ell)}}\tilde{C}^{(1)}_{\substack{lequ\\3322}} + \frac{\overline{m}_\tau^{(\ell)}}{\overline{m}_b^{(\ell)}}C_{\substack{ledq\\3333}} + \frac{\overline{m}_\mu^{(\ell)}}{\overline{m}_c^{(\ell)}}\tilde{C}^{(1)}_{\substack{lequ\\2222}} + \frac{\overline{m}_\mu^{(\ell)}}{\overline{m}_b^{(\ell)}}C_{\substack{ledq\\2233}}\right) \\
&\quad - 6\tilde{C}^{(1)}_{\substack{Hq\\33}} - 5\tilde{C}^{(1)}_{\substack{Hq\\22}} + 4\left(\frac{\overline{m}_b^{(\ell)}}{\overline{m}_c^{(\ell)}} - \frac{\overline{m}_c^{(\ell)}}{\overline{m}_b^{(\ell)}}\right)\tilde{C}^{(8)}_{\substack{quqd\\3223}} + 4\frac{\overline{m}_s^{(\ell)}}{\overline{m}_c^{(\ell)}}\tilde{C}^{(8)}_{\substack{quqd\\2222}} + 4\frac{\overline{v}^{(\ell)}}{\overline{m}_b^{(\ell)}}\tilde{C}_{Htb} \\
&\quad + 3\left(\frac{\overline{m}_b^{(\ell)}}{\overline{m}_c^{(\ell)}} - \frac{\overline{m}_c^{(\ell)}}{\overline{m}_b^{(\ell)}}\right)\tilde{C}^{(1)}_{\substack{quqd\\3223}} + 3\tilde{C}_{Hc} + 2\tilde{C}_{Hb} + \frac{\overline{v}^{(\ell)}}{\overline{m}_c^{(\ell)}}\frac{\tilde{C}_{cW}}{\overline{e}}\Bigg] \times 10^{-3} \\
&\quad + (2\times 10^{-4})\frac{\overline{v}^{(\ell)}}{\overline{m}_c^{(\ell)}}\frac{\tilde{C}_{cB}}{\overline{e}^{(\ell)}} + (4\times 10^{-5})\frac{\overline{v}^{(\ell)}}{\overline{m}_b^{(\ell)}}\frac{\tilde{C}_{bB}}{\overline{e}^{(\ell)}}\Bigg\} \,.
\end{aligned} \tag{4.7.11}$$

From the second line in Eq. 4.7.11 we see that the deviation from unity in the SM result is only 3%. We find that $\overline{\Gamma}_c^{(\ell)} + \overline{\Gamma}_b^{(\ell)}$ is a function of 60 Wilson coefficients, while the ratio $R_{c/b}$ in Eq. 4.7.11 is a function of 40 Wilson coefficients. This demonstrates again that we generally find the cancellation of flavor-universal Wilson coefficients

in this ratio. Again, imposing MFV we find this ratio becomes

$$\begin{aligned}\left[R_{c/b}-1\right]_{\text{MFV}} &= 0.03+\frac{(\overline{v}^{(\ell)})^2}{\Lambda_{\text{NP}}^2}\Bigg\{2.24\tilde{\mathcal{C}}^1_{bH}-2.22\tilde{\mathcal{C}}^1_{cH}+2.20\tilde{\mathcal{C}}^0_{HG}+\Bigg[8.5\tilde{\mathcal{C}}^0_{HB}\\ &\quad-4.5\tilde{\mathcal{C}}^{(1),2}_{\substack{quqd\\3333}}+4.4\tilde{\mathcal{C}}^0_{HWB}+4.2\tilde{\mathcal{C}}^0_{HD}+2.7\frac{\tilde{\mathcal{C}}^1_{bW}}{\overline{e}^{(\ell)}}+2.7\tilde{\mathcal{C}}^0_{HW}+2.6\tilde{\mathcal{C}}^{(3),0}_{\substack{Hq\\33}}\\ &\quad+1.9\tilde{\mathcal{C}}^{(3),0}_{\substack{Hq\\22}}-1.6\tilde{\mathcal{C}}^1_{tH}+1.5\frac{\tilde{\mathcal{C}}^1_{tW}}{\overline{e}^{(\ell)}}-1.3\left(\tilde{\mathcal{C}}^{(8),0}_{\substack{qu\\2222}}-\tilde{\mathcal{C}}^{(8),0}_{\substack{qd\\33}}\right)\\ &\quad+1.1\left(\frac{\tilde{\mathcal{C}}^1_{cG}}{g_3}-\frac{\tilde{\mathcal{C}}^1_{bG}}{g_3}\right)-1.0\left(\tilde{\mathcal{C}}^{(1),0}_{\substack{qu\\2222}}-\tilde{\mathcal{C}}^{(1),0}_{\substack{qd\\33}}\right)\Bigg]\times10^{-2}+\Bigg[-9\tilde{\mathcal{C}}^{(8),2}_{\substack{quqd\\3333}}\\ &\quad-6\tilde{\mathcal{C}}^{(1),0}_{\substack{Hq\\33}}-5\tilde{\mathcal{C}}^{(1),0}_{\substack{Hq\\22}}+5\tilde{\mathcal{C}}^2_{Htb}+3\tilde{\mathcal{C}}^0_{Hc}+2\tilde{\mathcal{C}}^0_{Hb}+2\frac{\tilde{\mathcal{C}}^1_{cW}}{\overline{e}^{(\ell)}}\Bigg]\times10^{-3}\\ &\quad+(3\times10^{-4})\frac{\tilde{\mathcal{C}}^1_{cB}}{\overline{e}^{(\ell)}}+(6\times10^{-5})\frac{\tilde{\mathcal{C}}^1_{bB}}{\overline{e}^{(\ell)}}\Bigg\},\end{aligned}\tag{4.7.12}$$

where we have used that $\mathcal{C}^{(1,3),0}_{\substack{Hq\\11}}=\mathcal{C}^{(1,3),0}_{\substack{Hq\\22}}$, a property we described in Section 3.5. This result is a function of 28 Wilson coefficients, far larger than the 3 Wilson coefficients present in the equivalent result for $R_{\tau/\mu}$. This number may be reduced further with additional assumptions, such as assuming some flavor universality for up- and down-type quarks, but such possibilities are not explored here. Studying Eq. 4.7.12 we see that by far the largest contributions are from the coefficients $\tilde{\mathcal{C}}^1_{bH}$, $\tilde{\mathcal{C}}^1_{cH}$ and $\tilde{\mathcal{C}}^0_{HG}$. We further find that the remaining operators that appear at LO in the individual processes, $\tilde{\mathcal{C}}^0_{H\Box}$, $\tilde{\mathcal{C}}^0_{HD}$, and $\tilde{\mathcal{C}}^0_{HWB}$ first contribute at NLO in the ratio $R_{c/b}$, and in particular the dependence on the coefficient $\tilde{\mathcal{C}}^0_{H\Box}$ cancels entirely. The contribution from $\tilde{\mathcal{C}}^0_{HG}$ is due to terms of the form $\alpha_s\ln^2(\overline{m}^{(\ell)}_f/m_H)$, so as remarked earlier in this section it would be desirable to resum such terms to obtain a more reliable prediction. We would wish to construct the analogue of Eq. 4.7.9 for $R_{c/b}$. Consider the three operators with the largest numerical contributions, $\tilde{\mathcal{C}}^1_{bH}$, $\tilde{\mathcal{C}}^1_{cH}$, and $\tilde{\mathcal{C}}^0_{HG}$. We find that while $\tilde{\mathcal{C}}^0_{HG}$ is generally well constrained, the infancy of measurements of $h\to b\bar{b}$ and $h\to c\bar{c}$ means that the constraints on $\tilde{\mathcal{C}}^1_{bH}$ and $\tilde{\mathcal{C}}^1_{cH}$ are sufficiently large that it is not constructive to consider the potential size of deviations from the SM as a result of these Wilson coefficients at this time [95].

Chapter 5

Conclusions

In this thesis we have calculated the complete set of NLO dimension-6 SMEFT contributions to the decay $h \to f\bar{f}$ for the phenomenologically viable final states $f \in \{b, c, \tau, \mu\}$. We began by introducing the aspects of the SM which are relevant to this calculation, including a discussion of renormalization at the one-loop level, throughout Chapter 1. In Chapter 2 we introduced the concept of EFTs, paying particular attention to the dimension-6 SMEFT. We saw that the dimension-6 SMEFT (under certain assumptions) provides a systematic way to parameterize the effects of heavy NP in a consistent manner in terms of Wilson coefficients. In turn, this enables us to describe any experimental deviations from SM predictions in terms of these Wilson coefficients, and opens the possibility for these deviations to be understood in terms of UV-complete theories. This provides a means to simultaneously test a large number of UV-complete theories.

In Chapter 3 we introduced the focus of this thesis, and motivated that the decay modes explored here are a viable avenue for constraining Wilson coefficients, with the current experimental status leaving ample room for NP. In this chapter we also introduced general aspects of calculations within the dimension-6 SMEFT beyond the specific decay modes considered, such as gauge fixing in the dimension-6 SMEFT and MFV in the small-mass limit. In Chapter 4 we introduced the main calculations of this thesis in full. We began by exploring the appropriateness of the diagonal CKM approximation in this calculation. This approximation is widely used in EW calculations in the SM, and we found that despite some technical differences when applying this approximation to the SMEFT (stemming from the possibility of amplitudes being a function of one CKM element rather than two), in practice for this particular calculation the diagonal CKM approximation remains viable. We also saw in Sections 4.3.3 and 4.3.4 that despite the renormalization of one-loop calculations in the dimension-6 SMEFT being broadly similar to those in the SM, it was also

necessary to implement several technical differences regarding the electric charge renormalization and the mixing of the Higgs with the Z- and neutral Goldstone bosons. We also saw that the mechanism of tadpole correction cancellation in the on-shell renormalization scheme in the SMEFT is more intricate than seen in the SM due to the introduction of tadpole corrections to the bare matrix elements and the electric charge – features not found in the SM.

Our calculation involved both EW and QCD corrections. We presented illustrative subsets of the full results in Sections 4.4.1 to 4.4.3. From our brief numerical analysis in Section 4.5 we saw that large NLO corrections arise from the QED-QCD corrections due to large logarithms from the on-shell renormalization of fermion masses, motivating that the renormalization of the fermion masses should be in the $\overline{\text{MS}}$ scheme. Despite this, we also found that a scheme in which some parameters are renormalized in the on-shell scheme while others are renormalized in the $\overline{\text{MS}}$ scheme results in the non-cancellation of tadpoles, leading to enhanced tadpole corrections, with the largest of these scaling as $m_t^4/(\hat{v}_T^2 m_H^2)$. This motivated the introduction of decoupling constants for the fermion mass and electric charge, linking the full theory with a five-flavor QED×QCD theory. This essentially allowed for a consistent way to renormalize the QED×QCD components of the fermion mass and electric charge in the $\overline{\text{MS}}$ scheme, while renormalizing the remaining components of the fermion mass and electric charge in the on-shell scheme. We found that decoupling these parameters in this way was equivalent to a new renormalization scheme. This renormalization scheme therefore allowed us to avoid enhanced corrections of both a QED×QCD and tadpole origin.

In Section 4.6 we presented the numerical results for the decay rates in the decoupled hybrid renormalization scheme. We first presented the results at the scale $\mu = m_H$. We found at NLO $h \to b\bar{b}$ receives contributions from 48 operators, $h \to c\bar{c}$ receives contributions from 47 operators, while $h \to \tau\bar{\tau}$ and $h \to \mu\bar{\mu}$ receive contributions from 40 operators. We also estimated the perturbative uncertainties to the LO and NLO results through scale variations. We advocated the introduction of two renormalization scales, μ_C for the Wilson coefficients, and μ_R for the remaining parameters, and adding the resulting uncertainties in quadrature. A brief analysis of the LO case showed that such a method was favorable to one in which both scales are varied simultaneously. From our analysis we found that while NLO corrections reduce the scale dependence of the decay rate, genuine NLO effects inaccessible to an RG analysis based on scale variations can be significant.

Finally, in Section 4.7 we considered the ratios of several of the calculated decay rates. We saw that, depending on the ratio in question, many flavor-universal Wilson coefficients either approximately, or exactly cancel in these ratios. This in

turn reduces the Wilson coefficient dependence of such ratios. We saw the example of $R_{\tau/\mu}$ which is a function of 26 Wilson coefficients, while $\overline{\Gamma}_{\tau}^{(\ell)} + \overline{\Gamma}_{\mu}^{(\ell)}$ is a function of 48. Similarly, $R_{c/b}$ is a function of 40 Wilson coefficients, while $\overline{\Gamma}_{c}^{(\ell)} + \overline{\Gamma}_{b}^{(\ell)}$ is a function of 60. We also explored the form of these ratios while imposing MFV. We found that in the case where the ratio is of decay rates where the final state fermion pairs have different charges under the SM symmetry group that imposing MFV results in another modest reduction of the number of contributing Wilson coefficients. Specifically in the ratio $R_{c/b}$, we find that imposing MFV reduces the number of Wilson coefficients to 28. However, in the case where the ratio involves final-state fermions with the same charge under the SM symmetry group, imposing MFV enormously reduces the Wilson coefficient dependence. We see in the case of $R_{\tau/\mu}$ that imposing MFV makes this ratio a function of only three Wilson coefficients. In this way, the ratio $R_{\tau/\mu}$ offers a potential test of MFV.

The analytic results for the decay rates calculated here are lengthy, therefore only a subset of the analytic results were provided. The full expressions for the decay rates calculated here may be found in the computer files of the arXiv submissions on which the work in this thesis is based [1,2]. We believe that the renormalization procedure, and the uncertainty analysis performed here can serve as a template for future NLO SMEFT calculations which aim to bring EW and QCD corrections into a single framework. The full analytic results may also serve to be useful for future global fits of Wilson coefficients to precision data, as well as for benchmarking all-purpose tools for automated NLO dimension-6 SMEFT calculations as they become available.

Appendix A

Dimension-6 SMEFT Operators in the Warsaw Basis

$1: X^3$	
Q_G	$f^{ABC} G^{A\nu}_{\mu} G^{B\rho}_{\nu} G^{C\mu}_{\rho}$
$Q_{\widetilde{G}}$	$f^{ABC} \widetilde{G}^{A\nu}_{\mu} G^{B\rho}_{\nu} G^{C\mu}_{\rho}$
Q_W	$\epsilon^{IJK} W^{I\nu}_{\mu} W^{J\rho}_{\nu} W^{K\mu}_{\rho}$
$Q_{\widetilde{W}}$	$\epsilon^{IJK} \widetilde{W}^{I\nu}_{\mu} W^{J\rho}_{\nu} W^{K\mu}_{\rho}$

$2: H^6$	
Q_H	$(H^\dagger H)^3$

$3: H^4 D^2$	
$Q_{H\Box}$	$(H^\dagger H)\Box(H^\dagger H)$
Q_{HD}	$\left(H^\dagger D_\mu H\right)^* \left(H^\dagger D_\mu H\right)$

$4: X^2 H^2$	
Q_{HG}	$H^\dagger H\, G^A_{\mu\nu} G^{A\mu\nu}$
$Q_{H\widetilde{G}}$	$H^\dagger H\, \widetilde{G}^A_{\mu\nu} G^{A\mu\nu}$
Q_{HW}	$H^\dagger H\, W^I_{\mu\nu} W^{I\mu\nu}$
$Q_{H\widetilde{W}}$	$H^\dagger H\, \widetilde{W}^I_{\mu\nu} W^{I\mu\nu}$
Q_{HB}	$H^\dagger H\, B_{\mu\nu} B^{\mu\nu}$
$Q_{H\widetilde{B}}$	$H^\dagger H\, \widetilde{B}_{\mu\nu} B^{\mu\nu}$
Q_{HWB}	$H^\dagger \sigma^I H\, W^I_{\mu\nu} B^{\mu\nu}$
$Q_{H\widetilde{W}B}$	$H^\dagger \sigma^I H\, \widetilde{W}^I_{\mu\nu} B^{\mu\nu}$

$5: \psi^2 H^3 + \text{h.c.}$	
Q_{eH}	$(H^\dagger H)(\bar{l}_p e_r H)$
Q_{uH}	$(H^\dagger H)(\bar{q}_p u_r \widetilde{H})$
Q_{dH}	$(H^\dagger H)(\bar{q}_p d_r H)$

$6: \psi^2 X H + \text{h.c.}$	
Q_{eW}	$(\bar{l}_p \sigma^{\mu\nu} e_r) \sigma^I H W^I_{\mu\nu}$
Q_{eB}	$(\bar{l}_p \sigma^{\mu\nu} e_r) H B_{\mu\nu}$
Q_{uG}	$(\bar{q}_p \sigma^{\mu\nu} T^A u_r) \widetilde{H}\, G^A_{\mu\nu}$
Q_{uW}	$(\bar{q}_p \sigma^{\mu\nu} u_r) \sigma^I \widetilde{H}\, W^I_{\mu\nu}$
Q_{uB}	$(\bar{q}_p \sigma^{\mu\nu} u_r) \widetilde{H}\, B_{\mu\nu}$
Q_{dG}	$(\bar{q}_p \sigma^{\mu\nu} T^A d_r) H\, G^A_{\mu\nu}$
Q_{dW}	$(\bar{q}_p \sigma^{\mu\nu} d_r) \sigma^I H\, W^I_{\mu\nu}$
Q_{dB}	$(\bar{q}_p \sigma^{\mu\nu} d_r) H\, B_{\mu\nu}$

Continued next page.

$7 : \psi^2 H^2 D$	
$Q_{Hl}^{(1)}$	$(H^\dagger i\overleftrightarrow{D}_\mu H)(\bar{l}_p\gamma^\mu l_r)$
$Q_{Hl}^{(3)}$	$(H^\dagger i\overleftrightarrow{D}^I_\mu H)(\bar{l}_p\sigma^I\gamma^\mu l_r)$
Q_{He}	$(H^\dagger i\overleftrightarrow{D}_\mu H)(\bar{e}_p\gamma^\mu e_r)$
$Q_{Hq}^{(1)}$	$(H^\dagger i\overleftrightarrow{D}_\mu H)(\bar{q}_p\gamma^\mu q_r)$
$Q_{Hq}^{(3)}$	$(H^\dagger i\overleftrightarrow{D}^I_\mu H)(\bar{q}_p\sigma^I\gamma^\mu q_r)$
Q_{Hu}	$(H^\dagger i\overleftrightarrow{D}_\mu H)(\bar{u}_p\gamma^\mu u_r)$
Q_{Hd}	$(H^\dagger i\overleftrightarrow{D}_\mu H)(\bar{d}_p\gamma^\mu d_r)$
Q_{Hud} + h.c.	$i(\widetilde{H}^\dagger D_\mu H)(\bar{u}_p\gamma^\mu d_r)$

$8 : (\bar{L}L)(\bar{L}L)$	
Q_{ll}	$(\bar{l}_p\gamma_\mu l_r)(\bar{l}_s\gamma^\mu l_t)$
$Q_{qq}^{(1)}$	$(\bar{q}_p\gamma_\mu q_r)(\bar{q}_s\gamma^\mu q_t)$
$Q_{qq}^{(3)}$	$(\bar{q}_p\gamma_\mu\sigma^I q_r)(\bar{q}_s\gamma^\mu\sigma^I q_t)$
$Q_{lq}^{(1)}$	$(\bar{l}_p\gamma_\mu l_r)(\bar{q}_s\gamma^\mu q_t)$
$Q_{lq}^{(3)}$	$(\bar{l}_p\gamma_\mu\sigma^I l_r)(\bar{q}_s\gamma^\mu\sigma^I q_t)$

$8 : (\bar{R}R)(\bar{R}R)$	
Q_{ee}	$(\bar{e}_p\gamma_\mu e_r)(\bar{e}_s\gamma^\mu e_t)$
Q_{uu}	$(\bar{u}_p\gamma_\mu u_r)(\bar{u}_s\gamma^\mu u_t)$
Q_{dd}	$(\bar{d}_p\gamma_\mu d_r)(\bar{d}_s\gamma^\mu d_t)$
Q_{eu}	$(\bar{e}_p\gamma_\mu e_r)(\bar{u}_s\gamma^\mu u_t)$
Q_{ed}	$(\bar{e}_p\gamma_\mu e_r)(\bar{d}_s\gamma^\mu d_t)$
$Q_{ud}^{(1)}$	$(\bar{u}_p\gamma_\mu u_r)(\bar{d}_s\gamma^\mu d_t)$
$Q_{ud}^{(8)}$	$(\bar{u}_p\gamma_\mu T^A u_r)(\bar{d}_s\gamma^\mu T^A d_t)$

$8 : (\bar{L}L)(\bar{R}R)$	
Q_{le}	$(\bar{l}_p\gamma_\mu l_r)(\bar{e}_s\gamma^\mu e_t)$
Q_{lu}	$(\bar{l}_p\gamma_\mu l_r)(\bar{u}_s\gamma^\mu u_t)$
Q_{ld}	$(\bar{l}_p\gamma_\mu l_r)(\bar{d}_s\gamma^\mu d_t)$
Q_{qe}	$(\bar{q}_p\gamma_\mu q_r)(\bar{e}_s\gamma^\mu e_t)$
$Q_{qu}^{(1)}$	$(\bar{q}_p\gamma_\mu q_r)(\bar{u}_s\gamma^\mu u_t)$
$Q_{qu}^{(8)}$	$(\bar{q}_p\gamma_\mu T^A q_r)(\bar{u}_s\gamma^\mu T^A u_t)$
$Q_{qd}^{(1)}$	$(\bar{q}_p\gamma_\mu q_r)(\bar{d}_s\gamma^\mu d_t)$
$Q_{qd}^{(8)}$	$(\bar{q}_p\gamma_\mu T^A q_r)(\bar{d}_s\gamma^\mu T^A d_t)$

$8 : (\bar{L}R)(\bar{R}L) + \text{h.c.}$	
Q_{ledq}	$(\bar{l}_p^j e_r)(\bar{d}_s q_{tj})$

$8 : (\bar{L}R)(\bar{L}R) + \text{h.c.}$	
$Q_{quqd}^{(1)}$	$(\bar{q}_p^j u_r)\epsilon_{jk}(\bar{q}_s^k d_t)$
$Q_{quqd}^{(8)}$	$(\bar{q}_p^j T^A u_r)\epsilon_{jk}(\bar{q}_s^k T^A d_t)$
$Q_{lequ}^{(1)}$	$(\bar{l}_p^j e_r)\epsilon_{jk}(\bar{q}_s^k u_t)$
$Q_{lequ}^{(3)}$	$(\bar{l}_p^j \sigma_{\mu\nu} e_r)\epsilon_{jk}(\bar{q}_s^k \sigma^{\mu\nu} u_t)$

Table A.1: *The 59 independent baryon number conserving dimension-6 operators built from Standard Model fields, in the notation of [130]. Classes 1-4 constitute the flavor-universal operators, while classes 5-8 are the flavor-dependent operators. The subscripts p, r, s, t are flavor indices, and σ^I are Pauli matrices. For particular operators, not all combinations of flavor indices are independent, see [135].*

Appendix B

Phase Space Integrals

As outlined in Section 4.1, the process of producing a decay rate from the corresponding amplitude requires the calculation of phase-space integrals. Specifically, the processes $h \to f\bar{f}$ at both LO and NLO requires the calculation of 2-body phase-space integrals, while the process $h \to f\bar{f}(g,\gamma)$ requires the calculation of 3-body final state integrals. Generically, an n-body phase-space integral measure takes the form

$$d\phi_n(p_{\text{in}};\{k_i\}) = \left\{\prod_{i=1}^{n}\frac{d^{d-1}\vec{k}_i}{(2\pi)^{d-1}}\frac{1}{2k_i^0}\right\}(2\pi)^d\delta^{(d)}\left(p_{\text{in}}-\sum_{i=1}^{n}k_i\right), \tag{B.0.1}$$

where the first argument specifies the ingoing momenta, while the second argument specifies the set out outgoing momenta. A semicolon is used to separate these momenta of two different types, and where p is used for incoming momenta, while k is used for outgoing momenta to further emphasize this distinction. While the 2-body phase-space integral is somewhat trivial to calculate, the 3-body phase-space integral requires a little more attention. While several numerical integrators exist to numerically calculate such integrals, often utilizing Monte-Carlo methods, we aim to calculate such integrals in an entirely analytic way.

In this section, in the context of the processes considered in this thesis, we first introduce the 2-body phase-space integral, and then introduce the 3-body phase-space integral, paying particular attention to the methods employed to regularize any IR poles.

B.1 2-Body Phase Space

Considering the process $h(p_H) \to f(k_f) + \bar{f}(k_{\bar{f}})$, we may use the 2-body instance of Eq. B.0.1, in d dimensions, such that the 2-body phase-space integral measure takes

the form

$$d\phi_2(p_H;\, k_f,\, k_{\bar{f}}) = \frac{d^{d-1}\vec{k}_f}{(2\pi)^{d-1}}\frac{1}{2k_f^0}\frac{d^{d-1}\vec{k}_{\bar{f}}}{(2\pi)^{d-1}}\frac{1}{2k_{\bar{f}}^0}(2\pi)^d\delta^{(d)}\left(p_H - k_f - k_{\bar{f}}\right)\,, \tag{B.1.1}$$

such that we may define the 2-body phase space integral over the corresponding matrix element to be

$$I_2 = \int d\phi_2(p_H;\, k_f,\, k_{\bar{f}})|\overline{\mathcal{M}}_{h\to f\bar{f}}|^2\,, \tag{B.1.2}$$

where the bar over the matrix element, $\overline{\mathcal{M}}_{h\to f\bar{f}}$, denotes that this matrix element has been summed over final-state spins.

We begin by considering the rest frame of the Higgs. In this frame the particles participating in this process have d-momentum vectors specified by

$$\begin{aligned} p_H &= (m_H,\, \vec{0})\,, \\ k_f &= (k_f^0,\, \vec{k}_f)\,, \\ k_{\bar{f}} &= (k_{\bar{f}}^0,\, \vec{k}_{\bar{f}})\,. \end{aligned} \tag{B.1.3}$$

Recognizing that we may split the momentum-conserving delta function in Eq. B.1.1 into a product of temporal and spatial components as

$$\delta^{(d)}\left(p_{\text{in}} - \sum_i k_i\right) = \delta(m_H - k_f^0 - k_{\bar{f}}^0)\delta^{(d-1)}(-\vec{k}_f - \vec{k}_{\bar{f}})\,, \tag{B.1.4}$$

we see we can immediately perform the integral over either $d\vec{k}_f$ or $d\vec{k}_{\bar{f}}$. Choosing to perform the integral over $d\vec{k}_{\bar{f}}$ brings Eq. B.1.2 into the form

$$I_2 = \frac{\pi^2}{(2\pi)^d}\int_{-\infty}^{+\infty}\frac{d^{d-1}\vec{k}_f}{(k_f^0)^2}\delta(m_H - 2k_f^0)|\overline{\mathcal{M}}_{h\to f\bar{f}}|^2\,. \tag{B.1.5}$$

We now find that it is simplest to perform the integral over $d^{d-1}\vec{k}_f$ by converting this to an integral over the magnitude of $\vec{k}_f$ and a $d-1$ dimensional spherical surface integral as

$$d^{d-1}\vec{k} = d|\vec{k}|d\Omega_{d-1}|\vec{k}|^{d-2}\,, \tag{B.1.6}$$

where

$$d\Omega_d = \sin^{d-2}(\phi_{d-1})\sin^{d-3}(\phi_{d-2})...\sin(\phi_1)d\phi_1...d\phi_{d-1}\,, \tag{B.1.7}$$

where ϕ_1 is defined over the range $[0,\, 2\pi]$, and the remaining angles are defined over the range $[0,\, \pi]$. The $h \to f\bar{f}$ matrix element, and thus also the matrix element

squared, has no angular dependence,[1] and so we may immediately integrate over all angles and use

$$\Omega_{d-1} = \frac{2\pi^{\frac{d-1}{2}}}{\Gamma\left(\frac{d-1}{2}\right)}\,, \tag{B.1.8}$$

such that Eq. B.1.5 now takes the form

$$I_2 = \frac{2^{1-d}\pi^{\frac{3-d}{2}}}{\Gamma\left(\frac{d-1}{2}\right)} \int_0^\infty d|\vec{k}_f| \frac{|\vec{k}_f|^{d-2}}{|\vec{k}_f|^2 + m_f^2} \delta\left(m_H - 2\sqrt{|\vec{k}_f|^2 + m_f^2}\right) |\overline{\mathcal{M}}_{h\to f\bar{f}}|^2\,. \tag{B.1.9}$$

We may then perform the integral over the delta function by applying the identity

$$\delta(f(x)) = \sum_{x_i} \frac{\delta(x - x_i)}{|f'(x_i)|}\,, \tag{B.1.10}$$

where x_i are the zeros of $f(x)$. Applying Eq. B.1.10 brings I_2 into the form

$$I_2 = \frac{2^{1-d}\pi^{\frac{3-d}{2}}}{\Gamma\left(\frac{d-1}{2}\right)} \int_0^\infty d|\vec{k}_f| \frac{|\vec{k}_f|^{d-2}}{|\vec{k}_f|^2 + m_f^2} \left\{\sum_{\pm} \frac{1}{2\beta_f} \delta\left(|\vec{k}_f| \pm \frac{m_H}{2}\beta_f\right)\right\} |\overline{\mathcal{M}}_{h\to f\bar{f}}|^2\,, \tag{B.1.11}$$

where β_f is the function seen in Eq. 4.2.6, and where now its kinematic origins become clear. Performing the final integral over $d|\vec{k}_f|$ gives

$$I_2 = \frac{2^{4-2d}\pi^{\frac{3-d}{2}} m_H^{d-4} \beta^{d-3}}{\Gamma\left(\frac{d-1}{2}\right)} |\overline{\mathcal{M}}_{h\to f\bar{f}}|\,. \tag{B.1.12}$$

In the instance of two massive final-state particles, as is considered here, the phase-space integral results in no IR divergences, and so we are free to simply replace $d \to 4$ in Eq. B.1.12 to produce the simple result

$$I_2 = \frac{\beta_f}{8\pi} |\overline{\mathcal{M}}_{h\to f\bar{f}}|\,. \tag{B.1.13}$$

B.2 3-Body Phase Space

B.2.1 General Phase Space Calculation

We now turn our attention to the 3-body final-state processes also considered in this work, these being $h(p_H) \to f(k_f) + \bar{f}(k_{\bar{f}}) + \gamma(k_\gamma)$ and $h(p_H) \to f(k_f) + \bar{f}(k_{\bar{f}}) + g(k_g)$. For simplicity of notation, in this section we will consider only the former of these two processes, with it understood that the techniques applied here are exactly analogous between the two cases.

[1] A feature which extends to all $1 \to 2$ processes.

To begin, we consider splitting the 3-body phase-space integral as a product of two 2-body phase-space integrals

$$d\phi_3 = \frac{dQ^2}{2\pi} d\phi_2(p_H;\, Q,\, k_\gamma) d\phi_2(Q;\, k_f,\, k_{\bar{f}})\,. \tag{B.2.1}$$

In this way, the fermion anti-fermion pair is considered as an independent 2-body final state system, the energy delivered to which is parameterized by the d-momenta, Q, over which we must integrate over all values. There is also a separate 2-body final state system where we consider the fermion anti-fermion pair as a single component with d-momenta Q, alongside the final-state photon. In total, we write the integral over the 3-body phase space considered here as

$$\begin{aligned} I_3 &= \int \frac{dQ^2}{2\pi} d\phi_2(p_H;\, Q,\, k_\gamma) d\phi_2(Q;\, k_f,\, k_{\bar{f}}) |\overline{\mathcal{M}}_{h\to f\bar{f}\gamma}|^2 \\ &= \int \frac{dQ^2}{2\pi} I_{3.2}\, I_{3.1}\,, \end{aligned} \tag{B.2.2}$$

where

$$\begin{aligned} I_{3.1} &= \int d\phi_2(Q;\, k_f,\, k_{\bar{f}}) |\overline{\mathcal{M}}_{h\to f\bar{f}\gamma}|^2\,, \\ I_{3.2} &= \int d\phi_2(p_H;\, Q,\, k_\gamma) I_{3.1}\,. \end{aligned} \tag{B.2.3}$$

We begin by computing $I_{3.1}$ where we are free to choose the reference frame in which to perform the integral. We choose the frame in which $Q = (Q^0,\, \vec{Q} = \vec{0})$, where the fermion anti-fermion pair are emitted back to back. There are an infinite number of d-momenta configurations which satisfy this condition, of which we are free to choose, and so we use

$$\begin{aligned} p_H &= (p_{\bar{H}}^-, 0, ..., |\vec{p_H}|), \\ k_f &= (p_f^0, 0, ..., |\vec{k}_f| \sin\theta, |\vec{k}_f| \cos\theta), \\ k_{\bar{f}} &= (k_{\bar{f}}^0, 0, ..., -|\vec{k}_{\bar{f}}| \sin\theta, -|\vec{k}_{\bar{f}}| \cos\theta), \\ k_\gamma &= (k_\gamma^0, 0, ..., 0, E_\gamma)\,, \end{aligned} \tag{B.2.4}$$

such that θ is the angle between the fermion, f, and the final-state photon. In this reference frame we may write

$$\begin{aligned} I_{3.1} &= \frac{\pi^2}{(2\pi)^d} \int d^{d-1}\vec{k}_f d^{d-1}\vec{k}_{\bar{f}} \frac{1}{k_f^0 k_{\bar{f}}^0} \delta(Q^0 - k_f^0 - k_{\bar{f}}^0) \delta^{(d-1)}(-\vec{k}_f - \vec{k}_{\bar{f}}) |\overline{\mathcal{M}}_{h\to f\bar{f}\gamma}|^2 \\ &= \frac{\pi^2}{(2\pi)^d} \int d^{d-1}\vec{k}_f \frac{1}{(k_f^0)^2} \delta(Q^0 - 2k_f^0) |\overline{\mathcal{M}}_{h\to f\bar{f}\gamma}|^2\,, \end{aligned} \tag{B.2.5}$$

where in the second line we have performed the integral over $d\vec{k}_{\bar{f}}$ to set $\vec{k}_{\bar{f}} = -\vec{k}_f$.

Similarly to as was seen in Eq. B.1.6 we may write this integral over $d^{d-1}\vec{k}_f$ as a product of an integral over the magnitude of the momenta and an integral over the surface of a $(d-1)$-sphere. However, unlike the case explored in Appendix B.1, in general, the matrix element $\mathcal{M}_{h\to f\bar{f}\gamma}$ is a function of the θ introduced in Eq. B.2.4. As such we can perform the integral over all but one of the angles in $d\Omega_{d-1}$. In particular we use the identity

$$\Omega_{d-1} = \int_0^\pi \frac{2\pi^{(d-2)/2}}{\Gamma(\frac{d-2}{2})} \sin^{d-3}\theta d\theta \,. \tag{B.2.6}$$

Changing variables as prescribed above, and again making use of the identity in Eq. B.1.10 brings $I_{3.1}$ into the form

$$I_{3.1} = \frac{2^{1-d}\pi^{\frac{2-d}{2}}}{\Gamma(\frac{d-2}{2})} \int_0^\infty d|\vec{k}_f| \frac{|\vec{k_f}|^{d-2}}{|\vec{k}_f|^2 + m_f^2} \left\{ \sum_\pm \frac{\delta\left(|\vec{k}_f| \pm \frac{\sqrt{Q^2}}{2}\beta_Q\right)}{2\beta_Q} \right\} \times \int_0^\pi d\theta \sin^{d-3}\theta |\overline{\mathcal{M}}_{h\to f\bar{f}\gamma}|^2 \,, \tag{B.2.7}$$

where we have used that in this frame $(Q^0)^2 = Q^2$ and where

$$\beta_Q = \sqrt{1 - \frac{4m_f^2}{Q^2}} \,. \tag{B.2.8}$$

Performing this final integral over $|\vec{k}_f|$ in $I_{3.1}$ gives

$$I_{3.1} = \frac{2^{4-2d}\pi^{\frac{2-d}{2}}}{\Gamma(\frac{d-2}{2})} (Q^2)^{\frac{d-4}{2}} \beta_Q^{d-3} \int_0^\pi d\theta \sin^{d-3}\theta |\overline{\mathcal{M}}_{h\to f\bar{f}\gamma}|^2 \,. \tag{B.2.9}$$

We now turn to computing $I_{3.2}$ from Eq. B.2.3. This integral takes the form

$$I_{3.2} = \frac{2^{4-2d}\pi^{\frac{2-d}{2}}}{\Gamma(\frac{d-2}{2})} (Q^2)^{\frac{d-4}{2}} \beta_Q^{d-3} \int \frac{d^{d-1}\vec{Q}}{(2\pi)^{d-1}} \frac{d^{d-1}\vec{k}_\gamma}{(2\pi)^{d-1}} \frac{1}{2Q_0} \frac{1}{2k_\gamma^0} (2\pi)^d \times \delta^{(d)}(p_H - Q - k_\gamma) \int_0^\pi d\theta \sin^{d-3}\theta |\overline{\mathcal{M}}_{h\to f\bar{f}\gamma}|^2 \,. \tag{B.2.10}$$

Performing the integral in Eq. B.2.10 introduces no new conceptual difficulties and we may follow the procedure laid out in Appendix B.1 and the previous parts of Appendix B.2.1: we perform the integral over either $d^{d-1}\vec{Q}$ or $d^{d-1}\vec{k}_\gamma$, change to spherical coordinates according to Eq. B.1.6, and apply the identity in Eq. B.1.10 to perform the remaining integral. We note however, that the only angular dependency in $|\overline{\mathcal{M}}_{h\to f\bar{f}\gamma}|$ was already integrated over in $I_{3.1}$ and so we can immediately integrate

over all angles of the $(d-1)$-sphere to find

$$I_{3.2} = \frac{2^{5-3d}\pi^{2-d}m_H^{2-d}}{\Gamma(d-2)}(Q^2)^{\frac{d-4}{2}}\beta_Q^{d-3}(m_H^2-Q^2)^{d-3}\int_0^\pi d\theta \sin^{d-3}\theta|\overline{\mathcal{M}}_{h\to f\bar{f}\gamma}|^2\,. \quad \text{(B.2.11)}$$

Finally, as we interpret Q^2 as the (squared) energy imparted to the fermion anti-fermion pair, the minimum amount of energy they can receive is enough to produce them stationary such that $Q^2 = 4m_f^2$, and the maximum amount of energy the fermion pair can receive is when the final-state photon receives no energy from the decaying Higgs (soft-photon limit), such that $Q^2 = m_H^2$. With this we can finally write this 3-body phase-space integral as

$$I_3 = \frac{2^{4-3d}\pi^{1-d}m_H^{2-d}}{\Gamma(d-2)}\int_{4m_f^2}^{m_H^2} dQ^2 \int_0^\pi d\theta (Q^2)^{\frac{d-4}{2}}\beta_Q^{d-3}(m_H^2-Q^2)^{d-3}\sin^{d-3}\theta|\overline{\mathcal{M}}_{h\to f\bar{f}\gamma}|^2\,. \quad \text{(B.2.12)}$$

B.2.2 Phase Space Slicing

Some momentum structures present in the squared amplitude $|\overline{\mathcal{M}}_{h\to f\bar{f}\gamma}|^2$ result in IR-poles when computing the 3-body phase-space integral as in Eq. B.2.12. As stated, these IR poles manifest in the soft-photon limit, equivalent to $Q^2 \to m_H^2$ in the context of Eq. B.2.12. In order to regulate these poles, like as was adopted in Section 1.2.2, we deform the number of dimensions so $d = 4-2\varepsilon$, such that the integral is regularized by a $1/\varepsilon$ pole. While computationally different, the techniques presented throughout this section are conceptually similar to those outlined in [141], and produce identical results, as found by our agreement with the results in [128] which applies the same methods.

The momentum structures leading to IR-divergences originate from a subset of real-emission diagrams. For such momentum structures, after integrating over θ in Eq. B.2.12, this integral takes the form

$$I = \int_0^{\beta_f} d\beta_Q \frac{1}{(\beta_f-\beta_Q)^{1+2\varepsilon}} f(\beta_Q)\,, \quad \text{(B.2.13)}$$

where we have changed variable such that the integration variable is now β_Q defined in Eq. B.2.8, where the IR-divergent nature of the squared amplitude is present in the $(\beta_f-\beta_Q)^{-1-2\varepsilon}$ term (which we call the divergent component), and where $f(\beta_Q)$ is some generic function which is finite over the limits of integration. We call $f(\beta_Q)$ the non-divergent component. To compute this integral we split the integration

range into a soft and hard region according to

$$\begin{aligned} \text{Hard:} \quad & 0 \leq \beta_Q \leq \beta_C \,, \\ \text{Soft:} \quad & \beta_C \leq \beta_Q \leq \beta_f \,, \end{aligned} \tag{B.2.14}$$

where β_C is a parameter separating the soft and hard regions. We further impose that β_C should be very close to the soft limit, β_f. As such, we may write the integral in Eq. B.2.13 as

$$\begin{aligned} I &= \int_{\beta_C}^{\beta_f} d\beta_Q \frac{1}{(\beta_f - \beta_Q)^{1+2\varepsilon}} f(\beta_Q) + \int_0^{\beta_C} d\beta_Q \frac{1}{(\beta_f - \beta_Q)^{1+2\varepsilon}} f(\beta_Q) \\ &= \left(\int_{\beta_C}^{\beta_f} d\beta_Q \frac{1}{(\beta_f - \beta_Q)^{1+2\varepsilon}} \right) \left[f(\beta_Q) \Big|_{\beta_Q \to \beta_f} \right] + \int_0^{\beta_C} d\beta_Q \frac{1}{(\beta_f - \beta_Q)^{1+2\varepsilon}} f(\beta_Q) \,. \end{aligned} \tag{B.2.15}$$

For the hard region, identified as the second term in both lines of Eq. B.2.15, analytical solutions exist for all $f(\beta_Q)$ that emerge in the process $h \to f\bar{f}(g, \gamma)$. We identify the soft region to be the first term on both lines of Eq. B.2.15. From the first line of Eq. B.2.15, we find that in this small region of integration the divergent component formally diverges while the non-divergent component remains static in the limit $\beta_C \to \beta_f$, hence we recover the form of the soft region of integration in the second line of Eq. B.2.15. Computing the integral in the soft region we find

$$I = -\frac{(\beta_f - \beta_C)^{-2\varepsilon}}{2\varepsilon} \left[f(\beta_Q) \Big|_{\beta_Q \to \beta_f} \right] + \int_0^{\beta_C} d\beta_Q \frac{1}{(\beta_f - \beta_Q)^{1+2\varepsilon}} f(\beta_Q) \,, \tag{B.2.16}$$

where the IR pole is now explicitly separated. As I should not be a function of the exact position of the split between the soft and hard regions, parameterized by β_C, we find that the β_C dependence in the soft and hard regions cancels between the sum of these two regions.

Appendix C

Feynman Diagram Subsets

C.1 QED-QCD Diagrams

In this section we present the subset of QED-QCD diagrams contributing to the processes considered in this work. Analytic results for these corrections are found in Section 4.4.1. In Fig. C.1 we give the QED corrections, while in Fig. C.2 we give the QCD corrections. As for the QED-QCD analytic results, we need not distinguish between the final-state fermion pairs in these diagrams, except to note that the QCD diagrams in Fig. C.2 only apply to final-state quark pairs. We report the first of these sets of diagrams overleaf.

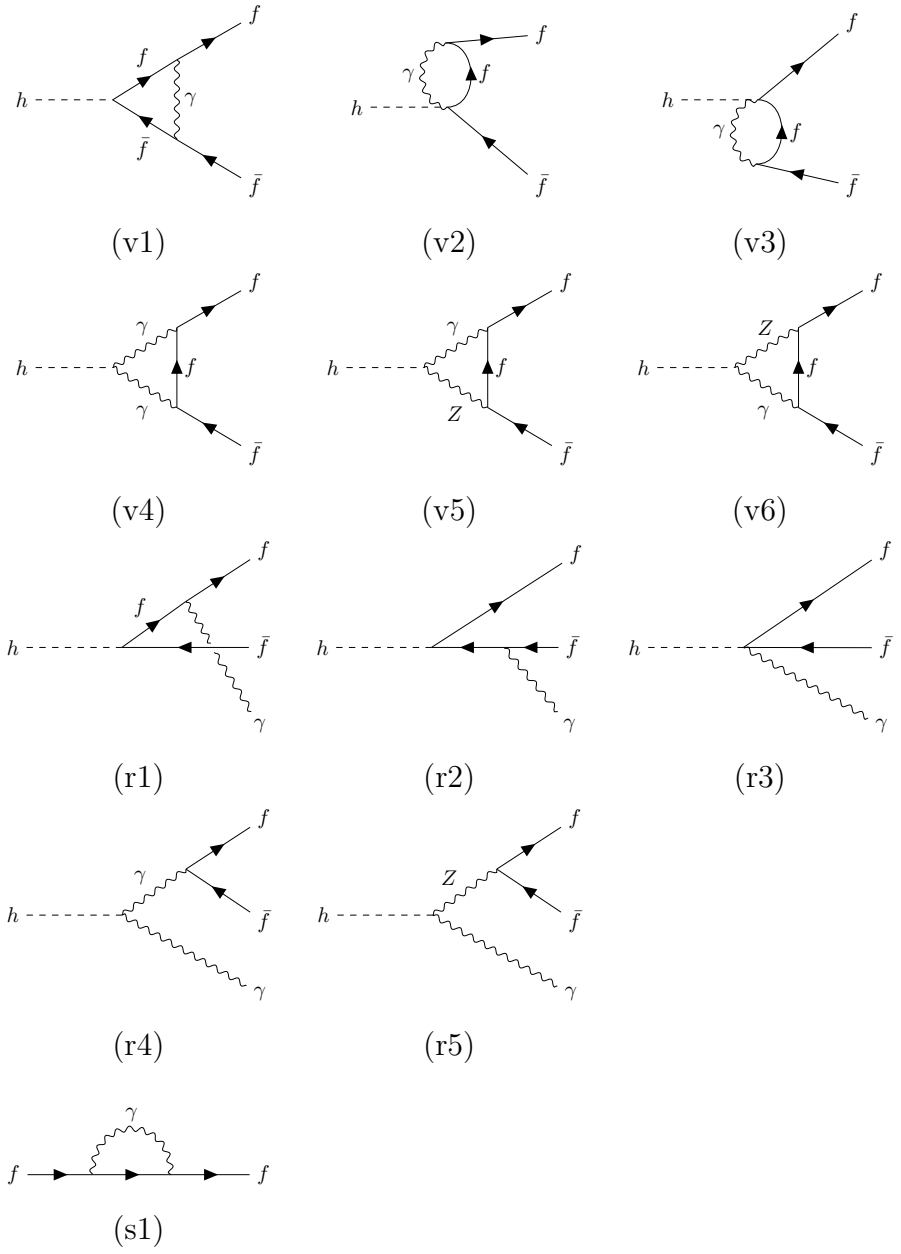

Figure C.1: *Diagrams showing the virtual (vi), real (ri), and self-energy (si) corrections from photons to the process $h \to f\bar{f}(\gamma)$. There is no visual distinction in these diagrams between SM vertices and dimension-6 effective vertices. Each diagram contains at most one dimension-6 SMEFT operator insertion. For the virtual corrections, (v1) receives SM contributions, as well as contributions from operators appearing in the LO decay rate, (v1-3) has Q_{fB}, Q_{fW} and their hermitian conjugate operator insertions, and (v4-6) receives contributions from the class-4 operators Q_{HB}, Q_{HW}, and Q_{HWB}. For the real corrections, (r1-2) receives SM contributions and contributions from operators appearing in the LO decay rate, (r1-3) has operator insertions from Q_{fB}, Q_{fW}, and their hermitian conjugates, and (r4-5) also has contributions from the class-4 operators listed above. The only QED self-energy diagram is shown in (s1), which receives SM as well as Q_{fB}, Q_{fW} and their hermitian conjugate contributions.*

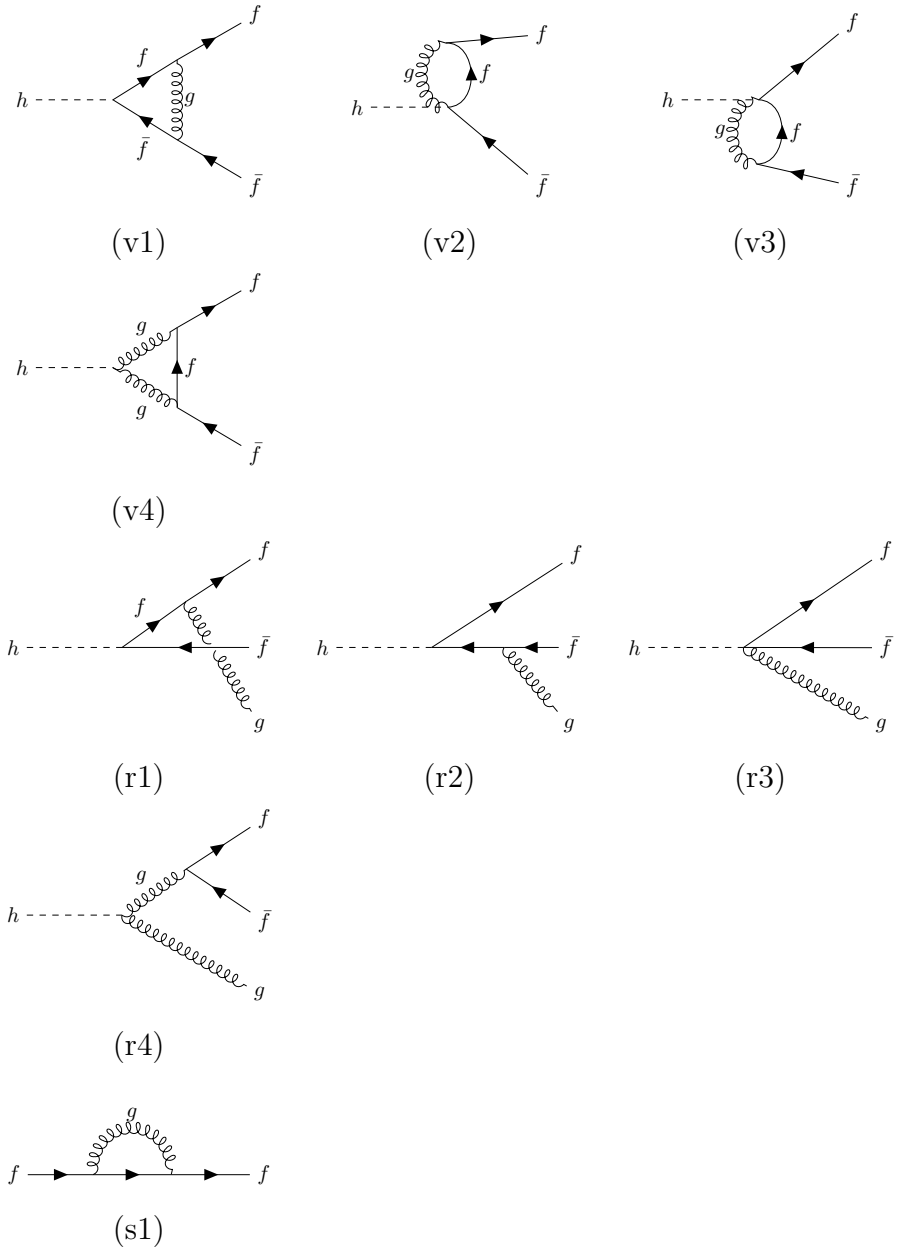

Figure C.2: *Diagrams showing the virtual (vi), real (ri), and self-energy (si) corrections from photons to the process $h \to f\bar{f}(g)$. There is no visual distinction in these diagrams between SM vertices and dimension-6 effective vertices. Each diagram contains at most one dimension-6 SMEFT operator insertion. For the virtual corrections, (v1) receives SM contributions, as well as contributions from operators appear in the LO decay rate, (v1-3) has Q_{fG} and its hermitian conjugate operator insertions, and (v4) receives contributions from the class-4 operators Q_{HG}. For the real corrections, (r1-2) receives SM contributions and contributions from operators appearing in the LO decay rate, (r1-3) has operator insertions from Q_{fG} and its hermitian conjugate, and (r4) also has contributions from the class-4 operator C_{HG}. The only contributing QCD self-energy diagram is shown in (s1), which receives SM as well as Q_{fG} and its hermitian conjugate contributions.*

C.2 Large m_t-Limit Diagrams

In this section we present the subset of diagrams contributing to the large-m_t limit subset of results, the analytical results for which are reported in Section 4.4.2. In Fig. C.3 we report the diagrams that contribute only to the process $h \to b\bar{b}$, while in Fig. C.4 we report the diagrams that contribute to $h \to f\bar{f}$ for all light fermions, including $f = b$.

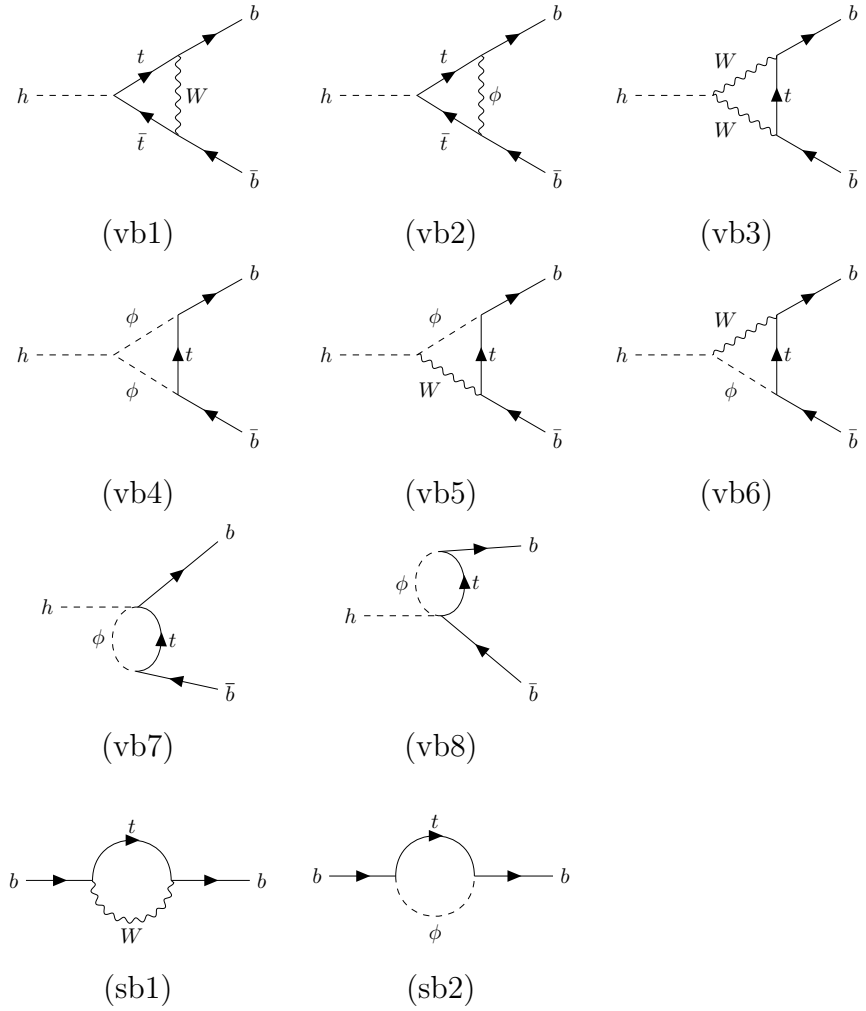

Figure C.3: *Diagrams unique to the process $h \to b\bar{b}$ contributing to the large-m_t from (vb1-9): the virtual corrections and (sb1-2): the two-point functions necessary for UV renormalization. Additional contributing diagrams that are not unique to $h \to b\bar{b}$ can be found in Fig. C.4. There is no distinction in the diagrams between a SM vertex and a dimension-6 effective vertex, but each diagram contains at most one dimension-6 SMEFT operator insertion.*

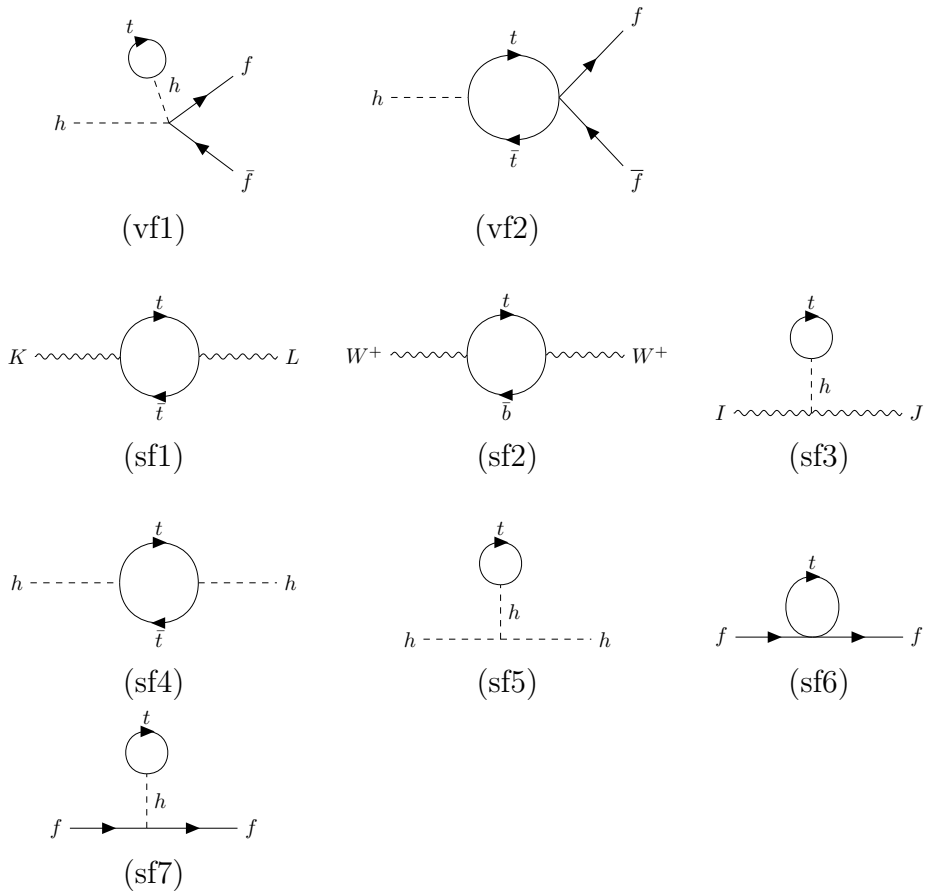

Figure C.4: *Diagrams contributing to the large-m_t corrections of the process $h \to f\bar{f}$ for all light fermions (including $f = b$) from (vf1-2): the virtual corrections and (sf1-7): the two-point functions necessary for UV renormalization. In these diagrams $KL = \{\gamma\gamma, ZZ, \gamma Z\}$ and $IJ = \{\gamma\gamma, ZZ, \gamma Z, WW\}$. There is no distinction in the diagrams between a SM vertex and a dimension-6 effective vertex, but each diagram contains at most one dimension-6 SMEFT operator insertion.*

Appendix D

Numerical Results for $h \to \mu\bar{\mu}$

In this section we report the numerical results for $h \to \mu\overline{\mu}$, including the analysis of scale uncertainties, which were omitted from the body of this work.

D.1 Results at $\mu = m_H$

For $h \to \mu\bar{\mu}$, using the values reported in Table 4.2 and setting $\mu = m_H$ we find that the LO expression in Eq. 4.6.2 takes the form seen in Eq. 4.6.5 with appropriate replacements, while the NLO expression in Eq. 4.6.2 evaluates to

$$\begin{aligned}
\Delta_\mu^{\rm NLO}(m_H) = 0.98 + \frac{(\overline{v}^{(\ell)})^2}{\Lambda^2_{\rm NP}}\Bigg\{ & 3.49\tilde{C}_{HWB} + 2.11\tilde{C}_{H\Box} - 1.50\frac{\overline{v}^{(\ell)}}{\overline{m}_\mu^{(\ell)}}\tilde{C}_{\mu H} + 1.20\tilde{C}_{HD} \\
& + 0.41\tilde{C}_{HB} + 0.14\tilde{C}_{HW} + \Bigg[- 9.0\tilde{C}^{(3)}_{\substack{Hq\\33}} - 7.9\tilde{C}_{Ht} + 5.2\tilde{C}^{(1)}_{\substack{Hq\\33}} - 4.6\tilde{C}_{tH} \\
& - 3.8\frac{m_t}{\overline{m}_\mu^{(\ell)}}\tilde{C}^{(1)}_{\substack{lequ\\2233}} + 2.4\tilde{C}_H + 2.0\left(\frac{\overline{m}_b^{(\ell)}}{\overline{m}_\mu^{(\ell)}}\tilde{C}_{\substack{ledq\\2233}} - \frac{\overline{m}_c^{(\ell)}}{\overline{m}_\mu^{(\ell)}}\tilde{C}^{(1)}_{\substack{lequ\\2222}} + \frac{\overline{m}_s^{(\ell)}}{\overline{m}_\mu^{(\ell)}}\tilde{C}_{\substack{ledq\\2222}}\right) \\
& + 1.5\tilde{C}^{(3)}_{\substack{Hl\\22}} - 1.0\left(\tilde{C}_{\substack{le\\2222}} + \frac{\overline{m}_\tau^{(\ell)}}{\overline{m}_\mu^{(\ell)}}\tilde{C}_{\substack{le\\2332}}\right)\Bigg] \times 10^{-2} + \Bigg[- 9\Bigg(\frac{\tilde{C}_{tB}}{\overline{e}^{(\ell)}} + \tilde{C}^{(3)}_{\substack{Hq\\11}} + \tilde{C}^{(3)}_{\substack{Hq\\22}} \\
& - \tilde{C}^{(1)}_{\substack{Hl\\22}} + \tilde{C}_{Hu} + \tilde{C}_{Hc}\Bigg) - 7\tilde{C}_W + 4\Bigg(\tilde{C}^{(1)}_{\substack{Hl\\11}} + \tilde{C}^{(1)}_{\substack{Hl\\33}} + \tilde{C}_{He} + \tilde{C}_{H\tau} - \tilde{C}^{(1)}_{\substack{Hq\\11}} - \tilde{C}^{(1)}_{\substack{Hq\\22}} \\
& + \tilde{C}_{Hd} + \tilde{C}_{Hs} + \tilde{C}_{Hb}\Bigg) - 3\left(\tilde{C}^{(3)}_{\substack{Hl\\11}} + \tilde{C}^{(3)}_{\substack{Hq\\22}}\right) + 2\frac{\tilde{C}_{tW}}{\overline{e}^{(\ell)}} + \frac{\overline{v}^{(\ell)}}{\overline{m}_\mu^{(\ell)}}\frac{\tilde{C}_{\mu W}}{\overline{e}^{(\ell)}}\Bigg] \times 10^{-3} \\
& + (4 \times 10^{-4})\left(\tilde{C}_{H\mu} - \frac{\overline{v}^{(\ell)}}{\overline{m}_\mu^{(\ell)}}\frac{\tilde{C}_{\mu B}}{\overline{e}^{(\ell)}}\right)\Bigg\}. \qquad \text{(D.1.1)}
\end{aligned}$$

In Table D.1 we also report the analogous results to those for in Table 4.3 for the process $h \to \mu\bar{\mu}$.

$h \to \mu\bar{\mu}$	SM	$\tilde{C}_{HWB}$	$\tilde{C}_{H\Box}$	$\frac{\overline{v}^{(\ell)}}{\overline{m}_{\mu}^{(\ell)}}\tilde{C}_{\mu H}$	$\tilde{C}_{HD}$
NLO QED	1.1%	-4.9 %	1.1%	1.1%	1.1%
NLO large-m_t	-1.1%	-0.7%	5.1%	4.4%	-4.4%
NLO remainder	-1.7%	-0.8%	-0.7%	0.8%	-0.6%
NLO correction	-1.7%	-6.4%	5.5%	6.3%	-3.9%

Table D.1: *Size of the NLO corrections for the process $h \to \mu\bar{\mu}$ split into QED, large-m_t and remainder corrections for the SM and the coefficients appearing in the LO decay rate.*

D.2 Scale Uncertainties

Here we report the scale uncertainties related to the process $h \to \mu\bar{\mu}$, using the quadrature method outlined in Section 4.6.2. Keeping only terms that contribute at the 5% level or more on the extreme values of their uncertainties, at LO we find

$$\begin{aligned}\Delta_{\mu}^{\rm LO}(m_H, m_H) = (1^{+0.002}_{-0.003}) + \frac{(\overline{v}^{(\ell)})^2}{\Lambda^2_{\rm NP}}\Big\{ \\ (3.74 \pm 0.14)\tilde{C}_{HWB} + (2.00 \pm 0.12)\tilde{C}_{H\Box} - (1.41 \pm 0.06)\frac{\overline{v}}{\overline{m}_{\mu}^{(\ell)}}\tilde{C}_{\mu H} \\ + (1.24 \pm 0.09)\tilde{C}_{HD} \pm 0.19\tilde{C}^{(1)}_{\substack{Hq \\ 33}} \pm 0.18\tilde{C}_{Ht} \pm 0.09\frac{m_t}{\overline{m}_{\mu}^{(\ell)}}\tilde{C}^{(1)}_{\substack{lequ \\ 2233}} \\ \pm 0.05\tilde{C}_{tH} \pm 0.05\tilde{C}^{(3)}_{\substack{Hq \\ 33}} + \dots \Big\}, \end{aligned} \tag{D.2.1}$$

while at NLO we find

$$\begin{aligned}\Delta_{\mu}^{\rm NLO}(m_H, m_H) = (0.98^{+0.0001}_{-0.0002}) + \frac{(\overline{v}^{(\ell)})^2}{\Lambda^2_{\rm NP}}\Big\{ \\ (3.49^{+0.00}_{-0.01})\tilde{C}_{HWB} + (2.11^{+0.00}_{-0.02})\tilde{C}_{H\Box} + (-1.50^{+0.01}_{-0.00})\frac{\overline{v}}{\overline{m}_{\mu}^{(\ell)}}\tilde{C}_{\mu H} + (1.20^{+0.00}_{-0.01})\tilde{C}_{HD} \\ + (0.41^{+0.01}_{-0.01})\tilde{C}_{HB} + (0.14^{+0.00}_{-0.00})\tilde{C}_{HW} + (-0.09^{+0.02}_{-0.00})\tilde{C}^{(3)}_{\substack{Hq \\ 33}} + (-0.08^{+0.03}_{-0.00})\tilde{C}_{Ht} \\ + (0.05^{+0.00}_{-0.03})\tilde{C}^{(1)}_{\substack{Hq \\ 33}} + (-0.05^{+0.01}_{-0.00})\tilde{C}_{tH} + \dots \Big\}. \end{aligned} \tag{D.2.2}$$

Appendix E

Select Full Mass Dependent Results

In this section we report the QED-QCD and four-fermion operator subsets of results, while retaining full mass dependence, which were reported in Sections 4.4.1 and 4.4.3 in the small-mass limit.

E.1 QED-QCD

Here, we report the full mass dependent results for the QED-QCD corrections. The small-mass limit results are listed in Section 4.4.1. We closely follow the presentation of the results Section 4.4.1, again allowing the reader to switch between the on-shell scheme and the hybrid renormalization scheme by setting $c_{m_f} = 0$ or $c_{m_f} = 1$ as defined in Eq. 4.3.14. We also make use of the expressions in Eq. 4.4.1, where these quantities now retain their full mass dependence. The reader may also recover the results in the recommended decoupled hybrid renormalization scheme by making use of the expression in Eq. 4.5.29. In order to simplify the results as much as possible, we will make use of the functions

$$\beta_f = \sqrt{1 - \frac{4m_f^2}{m_H^2}}\,, \qquad x_f = \frac{1-\beta_f}{1+\beta_f}, \qquad y_f = \frac{1-\beta_f^2}{4} = \frac{m_f^2}{m_H^2}\,,$$
$$z = \frac{M_Z^2}{m_H^2}\,, \quad \hat{\mu} = \frac{\mu}{m_H}\,. \tag{E.1.1}$$

In the SM, the on-shell scheme result may be written as a function of the hybrid renormalization scheme results in the exact same way as for the small-mass results seen in Eq. 4.4.2, with $\delta f^{(4)}_{(g,\gamma)}$ taking the same form as in Eq. 4.4.3. The NLO SM

result in the hybrid renormalization scheme is

$$\begin{aligned}\overline{\Gamma}^{(4,1)}_{f,(g,\gamma)} = \overline{\Gamma}^{(4,0)}_{f}\left(\frac{C_F\alpha_s\delta_{f,q}+Q_f^2\alpha}{\pi}\right)\frac{1}{\beta_f^3}\Bigg\{&\frac{3\beta_f}{8}\left(-1+7\beta_f^2\right)+\beta_f^3\left(3\ln(y_f)-4\ln(\beta_f)\right)\\&+\ln(x_f)\left[\frac{1}{16}\left(-3-34\beta_f^2+13\beta_f^4\right)+\beta_f^2(1+\beta_f^2)\left(-\frac{3}{2}\ln(y_f)+2\ln(\beta_f)\right)\right]\\&+\beta_f(1+\beta_f^2)\left[\frac{3}{2}\ln^2(x_f)+2\mathrm{Li}_2(x_f)+\mathrm{Li}_2(x_f^2)\right]+2\beta_f^3\left(1+\frac{3}{4}\ln\left(\frac{\mu^2}{m_f^2}\right)\right)\Bigg\}.\end{aligned} \tag{E.1.2}$$

The dimension-6 contribution differs from the form found in Eq. 4.4.4 and is instead given by

$$\Gamma^{(6,1)}_{f,(g,\gamma)} = \overline{\Gamma}^{(6,1)}_{f,(g,\gamma)} + 2c_{m_f}\Gamma^{(4,0)}_f\left[\delta f^{(4)}_{(g,\gamma)}\left(\frac{\hat{v}_T^2}{\sqrt{2}}C_{fH}+\frac{\Gamma^{(6,0)}_f}{\Gamma^{(4,0)}_f}\right)+\delta f^{(6)}_{(g,\gamma)}\right], \tag{E.1.3}$$

where

$$\delta f^{(6)}_{(g,\gamma)} = -\frac{\hat{v}_T m_f}{\sqrt{2}\pi}\left[\frac{\alpha_s C_F}{g_3}C_{cG}+\frac{\alpha Q_f}{e}\left(C_{cB}\hat{c}_w+C_{cW}\hat{s}_w\right)\right]\left(1+3\ln\left(\frac{\mu^2}{m_f^2}\right)\right). \tag{E.1.4}$$

The dimension-6 NLO corrections in the hybrid renormalization scheme are given by

$$\begin{aligned}\overline{\Gamma}^{(6,1)}_{f,(g,\gamma)} = \overline{\Gamma}^{(6,0)}_{f}\frac{\overline{\Gamma}^{(4,1)}_{f,(g,\gamma)}}{\overline{\Gamma}^{(4,0)}_{f}}+\frac{\hat{v}_T^2}{\pi}\overline{\Gamma}^{(4,0)}_{f}\Bigg\{&\frac{m_H^2}{\sqrt{2}\hat{v}_T m_f\beta_f^3}\Bigg(\delta_{f,q}\frac{C_F}{g_3}\alpha_s C_{fG}\\&+\frac{Q_f}{e}\alpha(C_{fB}\hat{c}_w+2T_f^3C_{fW}\hat{s}_w)\Bigg)\Bigg[\frac{\beta_f}{8}(15+4\beta_f^2-39\beta_f^4)\\&+\frac{3}{16}(1-\beta_f^2)\left((5+2\beta_f^2+17\beta_f^4)\ln(x_f)-24\beta_f^3\ln(y_f)\right)\\&+\frac{9}{2}(1-\beta_f^2)\ln\left(\frac{\mu^2}{m_H^2}\right)\Bigg]+\left(\delta_{f,q}C_F\alpha_s C_{HG}+Q_f^2\alpha c_{h\gamma\gamma}\right)\frac{1}{\beta_f^3}\Bigg[\frac{\beta_f}{2}(15-2\pi^2\beta_f\\&+23\beta_f^2)+\frac{1}{4}\Big(15+2\beta_f^2+7\beta_f^4-12\beta_f^2\ln(x_f)\Big)\ln(x_f)\\&+2\beta_f^2\Big(-3\beta_f+2\ln(x_f)\Big)\ln(y_f)+2\beta_f^2\left(6\mathrm{Li}(x_f)-\mathrm{Li}(x_f^2)\right)+6\beta_f^3\ln\left(\frac{\mu^2}{m_H^2}\right)\Bigg]\\&+c_{h\gamma Z}v_f Q_f\alpha F_{h\gamma Z}\left(z,\frac{\mu^2}{m_H^2},y_f\right)\Bigg\},\end{aligned} \tag{E.1.5}$$

where $c_{h\gamma\gamma}$ was reported in Eq. 4.3.27, $c_{h\gamma Z}$ was reported in Eq. 4.4.6 and where v_f is the vector coupling of fermions to the Z-boson. The function $F_{h\gamma Z}$ was fist reported in the small-mass limit in Eq. 4.4.7; here we report its full mass dependent form,

given by

$$
\begin{aligned}
F_{h\gamma Z}\left(z,\hat{\mu}^2,y_f\right) = {} & \frac{3}{4}\beta_f(8z-5) - \beta_f^3\left(\frac{39}{4}+\frac{z}{y_f}\right) - \frac{4}{3}\beta_f^2\pi^2\overline{z} + \frac{4}{3}\pi^2 z\overline{z} \\
& + 6\beta_f\left(\beta_f^2 - \frac{2}{3}z + \frac{(2y_f-\beta_f^2)z^2}{12y_f^2}\right)\ln(y_f) + 2(\beta_f^2-z)\overline{z}\ln(x_z)^2 \\
& - 4\beta_z z\overline{z}\ln(x_{\beta z}) + \ln(x_f)\Bigg[-\frac{1}{8}\Big(15+7\beta_f^4+8z(4z-7) \\
& + \beta_f^2(2+8z)\Big) + 2(z-\beta_f^2)\overline{z}\ln(x_z) + 4(\beta_f^2-z)\overline{z}\ln(1-x_f x_z) \\
& + 2(\beta_f^2-z)\overline{z}\ln(x_{\beta z})\Bigg] + \ln(x_z)\Bigg[\frac{\beta_f\beta_z z\left(\beta_f^2(2y_f+z)-2y_f z\right)}{2y_f^2} \\
& + 2(z-\beta_f^2)\overline{z}\ln(x_{\beta z})\Bigg] + 4\beta_f z\overline{z}\ln(\overline{z}) + \frac{\beta_f^3(\beta_f^2+2y_f)z^2\ln(z)}{2y_f^2} \\
& - 6\beta_f^3\ln\left(\hat{\mu}^2\right) + 4(\beta_f^2-z)\overline{z}\left(\mathrm{Li}_2\left(\frac{x_f}{x_z}\right) + \mathrm{Li}_2\left(x_f x_z\right)\right), \qquad \text{(E.1.6)}
\end{aligned}
$$

where

$$
\beta_z = \sqrt{1-\frac{4m_f^2}{M_Z^2}}, \quad x_z = \frac{1-\beta_z}{1+\beta_z}, \quad x_{\beta z} = \frac{\beta_f-\beta_z}{\beta_f+\beta_z}, \quad \overline{z} = 1-z\,. \qquad \text{(E.1.7)}
$$

Taking the small-mass limit of the results reported throughout this section we recover the results found throughout Section 4.4.1, as expected.

E.2 Four-Fermion Results

Here we present the full mass dependent dimension-6 SMEFT decay rate arising from the four-fermion operators, found in class 8 of Table A.1. The form of these results in the small-mass limit may be found in Section 4.4.3. We again present results without reference to any particular renormalization scheme, but allow the reader to choose a renormalization scheme through the choice of $\overline{c}_{m_f}$, defined below Eq. 4.4.10. The conversion to the recommended decoupled hybrid renormalization scheme, defined in Eq. 4.5.24 and equivalently in Eq. 4.5.27, may be performed using the simple conversion in Eq. 4.5.31.

We again split the result as

$$
\overline{\Gamma}^{(6,1)}_{f,(4\mathrm{F})} = \Gamma^{(6,1)}_{f,(4\mathrm{F})} - 2\Gamma^{(4,0)}_f \overline{c}_{m_f}\delta f^{(6)}_{(4\mathrm{F})}\,. \qquad \text{(E.2.1)}
$$

Keeping full mass dependence, the functions $\delta f^{(6)}_{(4\mathrm{F})}$ defined in Eq. 4.4.1 now read

$$
\begin{aligned}
\delta b^{(6)}_{(4\mathrm{F})} &= \frac{1}{16\pi^2 m_b}\Bigg\{ -2m_b^3\left[C^{(1)}_{\substack{qd\\3333}} + C_F C^{(8)}_{\substack{qd\\3333}}\right]\left(1+2\ln\left(\frac{\mu^2}{m_b^2}\right)\right)\\
&\quad -2m_s^3\left[C^{(1)}_{\substack{qd\\2332}} + C_F C^{(8)}_{\substack{qd\\2332}}\right]\left(1+2\ln\left(\frac{\mu^2}{m_s^2}\right)\right) + m_t^3\Bigg[(1+2N_c)C^{(1)}_{\substack{quqd\\3333}}\\
&\quad + C_F C^{(8)}_{\substack{quqd\\3333}}\Bigg]\left(1+\ln\left(\frac{\mu^2}{m_t^2}\right)\right) + m_c^3\Bigg[C^{(1)}_{\substack{quqd\\3223}} + C_F C^{(8)}_{\substack{quqd\\3223}} + 2N_c C^{(1)}_{\substack{quqd\\2233}}\Bigg]\\
&\quad \times\left(1+\ln\left(\frac{\mu^2}{m_c^2}\right)\right) + 2m_\tau^3 C_{\substack{ledq\\3333}}\left(1+\ln\left(\frac{\mu^2}{m_\tau^2}\right)\right)\\
&\quad + 2m_\mu^3 C_{\substack{ledq\\2233}}\left(1+\ln\left(\frac{\mu^2}{m_\mu^2}\right)\right)\Bigg\},\\
\delta c^{(6)}_{(4\mathrm{F})} &= \frac{1}{16\pi^2 m_c}\Bigg\{ -2m_c^3\left[C^{(1)}_{\substack{qu\\2222}} + C_F C^{(8)}_{\substack{qu\\2222}}\right]\left(1+2\ln\left(\frac{\mu^2}{m_c^2}\right)\right)\\
&\quad -2m_t^3\left[C^{(1)}_{\substack{qu\\2332}} + C_F C^{(8)}_{\substack{qu\\2332}}\right]\left(1+2\ln\left(\frac{\mu^2}{m_t^2}\right)\right) + m_b^3\Bigg[C^{(1)}_{\substack{qu\\3223}} + C_F C^{(8)}_{\substack{quqd\\3223}}\\
&\quad + 2N_c C^{(1)}_{\substack{quqd\\2233}}\Bigg]\left(1+\ln\left(\frac{\mu^2}{m_b^2}\right)\right) + m_s^3\Bigg[(1+2N_c)C^{(1)}_{\substack{qu\\2222}} + C_F C^{(8)}_{\substack{quqd\\2222}}\Bigg]\\
&\quad \times\left(1+\ln\left(\frac{\mu^2}{m_c^2}\right)\right) - 2m_\tau^3 C^{(1)}_{\substack{lequ\\3322}}\left(1+\ln\left(\frac{\mu^2}{m_\tau^2}\right)\right)\\
&\quad - 2m_\mu^3 C^{(1)}_{\substack{lequ\\2222}}\left(1+\ln\left(\frac{\mu^2}{m_\mu^2}\right)\right)\Bigg\},\\
\delta\tau^{(6)}_{(4\mathrm{F})} &= \frac{1}{16\pi^2 m_\tau}\Bigg\{ -2m_\tau^3 C_{\substack{le\\3333}}\left(1+2\ln\left(\frac{\mu^2}{m_\tau^2}\right)\right) - 2m_\mu^3 C_{\substack{le\\2332}}\left(1+2\ln\left(\frac{\mu^2}{m_\mu^2}\right)\right)\\
&\quad - 2N_c m_t^2 C^{(1)}_{\substack{lequ\\3333}}\left(1+\ln\left(\frac{\mu^2}{m_t^2}\right)\right) + 2N_c m_b^3 C_{\substack{ledq\\3333}}\left(1+2\ln\left(\frac{\mu^2}{m_b^2}\right)\right)\\
&\quad - 2N_c m_c^3 C^{(1)}_{\substack{lequ\\3322}}\left(1+2\ln\left(\frac{\mu^2}{m_c^2}\right)\right) + 2N_c m_s^3 C_{\substack{ledq\\3322}}\left(1+2\ln\left(\frac{\mu^2}{m_s^2}\right)\right)\Bigg\},\\
\delta\mu^{(6)}_{(4\mathrm{F})} &= \frac{1}{16\pi^2 m_\mu}\Bigg\{ -2m_\mu^3 C_{\substack{le\\2222}}\left(1+2\ln\left(\frac{\mu^2}{m_\mu^2}\right)\right) - 2m_\tau^3 C_{\substack{le\\2332}}\left(1+2\ln\left(\frac{\mu^2}{m_\tau^2}\right)\right)\\
&\quad - 2N_c m_t^2 C^{(1)}_{\substack{lequ\\2233}}\left(1+\ln\left(\frac{\mu^2}{m_t^2}\right)\right) + 2N_c m_b^3 C_{\substack{ledq\\2233}}\left(1+2\ln\left(\frac{\mu^2}{m_b^2}\right)\right)\\
&\quad - 2N_c m_c^3 C^{(1)}_{\substack{lequ\\2222}}\left(1+2\ln\left(\frac{\mu^2}{m_c^2}\right)\right) + 2N_c m_s^3 C_{\substack{ledq\\2222}}\left(1+2\ln\left(\frac{\mu^2}{m_s^2}\right)\right)\Bigg\}. \qquad \text{(E.2.2)}
\end{aligned}
$$

We again introduce notation to simplify the results via the functions

$$
\begin{aligned}
G_{8S}\left(\frac{m_f^2}{m_H^2},\frac{\mu^2}{m_H^2}\right) &= \beta_f^2\left(2+\beta_f\ln(x_f)-\ln(y_f)+\ln\left(\frac{\mu^2}{m_H^2}\right)\right),\\
G_{8V}\left(\frac{m_f^2}{m_H^2},\frac{\mu^2}{m_H^2}\right) &= -2\beta_f^2\left(3+\beta_f\ln(x_f)-2\ln(y_f)+2\ln\left(\frac{\mu^2}{m_H^2}\right)\right), \qquad \text{(E.2.3)}
\end{aligned}
$$

where β_f, x_f and y_f are found in Eqs. 4.2.6 and E.1.1. In presenting these results we also use the forms of $F_{(8S)}$ and $F_{(8V)}$ found in Eq. 4.4.24. Importantly, in the small-mass limit we recover the expressions

$$\lim_{m_f\to 0} G_{8S}\left(\frac{m_f^2}{m_H^2},\frac{\mu^2}{m_H^2}\right) = F_{8S}\left(0,\frac{\mu^2}{m_H^2}\right),$$
$$\lim_{m_f\to 0} G_{8V}\left(\frac{m_f^2}{m_H^2},\frac{\mu^2}{m_H^2}\right) = F_{8V}\left(0,\frac{\mu^2}{m_H^2}\right). \tag{E.2.4}$$

We also note that the functions $G_{(8S)}$ and $G_{(8V)}$ in Eq. E.2.3 are distinct from $F_{(8S)}$ and $F_{(8V)}$ in Eq. 4.4.24, despite converging to the same result in the small-mass limit. For $h \to b\bar{b}$ we find

$$\begin{aligned}\Gamma^{(6,1)}_{b,(4\mathrm{F})} = \frac{m_H^2\Gamma_b^{(4,0)}}{16\pi^2}\Bigg\{ &\left[C^{(1)}_{\substack{qd\\3333}} + C_F C^{(8)}_{\substack{qd\\3333}}\right] G_{8V}\left(\frac{m_b^2}{m_H^2},\frac{\mu^2}{m_H^2}\right) + \frac{m_s}{m_b}\left[C^{(1)}_{\substack{qd\\2332}} + C_F C^{(8)}_{\substack{qd\\2332}}\right]\\
&\times G_{8V}\left(\frac{m_s^2}{m_H^2},\frac{\mu^2}{m_H^2}\right) + \frac{m_t}{m_b}\left[(1+2N_c)C^{(1)}_{\substack{quqd\\3333}} + C_F C^{(8)}_{\substack{quqd\\3333}}\right] F_{8S}\left(\frac{m_t^2}{m_H^2},\frac{\mu^2}{m_H^2}\right)\\
&+ \frac{m_c}{m_b}\left[C^{(1)}_{\substack{quqd\\3223}} + C_F C^{(8)}_{\substack{quqd\\3223}} + 2N_c C^{(1)}_{\substack{quqd\\2233}}\right] G_{8S}\left(\frac{m_s^2}{m_H^2},\frac{\mu^2}{m_H^2}\right)\\
&+ 2\frac{m_\tau}{m_b} C_{\substack{ledq\\3333}} G_{8S}\left(\frac{m_\tau^2}{m_H^2},\frac{\mu^2}{m_H^2}\right) + 2\frac{m_\mu}{m_b} C_{\substack{ledq\\2233}} G_{8S}\left(\frac{m_\mu^2}{m_H^2},\frac{\mu^2}{m_H^2}\right)\Bigg\}.\end{aligned} \tag{E.2.5}$$

For $h \to c\bar{c}$ we find

$$\begin{aligned}\Gamma^{(6,1)}_{c,(4\mathrm{F})} = \frac{m_H^2\Gamma_c^{(4,0)}}{16\pi^2}\Bigg\{ &\left[C^{(1)}_{\substack{qu\\2222}} + C_F C^{(8)}_{\substack{qu\\2222}}\right] G_{8V}\left(\frac{m_c^2}{m_H^2},\frac{\mu^2}{m_H^2}\right)\\
&+ \frac{m_t}{m_c}\left[C^{(1)}_{\substack{qu\\2332}} + C_F C^{(8)}_{\substack{qu\\2332}}\right] F_{8V}\left(\frac{m_t^2}{m_H^2},\frac{\mu^2}{m_H^2}\right) + \frac{m_b}{m_c}\Bigg[C^{(1)}_{\substack{quqd\\3223}} + C_F C^{(8)}_{\substack{quqd\\3223}}\\
&+ 2N_c C^{(1)}_{\substack{quqd\\2233}}\Bigg] G_{8S}\left(\frac{m_b^2}{m_H^2},\frac{\mu^2}{m_H^2}\right) + \frac{m_s}{m_c}\left[(1+2N_c)C^{(1)}_{\substack{quqd\\2222}} + C_F C^{(8)}_{\substack{quqd\\2222}}\right]\\
&\times G_{8S}\left(\frac{m_s^2}{m_H^2},\frac{\mu^2}{m_H^2}\right) - 2\frac{m_\tau}{m_c} C^{(1)}_{\substack{lequ\\3322}} G_{8S}\left(\frac{m_\tau^2}{m_H^2},\frac{\mu^2}{m_H^2}\right)\\
&- 2\frac{m_\mu}{m_c} C^{(1)}_{\substack{lequ\\2222}} G_{8S}\left(\frac{m_\mu^2}{m_H^2},\frac{\mu^2}{m_H^2}\right)\Bigg\}.\end{aligned} \tag{E.2.6}$$

For $h \to \tau\bar{\tau}$ we find

$$\begin{aligned}\Gamma^{(6,1)}_{\tau,(4\mathrm{F})} = \frac{m_H^2\Gamma_\tau^{(4,0)}}{16\pi^2}\Bigg\{ &C_{\substack{le\\3333}} G_{8V}\left(\frac{m_\tau^2}{m_H^2},\frac{\mu^2}{m_H^2}\right) + \frac{m_\mu}{m_\tau} C_{\substack{le\\2332}} G_{8V}\left(\frac{m_\mu^2}{m_H^2},\frac{\mu^2}{m_H^2}\right)\\
&- 2N_c\frac{m_t}{m_\tau} C^{(1)}_{\substack{lequ\\3333}} F_{8S}\left(\frac{m_t^2}{m_H^2},\frac{\mu^2}{m_H^2}\right) + 2N_c\Bigg[\frac{m_b}{m_\tau} C_{\substack{ledq\\3333}} G_{8S}\left(\frac{m_b^2}{m_H^2},\frac{\mu^2}{m_H^2}\right)\\
&- \frac{m_c}{m_\tau} C^{(1)}_{\substack{lequ\\3322}} G_{8S}\left(\frac{m_c^2}{m_H^2},\frac{\mu^2}{m_H^2}\right) + \frac{m_s}{m_\tau} C_{\substack{ledq\\3322}} G_{8S}\left(\frac{m_s^2}{m_H^2},\frac{\mu^2}{m_H^2}\right)\Bigg]\Bigg\}.\end{aligned} \tag{E.2.7}$$

For $h \to \mu\bar{\mu}$ we find

$$\begin{aligned}\Gamma^{(6,1)}_{\mu,(4\mathrm{F})} = \frac{m_H^2 \Gamma^{(4,0)}_{\mu}}{16\pi^2}\Bigg\{ & C_{\substack{le\\2222}} G_{8V}\left(\frac{m_\mu^2}{m_H^2}, \frac{\mu^2}{m_H^2}\right) + \frac{m_\tau}{m_\mu} C_{\substack{le\\2332}} G_{8V}\left(\frac{m_\tau^2}{m_H^2}, \frac{\mu^2}{m_H^2}\right) \\ & - 2N_c \frac{m_t}{m_\mu} C^{(1)}_{\substack{lequ\\2233}} F_{8S}\left(\frac{m_t^2}{m_H^2}, \frac{\mu^2}{m_H^2}\right) + 2N_c \Bigg[\frac{m_b}{m_\mu} C_{\substack{ledq\\2233}} G_{8S}\left(\frac{m_b^2}{m_H^2}, \frac{\mu^2}{m_H^2}\right) \\ & - \frac{m_c}{m_\mu} C^{(1)}_{\substack{lequ\\2222}} G_{8S}\left(\frac{m_c^2}{m_H^2}, \frac{\mu^2}{m_H^2}\right) + \frac{m_s}{m_\mu} C_{\substack{ledq\\2222}} G_{8S}\left(\frac{m_s^2}{m_H^2}, \frac{\mu^2}{m_H^2}\right)\Bigg]\Bigg\}. \end{aligned} \tag{E.2.8}$$

Appendix F

Decoupling Constants

In this section we report the form of the fermion mass decoupling constants introduced in Section 4.5.2. The form of the electric charge decoupling constants are also listed in Section 4.5.2 in Eqs. 4.5.22 and 4.5.23. In reporting these results we write them in terms of the five-flavor QED×QCD theory parameters $\overline{m}_f^{(\ell)}$ and $\overline{e}^{(\ell)}$ to emphasize that we advocate the use of decoupling constants when adopting the decoupled hybrid renormalization scheme defined by Eq. 4.5.27. The decoupling constants are gauge-independent quantities which receive contributions from tadpole corrections. It is therefore convenient to split the decoupling constants into tadpole and non-tadpole contributions. As noted in Section 1.2.3, tadpoles are gauge-dependent quantities, and so this split into tadpole and non-tadpole contributions is gauge-dependent, although the sum of the tadpole and non-tadpole terms are necessarily gauge invariant. When reporting these results, we choose to write them with the tadpoles defined in Feynman gauge. The results are not simply a function of the tadpole functions defined in Eqs. 4.3.23 and 4.3.26, but rather of the finite parts of these tadpole functions in the small-mass limit. For convenience, we here list the finite part of the SM and dimension-6 SMEFT tadpole functions in the small-mass limit as

$$
\begin{aligned}
\tilde{T}^{(4)}_{\text{Feyn.}} &= \frac{1}{32\pi^2\overline{v}^{(\ell)}}\Bigg\{\hat{A}_0(M_W^2)(12M_W^2+2m_H^2)-8M_W^4+\hat{A}_0(M_Z^2)(6M_Z^2+m_H^2) \\
&\quad -4M_Z^4+3m_H^2\hat{A}_0(m_H^2)-8N_c m_t^2\hat{A}_0(m_t^2)\Bigg\}, \\
\tilde{T}^{(6)}_{\text{Feyn.}} &= \frac{\overline{v}^{(\ell)}}{32\pi^2}\Bigg\{4\left(C_{H\Box}-\frac{C_{HD}}{4}\right)m_H^2\left(\hat{A}_0(m_H^2)-\hat{A}_0(M_W^2)\right)-2C_{H\Box}m_H^2\hat{A}_0(M_Z^2) \\
&\quad -6C_H(\overline{v}^{(\ell)})^2\hat{A}_0(m_H^2)+\left(24\hat{A}_0(M_W^2)-16M_W^2\right)C_{HW}M_W^2+\left(3\hat{A}_0(M_Z^2)-2M_Z^2\right)M_Z^2 \\
&\quad \times\left[C_{HD}+4\left(C_{HW}\hat{c}_w^2+C_{HB}\hat{s}_w^2+C_{HWB}\hat{c}_w\hat{s}_w\right)\right]+4N_c\sqrt{2}\overline{v}^{(\ell)}m_tC_{tH}\hat{A}_0(m_t^2)\Bigg\} \\
&\quad +(\overline{v}^{(\ell)})^2\left[C_{H\Box}-\frac{C_{HD}}{4}+\frac{\hat{c}_w}{\hat{s}_w}\left(C_{HWB}+\frac{\hat{c}_w}{4\hat{s}_w}C_{HD}\right)\right]\tilde{T}^{(4)}_{\text{Feyn.}}\,,
\end{aligned}
\tag{F.0.1}
$$

where the tilde represents that the tadpole functions are the finite parts of the tadpole functions of Eqs. 4.3.23 and 4.3.26 in the small-mass limit, the superscript represents a contribution at mass dimension i, and $\hat{A}_0$ represents the finite part of the corresponding A_0 scalar loop function

$$\hat{A}_0(m^2) = m^2 + m^2 \ln\left(\frac{\mu^2}{m^2}\right) . \tag{F.0.2}$$

In the SM, we find that the decoupling constants for the final-state fermions relevant to the processes considered in this work, b, c, τ, and μ are

$$\begin{aligned}\zeta_{m_b}^{(4,1)} = \frac{1}{576\pi^2(\overline{v}^{(\ell)})^2}\Bigg\{ & M_Z^2\left(11 + 2\hat{c}_w^2 - 40\hat{c}_w^4\right) + 9m_t^2\left(\frac{6m_t^2}{m_t^2 - M_W^2} - 11\right) \\ & - \frac{54m_t^4\left(m_t^2 - 2M_W^2\right)}{\left(m_t^2 - M_W^2\right)^2}\ln\left(\frac{\mu^2}{m_t^2}\right) + 6\left(4M_W^2(1 - 2\hat{c}_w^2) + 7M_Z^2\right)\ln\left(\frac{\mu^2}{M_Z^2}\right) \\ & + \frac{18M_W^2\left(2m_t^4 - 7m_t^2M_W^2 + 2M_W^4\right)}{\left(m_t^2 - M_W^2\right)^2}\ln\left(\frac{\mu^2}{M_W^2}\right)\Bigg\} - \frac{1}{m_H^2\overline{v}^{(\ell)}}\tilde{T}_{\text{Feyn.}}^{(4)} ,\end{aligned} \tag{F.0.3}$$

$$\begin{aligned}\zeta_{m_c}^{(4,1)} = \frac{1}{576\pi^2(\overline{v}^{(\ell)})^2}\Bigg\{ & 182M_W^2 - 160M_W^2\hat{c}_w^2 - 49M_Z^2 + 36M_W^2\ln\left(\frac{\mu^2}{M_W^2}\right) + 6\Big(40M_W^2 \\ & - 32M_W^2\hat{c}_w^2 - 5M_Z^2\Big)\ln\left(\frac{\mu^2}{M_Z^2}\right)\Bigg\} - \frac{1}{\overline{v}^{(\ell)}m_H^2}\tilde{T}_{\text{Feyn.}}^{(4)} ,\end{aligned} \tag{F.0.4}$$

$$\begin{aligned}\zeta_{m_\tau}^{(4,1)} = \frac{1}{64\pi^2(\overline{v}^{(\ell)})^2}\Bigg\{ & 58M_W^2 - 40M_W^2\hat{c}_w^2 - 21M_Z^2 + 4M_W^2\ln\left(\frac{\mu^2}{M_W^2}\right) + \Big(72M_W^2 \\ & - 48M_W^2\hat{c}_w^2 - 22M_Z^2\Big)\ln\left(\frac{\mu^2}{M_Z^2}\right)\Bigg\} - \frac{1}{\overline{v}^{(\ell)}m_H^2}\tilde{T}_{\text{Feyn.}}^{(4)} ,\end{aligned} \tag{F.0.5}$$

$$\zeta_{m_\mu}^{(4,1)} = \zeta_{m_\tau}^{(4,1)} . \tag{F.0.6}$$

We split the dimension-6 SMEFT corrections according to

$$\zeta_{m_f}^{(6,1)} = -\frac{1}{m_H^2\overline{v}^{(\ell)}}\tilde{T}_{\text{Feyn.}}^{(6)} - \frac{1}{2m_H^2\overline{v}^{(\ell)}}\frac{\Gamma_f^{(6,0)}}{\Gamma_f^{(4,0)}}\tilde{T}_{\text{Feyn.}}^{(4)} + \zeta_{m_f,\text{ no-tad.}}^{(6,1)} , \tag{F.0.7}$$

where the term not proportional to tadpoles ("no-tad") is split further according to

$$\begin{aligned}\zeta_{m_f,\text{no-tad}}^{(6,1)} = \zeta_{m_f,\text{NL}}^{(6,1)} + \zeta_{m_f,\text{LH}}^{(6,1)}\ln\left(\frac{\mu^2}{m_H^2}\right) + \zeta_{m_f,\text{LW}}^{(6,1)}\ln\left(\frac{\mu^2}{M_W^2}\right) + \zeta_{m_f,\text{LZ}}^{(6,1)}\ln\left(\frac{\mu^2}{M_Z^2}\right) \\ + \zeta_{m_f,\text{Lt}}^{(6,1)}\ln\left(\frac{\mu^2}{m_t^2}\right) .\end{aligned} \tag{F.0.8}$$

For $f = b$ one finds

$$\begin{aligned}
\zeta^{(6,1)}_{m_b,\,\mathrm{NL}} = &-\frac{1}{1152(m_t^2-M_W^2)M_Z^2\pi^2\hat{s}_w^2}\Bigg\{C_{HD}\Big(M_W^2(45m_t^4\\
&-61m_t^2M_W^2-38M_W^4)+11M_Z^2(m_t^2-M_W^2)(M_Z^2-2M_W^2)\Big)\\
&-12C_{HWB}\hat{s}_w\hat{c}_wM_Z^2\left(-15m_t^4+17m_t^2M_W^2+16M_W^4+7m_t^2M_Z^2-7M_W^2M_Z^2\right)\\
&+6(m_t^2-M_W^2)M_Z^2\hat{s}_w^2\Bigg[-12C_{Htb}\frac{m_t}{\overline{m}_b^{(\ell)}}(m_t^2-M_W^2)+4C_{Hb}(5M_W^2-2M_Z^2)\\
&+4\sqrt{2}\frac{\overline{e}^{(\ell)}}{m_b^{(\ell)}}C_{bB}\hat{s}_wM_Z(4M_W^2-M_Z^2)+4\sqrt{2}\frac{\overline{e}^{(\ell)}}{m_b^{(\ell)}}C_{bW}M_W(6m_t^2+10M_W^2-M_Z^2)\\
&+3\sqrt{2}C_{bH}\frac{\overline{v}^{(\ell)}}{\overline{m}_b^{(\ell)}}(3m_H^2+2M_W^2+M_Z^2)+2(10M_W^2-M_Z^2)C^{(1)}_{\substack{Hq\\33}}\\
&-12\frac{m_t^3}{\overline{m}_b^{(\ell)}}\left((1+2N_c)C^{(1)}_{\substack{quqd\\3333}}+C_FC^{(8)}_{\substack{quqd\\3333}}\right)\Bigg]\\
&-6\sqrt{2}\overline{e}^{(\ell)}C_{tW}m_tM_W(m_t^2+5M_W^2)M_Z^2\hat{s}_w^2\\
&-2C^{(3)}_{\substack{Hq\\33}}\hat{s}_w^2M_Z^2\left(-15m_t^4+M_W^2(28M_W^2-M_Z^2)+m_t^2(5M_W^2+M_Z^2)\right)\Bigg\}\,,
\end{aligned}\tag{F.0.9}$$

$$\zeta^{(6,1)}_{m_b,\,\mathrm{LH}} = -\frac{3m_H^2\overline{v}^{(\ell)}}{32\sqrt{2}\overline{m}_b^{(\ell)}\pi^2}C_{bH}\,,\tag{F.0.10}$$

$$\begin{aligned}
\zeta^{(6,1)}_{m_b,\,\mathrm{LW}} = &\frac{M_W^3}{16\pi^2(m_t^2-M_W^2)^2}\Bigg\{\frac{2m_t^4-7m_t^2M_W^2+2M_W^4}{M_Z\hat{s}_w}\Bigg(C_{HWB}\\
&+\frac{M_W}{4M_Z\hat{s}_w}C_{HD}\Bigg)+3\sqrt{2}M_W^2\left(2(m_t^2-M_W^2)\frac{\overline{e}^{(\ell)}}{\overline{m}_b^{(\ell)}}C_{bW}-m_t\overline{e}^{(\ell)}C_{tW}\right)\\
&-\frac{(m_t^2-M_W^2)^2}{\sqrt{2}M_W}\frac{\overline{v}^{(\ell)}}{\overline{m}_b^{(\ell)}}C_{bH}+3\frac{m_t}{\overline{m}_b^{(\ell)}}M_W(m_t^2-M_W^2)C_{Htb}-3m_t^2M_WC^{(3)}_{\substack{Hq\\33}}\Bigg\}\,,
\end{aligned}\tag{F.0.11}$$

$$\begin{aligned}
\zeta^{(6,1)}_{m_b,\,\mathrm{LZ}} = &\frac{1}{16\pi^2}\Bigg\{-\frac{4M_W^4-14M_W^2M_Z^2+7M_Z^4}{12M_Z^2\hat{s}_w^2}C_{HD}+\frac{\hat{c}_w(3M_Z^2-2M_W^2)}{\hat{s}_w}C_{HWB}\\
&-(2M_W^2+M_Z^2)C_{Hb}+2(M_Z^2-M_W^2)\left(C^{(1)}_{\substack{Hq\\33}}+C^{(3)}_{\substack{Hq\\33}}\right)\\
&-\frac{1}{2\sqrt{2}}\Bigg(4M_Z(4M_W^2-M_Z^2)\left(\hat{c}_w\frac{\overline{e}^{(\ell)}}{\overline{m}_b^{(\ell)}}C_{bW}+\hat{s}_w\frac{\overline{e}^{(\ell)}}{\overline{m}_b^{(\ell)}}C_{bB}\right)+\frac{\overline{v}^{(\ell)}}{\overline{m}_b^{(\ell)}}M_Z^2C_{bH}\Bigg)\Bigg\}\,,
\end{aligned}\tag{F.0.12}$$

$$\begin{aligned}
\zeta^{(6,1)}_{m_b,\,\mathrm{Lt}} = &\frac{1}{16\pi^2}\Bigg\{\frac{m_t^3}{\overline{m}_b^{(\ell)}}\left((1+2N_c)C^{(1)}_{\substack{quqd\\3333}}+C_FC^{(8)}_{\substack{quqd\\3333}}\right)\\
&+\frac{m_t^3}{\overline{m}_b^{(\ell)}(m_t^2-M_W^2)}\left((m_t^2-4M_W^2)C_{Htb}-6\sqrt{2}m_tM_W\overline{e}^{(\ell)}C_{bW}\right)
\end{aligned}$$

$$- \frac{3M_W m_t^3 (m_t^2 - 2M_W^2)}{(m_t^2 - M_W^2)^2} \left(\sqrt{2}\overline{e}^{(\ell)} C_{tW} + \frac{m_t M_W}{4M_Z^2 \hat{s}_w^2} C_{HD} + \frac{m_t}{M_Z \hat{s}_w} C_{HWB} + \frac{m_t}{M_W} C^{(3)}_{\substack{Hq \\ 33}} \right) \Bigg\} . \tag{F.0.13}$$

For $f = c$ one finds

$$\begin{aligned}
\zeta^{(6,1)}_{m_c,\mathrm{NL}} = & -\frac{1}{1152\pi^2 M_Z^3 \hat{s}_w^3} \Big\{ C_{HD} M_Z \hat{s}_w \left(98 M_W^2 M_Z^2 - 49 M_Z^4 - 22 M_W^4\right) \\
& - 12 C_{HWB} M_W \left(17 M_Z^4 + 26 M_W^4 - 43 M_W^2 M_Z^2\right) + 18\sqrt{2} \frac{\overline{v}^{(\ell)}}{\overline{m}_c^{(\ell)}} C_{cH} M_Z^3 \hat{s}_w^3 \\
& \times \left(3 m_H^2 + 2 M_W^2 + M_Z^2\right) + 12 M_Z^3 \hat{s}_w^3 \Bigg[-\frac{\sqrt{2}}{\hat{c}_w} \frac{\overline{e}^{(\ell)} \overline{v}^{(\ell)}}{\overline{m}_c^{(\ell)}} C_{cB} \left(8 M_W^2 - 5 M_Z^2\right) \\
& + \frac{\sqrt{2}}{\hat{s}_w} \frac{\overline{e}^{(\ell)} \overline{v}^{(\ell)}}{\overline{m}_c^{(\ell)}} C_{cW} \left(14 M_W^2 - 5 M_Z^2\right) - C^{(1)}_{\substack{Hq \\ 22}} \left(20 M_W^2 - 11 M_Z^2\right) \\
& + C^{(3)}_{\substack{Hq \\ 22}} \left(38 M_W^2 - 11 M_Z^2\right) - 2 C_{Hc} \left(10 M_W^2 - 7 M_Z^2\right) \\
& + 12 \frac{m_t^3}{\overline{m}_c^{(\ell)}} \left(C^{(1)}_{\substack{qu \\ 2332}} + C_F C^{(8)}_{\substack{qu \\ 2332}} \right) \Bigg] \Bigg\} ,
\end{aligned} \tag{F.0.14}$$

$$\zeta^{(6,1)}_{m_c,\mathrm{LH}} = -\frac{3\sqrt{2} m_H^2}{64\pi^2} \frac{\overline{v}^{(\ell)}}{\overline{m}_c^{(\ell)}} C_{cH} , \tag{F.0.15}$$

$$\begin{aligned}
\zeta^{(6,1)}_{m_c,\mathrm{LW}} = & \frac{1}{32\pi^2 M_Z^5 \hat{s}_w^3} \Big\{ C_{HD} M_W^4 M_Z^3 \hat{s}_w + 4 C_{HWB} M_W^3 M_Z^4 \hat{s}_w^2 \\
& - \sqrt{2} \frac{\overline{v}^{(\ell)}}{\overline{m}_c^{(\ell)}} C_{cH} M_W^2 M_Z^5 \hat{s}_w^3 - 6\sqrt{2} \frac{\overline{e}^{(\ell)} \overline{v}^{(\ell)}}{\overline{m}_c^{(\ell)}} C_{cW} M_W^2 M_Z^5 \hat{s}_w^2 \Big\} ,
\end{aligned} \tag{F.0.16}$$

$$\begin{aligned}
\zeta^{(6,1)}_{m_c,\mathrm{LZ}} = & \frac{1}{192\pi^2 M_W M_Z^5 \hat{s}_w^3} \Big\{ C_{HD} M_W M_Z^3 \hat{s}_w \left(8 M_W^4 + 5 M_Z^4 - 10 M_W^2 M_Z^2\right) \\
& + 12 C_{HWB} M_W^2 M_Z^4 \hat{s}_w^2 \left(5 M_Z^2 - 4 M_W^2\right) - 3\sqrt{2} \frac{\overline{v}^{(\ell)}}{\overline{m}_c^{(\ell)}} C_{cH} M_W M_Z^7 \hat{s}_w^3 \\
& + 6\sqrt{2} \frac{\overline{e}^{(\ell)} \overline{v}^{(\ell)}}{\overline{m}_c^{(\ell)}} M_Z^6 \hat{s}_W^2 \left(8 M_W^2 - 5 M_Z^2\right) \left(C_{cB} \hat{s}_w - C_{cW} \hat{c}_w\right) \\
& + 48 M_W M_Z^7 \hat{s}_w^5 \left(C^{(3)}_{\substack{Hq \\ 22}} - C^{(1)}_{\substack{Hq \\ 22}} \right) + 12 C_{Hc} M_W M_Z^5 \hat{s}_w^3 \left(4 M_W^2 - M_Z^2\right) \Big\} ,
\end{aligned} \tag{F.0.17}$$

$$\zeta^{(6,1)}_{m_c,\mathrm{Lt}} = -\frac{1}{4\pi^2} \frac{m_t^3}{\overline{m}_c^{(\ell)}} \left\{ C^{(1)}_{\substack{qu \\ 2332}} + C_F C^{(8)}_{\substack{qu \\ 2332}} \right\} . \tag{F.0.18}$$

For $f = \tau$ we find

$$\begin{aligned}
\zeta^{(6,1)}_{m_\tau,\mathrm{NL}} = & -\frac{1}{128\pi^2 M_W M_Z^3 \hat{s}_w^3} \Big\{ -3 C_{HD} M_W M_Z \hat{s}_w \left(6 M_W^4 + 7 M_Z^4 - 14 M_W^2 M_Z^2\right) \\
& + 12 C_{HWB} M_W^2 M_Z^2 \hat{s}_w^2 \left(4 M_W^2 - 3 M_Z^2\right) + 2 M_Z^2 \hat{s}_w^3 \Bigg[\frac{6\sqrt{2}}{\hat{s}_w} \frac{\overline{v}^{(\ell)} \overline{e}^{(\ell)}}{\overline{m}_\tau^{(\ell)}} C_{\tau W} M_W M_Z
\end{aligned}$$

$$
\begin{aligned}
&\times \left(2M_W^2 - M_Z^2\right) + 2\sqrt{2}\frac{\overline{v}^{(\ell)}\overline{e}^{(\ell)}}{\overline{m}_\tau^{(\ell)}} C_{\tau B} M_Z^2 \left(4M_W^2 - 3M_Z^2\right) \\
&+ 8N_c \frac{m_t^3}{\overline{m}_\tau^{(\ell)}} C^{(1)}_{\substack{lequ \\ 3333}} M_W M_Z + \sqrt{2}\frac{\overline{v}^{(\ell)}}{\overline{m}_\tau^{(\ell)}} C_{\tau H} M_W M_Z \left(3m_H^2 + 2M_W^2 + M_Z^2\right) \\
&+ 2M_W M_Z \Bigg(\left(10M_W^2 - 7M_Z^2\right) C^{(1)}_{\substack{Hl \\ 33}} + \left(16M_W^2 - 7M_Z^2\right) C^{(3)}_{\substack{Hl \\ 33}} \\
&+ \left(10M_W^2 - 8M_Z^2\right) C_{H\tau} \Bigg) \Bigg] \Bigg\} ,
\end{aligned} \tag{F.0.19}
$$

$$
\zeta^{(6,1)}_{m_\tau,\,\mathrm{LH}} = -\frac{3\sqrt{2}m_H^2}{64\pi^2}\frac{\overline{v}^{(\ell)}}{\overline{m}_\tau^{(\ell)}} C_{\tau H} \,, \tag{F.0.20}
$$

$$
\begin{aligned}
\zeta^{(6,1)}_{m_\tau,\,\mathrm{LW}} = \frac{\hat{c}_w^2}{32\pi^2 M_Z \hat{s}_w^3} \Big\{ & 4C_{HWB} M_W M_Z^2 \hat{s}_w^2 + C_{HD} M_W^2 M_Z \hat{s}_w \\
& - \sqrt{2}\frac{\overline{v}^{(\ell)}}{\overline{m}_\tau^{(\ell)}} M_Z^3 \hat{s}_w^2 \left(6C_{\tau W}\overline{e}^{(\ell)} + C_{\tau H}\hat{s}_w\right) \Big\} \,,
\end{aligned} \tag{F.0.21}
$$

$$
\begin{aligned}
\zeta^{(6,1)}_{m_\tau,\,\mathrm{LZ}} = -\frac{1}{64\pi^2 M_W M_Z^3 \hat{s}_w^3} \Big\{ & C_{HD} M_W M_Z \hat{s}_w \left(22M_W^2 M_Z^2 - 12M_W^4 - 11M_Z^4\right) \\
& + 4C_{HWB} M_W^2 M_Z^2 \hat{s}_w^2 \left(6M_W^2 - 7M_Z^2\right) + \sqrt{2}\frac{\overline{v}^{(\ell)}}{\overline{m}_\tau^{(\ell)}} C_{\tau H} M_W M_Z^5 \hat{s}_w^3 \\
& + 6\sqrt{2}\frac{\overline{v}^{(\ell)}\overline{e}^{(\ell)}}{\overline{m}_\tau^{(\ell)}} M_Z^4 \hat{s}_w^2 \left(C_{\tau B}\hat{s}_w + C_{\tau W}\hat{c}_w\right) \left(4M_W^2 - 3M_Z^2\right) \\
& - 24\left(C^{(1)}_{\substack{Hl \\ 33}} + C^{(3)}_{\substack{Hl \\ 33}}\right) M_W M_Z^5 \hat{s}_w^5 + 12 C_{H\tau} M_W M_Z^3 \hat{s}_w^3 \left(2M_W^2 - M_Z^2\right) \Big\} \,,
\end{aligned} \tag{F.0.22}
$$

$$
\zeta^{(6,1)}_{m_\tau,\,\mathrm{Lt}} = -\frac{N_c}{8\pi^2}\frac{m_t^3}{\overline{m}_\tau^{(\ell)}} C^{(1)}_{\substack{lequ \\ 3333}} \,. \tag{F.0.23}
$$

The dimension-6 results for $f = \mu$ are similar to those for $f = \tau$, but are listed here for completeness

$$
\begin{aligned}
\zeta^{(6,1)}_{m_\mu,\mathrm{NL}} = -\frac{1}{128\pi^2 M_W M_Z^3 \hat{s}_w^3} \Big\{ & -3C_{HD} M_W M_Z \hat{s}_w \left(6M_W^4 + 7M_Z^4 - 14M_W^2 M_Z^2\right) \\
& + 12 C_{HWB} M_W^2 M_Z^2 \hat{s}_w^2 \left(4M_W^2 - 3M_Z^2\right) + 2M_Z^2 \hat{s}_w^3 \Bigg[\frac{6\sqrt{2}}{\hat{s}_w}\frac{\overline{v}^{(\ell)}\overline{e}^{(\ell)}}{\overline{m}_\mu^{(\ell)}} C_{\mu W} M_W M_Z \\
& \times \left(2M_W^2 - M_Z^2\right) + 2\sqrt{2}\frac{\overline{v}^{(\ell)}\overline{e}^{(\ell)}}{\overline{m}_\mu^{(\ell)}} C_{\mu B} M_Z^2 \left(4M_W^2 - 3M_Z^2\right) \\
& + 8N_c \frac{m_t^3}{\overline{m}_\mu^{(\ell)}} C^{(1)}_{\substack{lequ \\ 2233}} M_W M_Z + \sqrt{2}\frac{\overline{v}^{(\ell)}}{\overline{m}_\mu^{(\ell)}} C_{\mu H} M_W M_Z \left(3m_H^2 + 2M_W^2 + M_Z^2\right) \\
& + 2M_W M_Z \Bigg(\left(10M_W^2 - 7M_Z^2\right) C^{(1)}_{\substack{Hl \\ 22}} + \left(16M_W^2 - 7M_Z^2\right) C^{(3)}_{\substack{Hl \\ 22}} \\
& + \left(10M_W^2 - 8M_Z^2\right) C_{H\mu} \Bigg) \Bigg] \Bigg\} ,
\end{aligned} \tag{F.0.24}
$$

$$\zeta^{(6,1)}_{m_\mu,\mathrm{LH}} = -\frac{3\sqrt{2}m_H^2}{64\pi^2}\frac{\overline{v}^{(\ell)}}{\overline{m}^{(\ell)}_\mu}C_{\mu H}\,, \tag{F.0.25}$$

$$\begin{aligned}\zeta^{(6,1)}_{m_\mu,\mathrm{LW}} = \frac{\hat{c}_w^2}{32\pi^2 M_Z \hat{s}_w^3}\Big\{&4C_{HWB}M_W M_Z^2\hat{s}_w^2 + C_{HD}M_W^2 M_Z\hat{s}_w \\ &- \sqrt{2}\frac{\overline{v}^{(\ell)}}{\overline{m}^{(\ell)}_\mu}M_Z^3\hat{s}_w^2\left(6C_{\mu W}\overline{e}^{(\ell)} + C_{\mu H}\hat{s}_w\right)\Big\}\,,\end{aligned} \tag{F.0.26}$$

$$\begin{aligned}\zeta^{(6,1)}_{m_\mu,\mathrm{LZ}} = -\frac{1}{64\pi^2 M_W M_Z^3\hat{s}_w^3}\Big\{&C_{HD}M_W M_Z\hat{s}_w\left(22M_W^2M_Z^2 - 12M_W^4 - 11M_Z^4\right) \\ &+ 4C_{HWB}M_W^2M_Z^2\hat{s}_w^2\left(6M_W^2 - 7M_Z^2\right) + \sqrt{2}\frac{\overline{v}^{(\ell)}}{\overline{m}^{(\ell)}_\mu}C_{\mu H}M_W M_Z^5\hat{s}_w^3 \\ &+ 6\sqrt{2}\frac{\overline{v}^{(\ell)}\overline{e}^{(\ell)}}{\overline{m}^{(\ell)}_\mu}M_Z^4\hat{s}_w^2\left(C_{\mu B}\hat{s}_w + C_{\mu W}\hat{c}_w\right)\left(4M_W^2 - 3M_Z^2\right) \\ &- 24\left(C^{(1)}_{\substack{Hl\\22}} + C^{(3)}_{\substack{Hl\\22}}\right)M_W M_Z^5\hat{s}_w^5 + 12C_{H\mu}M_W M_Z^3\hat{s}_w^3\left(2M_W^2 - M_Z^2\right)\Big\}\,,\end{aligned} \tag{F.0.27}$$

$$\zeta^{(6,1)}_{m_\mu,\mathrm{Lt}} = -\frac{N_c}{8\pi^2}\frac{m_t^3}{\overline{m}^{(\ell)}_\tau}C^{(1)}_{\substack{lequ\\2233}}\,. \tag{F.0.28}$$

Bibliography

[1] J. M. Cullen, B. D. Pecjak and D. J. Scott, *NLO corrections to $h \to b\bar{b}$ decay in SMEFT*, *JHEP* **08** (2019) 173, [1904.06358].

[2] J. M. Cullen and B. D. Pecjak, *Higgs decay to fermion pairs at NLO in SMEFT*, *JHEP* **11** (2020) 079, [2007.15238].

[3] P. A. Dirac, *The quantum theory of the electron*, *Proc. Roy. Soc. Lond. A* **A117** (1928) 610–624.

[4] Z. Koba, T. Tati and S. i. Tomonaga, *On a Relativistically Invariant Formulation of the Quantum Theory of Wave Fields. II: Case of Interacting Electromagnetic and Electron Fields*, *Prog. Theor. Phys.* **2** (1947) 101–116.

[5] J. S. Schwinger, *On Quantum electrodynamics and the magnetic moment of the electron*, *Phys. Rev.* **73** (1948) 416–417.

[6] J. S. Schwinger, *Quantum electrodynamics. I A covariant formulation*, *Phys. Rev.* **74** (1948) 1439.

[7] R. Feynman, *Mathematical formulation of the quantum theory of electromagnetic interaction*, *Phys. Rev.* **80** (1950) 440–457.

[8] F. Englert and R. Brout, *Broken Symmetry and the Mass of Gauge Vector Mesons*, *Phys. Rev. Lett.* **13** (1964) 321–323.

[9] P. W. Higgs, *Broken Symmetries and the Masses of Gauge Bosons*, *Phys. Rev. Lett.* **13** (1964) 508–509.

[10] G. Guralnik, C. Hagen and T. Kibble, *Global Conservation Laws and Massless Particles*, *Phys. Rev. Lett.* **13** (1964) 585–587.

[11] S. Glashow, *Partial Symmetries of Weak Interactions*, *Nucl. Phys.* **22** (1961) 579–588.

[12] S. Weinberg, *A Model of Leptons*, *Phys. Rev. Lett.* **19** (1967) 1264–1266.

[13] A. Salam, *Weak and Electromagnetic Interactions*, *Conf. Proc. C* **680519** (1968) 367–377.

[14] H. Fritzsch, M. Gell-Mann and H. Leutwyler, *Advantages of the Color Octet Gluon Picture*, *Phys. Lett. B* **47** (1973) 365–368.

[15] M. E. Peskin and D. V. Schroeder, *An Introduction to quantum field theory*. Addison-Wesley, Reading, USA, 1995.

[16] M. D. Schwartz, *Quantum Field Theory and the Standard Model*. Cambridge University Press, 3, 2014.

[17] M. Srednicki, *Quantum field theory*. Cambridge University Press, 1, 2007.

[18] D. Y. Bardin and G. Passarino, *The standard model in the making: Precision study of the electroweak interactions*. 1999.

[19] F. Halzen and A. D. Martin, *QUARKS AND LEPTONS: AN INTRODUCTORY COURSE IN MODERN PARTICLE PHYSICS*. 1, 1984.

[20] T. Cheng and L. Li, *GAUGE THEORY OF ELEMENTARY PARTICLE PHYSICS*. 1984.

[21] J. Goldstone, *Field Theories with Superconductor Solutions*, *Nuovo Cim.* **19** (1961) 154–164.

[22] J. Goldstone, A. Salam and S. Weinberg, *Broken Symmetries*, *Phys. Rev.* **127** (1962) 965–970.

[23] Particle Data Group collaboration, M. Tanabashi et al., *Review of Particle Physics*, *Phys. Rev. D* **98** (2018) 030001.

[24] C. Wu, E. Ambler, R. Hayward, D. Hoppes and R. Hudson, *Experimental Test of Parity Conservation in β Decay*, *Phys. Rev.* **105** (1957) 1413–1414.

[25] N. Cabibbo, *Unitary Symmetry and Leptonic Decays*, *Phys. Rev. Lett.* **10** (1963) 531–533.

[26] M. Kobayashi and T. Maskawa, *CP Violation in the Renormalizable Theory of Weak Interaction*, *Prog. Theor. Phys.* **49** (1973) 652–657.

[27] L. Wolfenstein, *Parametrization of the Kobayashi-Maskawa Matrix*, *Phys. Rev. Lett.* **51** (1983) 1945.

[28] A. V. Manohar, *Introduction to Effective Field Theories*, *Les Houches Lect. Notes* **108** (2020) , [1804.05863].

[29] A. Denner, *Techniques for calculation of electroweak radiative corrections at the one loop level and results for W physics at LEP-200*, *Fortsch. Phys.* **41** (1993) 307–420, [0709.1075].

[30] G. Passarino and M. Veltman, *One Loop Corrections for e+ e- Annihilation Into mu+ mu- in the Weinberg Model*, *Nucl. Phys. B* **160** (1979) 151–207.

[31] M. Consoli, *One Loop Corrections to $e^+e^- \to e^+e^-$ in the Weinberg Model*, *Nucl. Phys. B* **160** (1979) 208–252.

[32] M. Veltman, *Radiative Corrections to Vector Boson Masses*, *Phys. Lett. B* **91** (1980) 95–98.

[33] M. Green and M. Veltman, *Weak and Electromagnetic Radiative Corrections to Low-Energy Processes*, *Nucl. Phys. B* **169** (1980) 137–164.

[34] G. 't Hooft and M. Veltman, *Scalar One Loop Integrals*, *Nucl. Phys. B* **153** (1979) 365–401.

[35] K. Aoki, Z. Hioki, M. Konuma, R. Kawabe and T. Muta, *Electroweak Theory. Framework of On-Shell Renormalization and Study of Higher Order Effects*, *Prog. Theor. Phys. Suppl.* **73** (1982) 1–225.

[36] J. Fleischer and F. Jegerlehner, *Radiative Corrections to Higgs Decays in the Extended Weinberg-Salam Model*, *Phys. Rev. D* **23** (1981) 2001–2026.

[37] M. Krause, R. Lorenz, M. Muhlleitner, R. Santos and H. Ziesche, *Gauge-independent Renormalization of the 2-Higgs-Doublet Model*, *JHEP* **09** (2016) 143, [1605.04853].

[38] A. Denner, L. Jenniches, J.-N. Lang and C. Sturm, *Gauge-independent $\overline{MS}$ renormalization in the 2HDM*, *JHEP* **09** (2016) 115, [1607.07352].

[39] S. Actis, A. Ferroglia, M. Passera and G. Passarino, *Two-Loop Renormalization in the Standard Model. Part I: Prolegomena*, *Nucl. Phys. B* **777** (2007) 1–34, [hep-ph/0612122].

[40] K.-i. Aoki, Z. Hioki, R. Kawabe, M. Konuma and T. Muta, *ELECTROWEAK RADIATIVE CORRECTIONS TO HIGH-ENERGY neutrino e SCATTERINGS*, *Prog. Theor. Phys.* **65** (1981) 1001.

[41] T. Kinoshita, *Mass singularities of Feynman amplitudes*, *J. Math. Phys.* **3** (1962) 650–677.

[42] T. Lee and M. Nauenberg, *Degenerate Systems and Mass Singularities*, *Phys. Rev.* **133** (1964) B1549–B1562.

[43] T. Appelquist and J. Carazzone, *Infrared Singularities and Massive Fields*, *Phys. Rev. D* **11** (1975) 2856.

[44] D. J. Gross and F. Wilczek, *Ultraviolet Behavior of Nonabelian Gauge Theories*, *Phys. Rev. Lett.* **30** (1973) 1343–1346.

[45] H. Politzer, *Reliable Perturbative Results for Strong Interactions?*, *Phys. Rev. Lett.* **30** (1973) 1346–1349.

[46] M. Neubert, *Les Houches Lectures on Renormalization Theory and Effective Field Theories*, *Les Houches Lect. Notes* **108** (2020) , [1901.06573].

[47] L. Faddeev and V. Popov, *Feynman Diagrams for the Yang-Mills Field*, *Phys. Lett. B* **25** (1967) 29–30.

[48] A. Neitzke, *Applications of qft to geometry*, 2017. https://web.ma.utexas.edu/users/neitzke/teaching/392C-qft-geometry/qft-geometry.pdf.

[49] E. Fermi, *An attempt of a theory of beta radiation. 1.*, *Z. Phys.* **88** (1934) 161–177.

[50] J. Fuentes-Martin, J. Portoles and P. Ruiz-Femenia, *Integrating out heavy particles with functional methods: a simplified framework*, *JHEP* **09** (2016) 156, [1607.02142].

[51] B. Grinstein, *TASI-2013 Lectures on Flavor Physics*, in *Theoretical Advanced Study Institute in Elementary Particle Physics: Particle Physics: The Higgs Boson and Beyond*, 1, 2015, 1501.05283.

[52] B. Grinstein, *Minimal flavor violation*, in *4th International Workshop on the CKM Unitarity Triangle (CKM 2006)*, 6, 2007, 0706.4185.

[53] G. D'Ambrosio, G. Giudice, G. Isidori and A. Strumia, *Minimal flavor violation: An Effective field theory approach*, *Nucl. Phys. B* **645** (2002) 155–187, [hep-ph/0207036].

[54] S. Weinberg, *Phenomenological Lagrangians*, *Physica A* **96** (1979) 327–340.

[55] W. Buchmuller and D. Wyler, *Effective Lagrangian Analysis of New Interactions and Flavor Conservation*, *Nucl. Phys. B* **268** (1986) 621–653.

[56] B. Grzadkowski, M. Iskrzynski, M. Misiak and J. Rosiek, *Dimension-Six Terms in the Standard Model Lagrangian*, *JHEP* **10** (2010) 085, [1008.4884].

[57] R. Contino, M. Ghezzi, C. Grojean, M. Muhlleitner and M. Spira, *Effective Lagrangian for a light Higgs-like scalar*, *JHEP* **07** (2013) 035, [1303.3876].

[58] A. Falkowski, *Higgs Basis: Proposal for an EFT basis choice for LHC HXSWG*, *LHCHXSWG-INT-2015-001* .

[59] L. Lehman, *Extending the Standard Model Effective Field Theory with the Complete Set of Dimension-7 Operators*, *Phys. Rev. D* **90** (2014) 125023, [1410.4193].

[60] B. Henning, X. Lu, T. Melia and H. Murayama, *2, 84, 30, 993, 560, 15456, 11962, 261485, ...: Higher dimension operators in the SM EFT*, *JHEP* **08** (2017) 016, [1512.03433].

[61] H.-L. Li, Z. Ren, J. Shu, M.-L. Xiao, J.-H. Yu and Y.-H. Zheng, *Complete Set of Dimension-8 Operators in the Standard Model Effective Field Theory*, 2005.00008.

[62] C. W. Murphy, *Dimension-8 Operators in the Standard Model Effective Field Theory*, 2005.00059.

[63] R. Alonso, E. E. Jenkins, A. V. Manohar and M. Trott, *Renormalization Group Evolution of the Standard Model Dimension Six Operators III: Gauge Coupling Dependence and Phenomenology*, *JHEP* **04** (2014) 159, [1312.2014].

[64] T. Aoyama, T. Kinoshita and M. Nio, *Revised and Improved Value of the QED Tenth-Order Electron Anomalous Magnetic Moment*, *Phys. Rev. D* **97** (2018) 036001, [1712.06060].

[65] D. Hanneke, S. Hoogerheide and G. Gabrielse, *Cavity Control of a Single-Electron Quantum Cyclotron: Measuring the Electron Magnetic Moment*, *Phys. Rev. A* **83** (2011) 052122, [1009.4831].

[66] CDF collaboration, F. Abe et al., *Observation of top quark production in $\bar{p}p$ collisions*, *Phys. Rev. Lett.* **74** (1995) 2626–2631, [hep-ex/9503002].

[67] G. M. Pruna and A. Signer, *The $\mu \to e\gamma$ decay in a systematic effective field theory approach with dimension 6 operators*, *JHEP* **10** (2014) 014, [1408.3565].

[68] C. Hartmann and M. Trott, *On one-loop corrections in the standard model effective field theory; the $\Gamma(h \to \gamma\,\gamma)$ case*, *JHEP* **07** (2015) 151, [1505.02646].

[69] C. Hartmann and M. Trott, *Higgs Decay to Two Photons at One Loop in the Standard Model Effective Field Theory*, *Phys. Rev. Lett.* **115** (2015) 191801, [1507.03568].

[70] C. Hartmann, W. Shepherd and M. Trott, *The Z decay width in the SMEFT: y_t and λ corrections at one loop*, *JHEP* **03** (2017) 060, [1611.09879].

[71] M. Ghezzi, R. Gomez-Ambrosio, G. Passarino and S. Uccirati, *NLO Higgs effective field theory and κ-framework*, *JHEP* **07** (2015) 175, [1505.03706].

[72] S. Dawson and P. P. Giardino, *Higgs decays to ZZ and $Z\gamma$ in the standard model effective field theory: An NLO analysis*, *Phys. Rev.* **D97** (2018) 093003, [1801.01136].

[73] S. Dawson and P. P. Giardino, *Electroweak corrections to Higgs boson decays to $\gamma\gamma$ and W^+W^- in standard model EFT*, *Phys. Rev.* **D98** (2018) 095005, [1807.11504].

[74] S. Dawson and A. Ismail, *Standard model EFT corrections to Z boson decays*, *Phys. Rev.* **D98** (2018) 093003, [1808.05948].

[75] S. Dawson and P. P. Giardino, *Electroweak and QCD corrections to Z and W pole observables in the standard model EFT*, *Phys. Rev.* **D101** (2020) 013001, [1909.02000].

[76] N. Deutschmann, C. Duhr, F. Maltoni and E. Vryonidou, *Gluon-fusion Higgs production in the Standard Model Effective Field Theory*, *JHEP* **12** (2017) 063, [1708.00460].

[77] M. Grazzini, A. Ilnicka and M. Spira, *Higgs boson production at large transverse momentum within the SMEFT: analytical results*, *Eur. Phys. J.* **C78** (2018) 808, [1806.08832].

[78] R. Boughezal, C.-Y. Chen, F. Petriello and D. Wiegand, *Top quark decay at next-to-leading order in the Standard Model Effective Field Theory*, *Phys. Rev.* **D100** (2019) 056023, [1907.00997].

[79] A. Dedes, K. Suxho and L. Trifyllis, *The decay $h \to Z\gamma$ in the Standard-Model Effective Field Theory*, *JHEP* **06** (2019) 115, [1903.12046].

[80] E. Vryonidou and C. Zhang, *Dimension-six electroweak top-loop effects in Higgs production and decay*, *JHEP* **08** (2018) 036, [1804.09766].

[81] J. Baglio, S. Dawson and I. M. Lewis, *An NLO QCD effective field theory analysis of W^+W^- production at the LHC including fermionic operators*, *Phys. Rev.* **D96** (2017) 073003, [1708.03332].

[82] S. Dawson, P. P. Giardino and A. Ismail, *Standard model EFT and the Drell-Yan process at high energy*, *Phys. Rev.* **D99** (2019) 035044, [1811.12260].

[83] C. Degrande, B. Fuks, K. Mawatari, K. Mimasu and V. Sanz, *Electroweak Higgs boson production in the standard model effective field theory beyond leading order in QCD*, *Eur. Phys. J.* **C77** (2017) 262, [1609.04833].

[84] C. Zhang, *Effective field theory approach to top-quark decay at next-to-leading order in QCD*, *Phys. Rev.* **D90** (2014) 014008, [1404.1264].

[85] C. Zhang and F. Maltoni, *Top-quark decay into Higgs boson and a light quark at next-to-leading order in QCD*, *Phys. Rev.* **D88** (2013) 054005, [1305.7386].

[86] C. Zhang, *Single Top Production at Next-to-Leading Order in the Standard Model Effective Field Theory*, *Phys. Rev. Lett.* **116** (2016) 162002, [1601.06163].

[87] C. Degrande, F. Maltoni, K. Mimasu, E. Vryonidou and C. Zhang, *Single-top associated production with a Z or H boson at the LHC: the SMEFT interpretation*, *JHEP* **10** (2018) 005, [1804.07773].

[88] O. Bessidskaia Bylund, F. Maltoni, I. Tsinikos, E. Vryonidou and C. Zhang, *Probing top quark neutral couplings in the Standard Model Effective Field Theory at NLO in QCD*, *JHEP* **05** (2016) 052, [1601.08193].

[89] F. Maltoni, E. Vryonidou and C. Zhang, *Higgs production in association with a top-antitop pair in the Standard Model Effective Field Theory at NLO in QCD*, *JHEP* **10** (2016) 123, [1607.05330].

[90] R. Grober, M. Muhlleitner, M. Spira and J. Streicher, *NLO QCD Corrections to Higgs Pair Production including Dimension-6 Operators*, *JHEP* **09** (2015) 092, [1504.06577].

[91] T. Neumann and Z. E. Sullivan, *Off-Shell Single-Top-Quark Production in the Standard Model Effective Field Theory*, *JHEP* **06** (2019) 022, [1903.11023].

[92] D. de Florian, I. Fabre and J. Mazzitelli, *Higgs boson pair production at NNLO in QCD including dimension 6 operators*, *JHEP* **10** (2017) 215, [1704.05700].

[93] A. Crivellin, S. Najjari and J. Rosiek, *Lepton Flavor Violation in the Standard Model with general Dimension-Six Operators*, *JHEP* **04** (2014) 167, [1312.0634].

[94] A. Dedes, M. Paraskevas, J. Rosiek, K. Suxho and L. Trifyllis, *The decay $h \to \gamma\gamma$ in the Standard-Model Effective Field Theory*, *JHEP* **08** (2018) 103, [1805.00302].

[95] J. Ellis, C. W. Murphy, V. Sanz and T. You, *Updated Global SMEFT Fit to Higgs, Diboson and Electroweak Data*, *JHEP* **06** (2018) 146, [1803.03252].

[96] R. Aoude, T. Hurth, S. Renner and W. Shepherd, *The impact of flavour data on global fits of the MFV SMEFT*, 2003.05432.

[97] G. T. Bodwin and H. S. Chung, *New method for fitting coefficients in standard model effective theory*, *Phys. Rev. D* **101** (2020) 115039, [1912.09843].

[98] I. Brivio, S. Bruggisser, F. Maltoni, R. Moutafis, T. Plehn, E. Vryonidou et al., *O new physics, where art thou? A global search in the top sector*, *JHEP* **02** (2020) 131, [1910.03606].

[99] A. Buckley, C. Englert, J. Ferrando, D. J. Miller, L. Moore, M. Russell et al., *Constraining top quark effective theory in the LHC Run II era*, *JHEP* **04** (2016) 015, [1512.03360].

[100] S. Dawson, S. Homiller and S. D. Lane, *Putting standard model EFT fits to work*, *Phys. Rev. D* **102** (2020) 055012, [2007.01296].

[101] LHC Higgs Cross Section Working Group collaboration, D. de Florian et al., *Handbook of LHC Higgs Cross Sections: 4. Deciphering the Nature of the Higgs Sector*, 1610.07922.

[102] ATLAS collaboration, G. Aad et al., *Observation of a new particle in the search for the Standard Model Higgs boson with the ATLAS detector at the LHC*, *Phys. Lett. B* **716** (2012) 1–29, [1207.7214].

[103] CMS collaboration, S. Chatrchyan et al., *Observation of a New Boson at a Mass of 125 GeV with the CMS Experiment at the LHC*, *Phys. Lett. B* **716** (2012) 30–61, [1207.7235].

[104] ATLAS, CMS collaboration, G. Aad et al., *Combined Measurement of the Higgs Boson Mass in pp Collisions at $\sqrt{s} = 7$ and 8 TeV with the ATLAS and CMS Experiments*, *Phys. Rev. Lett.* **114** (2015) 191803, [1503.07589].

[105] ATLAS collaboration, M. Aaboud et al., *Observation of $H \to b\bar{b}$ decays and VH production with the ATLAS detector*, *Phys. Lett.* **B786** (2018) 59–86, [1808.08238].

[106] CMS collaboration, A. M. Sirunyan et al., *Observation of Higgs boson decay to bottom quarks*, *Phys. Rev. Lett.* **121** (2018) 121801, [1808.08242].

[107] CMS collaboration, A. M. Sirunyan et al., *Observation of the Higgs boson decay to a pair of τ leptons with the CMS detector*, *Phys. Lett.* **B779** (2018) 283–316, [1708.00373].

[108] ATLAS collaboration, M. Aaboud et al., *Cross-section measurements of the Higgs boson decaying into a pair of τ-leptons in proton-proton collisions at $\sqrt{s} = 13$ TeV with the ATLAS detector*, *Phys. Rev.* **D99** (2019) 072001, [1811.08856].

[109] ATLAS collaboration, M. Aaboud et al., *Search for the dimuon decay of the Higgs boson in pp collisions at $\sqrt{s} = 13$ TeV with the ATLAS detector*, *Phys. Rev. Lett.* **119** (2017) 051802, [1705.04582].

[110] CMS collaboration, A. M. Sirunyan et al., *Search for the Higgs boson decaying to two muons in proton-proton collisions at $\sqrt{s} = 13$ TeV*, *Phys. Rev. Lett.* **122** (2019) 021801, [1807.06325].

[111] ATLAS collaboration, M. Aaboud et al., *Search for the Decay of the Higgs Boson to Charm Quarks with the ATLAS Experiment*, *Phys. Rev. Lett.* **120** (2018) 211802, [1802.04329].

[112] CMS collaboration, A. M. Sirunyan et al., *A search for the standard model Higgs boson decaying to charm quarks*, *JHEP* **03** (2020) 131, [1912.01662].

[113] M. Ruan, *Higgs Measurement at e^+e^- Circular Colliders*, *Nucl. Part. Phys. Proc.* **273-275** (2016) 857–862, [1411.5606].

[114] K. Fujii et al., *Physics Case for the International Linear Collider*, 1506.05992.

[115] H. Abramowicz et al., *Higgs physics at the CLIC electron–positron linear collider*, *Eur. Phys. J.* **C77** (2017) 475, [1608.07538].

[116] J. Ellis, P. Roloff, V. Sanz and T. You, *Dimension-6 Operator Analysis of the CLIC Sensitivity to New Physics*, *JHEP* **05** (2017) 096, [1701.04804].

[117] G. Durieux, C. Grojean, J. Gu and K. Wang, *The leptonic future of the Higgs*, *JHEP* **09** (2017) 014, [1704.02333].

[118] A. Denner and S. Dittmaier, *Electroweak Radiative Corrections for Collider Physics*, *Phys. Rept.* **864** (2020) 1–163, [1912.06823].

[119] R. Gauld, B. D. Pecjak and D. J. Scott, *One-loop corrections to $h \to b\bar{b}$ and $h \to \tau\bar{\tau}$ decays in the Standard Model Dimension-6 EFT: four-fermion operators and the large-m_t limit*, *JHEP* **05** (2016) 080, [1512.02508].

[120] A. Dedes, W. Materkowska, M. Paraskevas, J. Rosiek and K. Suxho, *Feynman rules for the Standard Model Effective Field Theory in R_ξ -gauges*, *JHEP* **06** (2017) 143, [1704.03888].

[121] W. R. Inc., "Mathematica, Version 12.1." https://www.wolfram.com/mathematica.

[122] A. Alloul, N. D. Christensen, C. Degrande, C. Duhr and B. Fuks, *FeynRules 2.0 - A complete toolbox for tree-level phenomenology*, *Comput. Phys. Commun.* **185** (2014) 2250–2300, [1310.1921].

[123] T. Hahn and M. Perez-Victoria, *Automatized one loop calculations in four-dimensions and D-dimensions*, *Comput. Phys. Commun.* **118** (1999) 153–165, [hep-ph/9807565].

[124] T. Hahn, *Generating Feynman diagrams and amplitudes with FeynArts 3*, *Comput. Phys. Commun.* **140** (2001) 418–431, [hep-ph/0012260].

[125] H. H. Patel, *Package-X 2.0: A Mathematica package for the analytic calculation of one-loop integrals*, *Comput. Phys. Commun.* **218** (2017) 66–70, [1612.00009].

[126] A. Helset, M. Paraskevas and M. Trott, *Gauge fixing the Standard Model Effective Field Theory*, *Phys. Rev. Lett.* **120** (2018) 251801, [1803.08001].

[127] M. Misiak, M. Paraskevas, J. Rosiek, K. Suxho and B. Zglinicki, *Effective Field Theories in R_ξ gauges*, *JHEP* **02** (2019) 051, [1812.11513].

[128] B. A. Kniehl, *Radiative corrections for $H \to f$ anti-f (γ) in the standard model*, *Nucl. Phys. B* **376** (1992) 3–28.

[129] R. Gauld, B. D. Pecjak and D. J. Scott, *QCD radiative corrections for $h \to b\bar{b}$ in the Standard Model Dimension-6 EFT*, *Phys. Rev. D* **94** (2016) 074045, [1607.06354].

[130] E. E. Jenkins, A. V. Manohar and M. Trott, *Renormalization Group Evolution of the Standard Model Dimension Six Operators I: Formalism and lambda Dependence*, *JHEP* **10** (2013) 087, [1308.2627].

[131] E. E. Jenkins, A. V. Manohar and M. Trott, *Renormalization Group Evolution of the Standard Model Dimension Six Operators II: Yukawa Dependence*, *JHEP* **01** (2014) 035, [1310.4838].

[132] T. Corbett, A. Helset and M. Trott, *Ward Identities for the Standard Model Effective Field Theory*, *Phys. Rev. D* **101** (2020) 013005, [1909.08470].

[133] K. Chetyrkin, B. A. Kniehl and M. Steinhauser, *Virtual top quark effects on the H —> b anti-b decay at next-to-leading order in QCD*, *Phys. Rev. Lett.* **78** (1997) 594–597, [hep-ph/9610456].

[134] S. Larin, T. van Ritbergen and J. Vermaseren, *The Large top quark mass expansion for Higgs boson decays into bottom quarks and into gluons*, *Phys. Lett. B* **362** (1995) 134–140, [hep-ph/9506465].

[135] A. Celis, J. Fuentes-Martin, A. Vicente and J. Virto, *DsixTools: The Standard Model Effective Field Theory Toolkit*, *Eur. Phys. J. C* **77** (2017) 405, [1704.04504].

[136] A. Bednyakov, B. Kniehl, A. Pikelner and O. Veretin, *On the b-quark running mass in QCD and the SM*, *Nucl. Phys. B* **916** (2017) 463–483, [1612.00660].

[137] R. Akhoury, H. Wang and O. I. Yakovlev, *On the Resummation of large QCD logarithms in Higgs —> gamma gamma decay*, *Phys. Rev. D* **64** (2001) 113008, [hep-ph/0102105].

[138] T. Liu and A. A. Penin, *High-Energy Limit of QCD beyond the Sudakov Approximation*, *Phys. Rev. Lett.* **119** (2017) 262001, [1709.01092].

[139] Z. L. Liu and M. Neubert, *Factorization at subleading power and endpoint-divergent convolutions in $h \to \gamma\gamma$ decay*, *JHEP* **04** (2020) 033, [1912.08818].

[140] J. Wang, *Resummation of double logarithms in loop-induced processes with effective field theory*, 1912.09920.

[141] B. A. Kniehl, *Radiative corrections for $H \to W^+W^-$ (γ) in the standard model*, *Nucl. Phys. B* **357** (1991) 439–466.

[142] J. Ellis, *TikZ-Feynman: Feynman diagrams with TikZ*, *Comput. Phys. Commun.* **210** (2017) 103–123, [1601.05437].